THEORETICAL AND EXPERIMENTAL INVESTIGATION OF PORE CONFINEMENT EFFECTS IN GAS CONDENSATE RESERVOIRS

By

Hosein Doryani Daryuni

BSc., MSc.

Submitted for the degree of **Doctor of Philosophy** in

Petroleum Engineering

Heriot-Watt University

Institute of Geoenergy Engineering

School of Energy, Geoscience, Infrastructure and Society

March 2022

The copyright in this thesis is owned by the author. Any quotation from the thesis or use of any of the information contained in it must acknowledge this thesis as the source of the quotation or information.

ABSTRACT

Unconventional resources play an important role to meet future energy demands. Recent advances in technology has made the production from unconventional reservoirs feasible. However, it is necessary to properly study the phase behavior and flow of fluids within these reservoirs as they are not well understood.

In this thesis, the impacts of fluid confinement effects, which refers to the impact the small pore spaces and pore walls on the fluid phase behaviour due to non-negligible interactions between pore walls and fluid molecules, on the phase behaviour of gas condensate systems within real unconventional rocks, were investigated. A novel experimental procedure was designed to measure dew point pressure (Pdew) of various gas-condensate fluid mixtures within different real shale rocks. Several experiments were performed to realistically study the impacts of gas condensate fluid composition, temperature, net stress and rock type on the extent of the pore confinement effects. The trends for the impacts of confinement Pdew of single component fluids and gas condensate mixtures were analyzed and it was observed that pore confinement would increase the Pdew of gas condensate mixtures while reduced the Pdew of single component fluids. The impacts of the presence of heavier components in the gas condensate mixture was found to be significant. In line with the experimental measurements, the equation of state describing confined fluid phase behavior of gas condensate mixtures was modified by modifications in binary interaction parameters. A new correlation based on the Lennard Jones interaction potential was presented to take into account the interactions between fluid and wall molecules. The proposed correlation was tuned based on the experimental results. The error of the predictability of the correlations for core sample and the fluids not used in its development was found to be within an acceptable range.

Based on the modified equation of state obtained, numerical simulations were performed to investigate the impacts of pore confinement on the performance of the unconventional reservoirs. It was noted that gas production was slightly higher using the confined fluid mode which was mainly attributed to the lower fluid viscosity due to confinement. When pressure drawdown (DP) was low, models with bulk fluid produced more condensate. However, when DP increased, models with confined fluid produced more. Considering dual porosity model, dual porosity-dual permeability model, adsorption, and diffusion did not alter these trends.

DEDICATION

To my lovely wife, Elahe

ACKNOWLEDGEMENT

It is a genuine pleasure to express my deep gratitude to my supervisor Prof. Mahmoud Jamiolahmady (Jami), for his technical guidance, insightful ideas and encouragement throughout this work. I always had his unconditional support, both in research and in my personal life all throughout these years. He will always be a role model to me for being a magnificent person. It was my greatest honor and pleasure to work under his supervision. I would like to also thank my second supervisor, Dr. Elli-Maria Charalampidou.

This work would have not been improved without the insightful and valuable technical comments and ideas that I received from Dr. Jingsheng Ma and Dr. Manouchehr Haghighi, who kindly accepted to review my thesis. I wish to express my sincerest thanks to them. It was my great pleasure to learn from them.

I would like to thank Shaun Ireland, Adam Sisson, Pantelis Tsolis, and Kristen Sondej for their technical lab support.

I would also like to thank my dear friends, Amir Heidari, Abdulelah Nasieef, Ifeanyi Seteyeobot, Victor Molokwu, Saeid Ataee, Ibrahim Alabdulwahab, Caroline Johnson, and Dr. Amir Farzaneh for their help over the course of this study.

And, I wish to thank my family, especially my lovely wife, Elahe, for her unconditional support, encouragement and patience during my PhD studies.

Research Thesis Submission

Name*:*	HOSEIN DORYANIDARYUNI		
School:	EGIS		
Version: *(i.e. First, Resubmission, Final)*	Final submission	Degree Sought:	PhD

Declaration

In accordance with the appropriate regulations I hereby submit my thesis and I declare that:

1. The thesis embodies the results of my own work and has been composed by myself
2. Where appropriate, I have made acknowledgement of the work of others
3. The thesis is the correct version for submission and is the same version as any electronic versions submitted*.
4. My thesis for the award referred to, deposited in the Heriot-Watt University Library, should be made available for loan or photocopying and be available via the Institutional Repository, subject to such conditions as the Librarian may require
5. I understand that as a student of the University I am required to abide by the Regulations of the University and to conform to its discipline.
6. I confirm that the thesis has been verified against plagiarism via an approved plagiarism detection application e.g. Turnitin.
7. Where the thesis contains published outputs under Regulation 6 (9.1.2) or Regulation 43 (9) these are accompanied by a critical review which accurately describes my contribution to the research and, for multi-author outputs, a signed declaration indicating the contribution of each author (complete)
8. Inclusion of published outputs under Regulation 6 (9.1.2) or Regulation 43 (9) shall not constitute plagiarism.

* *Please note that it is the responsibility of the candidate to ensure that the correct version of the thesis is submitted.*

Signature of Candidate*:*	*Hosein Doryani*	Date:	08/03/2022

Submission

Submitted By *(name in capitals):*	HOSEIN DORYANIDARYUNI
Signature of Individual Submitting:	*Hosein Doryani*
Date Submitted:	08/03/2022

For Completion in the Student Service Centre (SSC)

Limited Access	Requested	Yes		No		Approved	Yes		No	
E-thesis Submitted ***(mandatory for final theses)***										
Received in the SSC by *(name in capitals):*						Date:				

TABLE OF CONTENTS

Chapter 1: Introduction

1.1 Overview

Fluid phase behaviour in unconventional reservoirs depends on the interaction of fluid molecules with each other and also on the interactions taking place between fluid molecules and the pore wall. Hence, the properties of the fluids residing in very small nanopores of these rocks could be different compared to those observed as bulk in a PVT cell and conventional rock pore spaces due to fluid confinement effects. Fluid confinement is the term used to describe physico-chemical interactions for a system of fluid molecules whose phase behaviour and flow are affected by the surfaces of the void space of the pores. Such changes in fluid properties, depend on the geochemical and geophysical properties of the porous media, including its pore size distribution, rock surface structure, morphology, and mineralogy as well as other factors including the type of the fluid, pressure and temperature. Due to the difficulty involved in performing experimental studies to measure the fluid properties in such confined space, there are very limited sources of available data for the study of confined fluid phase behaviour. These data are limited to synthetic porous media with uniform pore size distribution and mainly with using pure components. Accordingly, this study is devoted to present a novel experimental method which can be applied to measure the extent of the pore confinement effects on fluid phase behaviour within real tight reservoir rocks. The main focus of the research is on effect of confinement on the dew point saturation pressure of gas-condensate fluids within real unconventional rocks. Considering that the current approaches in theoretical modelling the phase behaviour of gas condensate fluids in unconventional reservoirs are not able to predict the obtained results from experimental data with acceptable accuracy, the other element of this work is to propose a theoretical method, based on the experimental results, which can be used to model the confinement effects and evaluate its impact on recovery from unconventional gas-condensate reservoirs.

1.2 Unconventional Reservoirs

Production from unconventional reservoirs, i.e. tight oil and gas, shale oil and gas, heavy oil reservoirs as well as coalbed methane reservoirs, is not feasible without the use of

production stimulation techniques like horizontal wells and hydraulic fracturing(Cipolla *et al.*, 2009). Only in the past decades, with the advancement of the technologies and ever-increasing demand for the energy, it has been possible to produce from such reservoirs in an economically profitable manner. Most of unconventional reservoirs have significant proportion of nano-pores (Cipolla *et al.*, 2009). It is to note that in conventional reservoirs organic residues that had matured over time would migrate from the source rock to the reservoir sealed with a cap rock which has close zero permeability. On the other hand, in unconventional reservoirs, no migration takes place and the reservoir consists of a layer of significantly low permeability rock that has reached thermal maturity over time without any migration.

As demonstrated in Figure 1.1, tight and shale gas reservoirs are estimated to remain the main source of the gas production up until 2050 in the United States based on the annual energy outlook report in 2021 published by Energy Information Administration (EIA).

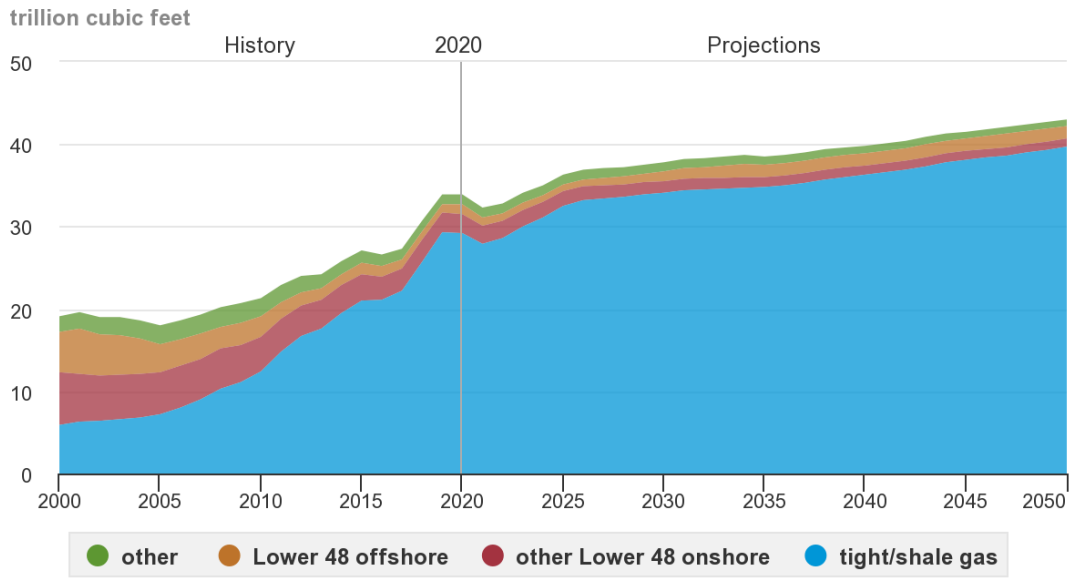

Figure 1.1: U.S. dry natural gas production by type, 2000-2050, Source: Annual Energy Outlook 2021

As of year 2020, 29.2 trillion cubic feet (tcf) of dry gas in the U.S. is produced from tight and shale gas reservoirs, and the corresponding value is projected to increase to 39.7 tcf by the year 2050. For crude oil (Figure 1.2), it is estimated that the current production of

11.5 million barrels per day would increase to 14 million barrels per day due to the contribution of tight oil reservoirs (*Annual Energy Outlook 2021*).

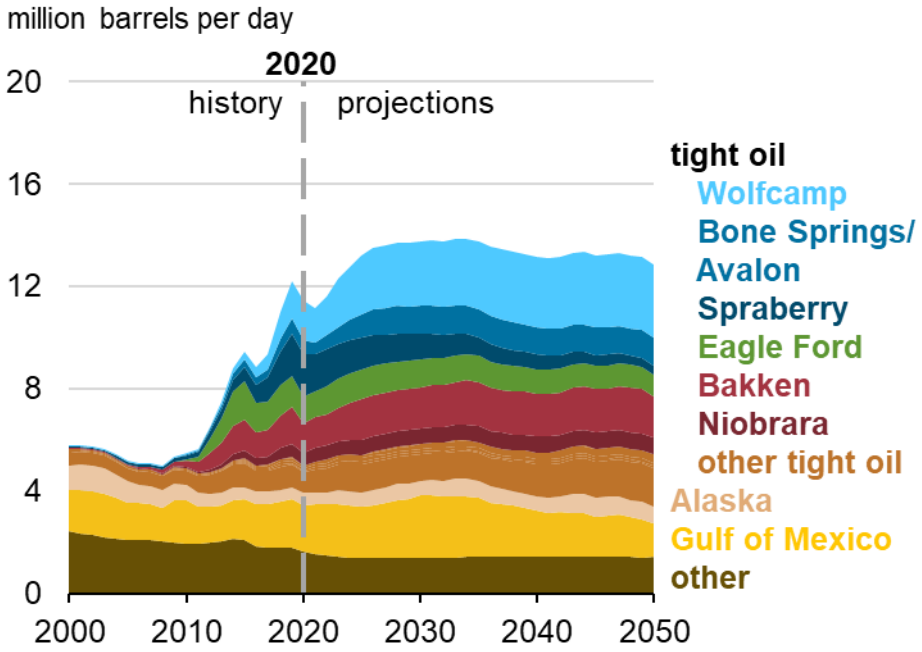

Figure 1.2: U.S. crude oil production, 2000-2050, Source: Annual Energy Outlook 2021

These predictions highlight the importance of unconventional reservoirs in future energy markets. The petrophysical and physicochemical data of the corresponding reservoir rocks and fluids should be properly measured and described in order to accurately estimate the hydrocarbon recovery from these reservoirs. However, due to the complicated nature of rocks and fluids properties in unconventional reservoirs, it is difficult to conduct appropriate theoretical and experimental studies for these reservoirs. Therefore, there are many uncertain parameters which require new and more specialized approaches to be determined. There are parameters and mechanisms affecting the fluid and flow behaviours in unconventional reservoirs which are different than those in conventional reservoirs including but not limited to micro- and nanoscale flow regimes, geomechanical effects, high capillary pressure and fluid confinement effects and deviations from bulk thermodynamic properties. In recent years, many theoretical and some experimental studies have been performed to study aforementioned mechanisms and effects in unconventional reservoirs. A brief description of each of them will be presented here. It should be noted that only pore confinement effects on fluid phase behaviour of gas-condensate fluid is the main area of interest in this study.

1.2.1 Micro- and Nanoscale Flow Regimes

Conventional, high permeability reservoirs which are usually referred to high quality reservoirs generally have pore sizes greater than 30 μm and pore throat size of 10 μm. The pore types in such reservoirs are referred to as macropores. When the size of the pore throats reduce to 1 μm, the type of the pore is referred to as micropores (Nelson, 2009). As depicted in Figure 1.3, the size of the pore throats in tight sandstones and shales is in the range of nanometers which is approximately of the size of an asphaltene molecules.

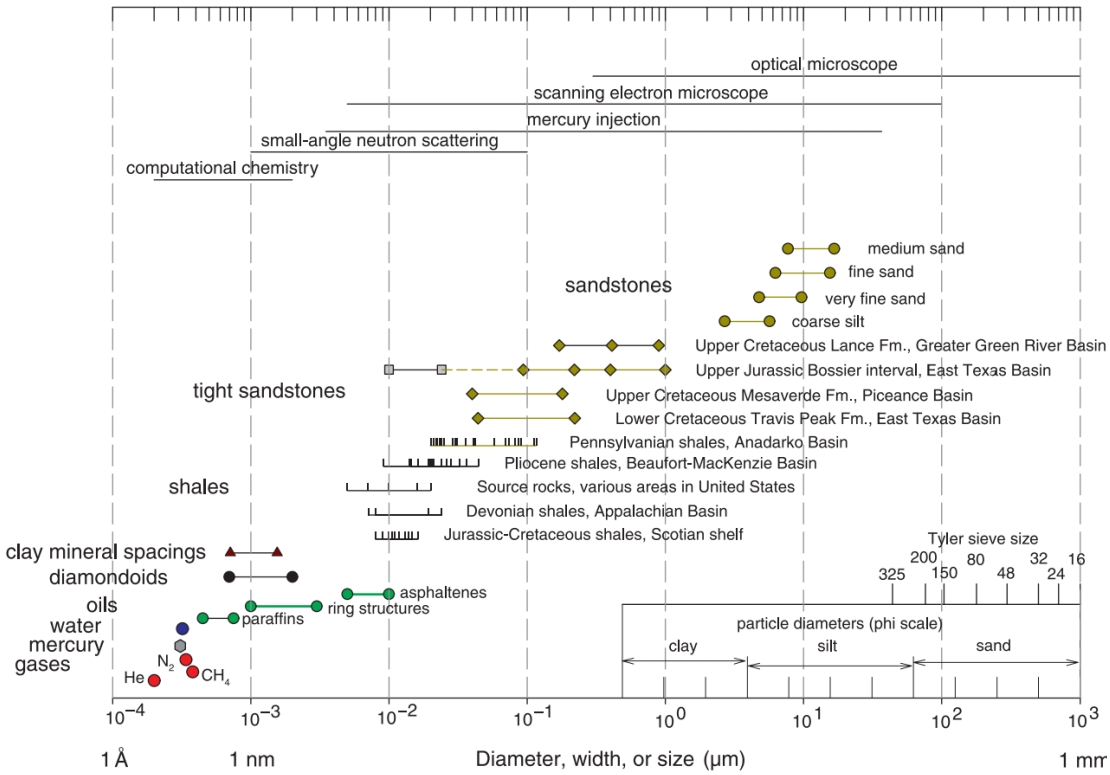

Figure 1.3: Sizes of the molecules and pore throats in different rocks and molecules (Nelson, 2009).

In unconventional rocks, where the fluid flows through very small pores, the molecular mean free path, which is an average distance over which a moving molecule substantially changes its direction or energy, typically as a result of one or more successive collisions with other molecules, is comparable to the size of the pores. In such conditions, the conventional Navier-Stokes equations for modelling fluid flow may no longer be valid mainly due to the significance of collisions taking place between gas molecules and pore wall compared to those occurring between molecules which are dominants in PVT cells

and large pores of conventional rocks (Nazari Moghaddam and Jamiolahmady, 2016b). Gas flow in nano- and microscale conduits has been widely modelled based on rarefied gas dynamics. Rarefied gas dynamics is based on the kinetic approach to gas flows. The term rarefaction refers to the gas phase, when it is becoming less dense and the intermolecular collisions become less important. For characterising and describing fluid flow within unconventional rocks, a dimensionless parameter, known as Knudsen number which is defined by the ratio of the mean free path (λ) to the flow characteristic length (D), is considered, which is expressed by Equation 1:

$$Kn = \frac{\lambda}{D} \qquad \text{Eq. 1.1}$$

Higher Knudsen number, i.e. increasing mean free path (which is usually associated with a decrease in pressure) or reducing the characteristic length (which is usually associated with smaller micro- and nanoscale channels), would result in higher importance of the rarefaction effect, which refers to less importance of fluid-fluid, compared to fluid-rock, intermolecular interactions. Different flow regimes can be defined based on Knudsen number (Zhang, Meng and Wei, 2012; Nazari Moghaddam and Jamiolahmady, 2016b).

1- For Knudsen numbers lower than 10^{-2}, the flow regime is considered to be continuum regime. This is a flow regime, which is usually occur in conventional reservoirs, where the pore size of the porous media is considerably higher than the molecular mean free path.
2- When Knudsen number is in the range of 10^{-2} and 10^{-1}, the fluid flow regime is considered to be in the slip flow regime. In slip flow regime, in near walls, the continuum flow is not valid while in the centre, away from the walls, the bulk fluid can be considered as continuum.
3- If Knudsen number lies within 10^{-1} and 10, the flow regime is considered to be in the transition flow regime region.
4- For Knudsen number higher than 10, the flow is considered to be free molecular regime where intermolecular forces among the fluid molecules can be ignored and fluid-wall interactions dominate the flow regime.

In unconventional reservoirs, as depicted in Figure 1.3, due to very small average pore size, which is in the nanometre range and is typically three orders of magnitude smaller than the pore average size in conventional reservoirs, it is very likely for Knudsen number to be higher than 10^{-2}. Hence, it is not accurate to consider the flow regime within

unconventional reservoirs to be in continuum regime. Fluid flow in unconventional reservoirs, can be in different regimes including slip, transition and even free molecular regime. It should also be considered that during the production from a reservoir, fluid flow might experience different regimes due to pressure depletion. One of the widely applied theoretical approaches to characterize such flow regimes occurring in unconventional reservoirs is to use the so-called "discrete particle-based atomistic simulations" such as molecular dynamics or Lattice-Boltzmann modeling (Cui *et al.*, 2018). However, the main drawback of these methods is that they can simulate processes in very short time scales in the range of ps or ns and they are mainly suitable for the systems in the range of nanometres rather than large filed scale studies. If the process is going to be extended for larger systems over extended period of time, then these simulations become time-consuming.

It has been shown in practice (Nazari Moghaddam, 2016) that the description of gas flow in micro- and nano-channels is also possible by solving N-S equations with modified boundary conditions for slip and transition flow regimes. With regard to slip flow in shale gas reservoirs, almost all researchers have used the models that were originally developed for micro-electromechanical systems (MEMS). These models can be divided into two separate approaches. In the first approach, researchers have considered the Dusty Gas Model (DGM), which assumes a linear combination of the "viscous flow" and the "gas diffusion" to predict the overall flow rate in nanopores. In this approach, the gas flow rate in the shale matrix is mostly correlated with viscous flow and free molecular flow regime. However, recent experimental observations have shown that gas mostly encounters slip flow and transition flow in shale and tight gas reservoirs and rarely experiences free-molecular flow. In addition, as the Knudsen diffusivity is based on simple kinetic theory, the DGM model becomes inaccurate, when strong potential energy gradients exist (Nazari Moghaddam, 2016). In the second approach, researchers have considered the dominant flow regime distinguished by the Knudsen number and developed flow equations suitable for that flow regime. Studies with this approach are mainly based on the Beskok and Karniadakis unified Hagen-Poiseuille-type model (1999) for volumetric gas flow (q_h) which is expressed in Equation 1.2.

$$q_h = f(Kn)\frac{\pi R_h^4}{8\mu}\frac{\Delta p}{L_h} \qquad \text{Eq. 1.2}$$

Where the flow condition function *f (Kn)* is given by:

$$f(Kn) = (1 + \alpha Kn)\left(1 + \frac{4Kn}{1 - bKn}\right) \qquad \text{Eq. 1.3}$$

Where *Kn* is the Knudsen number, α is the rarefaction dimensionless coefficient and *b* is the slip coefficient.

1.2.2 Geomechanical Effects

Geomechanical properties, including compressive strength, tensile strength, and elastic modulus of the rocks in unconventional reservoirs are different from conventional reservoirs. Permeability and porosity of porous media are dependent on the net stress or effective pressure (which is the difference between confining pressure and pore pressure). The stress dependency of the permeability of shale rocks is suggested to be due to the matrix shrinkage as well as fracture compression. Pore size distribution of the unconventional reservoirs are considered to be influenced by the net stress more than conventional reservoirs mainly due to lower values of abovementioned (compressive strength, tensile strength, and elastic modulus) rock mechanical properties, which in turn affects the flow regime prevailing in the pores (Gensterblum *et al.*, 2015).

An approach has been suggested is that the geomechanical effects on the permeability of the shale reservoirs to be coupled with the gas slippage effects in order to better estimate the apparent permeability. In such an approach non-slip permeability and modified average pore size can be estimated and this would lead to better prediction of apparent permeability of unconventional reservoirs under the impacts of geomechanical and gas-slippage effects. It has been shown that the Navier-Stokes equations with slip boundary conditions can approximately predict the flow behaviour for the entire system in the slip regime. In Gas Condensate Research Group at Heriot Watt University, Equation 1.4 has been proposed for the estimation of the apparent gas permeability of the shale rocks (Nazari Moghaddam and Jamiolahmady, 2016a). In the development of the following equation, it was assumed that the flow is steady and incompressible (due to low fluid density difference in each permeability measurement experiment). Also the gravity effect was ignored. Based on this approach, the apparent matrix permeability was estimated as a function of net stress assuming two separate exponential relationships for reduction of both non-slip permeability (intrinsic permeability) and average pore size. In other words, the slippage was considered in the flow equations by assuming slip boundary conditions

and the stress effect was taken into account in the same equation by assuming two exponential relationships for non-slip permeability and average pore size. Hence, in this equation the impacts of slippage is considered by using the general second order slip boundary conditions and the geomechanical effects are incorporated by considering two exponential relationships between non-slip permeability and average pore size.

$$K_a = K_{non-slip}\left[1 + 4C_1\left(\frac{\lambda}{R_c}\right) - 8C_2\left(\frac{\lambda}{R_c}\right)^2\right] \quad \text{Eq. 1.4}$$

where

$$K_{non-slip} = K_{int}[exp(\alpha \times \Delta P)] \quad \text{Eq. 1.5}$$

$$R_c = R_c^0[exp(\beta \times \Delta P)] \quad \text{Eq. 1.6}$$

where R_c^0 is the non-slip characteristic radius at a reference net stress, α and β are the fitting parameters obtained from experimental data, ΔP is the net stress difference from the reference pressure and C_1 and C_2 are the first and second order slip coefficients, respectively. The exponential correlations have been verified by experimental results. The fitting parameters can be obtained by few permeability measurements at different pore pressure and net stress.

1.2.3 High Capillary Pressure

In unconventional rocks, the average size of the pores in the system is very small. As a result, the capillary pressure in unconventional rocks is expected to be higher by several orders of magnitude. In conventional reservoirs, capillary pressure is within the range of approximately 400-500 psi. However, in unconventional reservoirs capillary pressure is in the range of 70000 psi (Donnelly *et al.*, 2016). Very high capillary pressure would have considerable impacts on the two phase flow in porous media. Also, capillary end effects (CEE) would significantly influence the measurements conducted in the lab to characterize the unconventional systems and obtaining relative permeability. A new experimental procedure and a new mathematically based method have recently been proposed by the Heriot-watt gas-condensate recovery research team to overcome the issue of CEE in laboratory measurements of relative permeability (Nazari Moghaddam and Jamiolahmady, 2019). Generally, most of the proposed methods for CEE corrections involve the requirement to have the information about in situ saturation or in situ pressure of the core plugs. Considering that the length of the unconventional core plugs is very small due to their ultralow permeability, this is experimentally very difficult to have

accurate in-situ saturation or pressure readings. In this method, four different flow rates are required to be injected for each flow rate ratio. For all flow rates, the pressure drop across the core and the measured wetting phase saturations (obtained by material balance) are used to solve the four pressure and four saturation equations simultaneously. From the results, the CEE length at each flow rate, corrected wetting phase saturation, average wetting phase saturation in the CEE region and the corresponding kr values can be obtained. The integrity of this method was evaluated with theoretically generated data. It should be mentioned that this study does not deal with CEE. In Chapter 6, the measured Kr obtained for a core sample similar to the one used in this study, was used. The Kr data was corrected for CEE.

1.2.4 Sorption and Desorption Processes

In unconventional reservoirs, fluid flow is considerably affected by the sorption and desorption processes. Adsorption process is dependent on pressure, temperature and total organic carbon content. Gas desorption rate would change during the course of production from hydrocabon reservoirs. In molecular point of view, adsorption/desorption energy, as presented in Equation 1.7, is an important parameter which can determine whether gas molecules can be adsorbed/desorbed from shale matrix.

$$E_{adsorption/desoption} = E_{adsorbate} + E_{host} - E_{adsorption/host} \qquad \text{Eq. 1.7}$$

Where $E_{adsorption/host}$, $E_{adsorbate}$, and E_{host} represent the single point energy of the matrix gas system, matrix and gas molecule, respectively (Hui *et al.*, 2019).

Adsorption process is usually expressed by adsorption isotherms. The Langmuir isotherm is one of the most widely used isotherm for the study of adsorption in unconventional gas reservoirs (Alafnan *et al.*, 2021). The basic from of Langmuir isotherm is developed for single component gas monolayer adsorption. It can be extended for multi-component fluids. Adsorption isotherms are also widely used method for obtaining capillary condensation (a process where the gas molecules form several layers on the rock surface due to high capillary pressure within small pores of a porous medium until the pore is completely filled with liquid condensed from vapour) data (Barsotti *et al.*, 2016). In a porous medium with uniform pore size distribution, adsorption isotherms exhibit a nearly vertical step. This is an indication of capillary condensation which is associated with rapid

pore filling. It should be mentioned that Langmuir adsorption isotherm, although being widely used for shale gas reservoirs, is not valid for capillary condensation which may occur in gas condensate reservoirs. The basic assumption of Langmuir isotherm, is the monolayer adsorption of molecules on the surface of the adsorbate. Capillary condensation isotherm is usually computed based on Kelvin equation or other adsorption isotherms types which consider the multi-layer adsorption. Application of the adsorption isotherms in the study of fluid phase behaviour and capillary condensation will be discussed in Section 2.2.2.

1.2.5 Fluid Confinement Effects

The average pore size of conventional porous media is in the range of micrometres and is several orders of magnitude higher than the fluid molecule diameters. As a result, in conventional reservoirs, the extent of the interactions among fluid molecules and pore walls, may be neglected compared to the interactions taking place between fluid molecules. In tight and shale reservoirs, on the other hand, the sizes of the pore space are comparable with the sizes of the fluid molecules. The interactions taking place between molecules and pore walls are strongly dependent on their distance between each other. Therefore, the interaction between molecules and pore walls cannot be ignored due to their high frequency collision contact. In such conditions, fluid molecule behaviour is affected by Van Der Waals (VdW) interactions (the interactions taking place at small space with respect to the distance of the two non-ionic molecules) with other fluid molecules as well as those with the pore surfaces. It is also possible to have Coulomb forces (forces that exist between ions and also is dependent on the distance) in confine space, however, these forces are not as common as VdW forces in the reservoirs. As mentioned, fluid confinement is the term used to describe interactions for a system of fluid molecules whose phase behaviour and flow are affected by the surfaces of the void space of the pores and fluid phase properties cannot be captured by conventional methods used for conventional reservoir. The left hand image in Figure 1.4 compares fluid molecules in an unconfined space, where relatively small portion of the molecules are affected by the pore walls (red circles) compared to those that are unaffected (blue circles). The right hand image displays the fluid molecules under the confinement effects, where relatively large portion of the molecules are affected by the pore walls.

It is well documented that the phase behaviour and therefore physical properties of the fluids confined in nanopores would be different compared to the bulk fluid phase behaviour (Barsotti *et al.*, 2016; Salahshoor *et al*., 2018; Tan *et al.*, 2020). Specifically, it has been verified that the critical properties of confined fluids will shift due to fluid confinement effects (Tan *et al.*, 2020). Also, the change in Pdew of gas condensate binary mixtures in porous medium with uniform pore size distribution is measured to be higher as a result of fluid confinement (Salahshoor and Fahes, 2020). Various theoretical models have also been developed to take into account the effects of pore confinement. One of the most common methods to study confinement effects was to simultaneously consider capillary condensation based on the Kelvin equation and shift in critical properties. However, the applicability of the proposed methods is not experimentally validated. A more detailed discussion on the proposed approaches will be presented in Chapter 2. Fluid confinement effects are the main topic of interest in this study and in the next chapter a general literature review of the ongoing research performed to study confinement effects will be presented. It will be shown that several theoretical approaches have been considered to take into account the impacts of confinement on the fluid phase behaviour. However these approaches produce conflicting results primarily because there are no or limited experimental data to verify them. In fact the available data are only limited to synthetic porous media with uniform pore size distribution and mainly using pure components.

More specifically to this work, there are very rare experimental data on the effect of confinement on gas-condensate fluid mixtures. Additionally these data have not been obtained using real porous rocks. The results of the experimental data obtained in this study, would then be utilized to modify Peng Robinson (PR) equation of state to predict gas condensate phase behaviour. It is an important step towards proper evaluation of reservoir performance based on modified EOS which can be used to capture the effects of confinement on the phase behaviour in unconventional reservoirs. The main advantage of the proposed would be the fact that it is based on more realistic experimental data using real unconventional shale samples which can be applied to unconventional reservoirs with more accuracy as compared to experiments performed on single component fluids in synthesized porous medium. Another impact of the intermolecular forces between pore surface and fluids residing in nanopores, is the heterogeneous distribution of fluid molecules which results in heterogeneous fluid properties, fluid molecules close to the pore surface will be denser compared to the molecules at the centre of the pore space.

Moreover, for unconventional gas condensate reservoirs, during the production, heavier components are expected to have higher possibility to be trapped in the smaller pores of the reservoirs which could lead to higher heterogeneity in the fluid distribution in unconventional reservoirs. Hence, higher discrepancy in the composition of the fluid is expected to be observed in nanopores and macropores within unconventional gas condensate reservoirs. It should be mentioned that in this study, the impacts of spatial heterogeneity will be considered to be reflected in the overall phase behaviour of the fluid in terms of its impacts on fluid Pdew. It should be noted that, there are very limited number of theoretical and experimental studies which have been dedicated to take into account the comparison between the extent of the impacts of confinement for different parameters, including different fluid composition, net stress, temperature, and rock type. In this study, for the first time, the relationship between these parameters and confinement effects, which could be very useful for the study of different unconventional gas condensate reservoirs, are experimentally evaluated. This study, is mainly devoted to investigate the effects of pore confinement on the changes in gas condensate Pdew, which is a crucial property in determining the phase behaviour of gas condensate fluids.

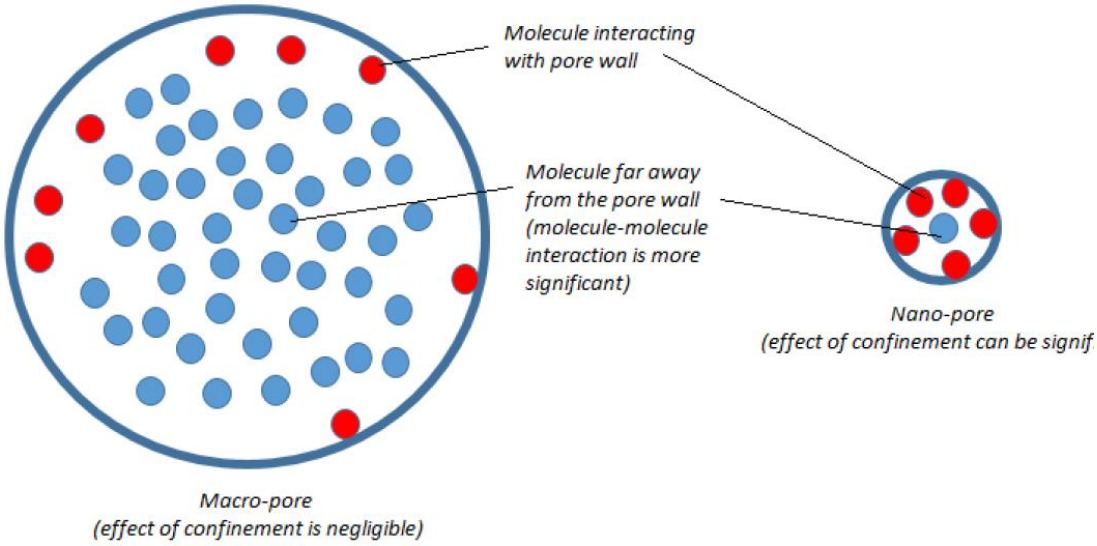

Figure 1.4: Schematic representation of confinement effect (source Haider (2015))

1.3 Gas Condensate Phase Behaviour

In this section, the general phase behaviour trend of a gas condensate fluid with a fixed composition is discussed.

A gas condensate reservoir is mainly composed of methane and other light hydrocarbons but it also contains some quantity of heavy hydrocarbon fractions.

Figure A.1 shows a typical phase diagram for gas condensate mixtures. As it can be observed the temperature of a gas condensate reservoir (T_R) is between critical temperature (T_C) and cricondentherm (T_{CT}). The line which connects the saturation pressures for the temperatures above critical point is known as the dew curve (blue line). In most cases the initial pressure of a gas condensate reservoir is above its Pdew. When the reservoir is producing, its temperature remains constant, while its pressure decreases. The purple line shows the direction at which a gas condensate reservoir is produced under natural depletion. Once the pressure reaches to the Pdew, heavier components of the fluid starts to drop out of the gas phase to form the condensate liquid. It is believed that heavier components are held within the gaseous phase by the attractive forces exerted on them by lighter components at high pressure but at lower pressure when these forces are not high enough to hold heavier molecules in the gas phase, liquid phase would be condensed out of the gas (Afidick *et al.*, 1994). The pressure corresponding to the condensing out of the first heavier molecules to form liquid is referred to as dew point pressure (Pdew). The extent of the liquid drop out and the pressure at which condensation occurs depends on the temperature and gas condensate composition. Further reduction of pressure, for a fluid with fixed composition, causes the re-vaporisation of liquid into gas and a second dew point pressure is observed. This is not observed in the field with continued production as the composition of the fluid becomes heavier with time due to production of the lighter gaseous fractions. Hence, in real field applications, due to change in the composition as a result of production, the second dew point is not as important as the first dew point pressure. Accordingly, in this study, the second dew point pressure is not an area of interest.

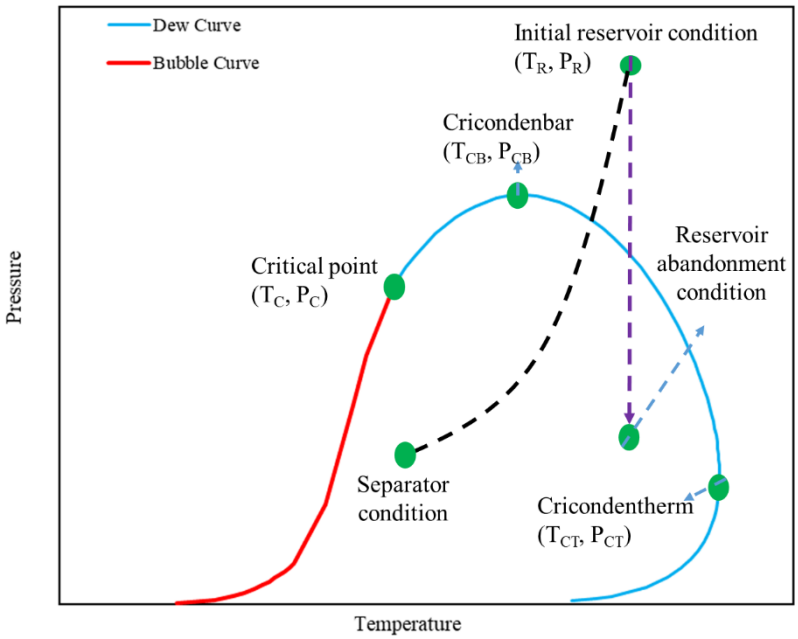

Figure 1.5: Typical P-T phase diagram of a gas condensate mixture

Cricondentherm is the maximum temperature point at which liquid and vapour can coexist. Cricondenbar is defined as the maximum pressure point at which liquid and vapour can coexist.

Two different trends for gas condensate mixture Pdew can be noticed. If the temperature is between critical temperature (T_C) and the temperature corresponding to the cricondenbar point (T_{CB}), by increasing temperature, Pdew of the gas condensate mixture increases. However, if the temperature is between the temperature corresponding to the cricondenbar point (T_{CB}) and cricondentherm (T_{CT}), by increasing temperature, Pdew of the gas condensate mixture decreases. This suggests that if the trend for the Pdew of a gas condensate fluid changes with temperature within the same range for different conditions, e.g. bulk or confined, its phase envelope has shifted, a trend which will be discussed in Chapter 4.

Intermolecular interactions taking place for gas condensate mixtures would make the fluid to have substantially different properties as compared to those fluids which do not exhibit retrograde behaviour, e.g. single component fluids (Afidick *et al.*, 1994). Considering that the pore confinement effects have noticeable influence on the intermolecular interactions, it is expected that the behaviour of gas condensate fluids will be affected in a different manner as compared to single component fluids. In other words, for gas condensate mixtures, the extent of the interactions taking place between heavier molecules and pore surface is different from lighter molecules. Heavier components are

expected to be adsorbed or trapped more in smaller pores compared to lighted components (Luo et al., 2021). Hence, the overall change in the behaviour of gas condensate mixture in confined space is expected to be different from the change in the behaviour of single component. As mentioned earlier, experimental results are required to validate the proposed theoretical approaches, however, due to the difficulties associated with the measurement of the fluid properties within porous medium, there is very small amount of data available for confined fluid phase behaviour in general, and in a more specific manner, smaller amount of data available for the study of gas condensate phase behaviour. There is no reported experimental data on real porous medium which also contributes to the insufficient confidence regarding the proposed theoretical methods applicable to real porous medium. Considering that there is only one experimental study in literature which measures the Pdew of gas condensate samples in confined space comprised of uniform distribution of pore size (Salahshoor and Fahes, 2020), one of the main research interests in this study is to experimentally examine how the Pdew of gas condensate mixtures would actually change within real rock samples instead of synthesized porous medium. Hence, it would be possible to modify/propose theoretical methods which can be applied to real reservoir conditions based on the results of the experiments conducted on real shale core samples.

1.4 Research Goals

This study focuses on the impacts of fluid confinement on the phase behaviour of gas condensate systems within real unconventional rocks. A novel experimental method has been proposed to measure dew point pressure of GC fluids within a number of shale rocks. In literature, there is only one research conducted to measure the Pdew of gas condensate fluids in confined space which its application is limited to synthetic porous medium and isobaric experiments which may not be of interest in gas condensate systems. A more detailed discussion on the presented method in literature will be provided in Chapter 2. The proposed method is employed to experimentally evaluate the confinement effects in a wide range of temperature and pressure. As mentioned obtaining accurate data based on the experimental measurements conducted on real shale samples and using multi-component fluids is of great importance for proper real unconventional reservoirs fluid characterization under the effects of confinement. The generated data are used to modify an equation of state (EOS) to more realistically predict the GC phase behaviour. A

numerical simulation exercise is then carried out to evaluate the impact of confinement on the results of series of single-well simulations. These findings serve as an asset to study gas condensate fluid and flow behaviours within unconventional reservoirs.

With the results of the experimental measurements and further theoretical evaluations performed in this study following questions are answered:

1- How does fluid confinement effects influence the dew point pressure (Pdew) of gas condensate mixtures in real shale core samples?
2- What is the impacts of fluid composition and richness, temperature, net stress, and rock type on the extent of the impact of the fluid confinement effects?
3- How can an EOS be modified to properly match the Pdew of gas condensate mixtures under the effects of fluid confinement?
4- What are the impacts of different parameters on the performance of a reservoir while considering the effects of confinement?

1.5 Scope of Dissertation

In chapter 1 fundamental concepts related to unconventional reservoirs and fluid confinement are introduced to lay a foundation for the research carried out in this thesis.

In chapter 2 the literature review of fluid confinement is presented, which include the results of other experimental and theoretical researches in the area of fluid confinement effects.

In chapter 3, the procedures for the experiments performed in this study are described. A novel experimental method is proposed, based on which the Pdew of fluids, as a crucial property in determining the phase behaviour of gas condensate fluids, in real unconventional rocks is measured. This novel method is used for varieties of fluid mixtures, over a wide range of pressure and temperature, for different rock types and under various net stress values. Different types of fluids, including single component fluid, i.e. ethane, binary component gas condensate fluids, i.e. mixtures of C1/nC5, C1/nC8, and C1/nC10 with different compositions, as well as a ternary mixture of C1/nC5/nC10 are used. The experiments were carried out at three different temperatures of 20, 40, and 60 °C. Three different net stress values of 500, 1000, and 2000 psi were used in the experiments conducted to study the impacts of net stress. Two types of shale

core samples, i.e. Eagle Ford and Barnett, were used in this research to compare the impacts of pore confinement effects on different rock types.

In chapter 4, first impact of pore confinement on the saturation pressure of a single component is demonstrating by presenting the results of the corresponding conducted experiment. As it will be discussed in chapter 2, most of the presented theoretical and experimental approaches are based on using single component fluids. Performing experiments to measure the saturation pressure of single component fluids helps to have a comparison between the presented approaches in the literature and this study. Moreover, it provides an approach which can be followed for real shale samples. Then, the results of novel experiments performed to investigate the impacts of fluid confinement on gas-condensate fluid mixture Pdew are presented. The impact of several parameters including, fluid type and composition, temperature, net stress and rock type are studied.

In the next part of this study, in chapter 5, an empirical correlation based on the Lennard-Jones (LJ) molecular potentials is suggested to be applied in the equation of state (EOS) to match the confined Pdew obtained from experimental results. This correlation accounts for the impacts of fluid type, rock type, pore size and also the temperature. 3-parameter Peng-Robinson (PR) EOS was employed to estimate the phase behaviour of different fluids in confined space.

Chapter 6 of this study is dedicated to series of single well reservoir simulations to evaluate the impact of confinement on gas and condensate recovery using selected shale rock and gas condensate fluid used in Chapter 3 and the modified EOS obtained in chapter 5.

Finally, chapter 7 is dedicated for conclusions and also some suggestions for future studies.

Chapter 2: Literature Review

Unlike conventional reservoirs where PVT properties is only a function of fluid-fluid interaction, in unconventional reservoirs with pore spaces of less than 100 nm, the rock-fluid interaction impacts on fluid properties is significant (Li and Sheng, 2017). Alongside with the exploitation from unconventional reservoirs, several attempts have been made to understand the physics of the fluid properties and fluid flow behaviour in such reservoirs. Most of the efforts have been devoted to theoretical modelling of the phase behaviour of fluids confined in nanopores. There are some experimental studies currently available in literature trying to validate and expand the understanding of how pore confinement effects might affect the phase behaviour of fluids in shale oil and gas reservoirs. However, these experiments are limited to synthetic porous media with uniform pore size distribution and mainly using pure components. In this chapter, in the first part, a general literature review on the theoretical researches performed to study the phase behaviour of confined fluid is presented. It will then be followed by the second part which is devoted to the overview of the experimental studies which have been proposed in literature to experimentally evaluate the phase behaviour changes in nanoporous systems.

2.1 Theoretical studies for confinement effects on phase behaviour in unconventional reservoirs

Theoretically, to take into account the impacts of pore confinement effects on phase behaviour (in a system with nanopores which are not limited to unconventional reservoirs), different approaches have been considered. Generally, these approaches fall within three main categories.

- Equation of state and VLE calculation modifications methods
- Molecular simulation methods
- Density functional theory methods

All these approaches are based on thermodynamic principles which should be considered for confinement effects. Here, a short description of the thermodynamic principles is presented followed by a literature review on theoretical studies conducted to account for nano-scaled pore confinement effects on fluid phase behaviour.

2.1.1 Thermodynamic principles considerations for confinement effects in unconventional reservoirs

In conventional thermodynamics (thermodynamic study of fluids at bulk state or fluids in a container with large space compared to the size of the molecules where the interactions between pore surface and fluid molecules can be neglected), there are two major assumptions which may not be applicable for thermodynamic studies in unconventional reservoirs. The first assumption is that surface tension does not depend on the curved surfaces. The second assumption is that the short range repulsive intermolecular forces which occur at very short distances between the molecules are considered to be negligible compared to the long range attractive intermolecular forces.

In conventional thermodynamics where the fluids of interest are residing in bulk space or pore spaces with the scales of considerably higher than 100 nanometres, the surface tension at the interface of the equilibrated surfaces is not based on curvature. At such scales, the impacts of confinement on the phase behaviour and saturation pressure is less than 3% (Li and Sheng, 2017).In contrast, while dealing with fluids within pore spaces with sub-micron scales, the assumption of flat interface is no longer valid.

Intermolecular forces are important factors affecting the phase behaviour. Vapour-Liquid Equilibrium (VLE) calculations can be used to obtain the dew point or bubble point of a fluid. However, such calculations are inaccurate due to neglecting the curved interface at equilibrium inside very small space. In order to overcome the deficiency of conventional VLE equations, applying Kelvin equation is considered to be the most fundamental approach. Kelvin equation, derived from Young-Laplace equation, is a description of saturation pressure for a curved interface between gas and liquid. Kelvin equation in its original form is as follows:

$$ln\frac{P}{P_{sat}} = \frac{2\sigma V_m}{rRT} \qquad \text{Eq. 2.1}$$

Where *P* is actual saturation pressure, *Psat* is the saturation pressure if the surface is flat, σ is the liquid/vapour surface tension, *Vm* is molar volume of the liquid, *R* is the universal gas constant, *r* is the radius of the droplet (or capillary), and T is the temperature. Kelvin equation is developed for single-component fluids and its application cannot be extended to compute the shift in saturation pressure for multi-component fluids like hydrocarbon reservoirs unless modified with further simplifying assumptions (Shapiro and Stenby,

1997; Al-Kindi and Babadagli, 2021). The drawback of Kelvin equation for fluids confined in very small pore spaces is that it assumes homogeneous density distribution for the fluids. Whereas, in reality, fluids within very small pore spaces, are considered to have spatially heterogeneous fluid properties, in particular fluid density (number of molecules per volume unit) profiles relative to the distance from the pore surface. Figure 2.1 shows a schematic distribution of the fluid molecules at the pore scale of with a pore size of the range of a few manometers.

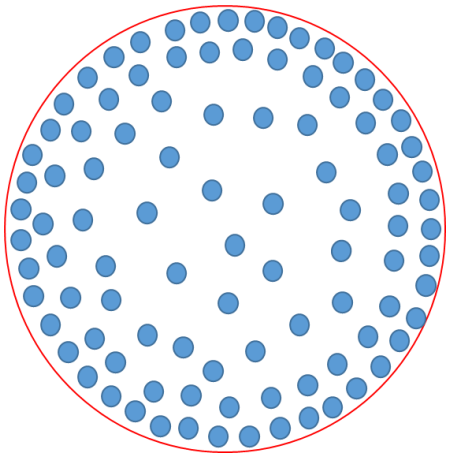

Figure 2.1: Schematic representation of fluid molecule distribution in nano-scaled pore space

As illustrated in Figure 2.1, the number of fluid molecules in the close proximity of the pore surface (i.e. fluid density) is higher than the number of molecules at the centre of the pore. Hence, due to pore surface-fluid interactions, there exist a heterogeneity of fluid properties in the pore space.

Also, as mentioned, Kelvin equation is derived from Young-Laplace equation. One main assumption in the derivation of Young-Laplace equation is the incompressibility of the fluid. Neglecting gas and condensate compressibilities in the equations could result in erroneous estimations for VLE calculations. Moreover, in Kelvin equation, the vapour volume is close to liquid volume at high pressure which results in the assumption that liquid and vapour density will be similar.

Thermodynamic equations of state generally are used for equilibrium calculations and usually take into account only the attractive (long-range) forces (Salahshoor *et al.*, 2018). VLE calculations can capture fluid properties with an acceptable range of accuracy for bulk fluids. However, when dealing with fluids existing in pore scales in the range of less than 100 nm, due to very small distance between molecules, short-range forces which

take into account the impact of pore proximity on the phase behaviour of confined fluids are also important and should not be ignored in the VLE calculations. Moreover, capillarity due to small pore space and large curvature as well as heterogeneity in fluid properties (e.g. density which is the result of short range forces and interactions) are other main parameters which are different for confined fluids in unconventional reservoirs.

2.1.2 Equation of State and VLE Calculation Modifications Methods

Equations of state (EOS) are thermodynamic tools by which the pressure, volume and temperature (PVT) properties of each fluid are linked or estimated. Two main categories of EOS consist of cubic and non-cubic equations. Non-cubic equations, like Virial EOS by which the pressure of a system in equilibrium is expressed as a power series of density, cannot capture complex hydrocarbon mixture properties mainly because virial coefficients are dependent on composition in an exact manner (Salahshoor *et al.*, 2018). As a result, in petroleum engineering applications, cubic EOS have gained more attention. Most popular and widely used cubic EOS are, Van der Waals (VdW), Peng-Robinson (PR), and Soave-Redlich-Kwong (SRK) EOS.

The original forms of these cubic EOS are not suitable for analysing the fluids in confined spaces. As mentioned, in such spaces, the interaction between fluid molecules and pore wall molecules makes the density of the fluids to be heterogeneous. Usually, the density of the fluid molecules (i.e. the number of the moles of molecules divided by the volume) adjacent to the pore wall is higher than the density of the fluid molecules in the pore body (Barsotti *et al.*, 2016). As a result, cubic EOS, which do not consider such effects and in their original form, would give estimation of fluid properties that are different from those in a confined medium. Several attempts have been made to implement the effects of nano-scale confinement on phase behaviour property estimations by the use of cubic EOS. Some methods involve the addition of another term in EOS to take into account the interaction between pore wall molecules and fluid molecules (Travalloni *et al.,* 2010). There are also some proposed approaches through which, the critical properties of the fluid molecules inside confined pore space is expected to change (Zarragoicoechea and Kuz., 2004; Ma *et al.,* 2013). However, due to lack of experimental data performed on confined space and the complexity of the systems under study, there are controversies in the results presented by different scholars. For instance, some researchers have utilized capillary pressure theory to consider the fluid-wall interactions (Wang et al.; 2013). Some

others have implemented MD simulations directly to tune their proposed EOS based on adding additional parameters into their modified EOS (Travalloni *et al.*, 2010). There are also some other researchers who only consider shift in critical properties to model the phase behaviour of unconventional reservoirs (Tan and Piri, 2015). There are also approaches which couple some of these methods for the modification of EOS based on additional terms with shifted critical properties and capillary pressure theory and adsorption isotherms (Dong *et al*., 2016). Liu and Zhang (2019) provided a great review over the theoretical studies performed on the phase behaviour of confined fluids. However, it should be noted that in most cases, the tuning of the parameters added or modified in the EOS due to confinement is performed by fitting the EOS model to the molecular simulations. As a consequence the obtained data for the models are subject to errors due to the assumptions made for the molecular simulations. This section provides a brief review of the studies conducted on EOS modification approaches for the study of confined fluids.

The fundamental concept of phase equilibrium of nano scale systems was first introduced by Hill (1962). The primary aim was to extend the applicability of the thermodynamics functions developed for macroscopic systems for smaller systems, e.g. single macromolecules or colloidal particles. Different formulations for the so-called nanothermodynamics were derived for different systems under study. It was suggested that, although a unique general equation can be derived for both macro- and nano-thermodynamic systems, it is advantageous to propose equations which are limited to specific applications. Some of the environmental variables, i.e. number of molecules, pressure, temperature, chemical potential or volume, were considered to be unique for each fluid ensemble for the thermodynamic analysis. This method is now the basis for molecular dynamic simulations as well.

The impact of capillary pressures on the phase behaviour of a multicomponent system was investigated thermodynamically by Brusilovsky (1992). This is the first reported attempt to provide an EOS for fluid phase behaviour under the effects of confinement. By modifying VdW EOS based on the capillarity equation, the results revealed that for smaller pores, since surface curvature increases, the bubble point would decrease, and the dew point would increase.

Diestler *et al.* (1998) by the use of VdW EOS and also according to perturbation theory analysed the single component confined fluids. The confined medium they considered was slit pores. They predicted that the critical temperature of the fluid would reduce due

to confinement. Critical pressure shift was not considered in their study. They also predicted that capillary condensation phenomenon would occur in the slit pores. However, their model was not able to satisfactorily estimate the confined fluid properties near critical point.

Based on different numerical models and thermodynamic analysis, shift in critical properties of confined fluids is well documented in the literature. The general form of the dimensionless shift in critical temperature based on the dimensionless ratio of the molecule size and flow path radius was suggested by Morishige and Shikimi (1998) for a single cylindrical pore. To study the phase behaviour of confined fluids, Zarragoicoechea and Kuz (2002) modified the VdW EOS. Using classical thermodynamics, they tried to explore the pressure tensor changes in a single nanopore as a result of pore size reduction. In their approach, they considered the particles to interact with each other via the Lennard-Jones (LJ) potential. LJ potential equation is shown in equation 2.2.

$$U(r_{12}) = 4\varepsilon\left[\left({}^{\sigma}/_{r_{12}}\right)^{12} - \left({}^{\sigma}/_{r_{12}}\right)^{6}\right] \qquad \text{Eq. 2.2}$$

where ε is the dispersion energy, r is the distance between the two interacting molecules, and σ is the distance at which the intermolecular potential is considered to be 0 which is usually referred to as LJ size parameter. In their approach, it was also assumed that the pore walls were inert, therefore the pore-wall interaction was ignored. With such assumptions they came up with a new equation which could be used to estimate the shift in critical temperature and pressure due to molecules being very close to each other in the confined space. The reduced form of the generalized VdW EOS which was presented in their study, is shown in equations 2.3 and 2.4. In these equations the tensorial nature of pressure is considered and hence, the expression for pressure in z direction is different from the expression for pressure in x and y directions.

$$p^*_{xx} = p^*_{yy} = \frac{T^*}{\vartheta^* - b^*} - \frac{a^* - \left[3\left({}^{c_1}/_{\sqrt{A}}\right) + 4\left({}^{c_2}/_{A}\right)\right]}{\vartheta^{*2}} \qquad \text{Eq. 2.3}$$

$$p^*_{zz} = \frac{T^*}{\vartheta^* - b^*} - \frac{a^* - 2\left({}^{c_1}/_{\sqrt{A}} + {}^{c_2}/_{A}\right)}{\vartheta^{*2}} \qquad \text{Eq. 2.4}$$

where the reduced coordinates are defined as $p^* = p\sigma^3/\epsilon$, $T^* = kT/\epsilon$, $\vartheta^* = (V/N)\sigma^{-3}$, $b^* = b\sigma^{-3}$, and $a^* = a/\epsilon\sigma^3$. A is the reduced area of the square section of the pore which is calculated by $A=LxLy/\sigma^2$. c_1 and c_2 are the values which are calculated with non-linear fitting.

Later (2004), they simplified their equation for the shift in critical temperature by the use of the adjusted parameters for VdW EOS and using the ratio suggested by Morishige and Shikimi (1998). Equation 2.5 shows the simplified relation that Zarragoicoechea and Kuz presented for the calculation of the shift in critical temperature due to confinement based on modified VdW EOS.

$$\frac{(T_c - T_{cp})}{T_c} = 0.9409\frac{\sigma}{r_p} - 0.2415\left(\frac{\sigma}{r_p}\right)^2 \qquad \text{Eq. 2.5}$$

where T_c is the bulk critical temperature, T_{cp} is the confined critical temperature, rp is the flow path characteristic radius, and σ is the LJ size parameter of the fluid molecules. Using the extended VdW EOS, Travalloni *et al.* (2010) investigated how the density and critical temperature of nitrogen in confined space (cylindrical pores with homogenous surface) would alter due to the effects of pore confinement. Moreover, they explored the impacts of considering different values for the interaction energy between fluid-wall molecules on the pore confinement effects. They proposed the following equation in which effects of pore size and fluid-wall interactions were considered. Their equation includes a term (f) added to the VdW EOS which considers the fluid-wall interactions.

$$P = \frac{RT}{(\vartheta - b_p)} - \frac{a_p}{\vartheta^2} - f(r_p, \delta_p, \varepsilon_p) \qquad \text{Eq. 2.6}$$

where δp and εp are the parameters that represent the potential width and potential energy between pore wall and fluid molecules, respectively. They extended their approach from single component fluids to mixtures by considering mixing rules for free energy and configurational energy. In their equation for mixtures, they used pore modified energy parameter (ap) and pore modified size parameter (bp) which could be calculated as follows:

$$a_p = \sum_i \sum_j x_i x_j a_{ij}\left(1 - \frac{b_i + b_j}{h(r_p)}\right) \qquad \text{Eq. 2.7}$$

$$b_p = \sum_i x_i b_i C_i(b_i, r_p) \qquad \text{Eq. 2.8}$$

Where h and C are functions of pore radius. Equations 2.7 and 2.8 are the general equations which could be applied for different EOSs including VdW, PR and SRK.The term in parenthesis in Equation 2.7 accounts for coordination number decrease with pore size reduction. In their model, fluid molecules were assumed to be hard spheres, whilst the pore space as absorbent cylindrical pores with constant radius. They calculated that

when the ratio of the pore radius to the molecular effective diameter is less than 20 (pore radius of 15 nm in this case), the effects of confined medium on the nitrogen critical properties would be noticeable and cannot be ignored. Using this model, they predicted that two different critical points may be obtained one of which correspond to the fluid-fluid interactions while the other one to the fluid-wall interactions.

Devegowda *et al.* (2012) extrapolated the numerical data of thermodynamic properties of confined n-alkane molecules presented by Singh *et al.* (2009) which was based on configurational-bias grand-canonical transition matrix Monte Carlo simulation to obtain correlations for critical properties of confined fluids for a wider range of applications. They proposed different correlations for each pore radius and the change in critical temperature and pressure was assumed to be dependent on the molecular weight of the fluid. They implemented modified PR EOS with shifted critical properties to create phase envelopes of the confined fluids. Gas viscosity was predicted to reduce due to the impacts of confinement and their EOS predicted lower liquid drop out (LDO) at a constant temperature over the whole estimated pressure range for the confined fluid. Accordingly, their numerical simulation results of a single-well radial synthetic reservoir model showed improved production from unconventional reservoirs due to confinement effects. They concluded that pore-wall confinement along with non-darcy effects associated with flow in nanopores would enhance the production from an unconventional reservoirs. They did not perform a proper evaluation on the effects of pore size distribution as their investigation was meant to be a exploratory work and it required further refinement and they simply considered the permeability to be the square of the pore diameter. Their work was restricted to models with a single pore diameter.

Wang et al. (2013) implemented the effects of capillary pressure into the Peng-Robinson EOS to estimate the oil phase behaviour. In their model, capillary pressure effects in fractures was ignored as the porosity and the permeability of the grids representing the fractures were much higher than the matrix grid blocks. Capillary pressure effect is applied to VLE calculations by considering the equal chemical potential for vapour and liquid. However, the phase pressures are different and are related to each other by capillarity equation described in equation 2.9.

$$P_{cap} = \frac{2\sigma_{VL}cos\theta}{r} \qquad \text{Eq. 2.9}$$

They indicated when the sizes of the pores are within the range of nanoscale, the effects of capillary pressure on the VLE of reservoir fluids becomes substantial. However, when

implementing Equation 2.9 for the simulation, IFT is usually obtained with Macleod-Sugden correlation. If this correlation ($\sigma^{\frac{1}{4}} = P_{ch}[(\rho_L - \rho_V)/M]$) is to be used for confined state of the fluid, as a result of the uncertain parameters including the density of the phases, it usually makes the IFT so low that the obtained capillary pressure from Equation 2.9 is not representative of unconventional reservoirs. In their approach, capillary pressure was calculated using an iterative Leverett J-function method in VLE calculations. They suggested that for any tight reservoir thermodynamic evaluation, numerical studies should consider the simultaneous effects of rock geomechanical properties, e.g. rock compaction behaviour, and the capillarity on production. In their study, it was not very clear how the impacts of confinement would be implemented. In other words, pore confinement effects are only implemented based on the fact that capillary pressure is high in unconventional reservoirs.

Teklu *et al.* (2014) used modified VLE to study the phase behaviour of reservoir fluid mixtures in unconventional reservoirs. In their study where the simulations were conducted on single pore models, different topics related to unconventional fluid phase behaviour were discussed. They considered how fluid critical properties, capillary pressure and minimum miscibility pressure (MMP) would change due to the effects of pore confinement. For the shift in critical temperature and pressure in nanopores they used Singh *et al.* (2009) modification approach for pore size radii of the range of 3nm to 30nm. They showed that the bubble point pressure, gas/oil (or gas/condensate) interfacial tension and MMP are decreased with confinement, whereas the upper Pdew of the phase envelope of fluid with a fixed composition, increases, whilst the lower Pdew decreases. As described in section 1.3, upper Pdew refers to the dew point curve for pressures above cricondentherm point pressure and the lower Pdew refers to the dew point curve for pressures below cricondentherm point pressure. Also, they concluded that the confinement effects on the fluid phase behaviour is marginal when the pore size is more than 20 nm.

Ma et al. (2013) used the data from Singh et al. (2009) to develop new equations for estimation of the shift in critical properties of pure components and mixtures under confinement. They considered a threshold ratio of $\left(\frac{D}{\sigma}\right) = 1.5$, with D as the pore diameter and σ as the LJ parameter size, for taking into account the impacts of confinement effects on the change in the critical temperature. However, such a consideration was not applied for critical pressure and a single equation was developed for changes in critical pressure.

Equations 2.10 and 2.11 present the relationships that Ma et al. found for the shift in critical properties due to confinement.

$$\Delta T_c = \frac{T_c - T_{cp}}{T_c} = 1.1775\left(\frac{D}{\sigma}\right)^{-1.338} \quad \text{for} \quad \left(\frac{D}{\sigma}\right) \geq 1.5$$

$$\Delta T_c = \frac{T_c - T_{cp}}{T_c} = 0.6 \quad \text{for} \quad \left(\frac{D}{\sigma}\right) \leq 1.5 \qquad \text{Eq. 2.10}$$

$$\Delta P_c = \frac{P_c - P_{cp}}{P_c} = 1.5686\left(\frac{D}{\sigma}\right)^{-0.783} \qquad \text{Eq. 2.11}$$

where D is pore diameter, and T_{cp} and P_{cp} are the confined critical properties. According to their modifications for nanopores, the Pdew of the ternary gas condensate mixture they used in their research was estimated to be lower for confined fluid compared to its bulk state. Later, Sanaei et al. (2014) evaluated the effects of phase behaviour and transport properties change due to confinement with the aid of the equations obtained by Ma et al (2013). Methane properties were estimated by applying the changes in the critical properties. They estimated that two-phase envelope shrinks when the pore size decreases and fluid starts to behave more like a dry gas. Moreover, Condensate and gas viscosity would decrease under confinement.

As discussed, in many proposed models, single (uniform) pore size was used to study the effects of confinement on the phase behaviour. The effects of the pore size distribution on the hydrocarbon phase behaviour was investigated by Wang *et al.* (2016) They used two nanopore systems with two different pore size distributions. They implemented capillarity equation (Eq. 2.9) for the VLE calculation which was done using the PR-EOS. They simulated constant composition expansion (CCE) and constant volume depletion (CVD) processes using their nanopores systems. They concluded that for a porous medium with a specific pore size distribution, phase transition from the single phase to two phase cannot be described by a single-phase envelope. In other words, pores with different sizes, have phase transitions at different times. This process includes the phase transition in the first favourable site. Then a thermodynamic equilibrium may be reached. Then in another favourable site, phase transition may occur followed by another thermodynamic equilibrium condition. For instance, in a porous system containing micro- and nano-channels, for a liquid hydrocarbon, during depressurization process, vaporization first takes place in larger micro pores. As a result, an equilibrium state would be achieved in larger pores which is not the same as that in smaller pores and also there would be new composition distribution for the gas in smaller pores. With further

reduction of the pressure, vaporization takes place in smaller pores as well and there would be a new equilibrium condition. It can be inferred that in a case with real pore size distribution, the process of phase and compositional change and subsequent thermodynamic equilibrium would be changing continuously. In other words, in a real core with wide pore size distribution range, the process of phase transition and equilibrium would take place according to the size of the pores which makes this a continuous process. They did not propose any conclusion on how to take into account the effects of pore size distribution on the phase behaviour of confined fluids.

Another approach for evaluating the effects of confinement and capillarity on the phase equilibria in nanopores was suggested by Tan and Piri (2015). They used perturbed-chain statistical associating fluid theory (PC-SAFT) whereby an EOS is coupled with a modified form of Young-Laplace equation to describe the phase behaviour of confined fluids in nanometre calendrical pores. They introduced a new term (an interaction parameter) in the Young-Laplace equation to extend and modify its application for nanopores. This new term takes into account the effects of the interaction between pore walls and the fluid. They suggested that this term can be a function of pore radius, type of the fluid and the lithology of the porous medium. They also stated that since it is an interaction term, it could be a function of temperature as well. The liquid density inside the nanopores was used to calculate the IFT for the curved surface in the pores. By tuning their proposed interaction parameters they were able to match the predicted results from their model to the experimental data of pure components. However, they stated that more experimental results were required to optimize the applicability of their method for hydrocarbon systems.

Dong *et al.* (2016) investigated the capillary pressure effect, critical shift, and adsorption on the behaviour of confined fluid using PR EOS. They adopted an improved Young-Laplace equation considering the adsorbed film at nanoscale. For the shift of the critical properties, they used the equations developed by Zarragoicoechea and Kuz (Eq. 2.5). They also employed similar expressions for critical pressure shift. They used two different adsorption isotherms to account for adsorption behaviour of hydrocarbon fluids. Lighter hydrocarbons ($\leq C_4$) were assumed to have monolayer adsorption (Langmuir) while heavier hydrocarbons ($\geq C_5$) would exhibit multilayer adsorption (BET) isotherm in their model. Langmuir isotherm refers to a type of isotherm, which describes an adsorption process in which the surface would be continuously occupied by fluid molecules as pressure increases. Once the surface is entirely covered with a single layer

of the molecules, no further adsorption can occur. The general form of the Langmuir isotherm can be expressed by equation 2.12.

$$\Gamma_L = V_L\left(\frac{P}{P + P_L}\right) \qquad \text{Eq. 2.12}$$

where Γ_L is the volume of the gas which is adsorbed at the pressure P per mass of the adsorbent, V_L is referred to as Langmuir volume and is the maximum volume of the gas that can be adsorbed on the surface per mass of the adsorbent, and P_L is the pressure at which half of the V_L can be adsorbed.

The concept of the BET adsorption isotherm is a generalization of the Langmuir adsorption. In fact, a BET isotherm is the extended Langmuir isotherm for typical multilayer adsorption on a surface. The general form of a BET isotherm can be expressed by equation 2.13. It is worth mentioning that the BET theory is a common concept for obtaining specific surface area of materials.

$$\frac{P}{V_{tot}(P_0 - P)} = \frac{1}{V_{mono}C} + \frac{C - 1}{V_{mono}C}\left(\frac{P}{P_0}\right) \qquad \text{Eq. 2.13}$$

where P_0 is saturation pressure, V_{tot} is the volume of the gas adsorbed, V_{mono} is the volume of the adsorbed gas when the surface is covered with monolayer, and C is the BET constant which is fixed for any given gas.

They reported that for the VLE calculation of pure components in confined space, capillary pressure and K-values would increase due to the existence of adsorption film. This effect would be more pronounced for the pores in the range of a few nanometres. For the binary mixture, it was estimated that when the difference between the two components is higher, the impacts of pore confinement would be higher as well.

The critical shifts of confined fluids in nanopores with considering the adsorption was studied by Zhang *et al.* (2019). They extended VdW and SRK EOS to perform VLE calculations of confined fluids. In their equations, they took into account the impacts of the existence of fluid adsorption on the effective pore radius. Their formulations for the shifts of critical temperature and pressure were equivalent for the two EOS used as expressed by equations 2.14 and 2.15.

$$\frac{T_c - T_{cp}}{T_c} = 2\frac{c_1}{\sqrt{\pi}a}\frac{\sigma_{LJ}}{r_p - \delta_{ad}} + 2\frac{c_2}{\sqrt{\pi}a}\left(\frac{\sigma_{LJ}}{r_p - \delta_{ad}}\right)^2 = 0.7179\frac{\sigma_{LJ}}{r_p - \delta_{ad}} - 0.0758\left(\frac{\sigma_{LJ}}{r_p - \delta_{ad}}\right)^2 \qquad \text{Eq. 2.14}$$

$$\frac{P_c - P_{cp}}{P_c} = 2\frac{c_1}{\sqrt{\pi}a}\frac{\sigma_{LJ}}{r_p - \delta_{ad}} + 2\frac{c_2}{\sqrt{\pi}a}\left(\frac{\sigma_{LJ}}{r_p - \delta_{ad}}\right)^2 = 0.7179\frac{\sigma_{LJ}}{r_p - \delta_{ad}} - 0.0758\left(\frac{\sigma_{LJ}}{r_p - \delta_{ad}}\right)^2 \quad \text{Eq. 2.15}$$

where δ_{ad} is the thickness of the adsorbed fluid.

The critical volume was found to be different for VdW and SRK EOS. A new correlation was also introduced to estimate adsorbed fluid thickness in nanopores and expressed by equation 2.16:

$$\delta_{ad} = \frac{m}{ln(r_p/\sigma_{LJ})} + n.\left(\frac{\sigma_{LJ}}{r_p}\right) \quad \text{Eq. 2.16}$$

where m and n were obtained by non-linear regression which were correlated to the molecular weight of the molecules. Hence, the fluid adsorption thickness was empirically correlated to the pore radius (r_p), LJ size parameter (σ_{LJ}) and also the molecular weight (MW) of the molecules. They implemented their adsorption thickness in the formulations of the critical properties change. Based on the results of their calculations, the compressibility factor of LJ fluids is independent of the effects of pore radius. However, the validity of their proposed approach, especially for the shift in critical pressure values, needed to be further modified by experimental results. Moreover, they did not suggest a proper approach for considering multi-component systems of gas condensate mixtures.

Luo et al. considered the heterogeneity and wide pore size distribution of the unconventional shale reservoirs has recently been considered by multi PVT study (Luo *et al.*, 2018a; Luo *et al.*, 2021). In their recent study (Luo *et al.*, 2021), they considered the porous medium to be divided into two regions of bulk (representing macropores, natural and hydraulic fractures) and nanoscale (representing nanopores which is generally considered as the pores less than 50 nm). The bulk region had a diameter of 10 μm. Nanoscale region was further divided to two regions with pore diameter of 15 and 5 nm. Fluid properties of the bulk region were estimated using original PR-EOS. Fluid properties at nanoscale (confined fluid properties) were estimated using confinement modified PR-EOS. In their study, they presented a physical explanation for the abnormal trend of observed production condensate/gas ratio (CGR), which was the continuous reduction of CGR during the production even for reservoir pressures above the Pdew. Their simulation suggested that heavier components of gas condensate mixtures will be trapped in nanopores. It was suggested that the nonequilibrium fluid distribution increases

the CGR drop because of the compositional selectivity of the nanopore in favor of intermediate and heavy hydrocarbons.

2.1.3 Molecular Simulation Methods

Laboratory experiments are costly and would take a long time to complete. An alternative method for evaluating pore confinement effects can be molecular simulations. However, the results of such simulations need to be validated with appropriate amount of experimental data, which are often very limited. In such simulations, usually, the average characteristics of each statistical ensemble is used to generate the macroscopic properties of the fluids.

Molecular mechanics, molecular dynamics and Monte Carlo simulations are the main subgroups of molecular simulations. In the study of pore confinement effects, usually the two latter, i.e. molecular dynamics and Monte Carlo simulations are used.

Molecular dynamics is based on Newton's equation of motion. The interaction between different atoms and molecules, from which the trajectories of each atom is obtained, are calculated according to the force fields. Molecular dynamic simulations are usually performed to model the novel phenomenon occurring at nano-confinement pore scales.

In Monte Carlo simulations, the movement of each particle is randomly chosen and observed. The simulation continues to perform these movement of the particles, until the minimum energy of the system is achieved. This minimum energy state is considered to be the state of the equilibrium in the system under study.

In general, molecular simulation methods have suggested that critical properties of fluid might change due to confinement effects. Usually, these methods correlate the extent of the change of the critical properties to the pore radius of the contained medium. It should be mentioned that in molecular dynamics simulations the main features and physics of a simple confined system can be captured. However, once the system size or complexity increases, high computational power is required and accuracy decreases as a result of the complexity in force fields. In this section, some of the studies which have been performed based on molecular simulations are presented.

Jiang *et al.* (2005) studied phase behaviour coexistence of n-alkanes on single-walled carbon nanotube bundle using the configurational-bias NVT Monte Carlo simulation. They used the united atom model for the fluids molecules. LJ potential with a spherical

cutoff length of 14.5 °A was used as the non-bonded dispersive interaction between different molecules. They used harmonic and cosine potential for intramolecular bending and dihedral torsion, respectively. Jorgensen mixing rules as expressed by equations 2.17 and 2.18, were used to obtain the LJ parameters.

$$\sigma_{ij} = \sqrt{\sigma_i \sigma_j} \qquad \text{Eq. 2.17}$$

$$\varepsilon_{ij} = \sqrt{\varepsilon_i \varepsilon_j} \qquad \text{Eq. 2.18}$$

They presented the results of their simulation in terms of the adsorption of pure and multi-component alkane mixtures. Comparing pure alkanes (C1 to nC5), they state that the adsorption of longer or heavier alkanes (nC4 and nC5) would be higher at low pressures and if the pressure is very low, there is almost no adsorption for lighter alkanes (C1 to C3). However, this trend would be reversed at higher pressures where the lighter alkanes would be more adsorbed compared to heavier alkanes. Based on their results for the case of the multicomponent mixture comprising of C1 to nC5, the adsorption of heavier components increases with pressure until reaching a maximum and with further increase in pressure the adsorption would decrease. However, the amount of adsorption for lighter alkanes experiences continuous increase with increasing pressure.

Hamada *et al.* (2007) investigated alteration of phase behaviour and thermodynamic properties of Lennard-Jones (LJ) particles in the confined space of nano-slit and nano-cylindrical pores. They used periodic boundary conditions for both of the medium used in their study. They obtained the equilibrium properties of the model confined fluid at constant μ, V, and T by the grand-canonical Monte Carlo (GCMC) simulation. Based on their results, it was suggested that these properties deviate from bulk value under confinement. They indicated that size of the pores in a nanoporous medium would alter the phase behaviour and thermodynamic properties of the fluids. Also, pore size would affect the interfacial behaviour of fluid-wall interface. They suggested that this could be due to the rise in the interactions between fluid molecules and also the potential energy, and most importantly, interactions between fluid-wall molecules.

Singh *et al.* (2009) used configurational-bias grand-canonical transition matrix Monte Carlo simulation results to examine the confinement effects on thermophysical properties of n-alkanes within a smooth and structureless slit. United-atom approach was selected to be used for n-alkane molecules. In order to describe the intermolecular potential, they used the Errington and Panagiotopoulos modified Buckingham potential expressed by equation 2.19.

$$U(r) = \left\{ \frac{\varepsilon}{1 - \frac{6}{\alpha}} \left[\frac{6}{\alpha} exp\left(\alpha \left[1 - \frac{r}{\sigma} \right] \right) - \left(\frac{\sigma}{r} \right)^6 \right] \right\} \qquad \text{Eq. 2.19}$$

In their approach μ, V, and T were held constant while allowing N (particle number) and U (energy) fluctuate. In order to estimate the vapour-liquid critical properties, they fit the coexistence densities to the law of the rectilinear diameter and the scaling law for the density. The critical pressure was calculated using an expression similar to Antoine equation, which was obtained from fitting the saturation pressure data of the molecular simulations. Their results indicated that, critical temperature of the confined fluid would reduce to a minimum value as the slit width reduces and the fluid flow approaches to two-dimensional flow. Also, the calculated critical pressure was found to increase to a constant maximum with decreasing the slit width.

In unconventional reservoirs, hydrocarbons can be found in three different states: free molecules, adsorbed molecules, and dissolved molecules. Jin and Firoozabadi (2016) focused on the thermodynamic modelling of phase behaviour of the dissolved hydrocarbons in unconventional reservoirs. For pores larger than 10 nm they used the conventional EOS with the effects of the curvature. However, they neglected adsorption for pores larger than 10 nm. For pores less than 10 nm, they used Density Functional Theory (DFT) and Grand Canonical Monte Carlo (GCMC) simulations to evaluate the critical properties of n-C4. They considered inhomogeneous density distributions and gas dissolution in kerogen to predict the phase behaviour of fluid in shale media with sub 10 nm pores. They reported that in pores less than 10 nm, surface adsorption becomes significant and fluids would have inhomogeneous density distribution caused by strong fluid/surface interactions. Moreover, their calculations showed that nanopore confinement would increase the Pdew of gas condensate mixtures.

More recently, de Andrade and Nojabaei (2021) presented a molecular dynamics study of nano-confinement effect on hydrocarbon fluid phase behaviour. They considered the fluid concentration distribution in organic shale rock with pore size distribution. In their study, they used pure ethane and pure n-heptane as well as the fluids which were confined in a carbon based structure, graphene, as the pore model. The All-Atom Optimized Potential for Liquid Simulation (OPLS-AA) force field was used to represent both pore and hydrocarbon molecules. NVT ensemble (thermodynamic ensemble with constant number of particles (N), constant volume (V), and constant temperature (T)) was used in their simulations. They simulated the phase behaviour and the molecular distribution of

the fluids in a confined space which is connected to a bulk space. They used two different set ups in their pore network system. The first one was a single 5-nm pore connected to the bulk system and the second one was the 2-nm and 5-nm pores connected to the bulk. Based on their results, all types of the hydrocarbon fluid molecules tend to get adsorbed onto the surface of the porous media. They suggested that bubble point pressure would be suppressed in nanopore confined space while the Pdew would probably increase. However, they stated that further studies are required to generalize this output.

Herdes *et al.* (2018) proposed a combined experimental, theoretical and molecular simulation framework for characterization of the fluid phase behaviour of hydrocarbon mixtures within shale rocks. In terms of the experimental part, they measured bulk IFT at high pressure high temperature conditions. They also measured the contact angle of various systems of CO2, water and n-decane at different temperature and pressure. The rock model was then characterized based on the nitrogen adsorption, thermogravimetric analysis and contact angle measurement. They used statistical associating fluid theory (SAFT) as the EOS and the resulting Mie intermolecular potential for the force field expressed by equation 2.20.

$$U(r) = \varepsilon \frac{\lambda}{\lambda - 6}\left(\frac{\lambda}{6}\right)^{6/6-\lambda}\left[\left(\frac{\sigma}{r}\right)^{\lambda} - \left(\frac{\sigma}{r}\right)^{6}\right] \qquad \text{Eq. 2.20}$$

where λ is the repulsion parameter of the interaction potential. Equation 2.20 is equivalent to equation 2.2 (LJ potential) if λ is set to be 12.

Also, the mixing rule suggested by Lafitte et al. was used for the force field parameters of mixtures. Their simulation results showed that, the organic pores with the radius 1 and 2 nm are mainly contributing towards the adsorption.

2.1.4 Discussions on the Proposed Theoretical Approaches for the Study of the Confinement Effects

It is widely believed that pure fluid critical properties would reduce due to the effects of confinement. However, for hydrocarbon mixtures, these theories lack general acceptance. As noted in previous sections, different approaches in the theoretical evaluation of the effects of fluid confinement have resulted in different outcomes. For instance, for pure components, depending on the force fields used, the coefficients which have been obtained based on non-linear regression vary from one set of equations to another. Even the form of the equations might not be the same as there are some researchers who have

presented equations in exponential form (Singh et al, 2009) while most of the equations are presented by a polynomial functions of the ratio ($\frac{\sigma}{r}$). Moreover, some of the assumptions made for the development of these proposed equations are not valid for real unconventional reservoirs. For example, in some of the cases (Zarragoicoechea and Kuz, 2002), the pore walls are considered to be inert. Hence, their interaction with the fluid molecules are neglected and only the interacting forces that molecules have due to close proximity in nano-scale confined space were considered.

Apart from such limiting assumptions, the application of the equations proposed for the shift in critical properties of single- component fluid for hydrocarbon mixtures is a matter of debate. In some methods, the proposed equations extend the applications for mixtures by simple mixing rules for critical properties. Some other methods, consider different adsorption isotherms for different molecules in confined fluids (Dong *et al.*, 2016). Another important part, which is missing in the proposed methods, is that most of them if not all do not include any parameter corresponding to the geochemical properties of the rocks including its mineralogy. The main reason could be due to the lack of experimental data on the real core samples or make comparison based on the synthetic porous samples but with different geochemical properties (i.e. synthetic porous samples made from different materials). The impact of pore size distribution is not very well established in literature. Most of the studies available, are concerned with single pore models. They do not consider wide range of pore size values on the extent of pore confinement. Another main drawback of the proposed methods lies within the fact that most of them are based on regressions performed on the data which has been obtained from molecular simulations or from the experiments which only consider single component fluid behaviour in porous media with uniform pore sizes.

Summary of different simulation and modelling work to study the effects of confinement on phase behaviour is presented in Table 2.1 for EOS and VLE calculation modification methods, Table 2.2 for Monte Carlo (MC) simulation and Table 2.3 for Molecular Dyanamic (MD) simulation approaches.

Table 2.1: Summary of different EOS and VLE calculation modification works to study the effects of confinement on phase behaviour

Equation of State and VLE Calculation Modifications Methods		
Reference	Type of porous medium/model	Results and notes
Zarragoicoechea and Kuz (2002 and 2004)	Single nanopore with infinite length. Modification of VdW EOS.	Shift in critical temperature based on flow path characteristic radius and LJ size parameter.

Travalloni et al. (2010)	Cylindrical pores with homogeneous surface. Extension of VdW EOS. For single component fluid and extended for multicomponent fluids.	The effects of confined medium could not be ignored when the ratio of the pore radius to the molecular effective diameter is less than 20.
Devegowda et al. (2012)	Modified PR-EOS with shifted critical properties.	Gas viscosity was predicted to be lower due to confinement. It is restricted to models with a single pore diameter.
Wang et al. (2013)	Modified PR-EOS coupled with capillary pressure.	Liquid viscosity and density was predicted to reduce. It is not clear on how confinement effects can be applied in their model.
Tan and Piri (2015)	PC-SAFT EOS coupled with modified capillary pressure	Introduced a capillary pressure fitting parameter. Critical pressure and temperature were predicted to be lower.
Li et al. (2014)	Density functional theory coupled with PR-EOS. Carbon-slit pores. Pure substances and mixtures.	For pure substances: Phase change was predicted to occur below the critical temperature and saturation pressure. For mixtures: Possibility of phase change above the cricondentherm was predicted.
Dong et al. (2016)	PR-EOS coupled with capillary pressure and adsorption theory	With pore size reduction: Capillary pressure was predicted to increase. Bubble point pressure was predicted to decrease. Dew point was predicted to increase.
Advantages and Disadvantages: EOS and VLE calculation modification methods benefit from simplicity and being easy to be implemented for field-scale studies. The effects of pore size can be demonstrated easier using these methods. However, for the methods with adding new terms in EOS, there is lack of theoretical explanation. There are usually semi-empirical correlations which ignores the heterogeneity of the fluid density in nanopores.		

Table 2.2: Summary of different Monte Carlo simulation works to study the effects of confinement on phase behaviour.

Monte Carlo Simulations		
Reference	Type of porous medium/model/components	Results and notes
Singh et al. (2009)	Configurational-bias grand-canonical transition-matrix Monte Carlo. Slit pores of graphite and mica. Constant mVT ensemble. Single component n-alkanes.	With decreasing pore size: Critical pressure shift continuously increases and critical temperature decreases up to a minimum then it becomes constant.
Pitakbunkate et al. (2015)	Grand canonical Monte Carlo. A graphite slab. Constant mVT ensemble. Pure hydrocarbons and a simple binary hydrocarbon mixture.	Critical temperature and pressure of pure component methane and ethane are reduced as the pore size decreases.

		Critical pressure and temperature of the confined mixture are lower than those of the bulk fluid. The phase diagram of the binary mixture shrinks as a result of the confinement.
Li et al. (2020)	Gibbs Ensemble Monte Carlo. Slit and cylindrical amorphous silica pore. Constant nVT ensemble. n-hexane.	System is subjected to temperature increase (and subsequent pressure increase) at each step. The strength of fluid−pore interaction effects was reported for the first time. As the surface energy decreases, the vapor pressure increases while the vapor temperature decreases. Sufficient reduction of the fluid−pore interactions could even elevate the vapor pressure above that of the bulk fluid.
Jin and Firoozabadi (2016)	Density Functional Theory coupled with Grand Canonical Monte Carlo	Critical temperature and pressure were predicted to continuously decrease with reduction in pore size.
Advantages and Disadvantages: MC simulation is a powerful tool for simple molecule systems and in general works good with constant temperature ensembles. However, it is difficult to perform simulations with multi-component or complex systems.		

Table 2.3: Summary of different Monte Carlo simulation works to study the effects of confinement on phase behaviour.

Molecular Dynamic Simulations		
Reference	Type of porous medium/model/components	Results and notes
Welch and Piri (2015)	Nano capillaries with square cross section. Constant NVT and NPT ensemble. Binary hydrocarbon mixture.	Explored retrograde condensation of the mixture at bulk phase, but not investigated phase transition in the nanopore by increasing pressure.
De Andrade and Nojabaei (2021)	OPLS-AA force field. Graphite nanopores with pore size distribution. Constant NVT ensemble. Binary hydrocarbon mixture.	Bubble point pressure would be suppressed in nanopore confined space while the upper Pdew would probably increase and lower Pdew would probably decrease. Confined space was introduced rather than changing pressure.
Advantages and Disadvantages: MD simulations are suitable for dense systems. Various data of different hydrocarbons can be obtained as opposed to experimental methods. However, it is challenging when dealing with coexisting phase behaviour near critical region. Also, the results from MD simulations highly depend on the choice of interaction potentials.		

As explained above, available theoretical researches have shed light in the study of fluid confinement effects, but due to the complexity of real unconventional reservoirs, validation of such studies for hydrocarbon mixtures residing in unconventional rocks is not possible mainly as a result of not having corresponding experimental data available.

The experimental study of fluid confinement effects although being difficult to perform, is a necessary step towards better understanding of the unconventional reservoirs.

2.2 Experimental Studies for Confinement Effects on Phase behaviour in Unconventional Reservoirs

There are different experimental studies which show that fluids phase behaviour in the confined space is different from that of the bulk state. These studies can be divided into two main categories. In the visual approach by which direct optical observation methods is employed, usually the lab on a chip technique is utilized. The Lab on a chip refers to the technology which allows laboratory analysis to be performed on the miniaturized scale. This method, is usually associated with devices containing micro- and nanochannels, which allow fluid flow within them. The benefit of this method is the possibility to directly observe the processes taking place within the nanochannels. However, this method cannot be easily applied to hydrocarbon systems where fluids are existing within rocks.

There are also, non-visual approach, which are usually conducted in porous media packed in metal holders. Several methods have been presented for fluid phase behaviour studies under pore confinement effects. These experimental methods include: Adsorption isotherm, differential scanning calorimetry (DSM), isochoric and diffusion studies.

2.2.1 Visual Experimental Methods

There have been efforts to imitate the phase behaviour and fluid flow within unconventional reservoirs by the use of nanochannel chips and high-resolution imaging devices. In this method, the nanochannel is filled with the fluid sample, then temperature and pressure changes slowly to observe the appearance of a second phase once equilibrium has been achieved.

The advantage of such methods is that the observer can actually visualize the formation of the liquid drops or gas bubbles within nanochannels. It should be mentioned that most of the experiments performed using this method have been dedicated to the oil phase. Sigmund *et al.* (1973) experimentally and numerically analysed the impact of porous media on phase behaviour of hydrocarbon binary mixtures based on the comparison

between a PVT cell packed with a porous medium and a conventional PVT cell. They reported that no significant differences in the bubble point and Pdew exist between the fluids in porous media or in the bulk. However, this was not the case for the surfaces with very high curvature. They added that such high curvature was unlikely to exist in the reservoirs as the finest pores are filled with the connate water.

Wang *et al.* (2014) used nanofluidic devices to visualize the effects of nanoconfinement on phase behaviour of alkanes. They observed that for pure hydrocarbons, the vaporization curve of the liquid suppressed due to the interaction between fluid and nanochannels. For multicomponent fluids, they stated that, since the lighter hydrocarbons first transform into gaseous phase, the molecular weight of the remaining liquid phase would increase. As a result, vaporization of the liquid in small pores would be suppressed. However, even with the most effective visualization devices, the process of capillary condensation and fluid confinement effects is not possible to be monitored using these methods in real shale rock samples.

Alfi *et al.* (2016) studied the phase behaviour of pure hydrocarbons (hexane, heptane and octane) inside nano-channels chips (Nano-channels with the depth of 50 nm and width of 5 μm). After introducing the fluid to the nano-channels, temperature was raised gradually at the rate of 12 °C/min while pressure was recorded. They managed to find bubble point pressures for the three components. It was found that there is a good agreement between predicted bubble point pressure and original PR-EOS suggesting that for pore sizes as small as 50 nm, the effect of confinement is negligible.

2.2.2 Adsorption Isotherm Methods

The most widely used experimental methods in order to determine the phase behaviour of the fluids in nanopores are the adsorption isotherm methods. High pressure adsorption isotherm measurements (high pressure adsorption isotherm measurements refers to the measurements which cover a wide range of pressures from 0 to 10000 psi and temperatures from 273 to 500 K) can be divided into two main groups of gravimetric and volumetric approaches. A comparative description of these methods is presented by Belmabkhout *et al.* (2004) and Barsotti *et al.* (2016). It should be mentioned that adsorption isotherm is not directly related to the scope of this study since it usually deals with capillary condensation determination of fluids using an operational condition which

is not similar to what occurs in unconventional reservoirs. However, adsorption isotherms provide valuable data in terms of fluid phase behaviour studies.

The basis of adsorption isotherm methods is the higher density of the fluid near pore walls, compared to the fluid density at the centre of the pores. During adsorption isotherm analysis, when a phase transition occurs, a sudden change in the amount of adsorbed fluid could be observed. For instance, for a gravimetric apparatus, the phase of a confined fluid is determined by the relationship between its adsorbed mass and pressure. In this method, at a constant temperature, a known volume of the fluid is introduced at each time. After reaching equilibrium, the change in mass and pressure of the sample would be recorded. Figure 2.2 shows the isotherm for CO2 in a synthetic porous medium. The data displayed in this specific figure, were obtained from the work of Barsotti *et al.* (2018), which used an apparatus that consisted of two chambers, one for bulk fluid and the other one for confined fluid. The fluid in the chamber for monitoring the bulk fluid behaviour is used to obtain the data that are used to correct the absolute data obtained from the chamber with confined fluid.

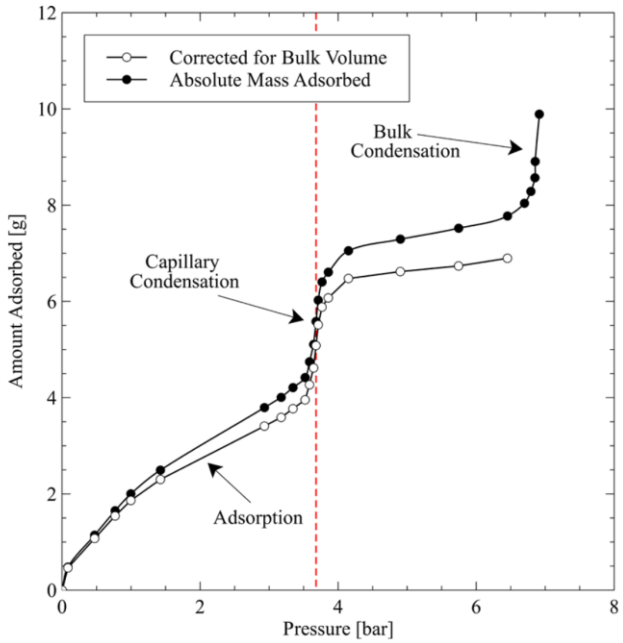

Figure 2.2: Adsorption isotherm for CO2 in a synthetic porous medium with a pore size of 3.7 nm (source: Barsotti *et al.*, 2018).

The significant difference between the mass of the fluid absorbed when it is in vapour or liquid phases, makes the transition between these phases to be corresponding to a steep change in the slope of the curve obtained from the experimental data. It can be observed that due to capillary condensation, the saturation pressure of CO2 is lower in the confined

space compared to the bulk value. The concept of capillary condensation is based on the intermolecular forces which can form fluids with multiple layers adsorbed onto the surfaces in small pores.

For single components, condensation occurs as a result of increase in fluid density due to pressure increase or multilayer adsorption. The latter is referred to as capillary condensation which is specific to unconventional reservoirs. In conventional reservoirs, it is unlikely to have capillary condensation. For multicomponent fluids, e.g. gas condensate mixtures, liquid drop out or condensation can occur due to pressure change (change in fluid-fluid interactions) or interactions between fluids and pore surface. The latter does not happen in conventional reservoirs. Interactions between fluids and pore surface result in the adsorption on the rock surface as well as increased tendency of the liquid molecules to be separated from gas phase. In unconventional reservoirs, for smaller pores both adsorption (capillary condensation) and liquid drop out can occur. However, in larger pores it is very likely to observe liquid drop out. It should be noted that the liquid drop out effects are translated into the change in the effective permeability and is not related to the adsorption amount observed. However, in capillary condensation, a gradient in the amount of adsorbed fluid is observed.

The dependency of the capillary condensation pressure value on the pore size of the porous medium is illustrated in Figure 2.3 which is obtained from the same work of Barsotti et al (2018). Figure 2.3 shows the adsorption isotherms of the n-pentane for another porous medium with similar type but different pore size values. In this figure, the red line highlights the obtained bulk saturation pressure whilst the blue lines show those under confined conditions in two homogeneous porous media with different pore sizes. As it can be observed, lower pore size values, has resulted in lower saturation pressure for n-pentane. The reason for the change in capillary condensation pressure values due to change in pore size, lies in the preference of the wetting fluids to wet the surface of the smaller pores. Based on capillarity equation, lower radius would result in higher capillary pressure. Hence, capillary condensation would occur with higher intensity in smaller pores.

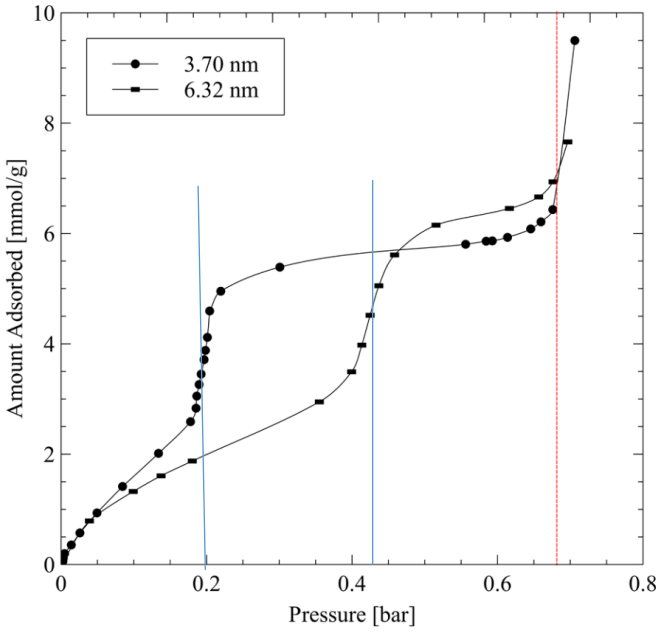

Figure 2.3: Adsorption isotherms for n-pentane in two porous media with similar type but different pore sizes of 3.7 nm and 6.32 nm (source: Barsotti *et al.*, 2018).

Adsorption isotherms are great tools for the study of ordered porous media where the porous space is consisted of similar pore structures. This method can provide useful information about the confinement effects on the extent of the shift in phase behaviour as it facilitates the study of nanopore confinement effects in the most basic manner, i.e. using synthesized samples with uniform pore structure. The performance of these isotherms are related to the pore size of the confined medium. However, while dealing with real shale samples, the range of the pore size of the porous media is quite wide, the sharp change in adsorption isotherm becomes a gentle change which makes the analysis of the adsorption isotherm for phase behaviour studies very difficult.

In another study, Barsotti and Piri (2021) evaluated the effects of pore size distribution on capillary condensation in nanoporous media using similar experimental approach. However, in their study, they synthesized different types of porous media with two and three different pore size values, namely large nanopores (L), medium nanopores (M), and small nanopores (S). Figure 2.4 shows the results of the adsorption isotherms obtained for n-pentane. In Figure 2.4 (a), the isotherms for the two pore size values of S and L are presented. It can be observed that two distinct phase transitions corresponding to the two pore size values can be observed. However, when porous medium is consisted of the two S and M pore size values, the difference between the two phase transition regions is not very clear. If the porous medium is consisted of several pore size values over a wide range of pore size distribution (as it is the case in real unconventional reservoirs), it is not easily

possible to pinpoint the pressure at which the phase transition has occurred. This is because the shift in the slope of the line which corresponds to the phase transition becomes so gentle that the estimation of the accurate phase transition pressure becomes extremely difficult.

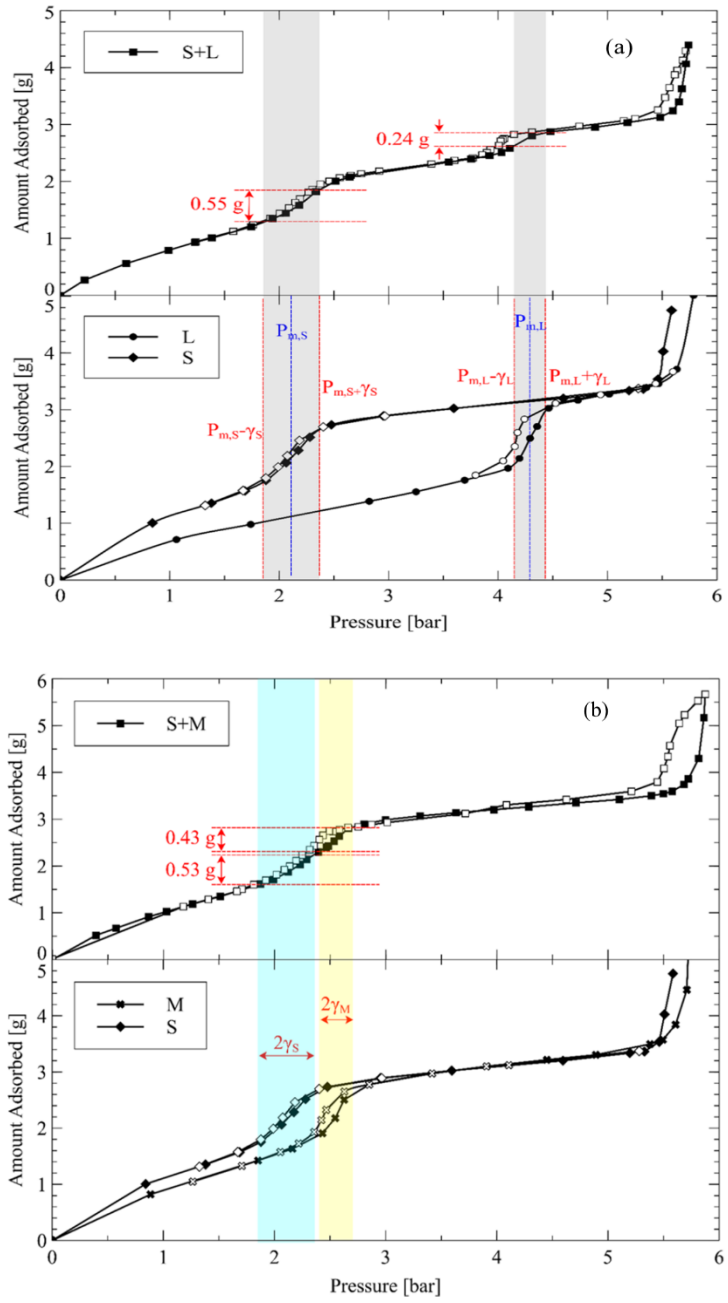

Figure 2.4: Adsorption isotherms for n-pentane in two different porous media each consisting of two distinct pore sizes (a) the porous medium with S and L pore sizes, (b) the porous medium with S and M pore sizes (Barsotti and Piri, 2021).

Additionally, it has been reported that a hysteresis loop can occur for adsorption and desorption in the region of the phase change where a sudden change occurs in the adsorption isotherms, which further complicates working with such isotherms.

There are some additional considerations, which should be taken into account while dealing with shale reservoirs. Since, the composition of the shale formations is complicated, there is a need to evaluate the effects of difference in composition on confinement effects. Also, we should bear in mind that due to difference in pore shape structure and surface chemistry among different shale formations, there is a need to conduct different experiments specific for each fluid and rock type to properly evaluate the effect of confinement for each case. It has also been suggested that kerogen in shale rock might be swollen due to adsorption and consequently the results of adsorption experiments may be affected by such phenomenon especially due to the shrinkage of the pore volume.

Most of the adsorption studies have been focused on the phase behaviour of pure hydrocarbon components. Main outcomes of the results obtained from adsorption analysis on pure components are: The saturation pressure of the confined fluid is lower than that of bulk fluid. The critical temperature of the fluids under the impacts of pore confinement is lower than that of bulk fluids. With a decrease in the pore size, the impact of pore confinement effects increase. As a result, when pore size increases, the fluid saturation pressure and critical temperature approach to the bulk values. A comprehensive literature survey on the application of adsorption isotherm measurements for investigating the capillary condensation and confinement effects has been presented by Barsotti *et al.* (2016). An extensive experimental data on adsorption isotherms has been presented by A. Russo *et al.*(2011). They measured the adsorption-desorption isotherms of different types of hydrocarbons including aromatic and aliphatic compounds using different types of synthetic porous materials. As mentioned before, Barsotti *et al.* (2018) used a gravimetric apparatus which was able to measure the pore confinement effects in different types of confined spaces for both static and dynamic conditions. They performed different experiments using binary and ternary mixtures in nanopores. Since their mixtures under study were predominantly made of CO2, the results of their experiments for capillary condensation pressures of the mixtures were very close to those of pure CO2. However, as mentioned, if a real shale sample and a multicomponent fluid is used, the measurement of the Pdew is very difficult as this method relies on a sharp shift in the adsorption isotherm to identify the Pdew and any change in the pore size would shift the point at which such sharp transition takes place. As a result, when the pore size of the sample has some significant variations throughout the core, the sharp change in the adsorption isotherm tends to become less identifiable. In such a case, there has been some

suggestions on how with some computational calculations, the approximate solution can be achieved, however, such calculations apart from being tedious, introduce errors in the measurement of the phase behaviour of confined fluids.

2.2.3 Differential Scanning Calorimetry Method

Differential scanning calorimetry (DSC) has recently been applied to study vapor-liquid phase transition of confined fluids. This method is based on evaluating thermal properties by measuring the heat of transformation of a process involved with a temperature change. DSC method is generally used to detect the temperature at which liquid phase turns into gas. During the thermal analysis of the heat capacity of the fluids, when phase transition occurs, a peak in the heat rate profile is observed by changing temperature. The corresponding temperature is regarded as the bubble point temperature.

Contrary results have been reported for the result obtained from this method. In general, the discrepancy comes from the way the data is analysed. Some studies have suggested that due to confinement, bubble point temperature increases, while other researchers suggest that the confinement effects would suppress the bubble point of the hydrocarbons. Applying this method for high pressure conditions is not very well established. It should be mentioned that this method is usually applied for bubble point measurements rather than dew point measurements as it is more convenient to deal with the thermogravimetric analysis of the phase transition from liquid to gas. This method could be applied for the Pdew measurement, however, the applicability of the method has only been considered at low temperatures and pressures which are not applicable for gas-condensate reservoirs temperature.

Luo *et al.* (2016) used two types of controlled pore glasses (CPG) to represent a porous medium. The average pore diameter of the first medium was 38.1 nm and for the second medium was 4.3 nm. Based on the experimental data obtained from DSC method performed at atmospheric pressure, they suggested that for pores with diameter of 38.1 nm and filled with n-octane and n-decane, the impacts of confinement on the bubble point was insignificant. However, they observed a different trend for the pores with diameter of 4.3 nm, where they found a difference, i.e. they found two peaks corresponding to two bubble points for the confined fluid. However, these authors did not present an acceptable explanation for such observations in their study.

Later, in another study Luo *et al.* (2018) indicated that in the case of using hydrocarbon mixtures, components with higher molecular weight, would prefer to adsorb onto the surface of the confined pores. However, lighter components prefer to remain in the pore body. Consequently, they suggested that under confinement, there would exist two distinct phases, making the composition distribution of the fluids inside nanopores to be heterogeneous.

Although these observation are important in the study of the phase transitions of confined fluids, still it is not very clear on how such approaches can be applied to real shale core samples where the range of the pore size distribution is wide and different range of pores with different size coexist in a samples.

2.2.4 Isochoric Method

This novel method has recently been proposed by Salahshoor and Fahes (2020). In this method, using two chambers, one for the bulk fluid and the other one for the fluid in a confined packed porous medium, the change in pressure due to decreasing and increasing temperature is recorded. The experiment starts when the fluid is considered to be single phase in both chambers. The temperature and pressure points obtained from the experiment are plotted in a P-T diagram. The appearance of the liquid phase and hence the corresponding dew point can be estimated by a change of slope in the fitted lines on P-T diagram. The results obtained from their study showed that the for a C2-C5 mixture, the confined Pdew is slightly higher than the bulk value. In this method, although being relatively fast, it is difficult to recognize the point at which the dew point is changed for complex gas condensate mixtures which may raise questions in the applicability of such a method for real unconventional gas condensate reservoirs.

In gas condensate reservoirs, the change of the properties by temperature is considered to be so slow that obtaining a change in the slope of a trend is not an error free task. Moreover, for gas condensate samples, with isobaric processes the phase behaviour changes are very difficult to pinpoint as the change in the trends are very minute and cannot be accurately obtained when using a mixture comprising of several components.

2.2.5 Diffusion Method

When the temperature is slightly above the critical point, i.e. the fluid is in supercritical conditions, the diffusion of the fluid would increase substantially. As a result, the increase in diffusion could be regarded as a sign of critical point. This method is usually performed by the pulsed field gradient nuclear magnetic resonance (NMR) experiments. NMR provides direct access to the key data of fluid behaviour in the container of interest. A method which is capable of recording the number of molecules and their dynamical properties. When by changing the external pressure, the NMR signal intensity is measured in a porous medium sample, adsorption isotherms can be obtained which then could be an indicator of the state of a fluid phase in the pores. Little experimental data are available using this method. The results obtained from this method suggest that the critical temperature of pure hydrocarbons reduces due to confinement effects. The application of this method for unconventional gas condensate reservoirs is not well documented. This method, is usually a way of obtaining critical temperature. Based on this method, the temperature at which the diffusivity of the fluids increases would be considered as the range which the fluid has become supercritical. Hence, the temperature at which the deviation in the diffusivity is observed is regarded as the critical temperature.

Zeigermann *et al.* (2009) used diffusion method to evaluate the critical point for pure n-pentane. They used two different types of nanopores with different sizes. The first porous glass material was made with Vycor particles of about 5μm size with an internal porous structure with mean pore diameter of about 5nm. The second porous material was made with ERM particles with size of 140-200 μm and the pore diameter of about 15nm. They observed that for both porous media, the critical temperature would reduce due to the presence of nano scale porous media. Also, based on their measurements, in the synthetic porous media with lower pore size radius, the confined critical temperature was lower. This method, is not very feasible with real rock materials and the geochemical properties of the porous container makes it difficult to perform error free measurements. Also, the results showed high dependency of the obtained confined critical temperature to the pore radius. When the range of the pore sizes is very wide, detecting or spotting the temperature at which diffusivity gas changed is not possible. As a result, this method cannot be applied to real reservoir rocks with variable pore size distributions.

2.2.6 Discussions on the Literature of the Experimental Approaches for the Study of Confinement Effects and Their Limitations

The majority of the available experimental studies, as described above, have focused on the phase behaviour of single component fluids in synthetic homogenous porous media. In most of these studies, the altered phase behaviour of confined fluids is confirmed. Most experimental results on single component fluids suggest that the saturation pressure of hydrocarbon gases would reduce due to increased impacts of capillarity and intermolecular forces. Most of these measurements confirm that for single component fluids, the critical temperature and pressure would reduce due to the impacts of pore confinement. However, there are very limited experimental data on the phase behaviour of multicomponent mixtures. In particular, there are limited experimental results which have been presented for binary and ternary gas condensate mixtures albeit in synthetic homogenous porous media. For instance, Salahshoor and Fahes (2020) conducted an isobaric study for the effects of confinement and observed that for the binary gas condensate mixture they used, Pdew of gas condensate mixture increased due to confinement. However, the results sometimes, are contradictory. In some studies, the phase envelope of the fluids is considered to be suppressed such as those measured by adsorption isotherms which suggested that saturation pressure will be lower such as those presented by Brasotti et al. (2018), while in some other studies, the Pdew of the gas condensate mixtures was measured through experimental studies such as the one presented by Salahshoor and Fahes (2020) or estimated through theoretical studies such as the one presented by Jin and Firoozabadi (2016) to be higher for the fluids under the effects of nanoconfinement. These results, may seem contradictory. However, it should be mentioned that the generalization of the findings from one approach or study with its specific limitations to other conditions of interest will not be accurate. Firstly, the results of each study is specific to the types of the fluid and porous medium employed in it. Having different fluid composition (e.g. single component or multiple component fluids), can result in different trends in observed data. For instance, the study conducted by Barsotti et al. (2018) was performed on single component fluids and using MCM41, while the study conducted by Salahshoor and Fahes (2020) was performed on a packed bed of nanoparticles with a mixture of C2-C5. Moreover, as mentioned earlier, in all of these experimental studies, the impacts of confinement on the phase behaviour of the fluids, was investigated using synthetic homogenous porous media. Hence, the pore size distribution is uniform and the effects of shale rock heterogeneous mineralogy are ignored. Having uniform pore size distribution is beneficial for sensitivity analysis which

could be performed in confined space because it would eliminate the influence of pore size distribution on other pertinent parameters like fluid composition. However, it is not very clear that if there exist a wide range of pore size in a porous medium which is the case for shale reservoirs, the impacts of pore confinement would be easily employable from the experiments performed on porous media with uniform pore size distribution. In other words, the current state of literature lacks sufficient reliable data for gas condensate mixtures in real unconventional rocks.

Although, such approaches may be beneficial to understand some of the mechanisms taking place in simple nanoporous materials and shed light for the study of the confinement effects on the phase behaviour, they are not applicable to real unconventional reservoirs. Their applications in real unconventional reservoirs will be a matter of debate from two aspects. Firstly, the geochemical structure of the synthesized porous media is totally different from naturally occurring unconventional rocks. For instance, in most experimental studies, either CPG or MCM has been used, which may have some common geochemical features similar to real shale reservoirs, but definitely they do not fully represent the real reservoir porous media. This could be very important as pore confinement effects is dependent on the mineralogy of the rock samples. Hence, it is not very clear how the presence of heterogeneous organic and inorganic compounds in the real rock sample might affect the extent of pore confinement if simplified porous medium is being used in the study of pore confinement effects. Secondly, the pore size distribution of a synthesized porous medium is very different from that of real porous media. Pore confinement effects are also dependent on the size of the pores. When dealing with real rock samples and real unconventional reservoirs, neglecting the effects of wide variations in pore size distribution, may result in the inaccurate evaluation of the overall performance of the reservoir. Even if a method can be employed to use real core samples, the governing conditions and the limitations in the methodology, impose a great degree of uncertainty and difficulty for obtaining a reliable data set for a specific reservoir with heterogeneous porous medium and wide range of pore size distribution.

A short summary of the experimental studies is presented in Table 2.4.

Table 2.4: Summary of different experimental works to study the effects of confinement on phase behaviour.

Reference	Methodology and operating conditions	Results and notes
Alfi et al. (2016)	Methodology: Lab on chip (Visual observation) for 50 nm nano-channels. Operating condition: Increase in temperature which results in pressure increase.	For pore sizes as small as 50 nm, the effect of confinement on bubble point of pure hydrocarbons was negligible.
Salahshoor and Fahes (2020)	Methodology: Isochoric (constant volume) for binary hydrocarbon mixture in a confined packed porous medium Operating condition: Changing temperature and subsequent change in pressure at constant volume.	confined Pdew was found to be slightly higher than the bulk value for binary C2-C5 mixture.
Luo et al. (2016)	Methodology: DSC using two types of CPG with different pore diameter. Operating condition: Changing temperature with constant pressure	Significant impacts of pore confinement was observed for pores with diameter of 38.1 nm.
Barsotti et al. (2021)	Methodology: Gravimetric adsorption isotherms for binary and ternary mixtures of hydrocarbons and CO2 in nanopores. Operating condition: Increase in pressure with injecting fluid at constant temperature.	Capillary condensation pressures of the mixtures were very close to those of pure CO2
Zeigermann et al. (2009)	Methodology: NMR diffusion for two different types of nanopores filled with pure n-heptane. Operating condition: Increase in pressure at constant temperature.	Confined critical temperature was lower in the nanopores with smaller diameters.

As presented in Table 2.4, operating conditions and methodologies for the experimental studies are different from what happens in the reservoirs. Figure 2.5 shows a schematic representation of the operating path (presented by green dashed arrow) on the phase diagram explored in experimental studies presented in literature. Figure 2.5a represents an isobaric path which is the path followed in DSC studies. Figure 2.5b and 2.5c are representative of isothermal operational condition which could be observed in NMR diffusion and adsorption isotherm measurement methods. These methods are usually associated with increasing pressure. However, in case of measuring desorption isotherm, impacts of pressure reduction on the amount of adsorbed phase is investigated. In case of using isothermal path presented in Figure 2.5c, lower Pdew may be obtained, however, it is not of great interest for the applications related to unconventional gas condensate

reservoirs. Figure 2.5d represents isochoric operational path which does not occur during the production life of an unconventional reservoir.

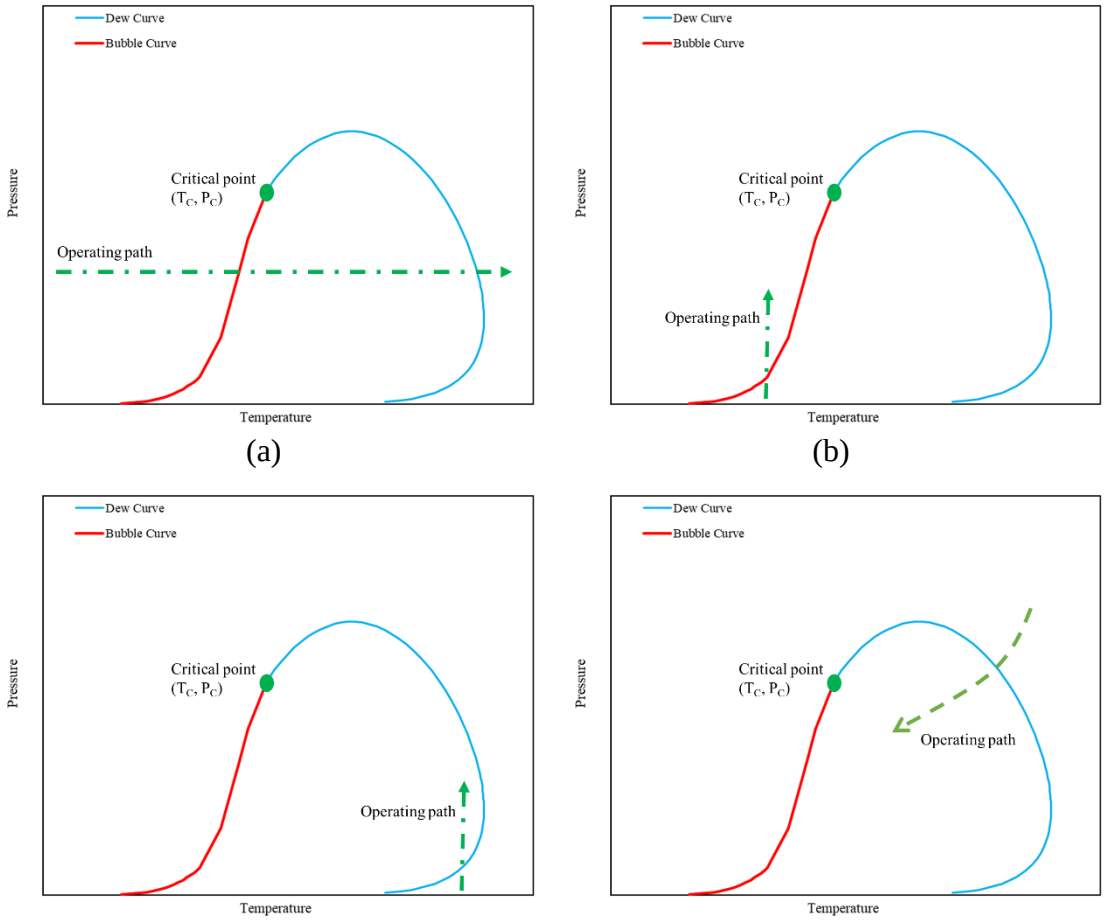

Figure 2.5: Schematic representation of operating path for experimental studies in literature

These presented operational conditions do not fully resemble to the production life of an unconventional gas condensate reservoir (as depicted in Figure 1.5). This could be considered as another shortcoming of the available experimental methodologies presented in literature. Hence, it is not very accurate to generalize the applicability of the proposed methods for gas condensate unconventional reservoirs.

Chapter 3: Experimental Methods and Procedures

The application of some of the presented experimental procedures is also not very clear for real gas condensate fluid mixtures which may comprise of many different organic compounds. Hence, the measurement of the impacts of confinement on the phase behaviour should be specific to the type of the reservoir rock and fluid systems. Nonetheless, it should be mentioned that the proposed methods for a porous media with uniform pore size distribution would help to disclose some of the main features of the interactions between fluid and pore walls.

In this study, a novel experimental framework is proposed to evaluate the extent of the impacts of confinement effects on the dew point pressure (Pdew) of gas condensate mixtures in unconventional reservoirs. The methodology implemented in this study is based on the fact that the ability of each fluid to flow in porous medium would reduce by the presence of other fluids (Honarpour and Mahmood, 1988). Accordingly, effective Pdew of a gas condensate system in porous medium is considered to be the pressure, at which the effective permeability of the injected gas into the core is reduced which is the result of the appearance of the second phase in the core in pores which contribute to the flow of the fluid. Based on this conjecture, measured Pdew is an effective value reflecting the overall fluid flow within porous medium. In other words, in a core sample, there might be some very small pores which are filled by condensate, but do not contribute significantly to the overall flow of the sample. These pores, due to the effects of capillarity might be filled with liquid earlier than those pores which contribute to flow. However, in this study, the effective Pdew in porous medium is not dependent on such pores because they do not have significant contribution to the production. As a result, having smaller pore size distribution may not be necessarily related to higher extent of pore confinement effects on effective Pdew of gas condensate mixtures in porous medium. The effective Pdew of fluids within conventional reservoirs are expected to be relatively the same as those of the bulk Pdew due to negligible influence and interactions of pore walls and fluids molecules. However, in unconventional reservoirs, due to non-negligible interactions between fluid molecules and pore walls, it is expected that the effective Pdew of the gas condensate mixtures in porous medium to be different from those observed in bulk state. In essence, the framework consists of the following three main steps:

1- Measurement of the bulk dew point pressure (Pdew) of the considered fluid sample. This step is quite important as the accurate measurement of the bulk Pdew is necessary to find out the extent of the difference between confined and bulk Pdew.

2- Measurement of Pdew in the chosen porous medium.

3- Comparing the results of the bulk Pdew value and the Pdew value measured in the porous medium. If there is a difference between these two values, then it can be concluded that fluid confinement effects influence the Pdew of the gas condensate samples.

These steps will be discussed extensively in later sections of this chapter. At this stage, some preparatory experimental stages which have been performed are discussed.

3.1 Gas Condensate Mixture Preparation

In order to confirm the existence of pore confinement effects, to validate the proposed method for measuring confined Pdew, and also to examine the impacts of the fluid composition on the extent of pore confinement effects, different types of binary and ternary gas condensate fluids were prepared. These fluids were mainly consisted of methane, as the abundant component existing in gas condensate reservoirs, with one or two heavier hydrocarbons like nC5, nC8 and nC10. Also, in this study, C2 was used as the single component which did not require any preparation and could directly be used for the experiments.

In order to prepare each gas condensate sample, after cleaning and vacuuming the rocking cell, a known amount of methane (based on its molar density) at room temperature but at a pressure well above the simulated bulk dew point pressure of the mixture, was injected into the cell. After leaving it for 24 hours to reach the equilibrium at constant pressure, other components were injected into the cell while making sure the pressure remains constant during the injection by increasing the volume of the fluid side in rocking cell. The pressure should be kept constant as the fluid volume calculation is usually performed based on constant pressure (Jalal Fahimpour, 2015). After injecting other components, the cell was left for at least 3 days. During this time, the rocking cell needs to be shaken occasionally, in order to facilitate the proper mixing of the components. All the data for the properties of the components used for the gas condensate sample preparation, i.e. fluid molar density and viscosity at each pressure, were collected from National Institute of

Standards and Technology (NIST) website. Gas condensate mixtures composition are summarized in Table 3.1.

Table 3.1: The composition of gas condensate mixtures used in this study.

Fluid	Composition (mole fraction)			
	C1	nC5	nC8	nC10
F1	0.896	0.104	0	0
F2	0.86	0.14	0	0
F3	0.922	0.078	0	0
F4	0.946	0.054	0	0
F5	0.92	0	0	0.08
F6	0.959	0	0	0.041
F7	0.923	0	0.077	0
F8	0.9	0	0.1	0
F9	0.951	0	0.049	0
F10	0.92	0.04	0	0.04

3.2 Core Samples Characterizations

In this study, two different types of shale rocks (from Eagle Ford and from Barnett shale reservoirs) were used for the study of pore confinement effects on the Pdew of fluids in porous media which are classified as unconventional reservoirs. In this study three different shale core samples (i.e. EF1 and EF2 from Eagle Ford and B1 from Barnett) were used. Core sample EF1 was used for method validation and preliminary experiments, while the majority of the main experiments to investigate the effects of pore confinement were conducted using core samples EF2 and B1. It should be noted that core samples EF1 and EF2 were collected from the same sections. These dried samples were received from Kocurek Industries and were by origin cut parallel to bedding. Also, two tight core samples, namely, Edward White and Crab Orchard with a permeability higher than the shale core samples were used for method validation. All the core samples were in 1.5 in diameters. Figure 3.1 shows the pictures of the core samples used in this study.

(a) (b) (c) (d)

Figure 3.1: Core samples used in this study, (a) EF1, (b) B1, (c) Edward White, and (d) Crab Orchard

Before conducting any pore confinement experiment, different characterization tests, including total organic carbon (TOC), X-ray Diffraction (XRD) analysis, Mercury injection capillary pressure (MICP), Scanning electron microscopy (SEM) as well as porosity and apparent permeability measurement tests were carried out on the shale rock samples. Porosity measurement experiments as well as all permeability measurement experiments were performed in our Gas Condensate Recovery lab while other characterization tests were performed by external companies.

The porosity of the core samples used for the measurement of the Pdew in porous media was measured by using the helium gas and Boyle's two cell porosimetry method (Nazari Moghaddam, 2016). Before performing any measurement, the core samples were placed in the oven at 105 °C while being connected to a vacuum pump to remove any fluid residue inside the core as much as possible and to make the fluid pressure inside the core to be close to zero. For porosity measurement the overburden pressure was set to be 500 psi while the helium pressure at which the measurement was conducted was set to be 100 psi. Helium porosimetry calculations is based on the ideal gas law, hence helium pressure should be as low as possible so that it behaves more similar to ideal gases. For each core, several porosity measurements, usually 5 experiments, were carried out to ensure a reliable value is obtained by making sure that helium transfer is established in all cells and the core.

The apparent permeability of the core samples was measured using steady state method. After cleaning the cores by injecting several pore volumes of methane, the rig was connected to a vacuum pump for at least 3 hours to ensure the system was completely vacuumed. Methane, as it can dissolve hydrocarbon, is usually used to clean the cores which are tight and may have traces of hydrocarbons in them. Hence, methane is the most

common gaseous solvent for hydrocarbons. The steady state apparent permeability measurement was then conducted at fluid pressure of 2500 psi and with the net stress value of 500 psi using nitrogen as the fluid. The apparent permeability of the unconventional and tight core samples is dependent on the fluid pressure inside the core as well as the net stress. Most of the experiments conducted for the effects of pore confinement, were carried out at pressures close to 2500 psi and the net stress was 500 psi except for those tests which were conducted to investigate the effects of net stress on pore confinement. Moreover, to have a basis for comparison of the apparent permeability of the core samples, this pressure was fixed for all the cores used in this study. As will be discussed in Section 4.1, for exploring the impacts of pore confinement on the phase behaviour of single component fluids, the apparent permeability of the core is also required to be measured. Similar approach for the measurement of the apparent permeability of the core was followed, except the fluid pressure values, which was dependent on the range of the saturation pressure inside the core.

It should be noted that prior to any porosity and permeability measurement performed in this study, it was made sure that the experimental facilities were leak tight at high pressures.

Total organic carbon (TOC) measurements, X-Ray diffraction (XRD) analysis, mercury injection capillary pressure (MICP), and scanning electron microscopy (SEM) tests were carried out on shale samples by external companies. The samples used for these characterization tests which were performed by external companies, were obtained from the same sections as those core samples used for porosity, permeability and effective permeability measurement tests (EF1, EF2, and B1). In other words, for these characterization experiments, two sets of data are reported for the two shale rock types used in this study. TOC analyses were performed on 1 g portions of ball-milled rock ground powder. To remove any inorganic carbon including carbonate minerals, the rock samples were firstly treated with hydrochloric acid. Then the samples were heated by a flow of a very hot oxygen in a carbon/sulphur analyser. Any carbon present in the samples would then be converted to carbon dioxide, which was measured by an infra-red detector. The carbon content was then calculated with respect to the original sample weight. The lower detection limit for the method is 0.2% TOC. Considering that the TOC of both samples are higher than 2.0 wt%, they can be considered as very good source rocks (Jarvie, 2012; S. Zhang *et al.*, 2018), which confirms they are suitable for the purpose of this study and previous studies performed in our group (Nazari Moghaddam, 2016).

Table 3.2 shows the basic properties of the shale core samples used in this study. Several core plugs were obtained from the Kocurek and the range of the measured values for porosity and permeability of the core samples (not only the ones used in this study but also those that have been tested before) are presented in Table 3.2. As mentioned earlier, TOC analyses were performed on powdered rock samples which are obtained from the same rock sections as of the core samples (i.e. EF1, EF2 or B1).

Table 3.2: Basic properties of the shale core samples used in this study.

Shale sample	TOC (%)	Porosity range (%)	Permeability range (mD)	Moisture condition
Eagle Ford	3.28	5 - 15	10^{-3}	Fully dry
Barnett	11.40	5 - 15	10^{-3}	Fully dry

XRD analysis was performed to obtain the Mineralogy of the samples. British Geological Survey (BGS) performed the quantitative whole-rock powder XRD analyses of the shale samples. Similar to TOC analysis, the samples used for XRD analysis were from the same section as those core samples used in this study. Table 3.3 summarizes the results of whole-rock powder XRD analyses. As it can be observed, the mineralogies of the two samples were in different ranges. The Eagle Ford sample primarily consist of calcite minerals while having notable quantity of quartz and also small amount of clay minerals in forms of mica and kaolinite. The Barnett sample, on the other hand, is mainly comprised of quartz minerals with higher phyllosilicates/clay minerals content as compared to the Eagle Ford sample. It is suggested that there is a direct relationship between the silicate content of a rock and its TOC. Moreover, higher carbonate content of a rock is usually associated with lower TOC. The comparison between the results of the TOC measurement and the mineralogy of the shale samples confirms this notion (S. Zhang *et al.*, 2018).

Table 3.3: Mineralogy of the shale samples obtained from whole-rock XRD analyses.

Shale sample	Silicates			Carbonates			Phyllosilicates/Clay minerals				Others		
	Quartz	Plagioclase	K-feldspar	Calcite	Dolomite	Siderite	Mica**	Kaolinite	Chlorite	Smectite	Pyrite	Fluorapatite	Gypsum

Eagle Ford	27.1	nd*	<0.5	68.4	nd	nd	1.0	1.6	nd	nd	<0.5	nd	1.2
Barnett	55.3	nd	nd	nd	nd	1.1	32.0	1.0	2.0	nd	0.8	7.8	nd

* Not detected

* Undifferentiated mica species possibly including muscovite, biotite, illite, and illite/smectite.

There are different methods to evaluate the pore structures of the unconventional porous media. These methods may be broadly classified into two main groups, namely observation description and fluid penetration methods.

Observation description methods, are referred to those which by the use of radiation techniques or optical visualizations, the pore structure of the porous media is directly observed and described. The most widely used methods which fall into this category are Scanning Electron Microscopy (SEM), Transmission Electron Microscopy (TEM), Nuclear Magnetic Resonance (NMR) and Small Angle X-Ray Scattering (SAXS).

On the other hand, in fluid penetration techniques a fluid is introduced into the porous media and its pore size distribution is obtained indirectly from fluid pressure, volume and/or mass. The most widely used methods in the fluid penetration techniques are Mercury Injection Capillary Pressure (MICP), liquid nitrogen adsorption and CO2 adsorption.

Core Laboratories Ltd., by employing Micromeritics Autopore V. apparatus, measured the capillary pressure of the core samples by the use of MICP method which was performed at very high pressures up to 55000 psi. For drainage, the non-wetting phase, i.e. mercury, was injected into the core sample. Initially, at low pressures, the incremental pressure increase for mercury injection was 0.5 psi. The corresponding value for higher pressures increased up to 25.0 psi. While keeping the injection pressure constant, the amount of invaded mercury was monitored. The system was considered to be in equilibrium if the difference between the injection pressure and the system pressure was less than 0.5% over a period of 60 seconds. In case of the increase in the difference, the pressure was again reset to the target pressure point until reaching equilibrium. This equilibration step is repeated at each pressure (Technical Writing, 2017). The MICP tests were conducted on thin rock samples of the two types (Eagle Ford and Barnett) of the shale rocks. Thin rock samples were obtained from the same sections as of the cores used for the pore confinement effects experiments.

Figure 3.2 illustrates the results of the capillary pressure measurements which were used to obtain pore throat size distributions for respective samples. For the simplicity, from now on, pore throat size distribution obtained from MICP is referred to as pore size distribution. As it can be observed, almost all of the pores of the Eagle Ford shale sample was filled by mercury. However, mercury was not able to fill nearly 40% of the pores of the Barnett shale sample even at the pressures as high as 55000 psi, which is equivalent to pore throat radius of 2 nm, indicating that nearly 40% of the pores are less than 2 nm in radius.

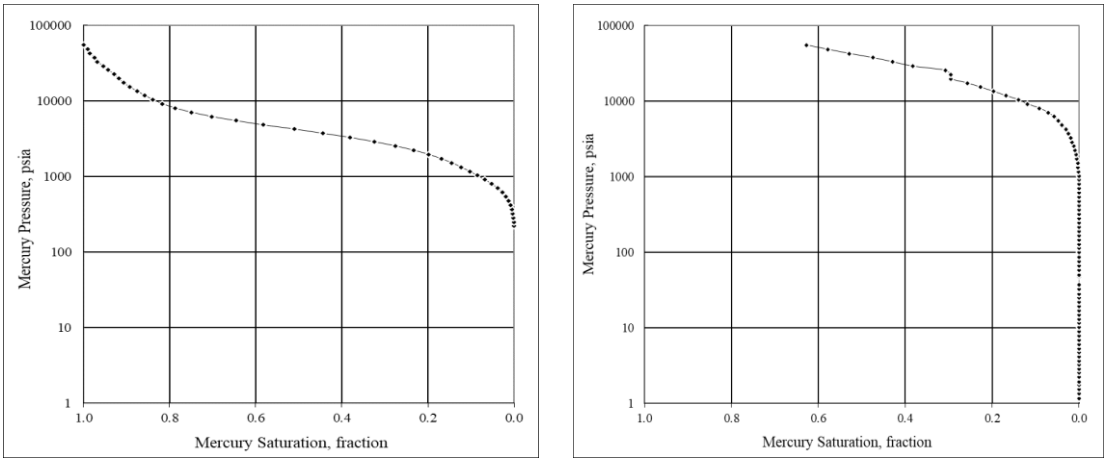

(a) (b)

Figure 3.2: MICP measurement results of (a) Eagle Ford and (b) Barnett rock samples.

Pore size distribution of the shale samples were obtained using MICP data. The pore radius can be obtained using the following capillary pressure equation (Washburn, 1921).

$$r = \frac{2\sigma cos\theta}{P_c} \qquad \text{Eq. 3.1}$$

where σ is interfacial tension between air and mercury (485 dynes/cm) and θ is contact angle between air and mercury (140°). A graph with the differential of a plot of pore volume injected versus pore throat radius would give a pore throat size distribution (PSD) function.

In this study, average pore size distribution of the core samples was estimated based on the measured pore size values. To do so, well known probability distribution functions were considered to find the best fit for the measured pore sizes. The advantage of using these distribution functions was that they could contain all pore size ranges (Nazari Moghaddam, 2016). This was particularly important for the case of the Barnett shale sample which 40% of its pores were not saturated during MICP measurements. In other

words, with employing probability distribution functions, those pores which were not filled with mercury will be considered in the estimation of the average pore size values.

As illustrated in Figure 3.3, the normal distribution and Gamma distribution functions are considered to be the best probability functions that can be fit to the pore sizes of the Eagle Ford and the Barnett shale samples, respectively. Table 3.4 summarizes the mean and standard deviation of the fitted probability distribution functions for the pore sizes of the shale samples. In this study, average pore radius values of the shale samples were considered to be equivalent to their mean pore size values.

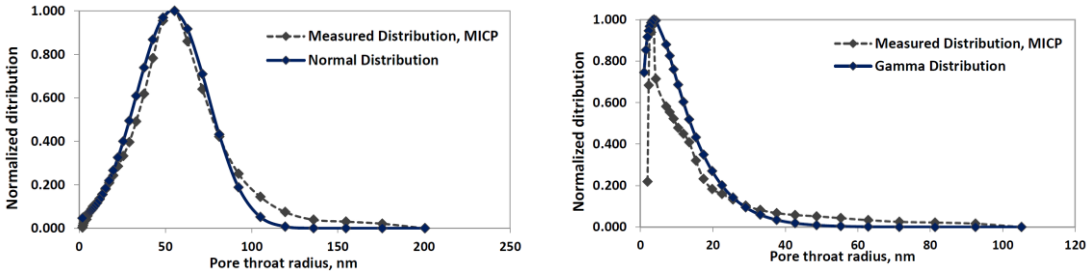

(a) (b)

Figure 3.3: Pore size distribution of (a) Eagle Ford, and (b) Barnett shale core samples with the best identified probability function

Table 3.4: The statistical parameters of the distribution functions fitted to the MICP pore size distribution measured on core sample used in this study and best fitted probability function.

Shale sample	Probability function	Mean (μ)	Standard deviation (σ)
Eagle Ford	Normal	54 nm	21 nm
Barnett	Gamma	11.25 nm	9.2 nm

SEM of the Eagle Ford shale sample was performed in this study. SEM can give valuable information on pore structures of the shale matrix especially during the study of the geomechanical effects on the shale matrix permeability where the additional data for rock fabric and distribution of organic materials and minerals can provide useful information (Dong *et al.*, 2018). Generally, there are two different main types of pores which exist in shale rocks. These groups can be classified as non-organic pores (which can also be found in conventional rocks) and organic pores. Also, in shale reservoirs, there are microfractures (MF) which can be considered as effective pores. The impacts of microfractures are significant especially in the fluid flow within unconventional shale

rocks. It is noted that these microfractures could be the products of the coring and post-coring processes. The SEM image of the polished thin sections of Eagle Ford shale is shown in Figure 3.4. As depicted in this figure, microfractures can be observed as shown by the red arrows. The contribution of these microfractures in fluid transport and the stress dependent behaviour of the shale rocks is significant (Nazari Moghaddam, 2016).

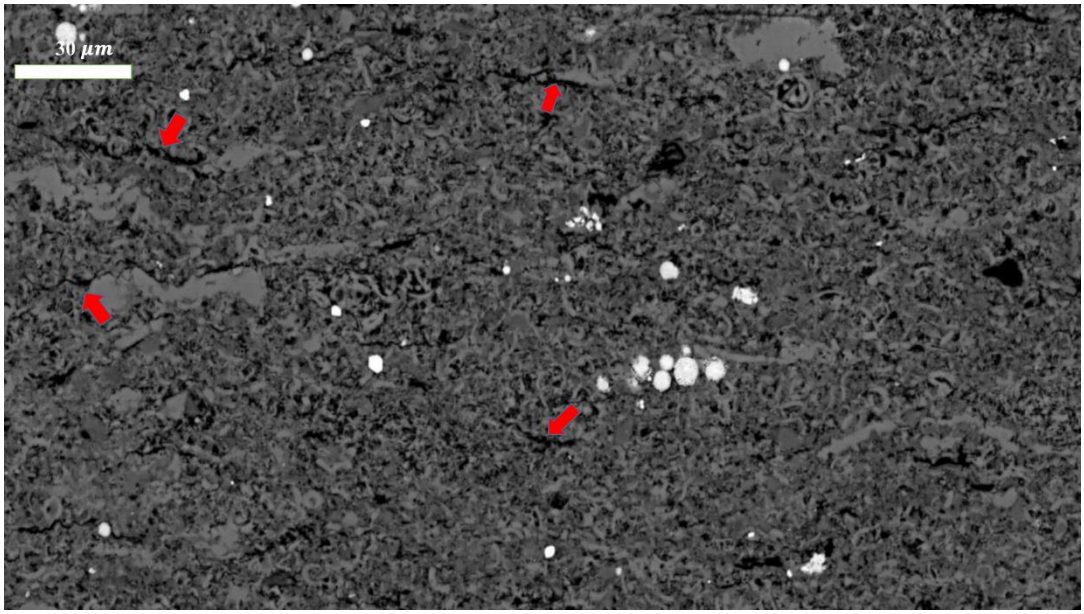

Figure 3.4: SEM image of the Eagle Ford shale sample which shows the interparticle microfractures (MF) by red arrows.

In addition to MFs, other types of non-organic pores such as interparticle and intraparticle pores can be detected in the SEM image of the sample. More information about the types of the pores can be observed in Figure 3.5. In Figure 3.5 (a) the length of the illustrated microfracture is approximately 60 μm. Figure 3.5 (b) shows the interparticle pore types denoted by the yellow arrows. These types of pores are usually associated with the primary pore network. These pores are the most common pore type found in the Eagle Ford (Nazari Moghaddam, 2016). Green arrows in Figure 3.5 (c) show the intraparticle pores. These pore types are considered to be the pores that exist within the boundary of a matrix grain. Framboidal pyrite type of pores is also shown in Figure 3.5 (c). These types of pores which are a subgroup of intraparticle pores, can be formed due to clustering of the grains. As it can be observed, framboidal pyrite types of pores can be easily noticed. t should be highlighted again that, in this research, TOC, XRD and SEM measurements were carried out by external companies.

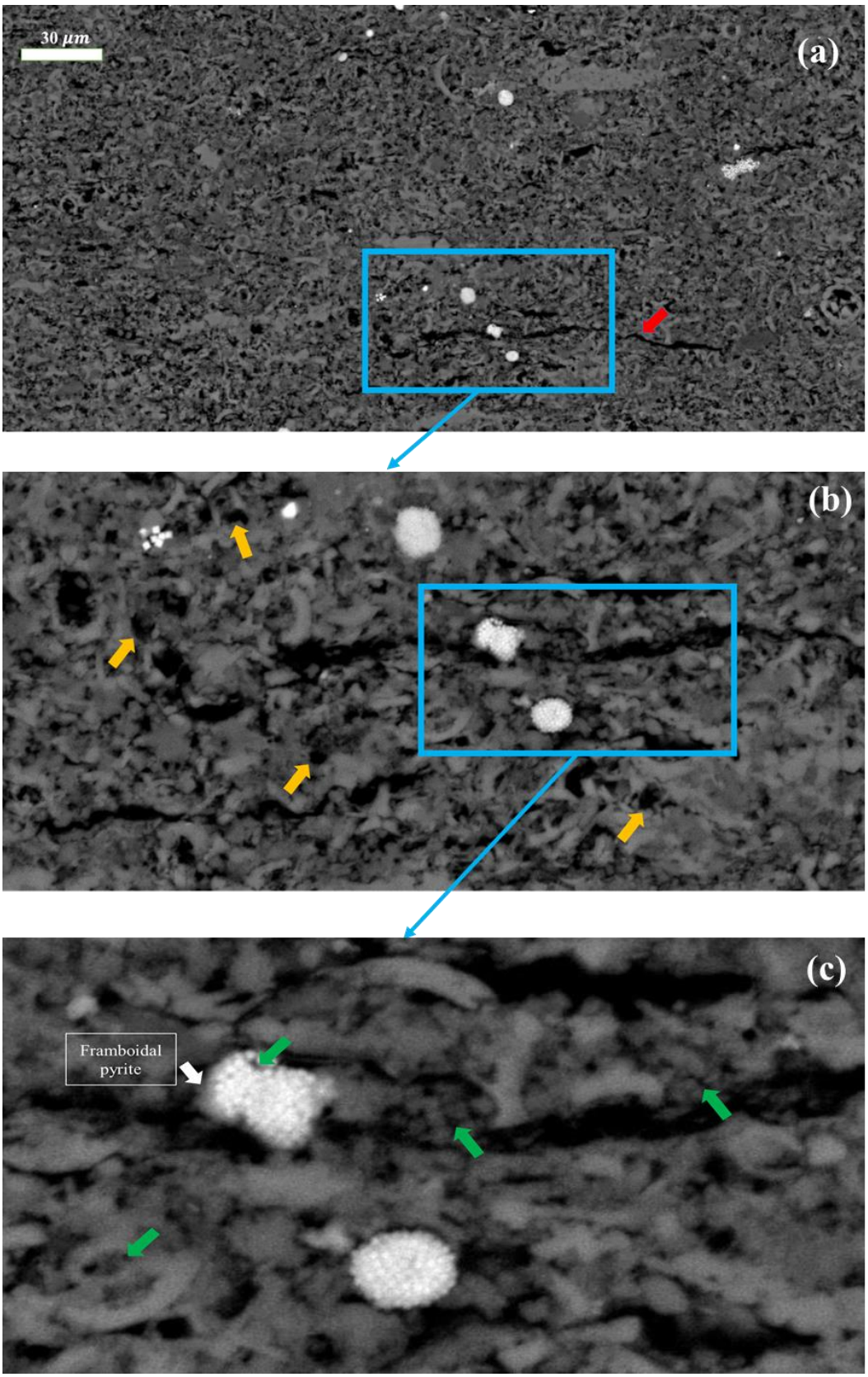

Figure 3.5: SEM Images of the Eagle Ford shale sample. Presence of framboidal pyrite and finer sediments inside a microfracture (shown by white arrows) which decreases the possibility of fracture propagation during the core preparation.

3.3 Bulk Dew Point Pressure Measurement

After preparing the fluid samples, the first experimental measurement step involves measuring the bulk Pdew of the prepared gas condensate samples without the presence of any porous medium. Measuring the bulk Pdew of the samples is an essential part of the measurements and great care and attention were taken to measure bulk Pdew accurately. For instance it should be considered that the pressure drop condensation (a phenomenon which occurs in experiments due to sudden decrease in pressure to values below the Pdew of gas condensate mixture which results in the appearance of condensate in the system) does not occur. Also, the process of reducing the fluid pressure should be as low as possible. Moreover, visual observations should be made so frequently as to prevent Pdew to be missed. A bulk Pdew measurement of gas condensate mixtures was based on conventional visual method and was conducted in an in-house modified phase equilibria apparatus. A schematic of the phase equilibria apparatus is shown in Figure 3.6. It should be mentioned that the employed PVT cell is equipped with 3 sight glasses positioned in different heights to capture the images inside the cell. These sight glasses are used to observe Pdew of the gas condensate mixture and measure its liquid drop.

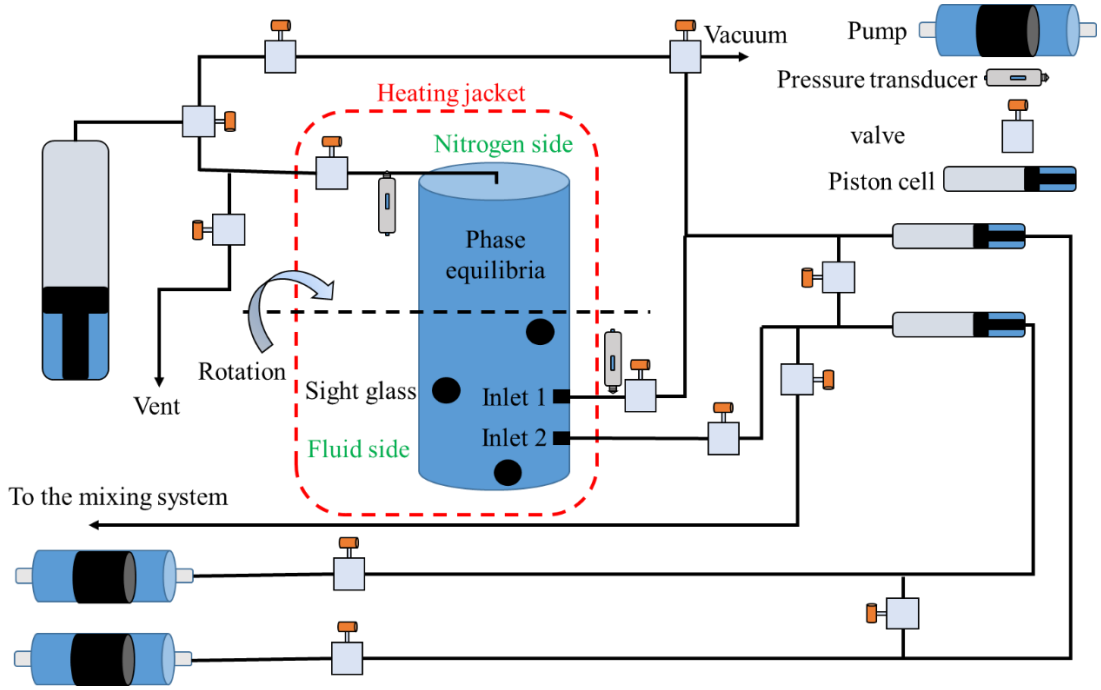

Figure 3.6: A schematic representation of the phase equilibria measurement apparatus used in this study.

Prior to transferring the GC fluid to the phase equilibria cell and measuring its bulk Pdew, the cell was cleaned by flushing methane at high pressure several times. Methane was used to remove any residual hydrocarbon fluids remained in the PVT cell. Then the visual cell was vacuumed. Next, the single phase gas condensate mixture was injected at a pressure well above the estimated bulk Pdew (the pressure values used in this study were at least 500 psi higher than the estimated Pdew) into the phase equilibria cell. In this study, estimated Pdew for each gas condensate sample was obtained from PVTi module of Eclipse Schlumberger Software Package. The cell was initially filled with methane to prevent pressure-drop condensation after the injection of the single-phase (which is in gas phase) gas condensate mixture. When a gas condensate fluid is introduced into a container which can be a PVT cell, fluid cell or even a porous medium, if the pressure inside the container is lower than the Pdew of the injected gas condensate at single gas phase, the gas condensate fluid experiences a sudden pressure drop which might result in the condensation of the liquid from the gas condensate sample. In this study, this phenomenon is referred to as pressure-drop condensation. If pressure-drop condensation is not prevented, the composition of the gas condensate sample would significantly change which results in the significant error in the measurement of gas condensate fluid properties including its Pdew. The injection of the single-phase continued until all initial methane was displaced through the venting system. This was achieved by displacing methane with single-phase gas condensate mixture volume equal to 2 PV of the visual cell (PV of the visual cell is 13 cc).

The visual cell temperature was then increased from room temperature to the desired value and the fluid was left in the cell to stabilize at least for 1 day. The desired temperature values were equivalent to the test temperatures. In this study, all the tests except those performed for the effects of temperature, were conducted at 20 °C to avoid complications on the performing and maintenance of the experimental set up. For those experiments performed for the effects of temperature, depending on the test temperatures, desired temperatures could be 20, 40 or 60 °C. The cell was then subjected to pressure drop by increasing the volume using a piston located at the top of the visual cell and controlled by nitrogen pressure. The position of the piston which could give the information about the volume of the fluid was monitored through the digital panel on the instrument. Through retraction on the nitrogen side, the pressure on the piston side was reduced and as a result the piston was moved upward and accordingly the volume of the fluid side increased and its pressure reduced. The dew point is a considered to be a point

at which a sudden change in the appearance of the fluid is observed. This change in the appearance is denoted as the formation of a cloud like phase in the cell. The rate of the pressure reduction in this study was maintained as low as possible in order to measure the bulk Pdew accurately. From the initial cell pressure until reaching the 100 psi above the predicted Pdew, the pressure was set to reduce at a rate of 5 psi/min, meaning that it would take 80 minutes to reduce the pressure by 400 psi. Further reduction in the pressure was carried out at a maximum rate of 1 psi/min. It is very important to reduce the pressure very slowly for two main reasons: the first reason is to make sure that the exact Pdew is not missed and secondly to make sure that the fluid is at relative equilibrium at all time during the bulk Pdew measurements. The set up was equipped with quartzdyne transducer with accuracy of 0.015% FS. Also, the temperature accuracy of the instrument was 0.1 °C. The measured bulk Pdew as well as maximum liquid drop out (MLDO) for the considered gas condensate mixtures at 20 °C are summarized in Table 3.4.

Table 3.4: Measured bulk Pdew and MLDO at 20 °C for the gas condensate mixtures used in this study.

Fluid	Bulk Pdew (psi)	MLDO (vol% of Vsat)	Corresponding pressure to MLDO (psi)
F1	2392	13	1750
F2	2493	25	2000
F3	2213	7	1500
F4	1891	3	1200
F5	5784	29	5050
F6	5264	14	3050
F7	4052	24	3000
F8	4110	31	3250
F9	3783	13	2600
F10	4538	18	4100

3.4 Porous Media Dew Point Pressure Measurement for Gas Condensate Mixtures

In this study, for the first time, a novel method for measurement of Pdew in porous media is presented. As mentioned earlier, this method is based on the change in the effective permeability of the injected gas in the presence of the liquid condensate phase in the porous medium. A steady state effective permeability measurement core-flood experimental set up was used with its schematic diagram depicted in Figure 3.7. The set up was equipped with the quartzdyne pressure transducer with the accuracy of 0.015% FS (Sensor Full Scale Error). Also, the dead volume of the core holder and lines was tried to be reduced to minimum using 1/16” lines. Although, in theory, the dead volume of the permeability measurement set up would not affect the pressure readings and hence the

permeability values, having high dead volume, could introduce slight errors on the measured pressures due to the large volume of fluids being present in the lines and fittings which are not contributing to the flow within porous medium. The dead volume of the experimental set up was measured using Boyle's two cell method to be 1.4 cc for the core holder and fittings, 1.6 cc for the lines, valves and external connections. Considering that there is small dead volume in the system (3 cc in total), it can be considered that the measured permeability is almost error free from the effects of dead volume. Moreover, in the measurement of the effective permeability, the saturation of the phases within the core sample is not of interest. Hence, the instrument dead volume does not have any influence on the results obtained from the measurements. Fluid properties and hence the measured effective permeability is dependent on the temperature. The variation in temperature of the experimental set up during the tests was 0.1 °C which is acceptable for performing accurate effective permeability. The core flood set up implemented in this study was capable of performing the experiments for pressures up to 10000 psi and temperature up to 150 °C. This brings additional benefit to the proposed method which enables the investigation of the fluid properties in unconventional reservoirs within a wide range of pressure and temperature which is applicable for most of unconventional shale reservoirs. However, in this study, the temperature range was up to 60 C and pressure range was up to 7000 psi.

In order to conduct the experiments for multicomponent gas condensate mixtures, the following steps are needed to be carried out.

1- Flush the core with methane by injecting several (at least 5 times) of the pore volume at high pressure (at least 500 psi above the Pdew of the gas condensate used in previous experiments).
2- The pressure inside the core is then reduced to atmospheric pressure and the core will be connected to vacuum pump to make the pressure inside the core to be close to zero, to possibly remove any adsorbed phase or condensate residue from the core.
3- Pressurize the core with methane to a pressure which is at least 500 psi higher than the measured bulk Pdew of the gas condensate sample. The injection should be continued until the ΔP of the injection (difference between inlet and outlet pressure) is stable. Getting the core to be fully saturated with methane would prevent any condensation dropout due to the sudden pressure drop after introducing the single phase gas condensate mixture.

4- Inject single phase gas condensate at a pressure of at least 500 psi higher than its bulk Pdew to displace the methane inside the core until the ΔP of the injection is becomes stable which is a sign of the core being fully saturated. The volume of the injected gas condensate was at least 1.5 times of the pore volume of the core sample for the experiments conducted in this study.
5- Let the single phase gas condensate inside the core to be stabilized. This is obtained if the fluctuation of the fluid pressure inside the core recorded by pressure transducers is less than 1 psi/hr.
6- Reduce the fluid pressure inside the core to reach the target pressure point. This is achieved by retracting on the pump from outlet. Target pressure points for each fluid could be different and dependent on the results of the effective permeability measurements. The selection of each target pressure point will be discussed in more details later in this section. During performing the initial stages of the experiments to establish the suitable approach for experimental procedure, the rate of the reduction in pressure was found to be as low as 1 psi/min to make sure that the reduction was slow enough to avoid significant fluctuation in pressure inside the core and maintain the relative fluid equilibrium during the fluid pressure reduction.
7- Let the fluid inside the core to be stabilized at the target pressure. Pressure fluctuation should be less than 1 psi/hr to consider the state of the fluid inside the core to be stable. During the experiments, it was found that in order to reach such stabilization criteria, it was needed to let the core to become stable for at least 12 hours.
8- Inject nitrogen to the core from the inlet part with constant rate and retract on the outlet with constant pressure (at the selected target pressure). Nitrogen should be used to minimize the adsorption effects on the effective permeability measurement. More importantly, nitrogen does not evaporate the condensate remained in the porous medium. Nitrogen injection for each pressure step should continue until a stabilized ΔP is obtained during the injection. The equilibrium state is determined if the fluctuation of the recorded ΔP is less than 0.1 psi over 3 hours. During the preliminary experiments, it was found that the volume of the injected nitrogen should be at least 5 times of the core pore volume (5-10 times in our experiments) to make sure that nitrogen has fully displaced the gas phase inside the core and stabilized ΔP is achieved. Nitrogen should be injected at a low

rate to make the ΔP across the core to be less than 50 psi. This is important as the estimation of gas properties (viscosity estimation and compressibility difference) at average pressure would have negligible error (Darabi *et al.*, 2012). Accordingly, the optimum rate of injection for nitrogen injection was found to be 2 cc/hr for the core samples used in this study to have a ΔP less than 50 psi. Hence, for all effective permeability measurements, the nitrogen injection rate was selected to be 2cc/hr. After establishing a stabilized DP, the effective permeability is then calculated based on Darcy equation. One sample calculation for the core sample EF2 at the target pressure of 2600 psi is presented as below:

Darcy equation: $K = \frac{Q}{A}\mu\frac{\Delta x}{\Delta P}$

Stabilized ΔP measured at the end of nitrogen injection: 19.81 psi = 136605.88 pa

Q (Rate): 2cc/hr=5.56E-10 m3/s

μ (N_2 viscosity at 2600 psi, Obtained from NIST): 0.0221 cp = 0.0000221 pa.s

Δx (Core length): 5.01 cm= 0.0501 m

D (Core diameter): 3.82 cm= 0.0382 m

Hence, K in m^2 would be:

$$K = \frac{5.56E-10}{\pi \times (0.0501)^2/4} \times 0.0000221 \times \frac{0.0501}{136605.88} \cong 3.9E-18\, m^2$$

Which the obtained permeability is approximately 3.9 μD.

It should be mentioned that in this study, the net stress was kept constant (500 psi) during all the stages of the injections and during the processes of effective permeability measurement except for the cases which the effects of net stress on pore confinement was the goal of the experiments. In other words, when the pressure inside the core increased (or reduced) the respective overburden pressure increase (or decreased) as well in order to maintain the net stress.

In this study, the first point was measured at a pressure of at least 500 psi above the measured bulk Pdew. At this pressure, the fluid in the core sample is believed to be still in single phase and this is an essential part as the apparent permeability of the core must be known at the pressures close to the Pdew. The core is again cleaned and the above procedure is repeated for another target pressure point. The final pressure point is selected to be the one at which the effective permeability is reduced considerably. Each target pressure point is selected based on the measured effective permeability. If the effective permeability does not become smaller enough to consider that point as a pressure at which

condensate has been formed, the next target pressure would be lower. However, if the measured effective permeability at the target pressure is lower enough, the next target pressure will be higher until an acceptable range for the Pdew is obtained. The range between the two pressure points at which the effective permeability changes, is considered as the range where the porous medium Pdew lies in. This is based on the fact that the effective permeability of the gas considerably reduces due to the presence of liquid phase. It should be mentioned that in shale core samples, changing pore (or fluid) pressure, can change the apparent permeability of the core due to slippage effects. In these experiments performed using gas condensate mixtures, the range of the pressure intervals (the difference between two consecutive pressures as the range noted as the confined Pdew range) considered as the target pressures is less than 50 psi (in most cases around 20 psi). As it was mentioned, during all of the stages of these experiments, the overburden pressure is altered in order to make sure that the net stress is kept constant during the experiments for all pressure points. As a result, the impacts of the changes in permeability due to factors like adsorption and slippage effect is minimal and, any changes in the effective permeability could be attributed to the formation of the liquid phase inside the core samples. It should be mentioned that it takes between 2 to 6 days to measure each effective permeability point.

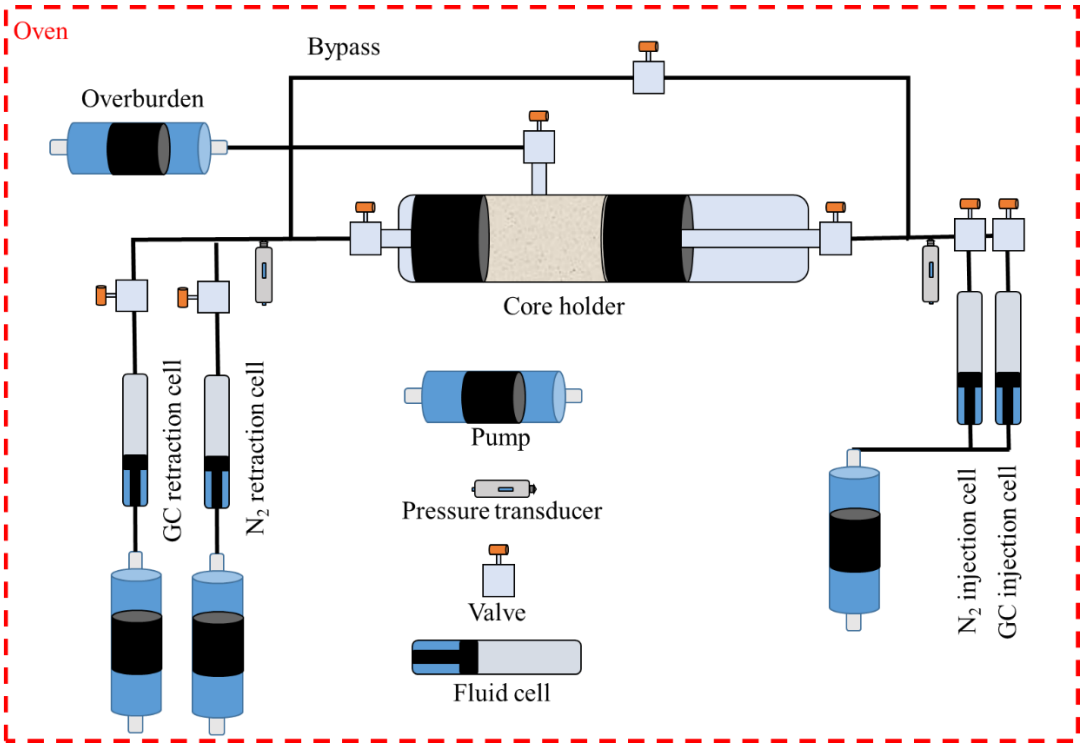

Figure 3.7: A schematic representation of the steady state effective permeability measurement apparatus used in this study.

3.5 Porous Media Dew Point Pressure Measurement for Single Component Fluids

The procedure described in section 3.1.4 was designed for gas condensate mixtures. This procedure was modified for measuring the dew point pressure of single component fluids. The modified procedure for single component fluids includes some additional steps and some modifications compared to the procedure described above for gas condensate mixtures. The main difference is related to the fact that for gas-condensate mixtures the liquid is formed when pressure drops whilst for pure components liquid is formed when pressure is increased. The initial state of the experiment should be at a point that the bulk critical pressure be higher than the starting pressure point. The set temperature (during the isotherm experiments) should also be lower than critical temperature. This affects the experimental procedure as in the former procedure for mixtures, pressure is progressively lowered as the test progresses whereas for the latter it is required to be increased. In other words, in the process presented for the gas condensate mixtures, the first pressure at which the experiment is performed, is considered to be higher than the measured bulk Pdew. However, in the case of single component fluid, the experiment starts at a pressure sufficiently below the measured bulk Pdew. Subsequent pressure points for single component fluids are higher as opposed to the gas condensate mixture where each new target pressure is lower than the previous one.

Due to many similarities to the procedure described for GC, the procedure for measuring single component fluids Pdew in a porous medium is described briefly below.

In the first step, the core is cleaned by methane similar to that followed for the gas condensate mixtures test. Then the target fluid is injected and allowed to reach a stabilised pressure well below the expected Pdew. Then pressure increases incrementally and effective permeability is measured at each pressure. This procedure continues until a considerable decrease in the measured effective permeability versus pressure is observed. However, these reductions in effective permeability is not solely related to the liquid condensation in core sample. In unconventional core samples with very low permeability, pore pressure influences the measured apparent permeability. At lower pressures, the gas permeability of unconventional core samples is higher due to the dominance of the gas slippage. In order to evaluate the results and determine the pressure at which condensation has occurred, series of single-phase apparent permeability measurements are also conducted with pore pressure being the same as those in the effective permeability measurements.

The apparent permeability measurement is not required for gas condensate mixtures, as the procedure is performed in descending pressure values. As a result, apart from performing the experiments at much higher pressures, which reduces the significance of gas slippage effects, by reducing fluid pressure at each consecutive pressure point, the measured permeability should increase if the permeability is only affected by gas slippage. Consequently, any significant reduction in permeability by reducing fluid pressure inside the core cannot be related to gas slippage and is only related to fluid condensation.

3.6 Comparison of the Bulk and Porous Media Pdew

In order to determine whether pore confinement effects would have influence on the Pdew of the confined fluid, the bulk Pdew measured in a PVT cell and that determined within a selected porous medium are compared. As mentioned in previous sections, the range of the pressure at which the effective permeability of the injected gas reduces noticeably, is considered as the pressure range at which condensation has occurred. Comparing this range with the measured bulk Pdew will show how the porous medium has affected the Pdew of the fluid. That is, if the bulk Pdew falls within the range of the porous medium Pdew, it can be considered that the pore confinement has negligible effects on the Pdew for the tested core sample. However, if the bulk Pdew, does not fall within the measured porous medium Pdew range, the change in Pdew in the porous medium is attributed to the confinement effects. In such a case, the effects of pore confinement on the Pdew and other gas condensate fluid properties cannot be ignored for further studies. Summary of the comparisons for the fluids used in this study based on the experiments conducted on core sample EF2 is presented in Table 3.5.

Table 3.5: Summary of the comparison between bulk and confined Pdew for core sample EF2

Fluid	Bulk Pdew (psi)	MLDO (%)	Range of measured confined Pdew (psi)	Difference in Pdew (psi)
F2	2493	25	2562 – 2581	69 – 88
F3	2213	7	2264 – 2281	51 – 68
F4	1891	3	1915 – 1935	24 – 44
F5	5784	29	6041 – 6063	257 – 279
F6	5264	14	5498 – 5519	234 – 255
F7	4052	24	4181 – 4205	129 – 153
F8	4110	31	4258 – 4275	148 – 165
F9	3783	13	3884 – 3904	101 – 121
F10	4538	18	4721 – 4740	183 – 202

3.7 Method Validation

In order to examine the reliability of the experimental method proposed in this study and to validate the procedure, some experiments using two types of tight and shale core samples were conducted. The goals for this exercise were: first, to examine the efficiency of the methodology which means whether it would be possible to apply the proposed method for different types of core samples using gas condensate mixtures. For a conventional core sample, we do not expect to see noticeable difference between bulk and porous media Pdew. An approach to check the validity of the proposed method, is to use a conventional core sample and measure the Pdew of a gas condensate fluid within that sample. Then, the porous media Pdew could be compared to the measured bulk Pdew. If the proposed approach is valid, there should be no noticeable difference between the two measured Pdew values. Accordingly, if for an unconventional core sample, same procedure is followed, and the measured porous media Pdew becomes different from measured bulk Pdew, the difference could be attributed to the impacts of confinement on the Pdew of gas condensate samples. Second to examine the accuracy of the methodology to evaluate if it would be possible to measure Pdew of confined fluids within an

acceptable range. For this purpose, fluid sample F1 was used to perform different experiments on 3 different core samples, namely Crab Orchard, Edward White and EF1 (an Eagle Ford shale sample). The basic properties of these core samples are summarized in Table 3.5.

Table 3.6: Basic properties of the core samples used for validation of the method proposed to measure confined Pdew.

Core sample	Length (cm)	Diameter (cm)	Porosity (%)	Permeability range (D)
Crab Orchard	7.05	3.85	7.2	6.0 E-6
Edward White	9.85	3.80	6.9	3.2 E-3
EF1 (Eagle Ford)	5.05	3.80	9.3	1.8 E-6

The apparent permeability of the core samples presented in this section was measured using nitrogen which is an inert gas at the fluid pressure of 2500 psi with the rate of 2 cc/hr. The results of the permeability measurement for these three rock samples using fluid sample F1 is presented in Figure 3.8. These measurements were conducted at 20 °C. The effective stress was 500 psi for all these measurements. The measured bulk Pdew of the fluid sample F1 was 2392 psi. For the case of tight Crab Orchard core sample with the apparent permeability of 6.0 μD, the effective nitrogen permeability was measured to be 5.9 and 5.8 μD at the pressure of 2500 and 2420 psi, respectively. This shows a reduction of only 0.1 μD, which is less than 2% reduction in the effective permeability. This difference is within the experimental error range and cannot be considered as a noticeable reduction in effective permeability caused by condensation in this porous medium. When fluid pressure inside the core reduced from 2420 to 2370 psi, it resulted in the decrease of the effective permeability from 5.8 to 4.7 μD. This is equivalent to almost 20% reduction of the apparent permeability of the core at 2500 psi. This reduction in the effective permeability is attributed to the formation of the liquid phase inside the core. Hence, the Pdew of the fluids sample F1 in the Crab Orchard tight core sample is considered to fall within the range of 2370 to 2420 psi. This range covers the measured bulk Pdew. In other words, the measured bulk falls within the range of Pdew measured in the rock, and hence it can be concluded that the effects of pore confinement on Pdew of the fluid sample F1 in the Crab Orchard tight core is negligible.

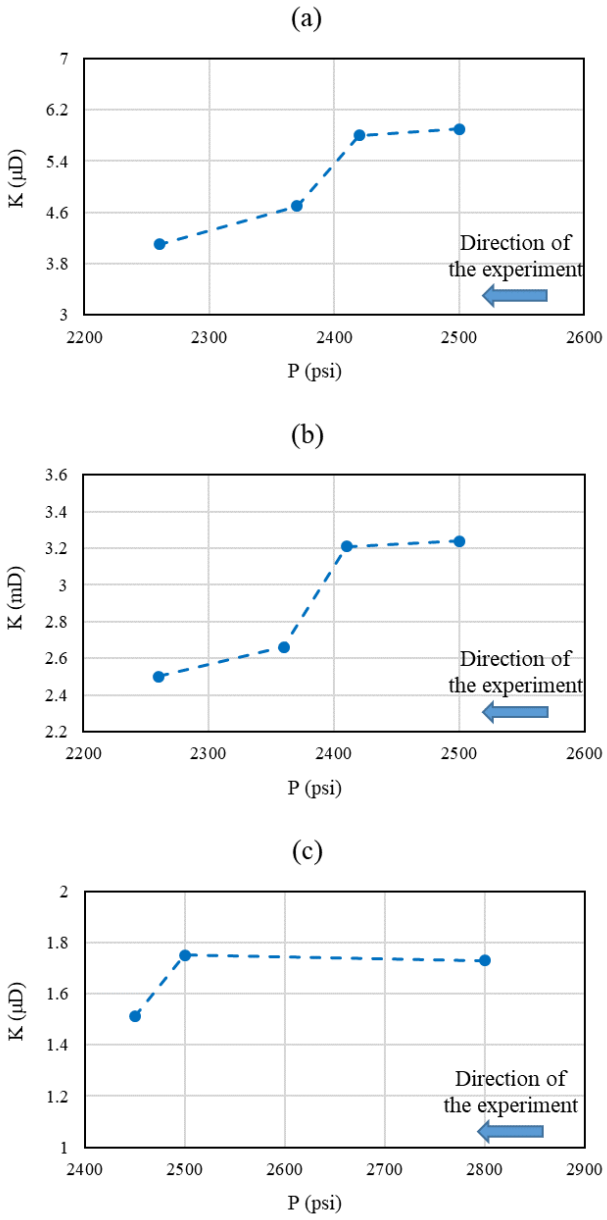

Figure 3.8: Effective permeability measured for (a) Crab Orchard tight, (b) Edward White, and (c) Eagle Ford shale core samples using fluid sample F1.

For the case of Edward White, similar approach was observed. In other words, the measured effective permeabilities at 2500 and 2410 psi were 3.24 and 3.21 mD, respectively. A very small difference in the measured permeability between the two pressure points (less than 1%) is noted which cannot be related to the formation of the liquid phase inside the core. However, further reduction in the pore pressure to 2360 psi, reduced the measured permeability to 2.66 mD, 18% reduction, which can be attributed to the existence of the second (liquid) phase inside the core. This shows that the Pdew in this porous medium falls within the range of 2360 and 2410 psi. Considering that the measured bulk Pdew of 2393 psi falls within the same range, it can be concluded that the

pore confinement has negligible effects on the Pdew of the gas condensate mixture in this rock too.

The same fluid was used for measuring the effective permeability for the Eagle Ford shale sample. As it can be observed, for the first pressure point in the experiment, i.e. 2800 psi, the effective permeability was measured to be 1.7 μD. The second pressure point was 2500 psi and the measured effective permeability slightly increased to 1.8 μD. This slight increase is mainly due to the experimental error in the measurement. When the pore pressure was reduced to 2450 psi, the measured effective permeability was reduced to 1.5 μD, which is equivalent to 13% reduction in the effective permeability. This reduction in the effective permeability can be attributed to the presence of the liquid inside the core. The results of the effective permeability measurement conducted on the Eagle Ford sample indicates that the Pdew of the gas condensate sample within this porous medium falls within the range of 2450 to 2500 psi. If this range is to be compared with the measured bulk Pdew of the gas condensate samples, i.e. 2393 psi, it can be observed that this pressure does not fall within the measured pressure range for this porous medium. These results indicate that the measured fluid Pdew within this porous medium is at least 57 psi higher than the bulk Pdew. For the sake of simplicity, from now on, if there is a difference between bulk Pdew and porous medium Pdew, porous medium Pdew is referred to as the confined Pdew.

In summary, the method presented in this study for measuring the effect of confinement on Pdew was validated using three types of core samples. Two tight core samples, i.e. Crab Orchard and Edward White, were used as well as a shale core sample. The experiments performed on the tight core samples showed that the proposed method for measuring the Pdew within a porous medium has acceptable integrity for the conventional or tight core samples showing Pdew similar to bulk Pdew.

To investigate this confinement effect, the pore size distributions of the two core samples with relatively close permeability, i.e. Crab Orchard and Eagle Ford core samples, are presented in Figure 3.9. It should be mentioned that the pore size distributions of these two samples are obtained based on the approach presented in section 3.2. It can be clearly observed that the pore size distribution of the Crab Orchard core sample with the majority of the pore throat radii being higher than 100 nm is significantly higher than that of the Eagle Ford core sample with the majority of the pore throat radii being lower than 100 nm. This confirms that confinement occurs in very small pores. However, as it will be

discussed in Chapter 4, smaller pores will not be necessarily be related to higher extent of the effects of pore confinement on the Pdew of gas condensate mixures.

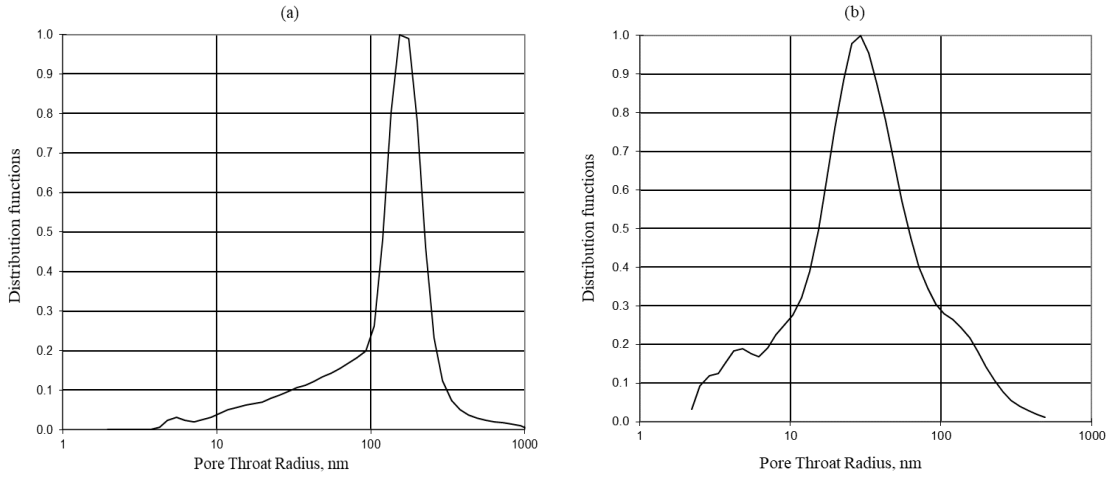

Figure 3.9: Pore size distribution of the core samples used for the validation method proposed confined Pdew measurements (a) Crab Orchard and (b) Eagle Ford core samples.

Chapter 4: Experimental Results and Discussions on the Effects of Pore Confinement on Gas Condensate Fluids Dew Point Pressure

Following verifying the experimental method as described in the previous chapter, in this chapter the results of experiments performed to evaluate the effect confinement on Pdew of a number of single component and GC mixtures fluids in several unconventional rocks under various conditions, are discussed.

4.1 Impacts of Confinement Effects on the Pdew of Single Component Fluids

In this section the results of the experiments performed on an Eagle Ford shale core sample (Sample EF2) using ethane (C2) as a single component fluid is presented and discussed. The basic properties of the EF2 core sample is presented in Table 4.1.

Table 4.1: The basic properties of the core sample used for the experiments to explore the effects of pore confinement with single component fluid.

Core sample	Length (cm)	Diameter (cm)	Porosity (%)	Apparent permeability (D)
EF2 (Eagle Ford)	5.01	3.82	15.0	4.4 E-6

As discussed in section 3.1.5, the proposed experimental method, is mainly consists of two sets of permeability measurement. Figure 4.1 shows the results of the experiments performed using ethane as the fluid sample and EF2 as the core sample at 20 °C. Net stress was kept at a constant value of 500 psi for all pressure points.

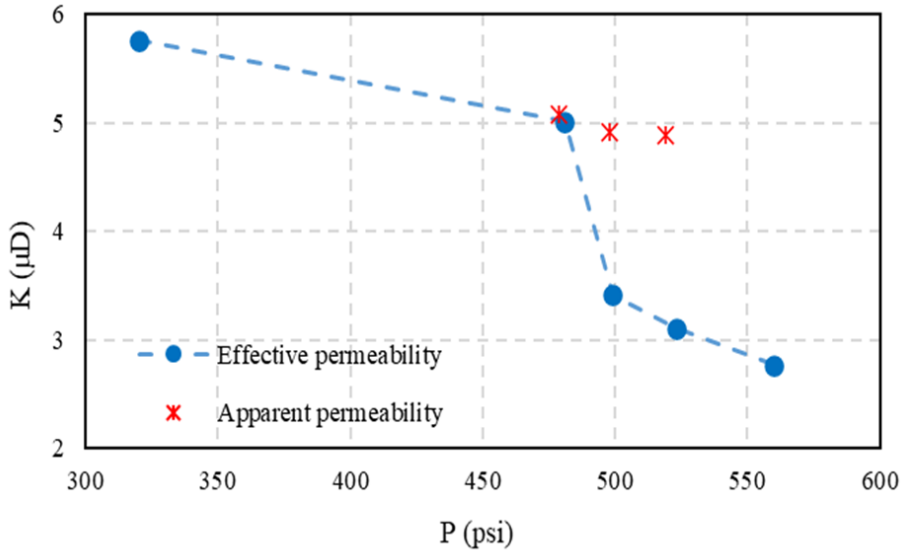

Figure 4.1: Effective and apparent permeability measured for the EF2 core sample using the single component fluid (C2).

The effective permeability of nitrogen in the presence of C2 in the core at fluid pressures of 320, 481, 499, 523, and 560 was measured to be 5.8 μD, 5.0 μD, 3.4 μD, 3.1 μD and 2.8 μD, respectively. By increasing pressure at each point, the effective permeability reduces. However, these reductions in pressure is not solely related to the liquid condensation in core sample. In unconventional core samples with very low permeability, and at lower pressures, the gas permeability is higher due to the dominance of the gas slippage. In order to determine the exact pressure at which condensation has occurred, series of single-phase apparent permeability measurements were also conducted with pore pressure being the same as those in the effective permeability measurements. As it can be observed in Figure 4, the apparent permeability of the shale core sample for pressures of 479, 498 and 519 psi was measured to be 5.1 μD, 4.9 μD, and 4.9 μD. Comparing these values of apparent permeability with the values of effective permeability, reveals that there is a noticeable difference between the measured effective permeability and apparent permeability from the pressure of 499 psi. This indicates that, Pdew of the C2 fluid sample in this porous medium lies between 481 and 499 psi which is at least 46 psi lower than the C2-bulk Pdew value of 545 psi at 20 °C. It should also be mentioned that, confined Pdew in porous media, for single component fluids, is less than bulk Pdew. This observation is in line with those reported in literature. That is, as noted in Chapter 2, many studies have indicated that the saturation pressure of the single component fluids decrease due to the confinement effects. However, those measurements were performed in synthetic homogenous nano-pores whilst this is for the first time in this research that the

Pdew of the single component fluid is measured within a real core sample. Additionally it will be shown later that an opposite trend is observed for GC fluid where confined Pdew is higher than bulk Pdew.

4.2 Impacts of Confinement Effects on the Pdew of Gas Condensate Mixtures

In this section, the results of the effective permeability measurement experiments using various gas condensate mixtures are presented. The impacts of different parameters, including fluid type and composition, temperature, net stress, and rock type on the extent of the effects of confinement on the phase behaviour of gas condensate mixtures are discussed. It should be mentioned that for all the experiments presented in this study, at least 4 pressure points were measured. Many of the experiments required 6 or 7 points to obtain the range of Pdew in porous medium.

4.2.1 Impacts of Fluid Type and Composition on Pore Confinement Effects on the Pdew of Gas Condensate Mixtures

Nitrogen effective permeability measurements for the EF2 core sample using fluid samples F2, F3, F4, at 20 °C were performed. Figure 4.2 shows the results of the corresponding effective permeability measurements. It should be mentioned that in these experiments, the net stress was maintained to be 500 psi during all the stages of these experiments.

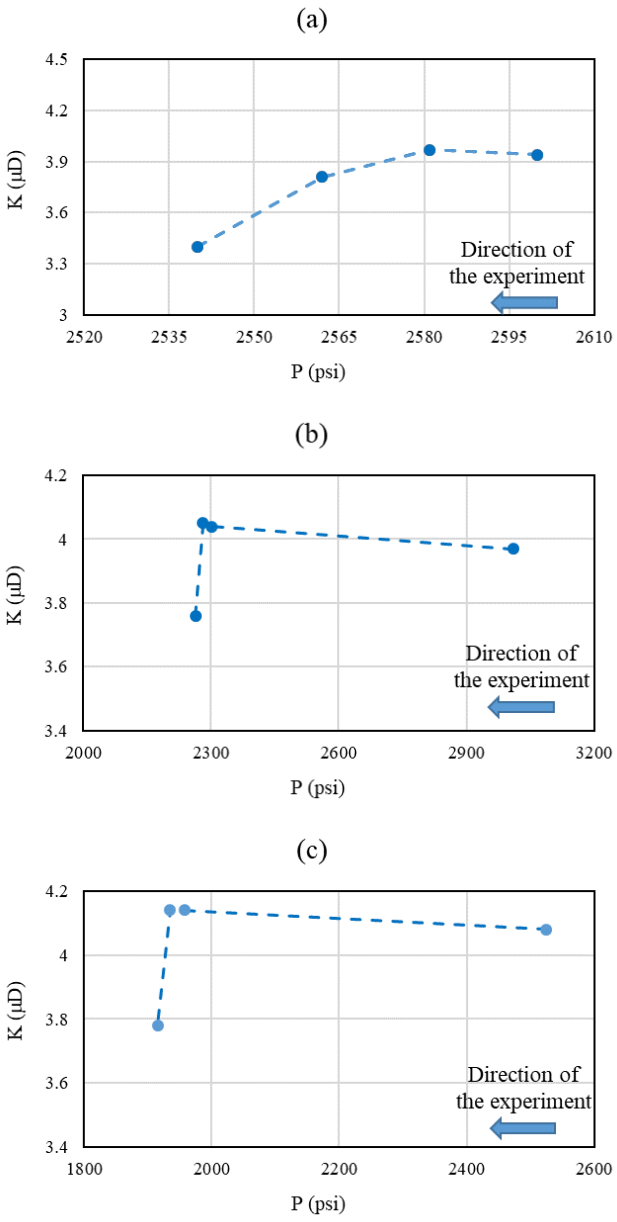

Figure 4.2: Effective permeability measurement for EF2 core sample using (a) Fluid sample F2, (b) Fluid Sample F3, and (c) Fluid sample F4.

From Figure 4.2 (a), it can be observed that in the case of fluid sample F2, the nitrogen effective permeability is 3.9 and 4.0 µD at the pressure points of 2600 and 2581 psi. When the pore pressure is at lower values of 2562 and 2540 psi, the effective permeability is at lower values of 3.8 and 3.4 µD, respectively. The effective permeability for the pore pressure of 2562 is 6% lower than the measured effective permeability for the pore pressure of 2581 psi. This shows that the confined Pdew of the fluid sample F2 falls within the range of 2562 to 2581 psi. The measured bulk Pdew of the sample is 2493 psi and compared to the range of the confined Pdew, it can be observed that the confined Pdew is at least 69 psi higher than the measured bulk Pdew.

A similar observation can be made for the fluid sample F3 as shown in Figure 4.2(b). The measured bulk Pdew for this sample is 2213 psi and the confined Pdew of the sample falls within the range of 2264 to 2281 psi as the nitrogen effective permeability reduces from 4.1 μD at the pressure point of 2281 psi to 3.8 μD at the pressure point of 3.8 μD. This shows that the effective permeability of the nitrogen reduces by 7% when the pore pressure drops from 2281 to 2264 psi. Comparing the values obtained for confined and bulk Pdew, it can be observed that the measured confined Pdew is at least 51 psi higher than the measured bulk Pdew.

The results for the fluid sample F4, shown in Figure 4.2(c), demonstrate that the confined Pdew falls within the range of 1915 to 1935 psi where the nitrogen effective permeability reduces by 9% from 4.1 μD to 3.8 μD for the pore pressure points of 1935 and 1915, respectively. Hence, the confined Pdew of the fluid sample F4 is at least 24 psi higher than its bulk Pdew. Table 4.2 summarizes the results of the experiments for the effective permeability measurements performed for the EF2 core sample using various C1+nC5 binary mixtures.

Table 4.2: A summary of the results of the effective permeability experiments for the EF2 core sample using three binary mixtures of C1+nC5.

Fluid	Composition (mole %)		Bulk Pdew (psi)	MLDO (%)	Range of measured confined Pdew (psi)	Difference in Pdew* (psi)
	C1	nC5				
F2	86	14	2493	25	2562 – 2581	69 – 88
F3	92.2	7.8	2213	7	2264 – 2281	51 – 68
F4	94.6	5.4	1891	3	1915 – 1935	24 – 44

*Difference in Pdew = Confine Pdew – Bulk Pdew

From Table 4.2, it can be observed that, for the binary mixtures comprising C1+nC5, when the concentration of the nC5 increases, and the MLDO of the gas condensate mixture increases and it becomes richer, the difference between the confined Pdew and bulk Pdew increases as well. This could be as a result of the higher interactions between heavier molecules and the pore walls which intensifies the extent of the impacts of pore confinement effects on gas condensate mixtures phase behaviour and Pdew. That is, the minimum difference between bulk and confined Pdew increases from 24 psi to 69 psi when the nC5 mole fraction in binary mixture increases from 0.054 to 0.14. These results confirm a unique trend for the extent of the Pdew changes due to pore confinement effects.

The study of the impacts of fluid composition was further investigated by using other types of binary gas condensate mixtures. The results of the effective permeability measurement for two different binary gas condensate mixtures comprised of C1 and nC10 (fluid samples F5 and F6) are shown in Figure 4.3.

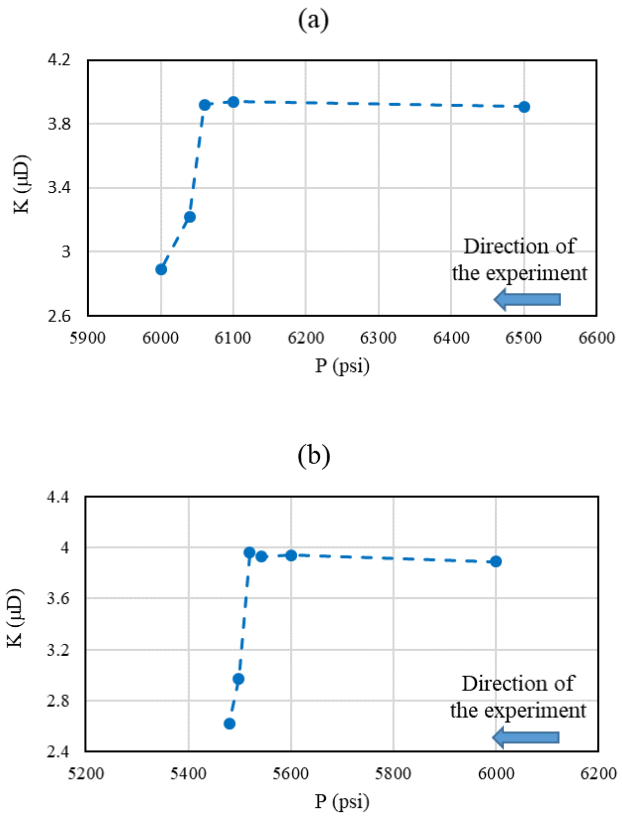

Figure 4.3: Effective permeability measurement for the EF2 core sample using (a) Fluid sample F5, and (b) Fluid Sample F6.

Measured bulk Pdew for the fluid sample F5 is 5784 psi. It can be observed from data of Figure 4.3(a) that for this fluid sample, the confined Pdew falls within the pressure range of 6040 to 6060 psi. At pressure 6060 psi, the nitrogen effective permeability is 3.9 μD and then reduces by 17% to 3.2 μD at the pressure of 6040 psi. This shows that the pore confinement effect has increased the confined Pdew for fluid sample F5 by at least 256 psi.

When it comes to fluid sample F6, the measured bulk Pdew is 5264 psi while the confined Pdew falls within the range of 5498 and 5519 psi. As noted in Figure 4.3(b), the measured nitrogen effective permeability for the two pressures of 5498 and 5519 psi are 3.0 μD and 4.0 μD, respectively. These values show that the formation of the liquid has decreased the effective permeability of nitrogen in this core by 25% in the presence of the fluid

sample F6. Therefore, the difference between measured bulk and confined Pdew in the case of using the fluid sample F6 is at least 234 psi. A summary of the results obtained based on the experiments performed on fluid samples F5 and F6 is presented in Table 4.3.

Table 4.3: A summary of the results of the effective permeability experiments for the EF2 core sample using two binary mixtures of C1+nC10.

Fluid	Composition (mole %)		Bulk Pdew (psi)	MLDO (%)	Range of measured confined Pdew (psi)	Difference in Pdew (psi)
	C1	nC10				
F5	92	8	5784	29	6041 – 6063	257 – 279
F6	95.9	4.1	5264	14	5498 – 5519	234 – 255

From Table 4.3, it can be observed that, when binary mixtures of C1+nC10 are used as the fluid samples, an increase in nC10 concentration results in higher difference between the measured bulk and confined Pdew. nC10 molecules are much bigger and heavier than C1 molecules, as a result, an increase in the concentration of nC10 results in elevated interactions between fluid molecules and pore walls.

The impact of fluid composition on the pore confinement was further examined using another binary gas condensate mixture type, comprising of C1 and nC8. The results of the nitrogen effective permeability measurement of the fluid samples F7, F8 and F9 are depicted in Figure 4.4.

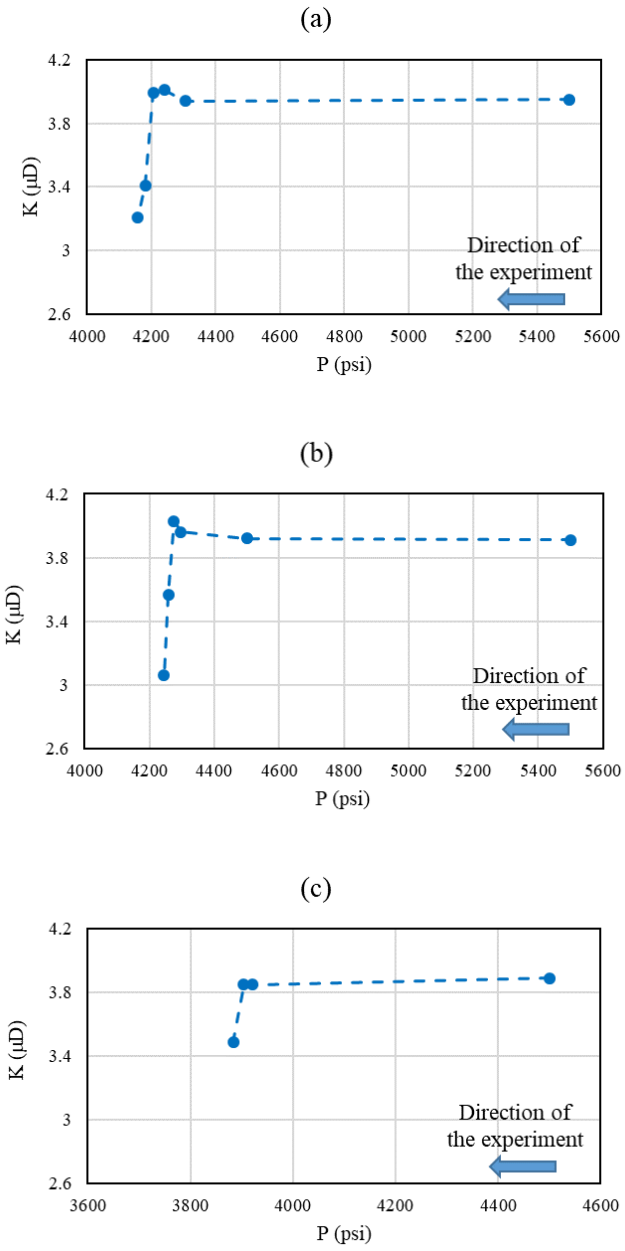

Figure 4.4: Effective permeability measurement for the EF2 core sample using (a) Fluid sample F7, (b) Fluid Sample F8, and (c) Fluid sample F9.

Fluid sample F7, has a measured bulk Pdew of 4052 psi. The nitrogen effective permeability was measured to be 4.0, 3.9, 4.0, and 4.0 μD at the first four measured pressure points of 5500, 4305, 4241, and 4205 psi, respectively. However, when the pore pressure further decreased to 4181 psi, the pressure substantially decreased by 15% from 4.0 μD to 3.4 μD, which was clearly indicative of the appearance of the liquid phase inside the core sample. These data, which are shown in Figure 4.4(a), demonstrate that the measured confined Pdew range for the fluid sample F7 is between 4181 and 4205 psi.

Hence, the difference between the measured bulk and confined Pdew for fluid sample F7 is at least 129 psi.

Measured bulk Pdew of fluid sample F8 is 4110 psi. For this fluid sample when the pore pressure decreased from 4275 to 4258 psi, the effective permeability of nitrogen reduced from 4.0 to 3.6 μD. This observation shows that for this fluid sample the confined Pdew has occurred in the range between 4258 and 4275 psi, indicating an increase of at least 148 psi for this fluid sample.

The effective permeability measurement data for the F9 fluid sample, which are shown in Figure 4.4(c), demonstrate that the confined Pdew is within the range of 3884 and 3904 psi as the measured effective permeability values are 3.9 and 3.5 μD, respectively. Therefore, confined Pdew of the fluid sample is at least 101 psi higher than its measured bulk Pdew of 3783 psi.

A summary of the results of the experiments performed using binary gas condensate mixtures of C1+nC8 is shown in Table 4.4.

Table 4.4: A summary of the results of the effective permeability experiments for the EF2 core sample using three binary mixtures of C1+nC10.

Fluid	Composition (mole %)		Bulk Pdew (psi)	MLDO (%)	Range of measured confined Pdew (psi)	Difference in Pdew (psi)
	C1	nC8				
F7	92.3	7.7	4052	24	4181 – 4205	129 – 153
F8	90	10	4110	31	4258 – 4275	148 – 165
F9	95.1	4.9	3783	13	3884 – 3904	101 – 121

Again, the main observation is that having heavier and richer fluids resulted in the higher difference between the confined and bulk Pdew. For instance, when the nC8 mole fraction increases from 0.049 to 0.1 for fluid samples F9 and F8, respectively, the minimum difference between confined and bulk Pdew also increases from 101 psi to 148 psi.

To consolidate the findings of the impacts of fluid composition on the pore confinement effects, a ternary gas condensate mixture comprising of C1, nC5 and nC10 was prepared. This sample was labelled as the fluid sample F10. This experiment also shows how the experimental method presented in this study can simply be extended to other types of gas condensate mixtures with many different types of components as it usually occurs in real gas condensate reservoirs. The results of the effective permeability measurement using fluid sample F10 are presented in Figure 4.5.

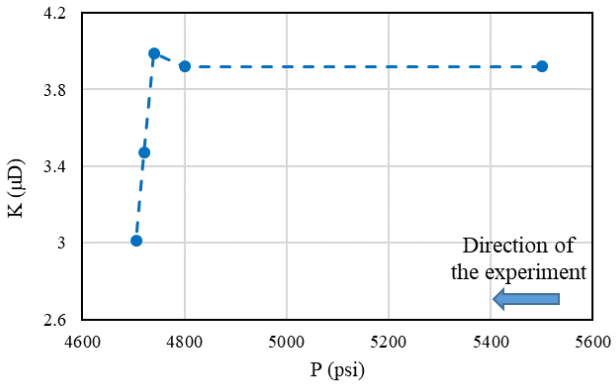

Figure 4.5: Effective permeability measurement for the EF2 core sample using sample F10.

As it can be observed in Figure 4.5, the effective permeability of nitrogen reduces from 3.9 µD to 3.5 µD when the pore pressure decreases from 4740 psi to 4721 psi. This shows that the confined Pdew of the ternary gas condensate fluid sample F10 is within the pressure range of 4721 and 4740 psi, which is at least 183 psi higher than the bulk Pdew of 4538 psi. Table 4.5 summarizes the key data for the experimental results of the effective permeability measurements using the ternary fluid sample F10.

Table 4.5: A summary of the results of the effective permeability experiments for the EF2 core sample using a ternary mixture of C1+nC5+nC10.

Fluid	Composition (mole %)			Bulk Pdew (psi)	MLDO (%)	Range of measured confined Pdew (psi)	Difference in Pdew (psi)
	C1	nC5	nC10				
F10	92	4	4	4538	18	4721 – 4740	183 – 202

Another way of looking at the impacts of fluid type and concentration, could be by comparing the difference between the binary mixtures where the heavier component varies with type and not by the concentration. Based on this, the results of the experiments already performed for the same core but using different fluid samples F3, F5 and F7 are summarized in Table 4.6. In these fluid samples, the methane and the second component concentrations are relatively similar and is around 92 and 8 mole %, respectively. However, the type of the second component vary.

Table 4.6: A summary of the results of the effective permeability experiments for the EF2 core sample using three binary mixture fluid samples of F3, F5, and F7.

Fluid	Composition (mole %)				Bulk Pdew (psi)	MLDO (%)	Range of measured confined Pdew (psi)	Difference in Pdew* (psi)
	C1	nC5	nC8	nC10				
F3	92.2	7.8	-	-	2213	7	2264 – 2281	51 – 68
F5	92	-	-	8	5784	29	6041 – 6063	257 – 279
F7	92.3	-	7.7	-	4052	24	4181 – 4205	129 – 153

It can be observed that for fluid sample F3, when the heavier component is nC5, the difference between bulk and confined Pdew is within the range of 51 to 68 psi. The corresponding ranges for the cases of nC10 and nC8 are 257 – 279 psi and 129 – 153 psi, respectively. This shows that the presence of heavier components significantly increases the impacts of pore confinement effects on the Pdew of gas condensate mixtures. Similar trend can be observed if the results of the experiments performed using fluid samples F4, F6 and F9 are to be compared. To avoid repetition, the results of this comparison are not summarized here.

To examine the effect of the fluid type and concentration simultaneously, the results for fluid samples F3, F5 and F10 can be compared. Table 4.7 summarizes the comparison between the results obtained from the experiments using these fluid samples.

Table 4.7: A summary of the results of the effective permeability experiments for the EF2 core sample using three gas condensate fluid samples of F3, F5, and F10.

Fluid	Composition (mole %)			Bulk Pdew (psi)	MLDO (%)	Range of measured confined Pdew (psi)	Difference in Pdew (psi)
	C1	nC5	nC10				
F3	92.2	7.8	-	2213	7	2264 – 2281	51 – 68
F5	92	-	8	5784	29	6041 – 6063	257 – 279
F10	92	4	4	4538	18	4721 – 4740	183 – 202

When it comes to the difference between bulk and confined Pdew, it can be observed that the impacts of the presence of heavier components is much higher. For instance, the difference between the measured bulk and confined Pdew of the fluid sample F3 with nC5 as the second component of this binary mixture is in the range of 51 to 68 psi. This difference for the tertiary fluid sample F10 with half of nC5 replaced by nC10 is 183 to 202 psi, which is much more. This difference becomes even larger when all nC5 in the binary fluid sample F3 is replaced by nC10 in the binary fluid sample F5. In other words,

the impacts of the presence of nC10 is much more than the impacts of the presence of nC5.

Another comparison can be made based on the results of the experiments for the fluid sample of F6 and the fluid samples of F7 and F8. The MLDO of the fluid sample F6 is 14% while the measured MLDO of the fluid samples F7 and F8, are 24% and 31%, respectively. However, as summarized in Table 4.8, the difference between bulk and confined Pdew of fluid sample F6, with nC10, falls within the range of 234-255 psi. This difference is much higher compared to the difference between the bulk and confined Pdew of the fluids samples of F7 and F8 with larger MLD difference but similar nC8, which fall within the range of 129-153 and 148-165 psi, respectively. Hence, it can be concluded that the impacts of the presence of the heavier components are higher than the fluid richness.

Table 4.8: A summary of the results of the effective permeability experiments for the EF2 core sample using three binary mixture fluid samples of F6, F7, and F8.

Fluid	Composition (mole %)			Bulk Pdew (psi)	MLDO (%)	Range of measured confined Pdew (psi)	Difference in Pdew (psi)
	C1	nC8	nC10				
F6	95.9	-	4.1	5264	14	5498 – 5519	234 – 255
F7	92.3	7.7	-	4052	24	4181 – 4205	129 – 153
F8	90	10	-	4110	31	4258 – 4275	148 – 165

The above observations can be related to fluid-fluid and rock-fluid molecular interactions. That is, in gas condensate mixtures, it is believed that the interactions between the light and heavy components of the mixture holds the fluid together as a single phase. By reduction in pressure, these interactions, which are attractive VdW forces would not be sufficient to hold the heavier components of the gas condensate mixture within the single phase gas. In the presence of the porous media, where the range of the pore size is within a few nanometres, the interactions between the fluid molecules and pore walls are also important. Since in gas condensate mixtures, heavier and bigger components have more interactions with pore walls, the presence of heavier components intensify the pore confinement effects more than the lighter and smaller components.

When single component fluids are compared with the multi-component mixtures of gas condensate, it is noted that the impact of confinement effects would change the fluid behaviour in different manners. In the case of single component gases, the close proximity to unconventional pore wall surfaces results in higher interactions between similar fluid

molecules, which in turn results in higher accumulation of the molecules near pore walls. This makes the single component fluid inside the pore and in the vicinity of the pore walls to be denser than the bulk state. As a result, the fluids tend to liquefy in lower pressures. However, when the nanopores within unconventional porous media, are filled with the fluids with retrograde behaviour, higher rock-fluid interactions taking place in near pore walls region causes the heavier molecules to be separated from the bulk easier and at higher pressures. Whereas in the bulk state, the fluid-fluid molecular interactions take place at the pressures above Pdew are sufficient to hold the molecules in the gas phase, but when additional interactions between fluid molecules and pore walls exist in unconventional rocks the threshold pressure for heavy components deposition, which is denoted as the Pdew, becomes higher.

4.2.2 Impacts of Temperature on Pore Confinement Effects on the Pdew of Gas Condensate Mixtures

In this section, the results of the experiments performed on gas condensate sample F7 at different temperatures of 20, 40, and 60 °C, are compared. All the experiments were performed on the EF2 shale core sample. During all the experiments, the net stress was fixed at 500 psi. The bulk properties of the fluid sample F7 at different temperatures are presented in Table 4.8. As it can be observed in this Table, by increasing the temperature, the measured Pdew of the gas condensate samples increases as well.

It has been suggested that, in real gas condensate mixtures with wide range of molecules, the presence of C7+ components, would result in such behaviour, whereby a subtle increase in temperature, the Pdew of the gas condensate mixtures would increase, however, further increase in temperature would result in a decrease in Pdew.

Table 4.8: Measured bulk Pdew and MLDO for the gas condensate fluid sample F7 at different temperatures of 20, 40, and 60 °C

Fluid	Composition (mole %)		Temperature (°C)	Bulk Pdew (psi)	MLDO (%)
	C1	nC8			
F7	92.3	7.7	20	4052	24
F7	92.3	7.7	40	4096	
F7	92.3	7.7	60	4108	

The results of the effective permeability measurement for fluid sample F7 at different temperatures are presented in Figure 4.6. As it can be observed, pore confinement effects

have increased the Pdew of the gas condensate mixture at higher temperatures as well. For instance, for the case of the measurements at 40 °C, the effective permeability of nitrogen decreases from 4.1 μD at 4298 psi to 3.5 μD at 4277 psi. Such a reduction in effective permeability within this pressure range shows that the condensate has been dropped out inside the core. As a result, confined Pdew falls within the range of 4277 to 4298 psi which is at least 181 psi higher than the measured bulk Pdew of 4096 psi for this fluid sample at 40 °C. By increasing the temperature from 40 °C to 60 °C, considerable effective permeability reduction has occurred at the range of 4182 and 4202 psi. That is the effective permeability reduces from 4.2 μD at 4202 psi to 3.4 μD at 4182 psi. Measured bulk Pdew of the fluid sample F7 s 4108 psi which is at least 74 psi lower than the measured range for the confined Pdew.

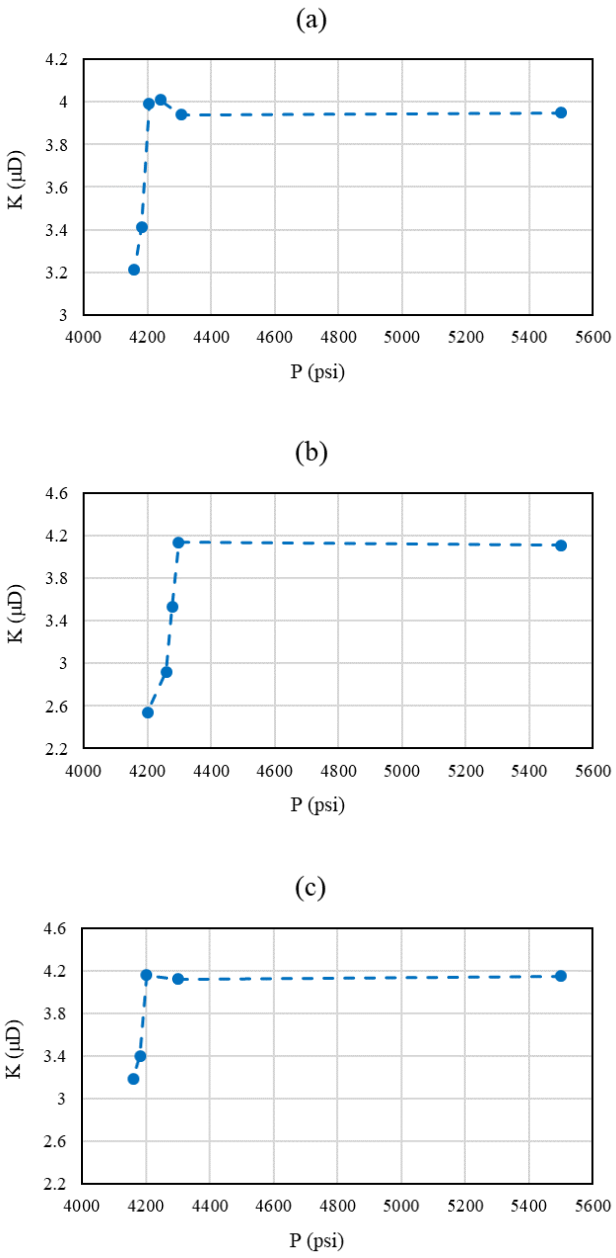

Figure 4.6: Effective permeability measurement for the EF2 core sample using fluid sample F7 at the temperature of (a) 20 °C, (b) 40 °C, and (c) 60 °C.

Table 4.9 summarizes the data for the measurements performed on the EF2 core sample using the binary fluid sample F7 to investigate the effects of temperature on confined Pdew.

Table 4.9: A summary of the results of the effective permeability experiments for the EF2 core sample using the gas condensate fluid sample F7 at three different temperature values.

Fluid	Temperature (°C)	Bulk Pdew (psi)	MLDO (%)	Range of measured confined Pdew (psi)	Difference in Pdew (psi)
F7	20	4052	24	4181 – 4205	129 – 153
F7	40	4096	18	4277 – 4298	181 – 202
F7	60	4108	15	4182 – 4202	74 – 94

It can be observed that, first, by an increase in the temperature from 20 to 40 °C, the difference between measured bulk and confined Pdew increases from the range of 129 – 153 psi to the range 181 – 202 psi. However, further increase in temperature to 60 °C, substantially reduces the difference between measured bulk and confined Pdew to the range of 74 – 94 psi.

The relative impacts of temperature seems to be highly dependent on the type of the fluid and also the porous medium. Further investigations are required to take into account the impacts of temperature. However, it can be suggested that, the impacts of temperature on the pore confinement effects would be based on the resultant net interactions taking place among fluid-fluid molecules and fluid-wall molecules. If one is to consider the gas condensate mixture phase envelope, the presence of the heavier molecules would result in expanding the phase envelope. As discussed in Section 1.3, the phase behaviour and the trend of the Pdew with changing temperature depends on the range at which the temperature lies as compared to the phase envelope. If the temperature falls within the range of T_C (critical temperature) and T_{CB} (the temperature corresponding to cricondenbar point), an increase in temperature results in higher Pdew. However, if the temperature falls within the range of T_{CB} and T_{CT} (the temperature corresponding to cricondentherm point), an increase in Pdew results in lower Pdew. In this study, the change in the trend for the impacts of temperature is the sign of the shift in the phase envelope of the gas condensate mixture due to confinement effects. In the next chapter, the confinement induced modifications on the EOS and its effects on the phase envelope will be further discussed.

4.2.3 Impacts of Net Stress on Pore Confinement Effects on the Pdew of Gas Condensate Mixtures

In this section, the impacts of net stress on the Pdew of four different gas condensate mixtures, namely fluid samples F4, F5, F7, and F10 are discussed. The experiments have been performed at three different net stress of 500, 1000, and 2000 psi for each fluid.

The impacts of net stress affects the permeability measurement values due to geomechanical effects. As it was mentioned in Chapter 1, during production from the reservoirs, the pore pressure reduces and the net stress increases resulting in two different simultaneous effects which could influence the measured apparent permeability of the unconventional shale core samples. First, an increase in the net stress results in the compaction of the rock and reducing the pore volume of the rock. During this process, fractures within the rock may be closed. This would result in the decrease of the measured apparent permeability. On other hand, production from the reservoirs and the resultant reduction in pressure results in the increase of the slippage rarefied flow within the rock which increases the apparent permeability. Figure 4.7 shows the comparison between the nitrogen effective permeability for different ranges of pore pressure which have been investigated in this study. It should be mentioned that there have been several studies which have been performed to evaluate geomechanical effects on the apparent permeability of the shale core samples.

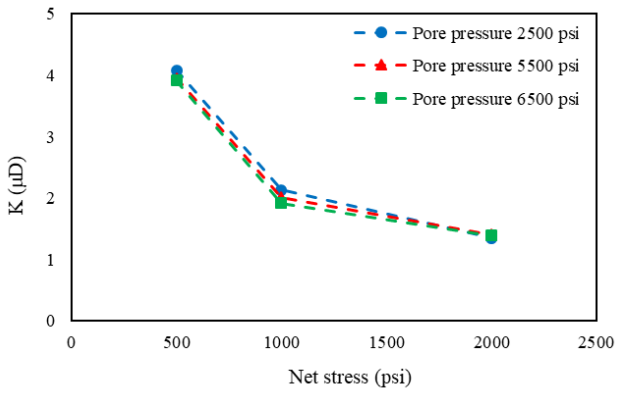

Figure 4.7: Effective permeability measurements of core sample EF2 at three different net stress corresponding to three pore pressure values of 2500 psi (blue), 5500 psi (red), and 6500 psi (green).

The results in Figure 4.7 show that changes in pore pressures at high pressure ranges, does not contribute to any difference in the measured effective permeability. For instance, when the net stress is fixed at 500 psi, the effective permeability is in the range of 4.0 μD.

However, change in the net stress, significantly reduces the measured effective permeability for all three pore pressure values. For unconventional gas condensate reservoirs, the impacts of net stress and its influence on the effective permeability cannot be ignored. As a result, the range of the effective permeability values are lower for cases with higher net stress.

The results of the effective permeability measurements at three different net stress values using the fluid sample F4 are shown in Figure 4.8. In this figure only those values have been presented which correspond to the range at which confined Pdew was observed. As it can be observed, in order to better compare the results of the experiments, the results all three sets of measurements are shown in the same graph.

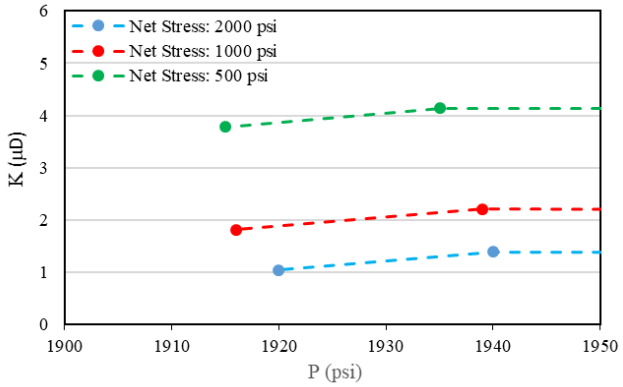

Figure 4.8: Effective permeability measurements for the EF2 core sample using the lean fluid sample F4 at three net stress values of 500 psi (green), 1000 psi (red), and 2000 psi (blue).

It can be observed that at different net stress values, the confined Pdew for the fluid sample F4 falls within a similar range. For example, the confined Pdew of the fluid F4 with net stress of 1000 psi, falls within the pressure range of 1916 to 1939 psi. Similarly, the range at which the confined induced condensation occurs for the case of net stress of 2000 psi is 1920 to 1940 psi. Fluid sample F4 is the leanest fluid sample in this study with MLDO of 3%. These results show that for this lean fluid sample, the impact of net stress on the extent of pore confinement effects is negligible. Table 4.10 summarizes the same results evaluating the impact of net stress on pore confinement effects using fluid sample F4. As it can be observed, the differences between the confined and bulk Pdew are in the ranges of 24 – 44 psi, 25 – 48 psi, and 29 – 49 psi for the cases with net stress of 500, 1000, and 2000 psi, respectively.

Table 4.10: A summary of the results of the effective permeability experiments for the EF2 core sample using the lean gas condensate fluid sample F4 at three different net stress values.

Fluid	Net stress (psi)	Bulk Pdew (psi)	MLDO (%)	Range of measured confined Pdew (psi)	Difference in Pdew (psi)
F4	500	1891	3	1915 – 1935	24 – 44
F4	1000	1891	3	1916 – 1939	25 – 48
F4	2000	1891	3	1920 – 1940	29 – 49

The impacts of net stress using a richer fluid was also considered in this study. Accordingly fluid sample F5, with MLDO of 29% was used. The results of the effective permeability measurement at the same three different net stress values are shown in Figure 4.9.

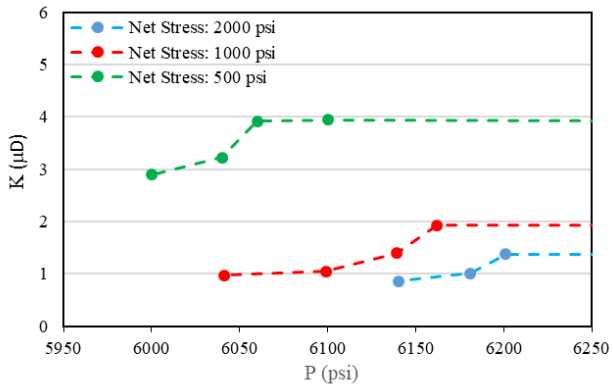

Figure 4.9: Effective permeability measurements for the EF2 core sample using the rich fluid sample F5 at three net stress values of 500 psi (green), 1000 psi (red), and 2000 psi (blue).

It can be observed that unlike the case of fluid sample F4, for fluid sample F5, the impact of net stress is not negligible on the extent of the effects of confinement. For instance, for the case of net stress value of 500 psi, the difference between measured confined and bulk Pdew is at least 257 psi. The green line in the plot represents the case of net stress value of 500 psi where the effective permeability significantly is reduced from 3.9 μD to 3.2 μD when the pressure is decreased from 6063 to 6041 psi. For the case of net stress equivalent to 1000 psi, confined Pdew falls within the range of 6139 to 6162 psi. This range is considerably higher than the range observed for the net stress of 500 psi. Similarly, further increase of the net stress results in further increase in the difference between confined and bulk Pdew. That is, increasing the net stress to 2000 psi, results in

the confined Pdew to occur within the range of 6181 to 6201 psi which is clearly higher than the other two measured ranges for cases with the net stress of 500 and 1000 psi.

Table 4.11 summarizes the results of the effective permeability measurement experiments conducted to evaluate the impact of net stress on pore confinement effects using the rich fluid sample F5. As it can be observed, the differences between the confined and bulk Pdew are in the ranges of 257 – 279 psi, 355 – 378 psi, and 397 – 417 psi for the cases with net stress of 500, 1000, and 2000 psi, respectively.

Table 4.11: A summary of the results of the effective permeability experiments for the EF2 core sample using the rich gas condensate fluid sample F5 at three different net stress values.

Fluid	Net stress (psi)	Bulk Pdew (psi)	MLDO (%)	Range of measured confined Pdew (psi)	Difference in Pdew (psi)
F5	500	5784	29	6041 – 6063	257 – 279
F5	1000	5784	29	6139 – 6162	355 – 378
F5	2000	5784	29	6181 – 6201	397 – 417

Further investigation on the impact of net stress on pore confinement effects was carried out using another fluid sample. For this purpose, fluid sample F7 was used as the next binary gas condensate mixtures. This fluid sample has an intermediate-to-rich bulk MLDO of 24 %. The comparison between the results of the effective permeability measured for the same core sample at the same three values of net stress are plotted in Figure 4.10.

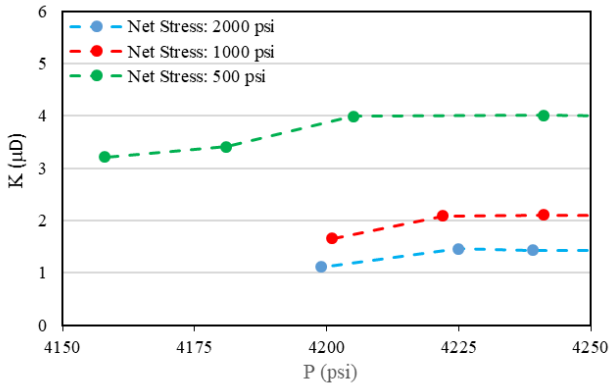

Figure 4.10: Effective permeability measurements for the EF2 core sample using the intermediate-to-rich fluid sample F7 at three net stress values of 500 psi (green), 1000 psi (red), and 2000 psi (blue).

The measured confined Pdew of the fluid sample F7, falls within the range of 4181 to 4205 psi when the net stress is 500 psi. The respective range when the net stress is 1000 psi, is 4201 to 4222 psi. There is a minor difference between these two ranges, however, when the net stress increases to 2000 psi, the observed range of 4199 to 4225 psi is very similar to that of the case with the net stress of 1000 psi.

Table 4.12 summarizes the results of the experiments for evaluation of the impact of net stress on pore confinement effects using fluid sample F7. As it can be observed, the differences between the confined and bulk Pdew are in the ranges of 257 – 279 psi, 355 – 378 psi, and 397 – 417 psi for the cases with net stress of 500, 1000, and 2000 psi, respectively.

Table 4.11: A summary of the results of the effective permeability experiments for the EF2 core sample using the intermediate-to-rich gas condensate fluid sample F7 at different net stress values

Fluid	Net stress (psi)	Bulk Pdew (psi)	MLDO (%)	Range of measured confined Pdew (psi)	Difference in Pdew (psi)
F7	500	4052	24	4181 – 4205	129 – 153
F7	1000	4052	24	4201 – 4222	149 – 170
F7	2000	4052	24	4199 – 4225	147 – 173

Fluid sample F10, as a ternary gas condensate mixture was also used to examine the impact of net stress on pore confinement effects. This fluid sample has an intermediate bulk MLDO of 18 %. The two components that were added to methane to prepare this gas condensate mixture, are the intermediate nC5, and the heavy nC10, components. A comparison of the results of this fluid sample with those of other binary fluid samples, the relative impacts of each component can also be highlighted. The comparison between the results of the effective permeability measurements of the EF2 core sample at the same three values of the net stress are plotted in Figure 4.11.

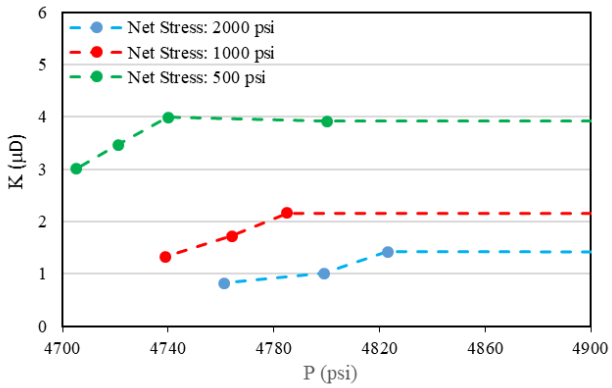

Figure 4.11: Effective permeability measurements of EF2 core sample using the intermediate fluid sample F10 at the net stress of 500 psi (green), 1000 psi (red), and 2000 psi (blue).

It can be observed that for fluid sample F10, like fluid sample F5, the impact of net stress is not negligible on the extent of the effects of confinement. For instance, for the case of net stress value of 500 psi, the difference between measured confined and bulk Pdew is at least 183 psi. The green line in the plot represents the case of the net stress value of 500 psi where the effective permeability is significantly reduced from 4.0 μD to 3.5 μD when the pressure is decreased from 4740 to 4721 psi. For the case of net stress equivalent to 1000 psi, confined Pdew falls within the range of 4764 to 4785 psi. This range is higher than the range observed for the net stress of 500 psi. Similarly, further increase of the net stress results in further increase in the difference between confined and bulk Pdew. That is, increasing the net stress to 2000 psi, results in the confined Pdew to occur within the range of 4799 to 4823 psi which is clearly higher than the other two measured range for cases with the net stress of 500 and 1000 psi.

Table 4.11 summarizes the results of the effective permeability measurement experiments conducted to evaluate of the impact of net stress on pore confinement effects using the fluid sample F10. As it can be observed, differences between the confined and bulk Pdew are in the ranges of 183 - 202 psi, 226 – 247 psi, and 261 – 285 psi for the cases with net stress of 500, 1000, and 2000 psi, respectively. If we compare these values with the corresponding values for the case of fluid sample F5 and fluid sample F7, it can be concluded that for this fluid, the differences due to the change in net stress is higher compared to fluid sample F7 while being less compared to fluid sample F5. It should be noted that the richness of the fluid sample F7 with MLDO of 24% is higher than the richness of the fluid sample F10 with MLDO of 18%. This observation shows that, the richness of a fluid on its own cannot explain the higher impact of net stress on the extent

of the pore confinement effects. In fact, it can be suggested that, it is the presence of larger molecules with higher molecular weights that gives rise to the pore confinement effects in unconventional porous media.

Table 4.11: Summary of the results of the effective permeability experiments for the EF2 core sample using the intermediate gas condensate fluid sample F7 at three different net stress values.

Fluid	Net stress (psi)	Bulk Pdew (psi)	MLDO (%)	Range of measured confined Pdew (psi)	Difference in Pdew (psi)
F10	500	4538	18	4721 – 4740	183 – 202
F10	1000	4538	18	4764 – 4785	226 – 247
F10	2000	4538	18	4799 – 4823	261 – 285

4.2.4 Impacts of Rock Type on the confined Pdew

Another important aspect, which could influence the extent of the confinement effects in unconventional reservoirs is the rock type. To investigate this effect, nitrogen effective permeability measurement using two different types of gas condensate mixtures, namely fluid sample F7 and fluid sample F10, was performed on the Barnett shale core sample. The basic properties of the Barnett shale core sample are summarized in Table 4.12.

Table 4.12: The basic properties of the Barnett core sample used for the experiments of the effects of rock type with fluid sample F7.

Core sample	Length (cm)	Diameter (cm)	Porosity (%)	Apparent permeability (D)
B1 (Barnett)	5.08	3.95	9.4	3.1 E-6

The results of the comparison between nitrogen effective permeability in Eagle Ford (EF2) and Barnett (B1) shale core samples using fluid sample F7 are presented in Figure 4.12. The net stress for these measurements was fixed at 500 psi.

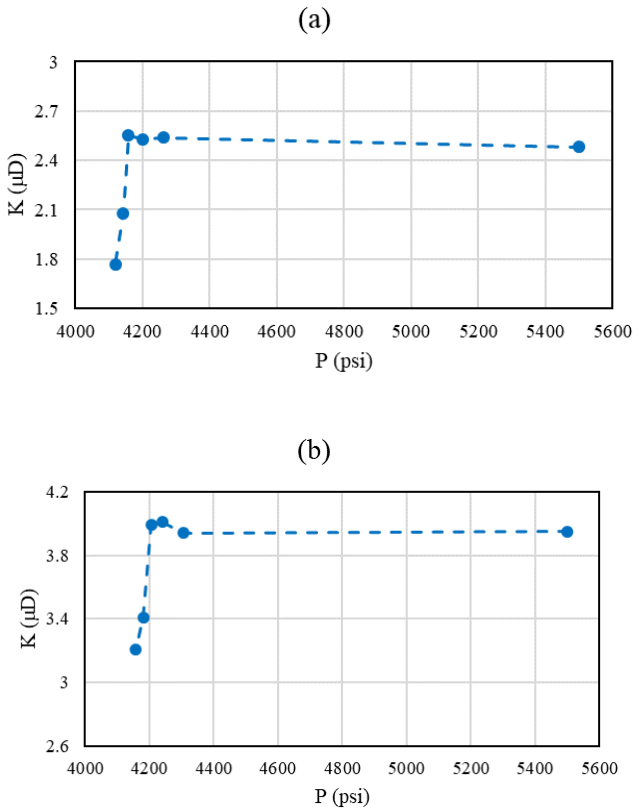

Figure 4.12: Effective permeability measurement using fluid sample F7 for the (a) Barnett (B1), and (b) Eagle Ford (EF2) shale core samples.

As it can be observed, for the case of Barnett shale core sample, in the conducted experiment, the effective permeability reduced from 2.6 μD to 2.1 μD when the pressure dropped from 4158 to 4142 psi. As a result, for the B1 core sample, the confined Pdew falls within the range of 4142 to 4158 psi. The corresponding range for the EF2 core sample is 4181 to 4205 psi. Accordingly, the impacts of pore confinement effects on the Pdew of the fluid sample F7 is more pronounced for the EF2 core sample.

In another set of experiments, the change of the Pdew of fluid sample F10 due to pore confinement effects in the B1 core sample was examined. Figure 4.13 shows a comparison between the results of the effective permeability measurements for EF2 and B1 core samples using the fluid sample F10.

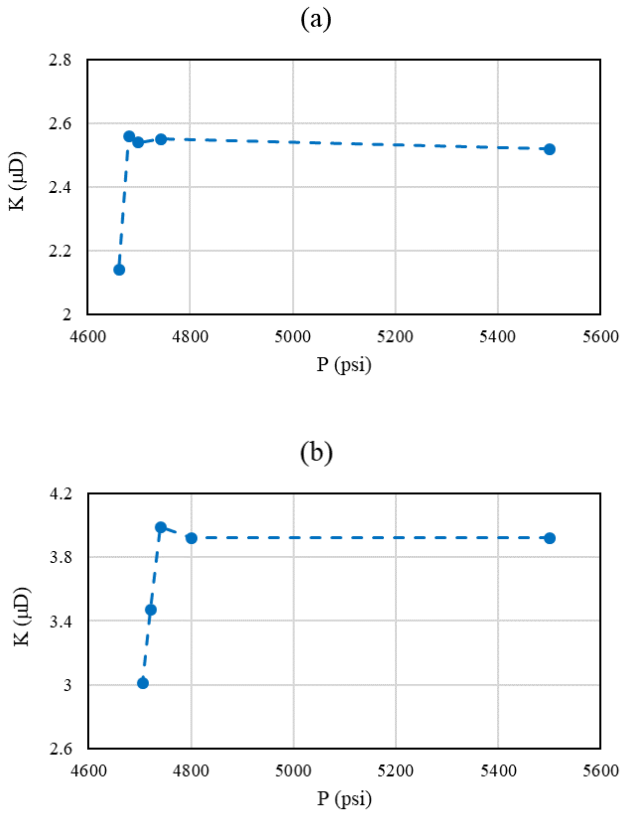

Figure 4.13: Effective permeability measurements, using fluid sample F10, for the (a) Barnett (B1), and (b) Eagle Ford (EF2) shale core samples.

In these experiments, the significant drop in the effective permeability of the nitrogen from 2.6 µD to 2.1 µD for the B1 core sample occurred when the pressure dropped from 4680 psi to 4661 psi. As a result, confined Pdew of the fluid sample F10 falls within the range of 4661 psi to 4680 psi. The corresponding range for the EF2 core sample is 4721 to 4740 psi. Table 4.13 summarizes the comparisons between the two core samples used in this study.

Table 4.13: Summary of the results of the effective permeability experiments for B1 and EF2 core samples and using two gas condensate fluid samples of F7 and F10.

Core sample	Fluid	Bulk Pdew (psi)	MLDO (%)	Range of measured confined Pdew (psi)	Difference in Pdew (psi)
B1	F7	4052	24	4181 – 4205	129 – 153
EF2	F7	4052	24	4142 – 4158	90 – 106
B1	F10	4538	18	4721 – 4740	183 – 202
EF2	F10	4538	18	4661 – 4680	123 – 142

As it is demonstrated in Table 4.13, the extent of the difference between bulk and confined Pdew for both fluid types is higher for the EF2 core sample compared to the B1 core

sample. The pore size distribution measurements and corresponding calculations presented in Figure 3.3 showed that the mean value for the pore radius size of the Barnett shale is 11.25 nm whereas the corresponding value for the Eagle Ford shale is 54 nm. It was expected that the impacts of confinement on the Pdew of the fluid sample F7 would be higher for B1 sample. However, the comparison of the results of the effective permeability for these two shale samples shows that the effects of pore confinement is more pronounced for the Eagle Ford core sample with higher mean pore size. These results demonstrate that to take into account the effects of confinement, ignoring the type of the rock and its mineralogy would result in erroneous estimations. Accordingly, it suggests that, only considering the average value for the pore size within unconventional rocks as the representative length of the porous medium, would not be sufficient. However, in order to achieve a unified and suitable approach for the study of the confinement effects within real porous media, the use of mean pore size is useful providing that another suitable physical shape factor is defined for each specific rock type to take into account the effects of rock geophysical and geochemical properties. In Chapter 5, this approach is undertaken to obtain a modified EOS for the study of the fluid phase behaviour.

4.3 Concluding Remarks on Experimental Results of the Measurement of Pore Confinement Effects in Real Shale Core Samples

In this study, a new experimental method for measuring the effects of pore confinement on the Pdew of the single component fluids as well as gas condensate mixtures was presented. The impacts of fluid composition, temperature, net stress and rock type was experimentally evaluated. Following findings were obtained during the course of the experiments performed in this chapter:

- Pore confinement effects increased Pdew of gas condensate mixtures while it reduced Pdew of the tested single component gas. The main reason can be attributed to the increased interactions between fluid molecules and pore walls. For the single component fluid, the interactions between fluid molecules and pore walls, attracts fluid molecules toward the pore walls. Hence near the pore walls there would be a fluid region with higher density compared to the bulk phase. As a result, the accumulation of the single component fluid molecules makes Pdew to occur at lower pressures in the confined space. For gas condensate mixtures, heavier molecules tend

to be more interacting with the pore walls. As a result, a process with a mechanism similar to retrograde condensation dictates that for gas condensate mixtures confined in small pore spaces to have higher Pdew. In other words, increased the interactions between heavier components and the pore wall in gas condensate mixtures makes them to drop out from the gas phase at higher pressures compared to bulk Pdew. The trend of the results for gas condensate mixtures were in good agreement with those experimental results reported by Salahshoor and Fahes (2020) or the theoretical results reported by Jin and Firoozabadi (2016).

- For gas condensate mixtures with similar components, as the concentration of the heavier component increased, the confined Pdew was higher. This is argued to due to the presence of heavier molecules that increases the interactions between pore walls and fluid molecules, hence, the pore confinement effects which are created due to the non-negligible interactions between fluid molecules and pore walls would be intensified in the presence of heavier molecules. As a result, for different gas condensate mixtures with similar components but different composition, the difference between the bulk and confined Pdew for the mixture with higher amount of heavier molecules is higher.
- The richness of the gas condensate mixture which is represented by its maximum liquid drop out (MLDO), was not as an important factor as the presence of heavier components in the mixture. In other words, it is possible that the pore confinement effects would be higher for a gas condensate mixture with a lower MLDO compared to another gas condensate mixture with a higher MLDO. The presence of heavier molecules, or higher concentrations of heavier molecules, on the other hand, was shown to be the main reason for such observations, i.e., the heavier molecules the higher the effects of confinement would be.
- Initially, by an increase in temperature, the difference between confined Pdew and bulk Pdew increased. However, further increase in the temperature resulted in a considerable decrease in the difference between bulk and confined Pdew. This non-monotonic difference in the trends observed for the measured confined and bulk Pdew based on a change in temperature, suggests the alteration of the phase envelope of gas condensate mixtures due to confinement.
- The impacts of net stress was shown to be highly dependent on the fluid type. For lean fluids, or fluids with very low content of heavier components, the net stress had negligible impacts on the extent of the confinement effects. However, when gas condensate mixture contains heavier molecules, the impacts of net stress was not

negligible anymore. Moreover, it was observed that, the effective permeability of the shale cores under study was very sensitive to the net stress. Higher net stress values, considerably reduced the effective permeability of the core samples due to the increased geomechanical effects on the compaction of the rock matrix and closure of the fractures.

- Unconventional rock type was also another contributing factor which influenced the extent of the pore confinement effects. It was observed that for the B1 core sample with a mean pore radius value of 11.25 nm, the effects of pore confinement was less noticeable compared to the EF2 core sample with a mean pore radius value of 54 nm. This observation suggests that the confinement effects is not only dependent on the pore size distribution of the porous media, but also the geophysical and geochemical properties of the porous medium play an important role in the extent of the confinement effects. It should be mentioned that there is no study which takes into account the effects of the porous medium type on the extent of the deviation in fluid phase behaviour in confined space. Hence, there is no reported justification for the observed trend for comparison of the results obtained from B1 and EF2 core samples. Hence, more experiments need to be conducted to obtain general understandings regarding the impacts of rock type.

The novel experimental results presented in this chapter help to gain a better understanding of the impacts of different parameters that are influential in determining the effect of confinement on the phase behaviour of the gas condensate mixtures. These results also provide valuable source of data to verify the proposed theoretical methods and their applications for estimating the level of confinement in unconventional gas-condensate reservoirs. More specifically, these results can be used as the basis for the development of modified EOS which can be used to describe the behaviour of gas condensate mixtures under confinement something which has been discussed in the next chapter.

Chapter 5: Empirical Modifications on Equation of State for Confinement Effects

In chapter 2, a brief review of the suggested approaches in the literature for modelling the phase behaviour of confined fluids using modified equations of state was presented. In this chapter, based on the experimental results obtained from the confined fluids Pdew measurements, a new approach for describing the confinement effects for gas condensate mixtures phase behaviour is introduced.

As discussed in chapter 4, the results of confined Pdew measurements showed different trends for single component fluid and multi-component gas condensate mixtures. In other words, due confinement effects, Pdew of a single component gas decreases, whereas, Pdew of a gas condensate mixtures increases. These observations, suggest that, approaches which are considered for confined single component fluid EOS modelling, need further modifications when they are applied to gas condensate mixtures. As mentioned, the majority of the proposed approaches for the EOS modifications, are based on the phase behaviour of single component fluids in confined containers with uniform pore size distributions. Relatively good agreement is obtained between the experimental data and the numerical predictions for such systems. However, due to the lack of experimental data, the extension of the proposed methods is not easily applicable to express confinement effects in real unconventional rocks.

In this chapter, after a brief introduction to the PR EOS, the method and formulations undertaken to modify the EOS for confined fluids are discussed. The method, involves estimation of the change in critical properties of the components due to confinement based on the general form of the equation proposed by Zarragoicoechea and Kuz (2004). The tuning parameters for the equations are obtained from single component confined Pdew measurements. Once the critical properties are modified, the binary interaction parameters (BIPs) are modified based on intermolecular forces between different molecules and pore walls. Lennard-Jones (LJ) potential is used to estimate the modified BIP for different mixtures. Finally the results of the experimental measurements are compared with the suggested modified EOS.

5.1 Peng-Robinson (PR) Equation of State

In 1976, PR EOS was presented as an attempt to improve the accuracy of the well-known Redlich-Kwong (RK) EOS for the estimation of the liquid phase density (Peng and Robinson, 1976). Later, the capability of the PR EOS and its high accuracy for retrograde gas phase behaviour studies was highlighted. It was demonstrated that PR EOS has a good potential to predict the phase behaviour even for near critical regions of gas condensate mixtures (Slot-Petersen, 1989). Equations 5.1 to 5.6 presents the formulations for original PR EOS with two constants a and b.

$$P = \frac{RT}{\vartheta - b} - \frac{a}{\vartheta(\vartheta + b) + b(\vartheta - b)} \qquad \text{Eq. 5.1}$$

with:

$$a = a_c \alpha \qquad \text{Eq. 5.2}$$

$$\alpha = \left[1 + \kappa\left(1 - \sqrt{T_r}\right)\right]^2 \qquad \text{Eq. 5.3}$$

$$\kappa = 0.37464 + 1.54226\omega - 0.26992\omega^2 \qquad \text{Eq. 5.4}$$

$$a_c = \Omega_a \frac{R^2 T_c^2}{P_c} = 0.45724 \frac{R^2 T_c^2}{P_c} \qquad \text{Eq. 5.5}$$

$$b = \Omega_b \frac{RT_c}{P_c} = 0.07780 \frac{RT_c}{P_c} \qquad \text{Eq. 5.6}$$

Where Tc and Pc are critical temperature and pressure, respectively. a and b are VdW attractive parameter and covolume parameter, respectively. T_r is the reduced temperature and ω is the acentric factor.

One of the most widely used modifications for PR EOS is the volume translation modification which introduces a new term c into the original PR EOS which makes it a 3-Parameter EOS taking a general form as presented in equation 5.7 (Péneloux, Rauzy and Fréze, 1982)

$$P = \frac{RT}{\vartheta + c - b} - \frac{a}{(\vartheta + c)(\vartheta + c + b) + b(\vartheta + c - b)} \qquad \text{Eq. 5.7}$$

Modifications for the volume parameter in PR EOS, improved its predictions, especially for ϑ^l, which is the liquid molar volume.

Peng and Robinson used the classical mixing rules of Zudkevitch and Joffe (1970) to extend their EOS to mixtures.

$$a = \sum_{i=1}^{n}\sum_{j=1}^{n} x_i x_j a_{ij} \qquad \text{Eq. 5.8}$$

$$a_{ij} = \sqrt{a_i a_j}\left(1 - \delta_{ij}\right) \qquad \text{Eq. 5.9}$$

$$b = \sum_{i=1}^{n} x_i b_i \qquad \text{Eq. 5.10}$$

where δ_{ij} is binary interaction parameter (BIP) which is an empirical parameter that is used to for the correction of the deviations observed between the prediction of the EOS and the experimentally obtained data. There is no known solid theoretical basis for BIP, i.e., it is a parameter which accounts for the interactions between different types of molecules. It can be considered as a parameter which shows the extent of the non-ideality of a mixture (Coutinho *et al.*, 1994). Several studies have suggested equations for prediction of BIPs. Generally, the presented equations in literature for estimating BIP are in different forms of temperature, or molecular weight or acentric factor functions (Shinta and Firoozabadi, 1997; Mulliken and Sandler, 2002; Venkatramani and Okuno, 2015).

5.2 Confinement Induced Changes in Critical Properties

As mentioned in chapter 2, Morishige and Shikimi (1998) experimentally found that shifts in the critical properties can be scaled properly, in dimensionless form (i.e. the ratio of $\frac{\varphi_c - \varphi_{cp}}{\varphi_c}$ in which φ_c and φ_{cp} are bulk and confined critical properties, respectively) and presented in terms of the ratio $\left(\frac{\sigma}{r_p}\right)$ where σ is the LJ size parameter and r_p is the porous characteristic radius or length. Accordingly, Zarragoicoechea and Kuz (2004) developed the following form of the equation for the shift of confined critical properties.

$$\frac{\left(\varphi_c - \varphi_{cp}\right)}{\varphi_c} = 0.9409\frac{\sigma}{r_p} - 0.2415\left(\frac{\sigma}{r_p}\right)^2 \qquad \text{Eq. 5.11}$$

There are also several other similar attempts to obtain the best equations for critical properties shifts due to pore confinement. For instance, Zhang *et al.* (2018) developed the following equation:

$$\frac{(\varphi_c - \varphi_{cp})}{\varphi_c} = 0.7179\frac{\sigma}{r_p} - 0.0758\left(\frac{\sigma}{r_p}\right)^2 \qquad \text{Eq. 5.12}$$

Other quadratic equations follow the same formats.

One can write a general form of these equations based on the following equation:

$$\frac{(\varphi_c - \varphi_{cp})}{\varphi_c} = A\frac{\sigma}{r_p} + B\left(\frac{\sigma}{r_p}\right)^2 \qquad \text{Eq. 5.13}$$

where A and B are the coefficients, which are usually determined by non-linear least square regression.

The accuracy of each correlation, is dependent on the set of the data which is used and also on the regression method applied. The source of the data sets that are used for obtaining these coefficients is either the results of MD simulations or the results of experiments conducted on single component fluids in a container of nanopores with a uniform pore size distribution.

In this study, the results of the experiments conducted on single component fluids is employed to obtain these coefficients. The geochemical and geophysical properties of the rocks are believed to influence the extent of the confinement effects, hence, the coefficients obtained from such experiments is specific to the type of porous medium used in the experiments. In this study, for the first time, the correlations for shift in critical properties were obtained from the experiments conducted on a real shale core sample and for gas-condensate mixtures. Having higher number of parameters (including fluid viscosities, densities and in case of gas condensate mixtures, LDO) would result in obtaining more accurate values for A and B in Equation 5.13. However, apart from the measurements conducted in this study to obtain Pdew (as one of the most important variables in tuning any correlation for fluid phase behaviour), there is no experimental data available for other parameters which could be used to further increase the accuracy of the estimations obtained based on Equation 5.13.

Pore size distributions in unconventional rocks are not uniform. Considering that the characteristic length of a porous medium plays an important role on the extent of the impacts of confinement on phase behaviour, it would be of great interest that a

representative pore radius to be defined. In this study, the average of pore sizes obtained from the normalized pore size distribution is used as the characteristic length of the porous medium under study and employed as the pore radius (r_p) in the corresponding equations.

As noted in chapter 4, measured confined Pdew of the single component (C2) fluid is between 481 and 499 psi, whereas the bulk Pdew of C2 is 545 psi at 20 °C. Equation 5.13 was employed and the optimum values for A and B were obtained to match the confined Pdew of C2 by changing the critical properties as expressed by Equation 5.13. During the fitting process, it was observed that it was not possible to get a good match if the same coefficients for critical pressure and temperature were used. In other words, the extent of a change in the critical pressure should be higher than that in the critical temperature to get a good match. The final fitted equations for the dimensionless shift of confined pressure and temperature are presented in equations 5.14 and 5.15, respectively.

$$\frac{(P_c - P_{cp})}{P_c} = 2.49\frac{\sigma}{r_p} - 0.64\left(\frac{\sigma}{r_p}\right)^2 \qquad \text{Eq. 5.14}$$

$$\frac{(T_c - T_{cp})}{T_c} = 1.65\frac{\sigma}{r_p} - 0.4\left(\frac{\sigma}{r_p}\right)^2 \qquad \text{Eq. 5.15}$$

The impact of different pore sizes in unconventional rocks is inherent in the coefficient which is obtained for each specific type of rock. As a result, the coefficients used in these equations are specific to the rock type used in this study. This suggests that other experiments are required to propose a general equation for shift in critical properties in different rocks.

Bulk and confined phase curves of C2 are depicted in Figure 5.1. As it can be observed, pore confinement has shifted the saturation curve downward. For other components used in this study, same equations were used to obtain shifted critical properties.

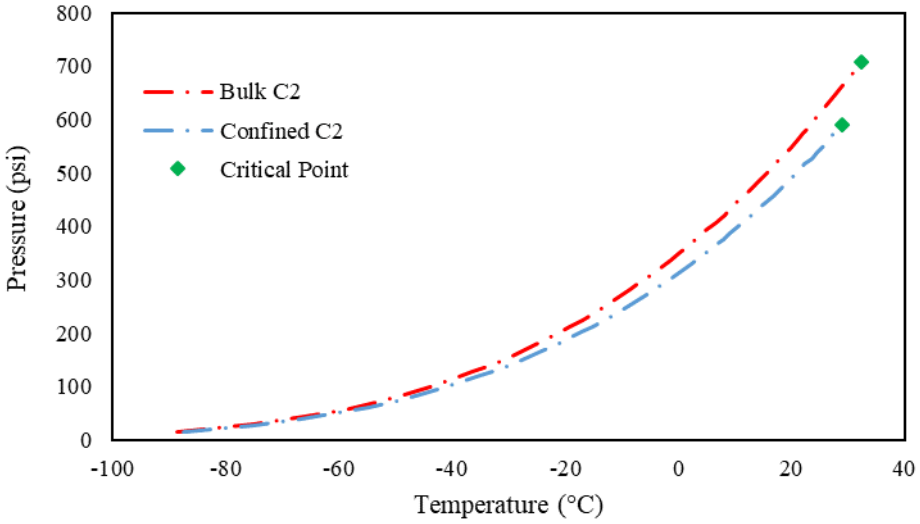

Figure 5.1: Ethane bulk and confined saturation curves.

Critical point is the end point of saturation pressure line separating the liquid and gas phases. Accordingly, critical temperature (Tc) can be considered as a measure of the strength of the intermolecular attraction forces of the fluid molecules in the gaseous phase, i.e. the weaker are the attraction intermolecular forces, the more difficult it is to liquefy that gas and hence, the lower is its critical temperature. For a single component fluid, above Tc, the molecules have too much kinetic energy for the intermolecular attractive forces to hold them together in a separate liquid phase. The explanation for the decrease in Tc is the weaker role of the fluid-fluid interactions in narrow pores as compared to the fluid-wall interactions. The confined fluid is denser than the bulk fluid, because the attractive potential of nanopores walls bring fluid molecules closer to the walls and also to interact strongly with each other. Consequently, the confined fluid condenses at lower pressure than the bulk fluid does. This phenomenon may shift the phase curve to a lower critical temperature and pressure, and a different critical density.

There are studies that suggested the change in critical properties should only be used for considering the effects of confinement. For mixtures, they have suggested that simple mixing rules can be applied with shifted critical properties to take into account the impacts of confinement. However, this approach does not give proper results for gas condensate mixtures. As discussed in Chapter 4, the impact of confinement effects the single component fluid Pdew and gas condensate mixtures Pdew is different, i.e. Pdew of single component fluid decreases while Pdew of gas condensate mixtures increase due to the effects of pore confinement. Solely considering critical properties shift cannot capture such fluid behaviours. To demonstrate the impact of different trends for single component

and multi-components mixtures, the available equations suitable for predicting the single-component saturation pressure due to confinement, which are based on the shift in the corresponding critical properties, were used as the starting point for predicting Pdew of GC mixtures used in this study. The results of employing these different formulations are compared with the experimental data from this study in table 5.1.

Table 5.1: Comparison between different proposed equations for prediction of confined Pdew of fluid samples used in this study

Fluid	**Bulk Pdew (psi)**	**Range of measured confined Pdew (psi)**	**Zarragoicoechea and Kuz (2004)**	**Zhang *et al.* (2018)**	**Sun et al. (2015)**
F1	2392	2450 - 2500	2367	2374	2287
F2	2493	2562 - 2581	2479	2484	2388
F3	2213	2264 - 2281	2179	2202	2112
F4	1891	1915 - 1935	1843	1882	1801
F5	5784	6041 - 6063	5808	5833	4286
F6	5264	5498 - 5519	5288	5312	3875
F7	4052	4181 - 4205	4003	4014	3846
F8	4110	4258 - 4275	4065	4075	3901
F9	3783	3884 - 3904	3735	3747	3596
F10	4538	4721 - 4740	4472	4473	4295

As it can be observed, none of the proposed formulations could properly predict the confined Pdew of the gas condensate mixtures. In fact, all of these formulations are based on the reduction of critical pressure and temperature as a result of confinement, which makes the resulting predicted confined Pdew of the gas condensate mixtures to be lower than the bulk value. This suggests that these formulations are only valid for single component fluids and also in specific conditions under which these formulations have been tuned and obtained. For a gas condensate mixture, if one is supposed to get a proper match for confined Pdew by just changing the critical properties, the critical properties should be forced to increase. Considering that the downward shift in critical properties due to confinement has been verified experimentally, modifications in addition to shift in the critical properties of the corresponding single-components, are required for prediction of gas condensate mixture phase behaviour in confined space.

5.3 BIP Modifications

As mentioned in previous sections, the trend of the impacts of confinement on the Pdew of fluids is different for single component fluids and gas condensate mixtures. This suggests that apart from the widely used approaches (i.e. shift in critical properties) for the prediction of the phase behaviour of confined fluids which are based on the results obtained for single component fluids, it is required to take into account another approach which is suitable for mixtures.

The first attempt in this study to modify PR EOS for confined fluids, was based on modifying VdW attraction parameters. This approach was based on increasing the attraction parameter value based on different force field potentials. That is, the term $U_{fw(LJ)}$ was added to the VdW attraction parameter as shown in equation 5.16.

$$a_{ij-conf} = a_{ij-bulk} + U_{fw(LJ)} \qquad \text{Eq. 5.16}$$

where $a_{ij-conf}$ is the VdW interaction parameter for the confined i and j molecules, $a_{ij-bulk}$ is the VdW interaction parameter for the bulk state of the molecules and is represented as equation 5.9, and $U_{fw(LJ)}$ is the confinement induced attraction term. However, this equation was not able to properly match the experimental results. The main reasons for the deficiency of this approach was its low flexibility with the type of the molecules and porous medium which sometimes resulted in the divergence in the VLE calculations.

As mentioned before, binary interaction parameters, do not have any solid theoretical background. These parameters aimed to capture the non-ideal interactions among different types of molecules. The interactions between pore walls and fluid molecules can be modelled with VdW forces taking place between two similar/dissimilar non-polar molecules.

In this study, pore confinement effects were assumed to have two different types of impacts on single-component and multi-component mixture confined fluids. Figure 5.2 represents a schematic of a pore filled with different types of fluids, i.e. single component and binary component fluids. In Figure 5.2 (a) the pore is filled with a single component fluid. In this system, the fluid phase behaviour is determined by the magnitude of the interactions taking place between similar fluid molecules and that between fluid molecules and pore walls. Depending on the size of the pore and the size of the fluid molecules, the impacts of pore walls may be important. In the open literature, the

interactions taking place between each single component fluid and the pore walls are translated into the shift of the critical properties (Barsotti *et al.*, 2016; Salahshoor *et al.*, 2018; Tan *et al.*, 2020), which was observed and adopted too. In other words, in a porous medium with nanopores where these pores are filled with single component fluid, the interactions between similar molecules and the pore walls would influence the critical temperature and pressure. Hence, the effective influence of pore confinement effects on the values of U_{1w} defined as the interaction between pore walls and type 1 fluid molecules would change the critical properties of the type 1 fluid molecules in the confined space. This influence would exist even in the presence of other types of molecules of a mixture. However, in the case of the porous medium filled with a fluid comprising of two types of molecules, and as depicted in Figure 5.2 (b), pore walls would have similar effects on U_{22} and U_{2w}. In other words, the critical properties of the confined type 2 fluid would also be changed due to the confinement in a similar way to type 1 fluid critical properties. However, when there is more than one type of fluid component, another interaction exist in the system. U_{12} is a non-ideal interaction taking place between type 1 and type 2 fluid molecules. In this study, it is assumed that the pore walls would influence this type of interactions as well. The influence of the pore walls on U_{12} is called the confinement induced mixture interactions. As a result, U_{12} is a function of two interaction parameters. Equation 5.17 is a new equation proposed in this study based on which the effects of confinement on the phase behaviour of different mixtures can be predicted. In this equation, total binary interaction parameter (BIP_{total}) is introduced which is simply the summation of the bulk binary interaction parameter (BIP_{bulk}) of type 1 and type 2 fluid molecules and the confined binary interaction parameter $\left(BIP_{confined}\right)$ which is influenced by the level of confinement effects. It should be mentioned that BIP_{bulk} is the value, which can be obtained from bulk Pdew measurements and, $BIP_{confined}$ needs to be determined by experimental results under confinement. The remainder of this chapter is dedicated to propose an equation to estimate the $BIP_{confined}$ based on tuning the EOS predictions to match the results of the experiments performed in this study.

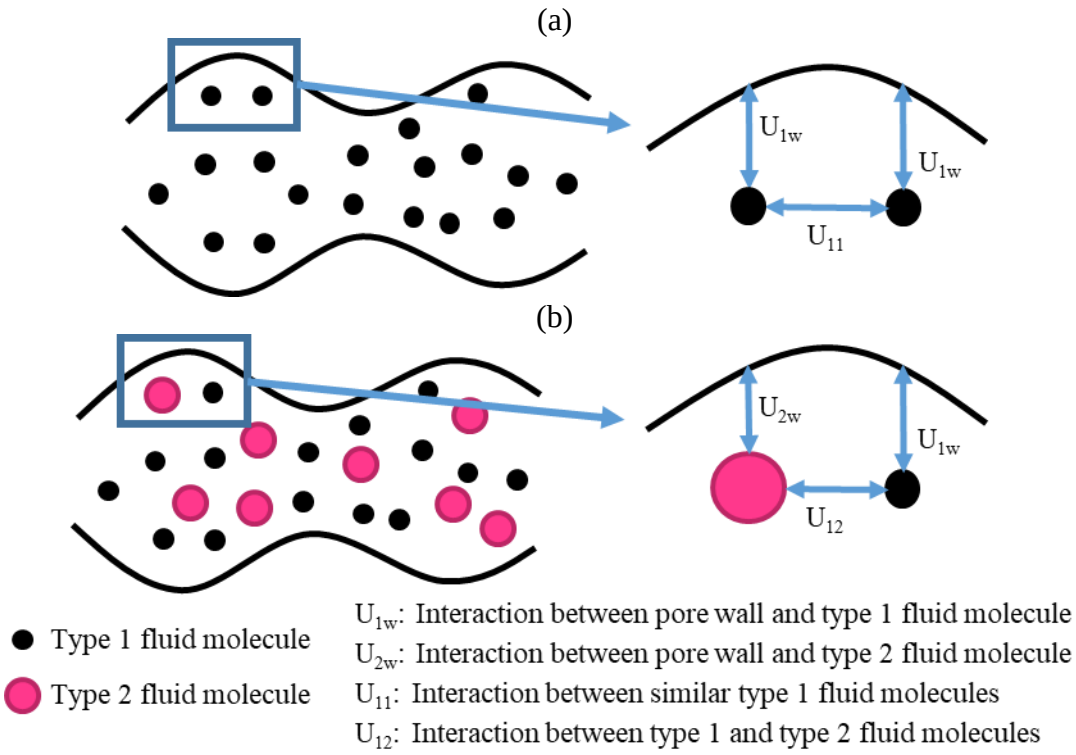

Figure 5.2: Schematic of different interactions taking place in a pore filled with (a) similar fluid molecules of a single-component and (b) different fluid molecules of a binary mixture.

$$BIP_{total} = BIP_{bulk} + BIP_{confined} \qquad \text{Eq. 5.17}$$

BIP_{bulk} is easily attainable through bulk Pdew measurements. For the simplicity and the accuracy of the calculations for the values of the $BIP_{confined}$, following term (α) is defined as the characteristic parameter:

$$\alpha = \frac{BIP_{confined}}{BIP_{bulk}} \qquad \text{Eq. 5.18}$$

In physical term, α can be defined as below:

$$\alpha = \frac{Fluid - Wall\ interaction\ potential}{Fluid\ interaction\ potential}$$

Fluid-wall interaction potential would tend to be zero when the pore radius is sufficiently large to ignore fluid-wall interactions. In this study, in order to estimate the fluid-wall interactions, it is assumed that the pore wall surface is covered with the heavier molecule of the binary mixture components. Moreover, the interactions taking place between each fluid component and pore walls are assumed to be a function of the LJ potential defined

by Equation 2.2. These component fluid interaction potentials can be estimated by different well-known intermolecular potentials like LJ, Steel, or TraPPe (Liu and Zhang, 2019). The mixture fluid interaction potential is then assumed to be a linear function of the components LJ potentials and their mole fractions. The advantage of using the LJ potential is being simple yet giving the realistic values for intermolecular interactions between non-polar molecules. An additional term is also added to take into account the fluid-wall affinity which depends on the mineralogy and morphology of the porous medium as well as the type of the fluid used for measurements. Hence, equation 5.19 can be proposed in a simplified form to estimate $BIP_{confined}$ for a binary mixture.

$$\alpha = A_{fw}\frac{[z_1U_{12} + z_2U_{22}]}{U_{12}} \qquad \text{Eq. 5.19}$$

with

$$\varepsilon_{12} = \sqrt{\varepsilon_1\varepsilon_2} \qquad \text{Eq. 5.20}$$

$$\sigma_{12} = \frac{1}{2}(\sigma_1 + \sigma_2) \qquad \text{Eq. 5.22}$$

$$U_{12} = 4\varepsilon_{12}\left[\left(\frac{\sigma_{12}}{r_p}\right)^{12} - \left(\frac{\sigma_{12}}{r_p}\right)^{6}\right] \qquad \text{Eq. 5.23}$$

$$U_{22} = 4\varepsilon_2\left[\left(\frac{\sigma_2}{r_p}\right)^{12} - \left(\frac{\sigma_2}{r_p}\right)^{6}\right] \qquad \text{Eq. 5.24}$$

where ε_1 and ε_2 are the LJ dispersion energy parameters for fluid's component 1 and 2 molecules, respectively. σ_1 and σ_2 are the LJ size parameters of fluid's component 1 and 2, respectively. z_1 and z_2 are the molar fractions of fluid component 1 and 2, respectively. It should be noted that in these equations, fluid component 2 is considered to be heavier than component 1 with higher affinity towards the rock surface. A_{fw} is the fluid-wall affinity coefficient which depends on the pore wall geochemical and geophysical properties as well as fluid type and temperature. U_{12} is the LJ intermolecular interaction between fluid component 1 and 2. U_2 is the LJ intermolecular interaction potential between similar molecules of component 2. As mentioned, it is assumed that for the considered binary mixture, the surface of the rock is covered with the heavier molecule (i.e. component 2). Hence, the interactions between the rock and the fluid molecules were simplified to the interactions between fluid molecules (component 1 and component 2) and the pore wall and heavier molecules of the fluids (rock and component 2). The

impacts of rock properties are linearly correlated to the fluid-wall potential by parameter A_{fw} which can be estimated experimentally.

5.4 PR EOS Modifications

In this study, the 3-parameter PR EOS was used to predict the phase behaviour of the confined binary gas condensate mixtures. The LBC viscosity correlation was used to predict fluid viscosities. Different parameters, including BIPs, Ω_a, Ω_b, S-shift, Vc and Zc, were considered for regression. During the regression process it was observed that the most effective regression parameters were BIPs, Ω_a, Ω_b, and S-shift to match the observed bulk LDO and Pdew for different gas condensate mixtures. The EOS confinement induced modifications involved the critical properties shift due to confinement as well as adding the parameter $BIP_{confined}$ to obtain BIP_{total}. In obtaining $BIP_{confined}$, A_{fw} since being unknown, served as a tuning parameter for each rock-fluid system. Table 5.2 shows bulk (Tc and Pc) and confined (Tcp and Pcp) critical properties of different components used for gas condensate fluid mixtures. Bulk critical properties of different components were obtained from NIST website. Confined critical properties were estimated based on equations 5.14 and 5.15 proposed for single-component under confinement.

Table 5.2: Bulk and confined critical properties used for EOS tuning in this study

Component	Pc (psi)	Tc (°F)	Pcp (psi)	Tcp (°F)
C1	666.45	-116.59	655.50	-120.33
C5	488.78	385.61	479.87	375.40
C8	360.56	564.17	352.45	548.91
C10	306.03	660.11	298.67	642.26

At this stage, first the best $BIP_{confined}$ values for each fluid is determined by a simple regression to match some of the measured data. Then the predictive capability of the proposed equation for is examined for other measured data not used for its development. Table 5.3 shows the results of the $BIP_{confined}$ obtained from the tuning of the EOS prediction to some of the measured data..

Table 5.3: Different tuned BIP values for gas condensate fluid mixtures.

Fluid	Bulk Pdew (psi)	Range of measured confined Pdew (psi)	BIP_{bulk}	BIP_{total}	$BIP_{confined}$
F2	2493	2562 – 2581	0.001	0.021	0.020
F3	2213	2264 – 2281	0.001	0.028	0.027
F4	1891	1915 – 1935	0.002	0.034	0.033
F5	5784	6041 – 6063	0.039	0.078	0.039
F6	5264	5498 – 5519	0.041	0.081	0.040
F7	4052	4181 – 4205	0.016	0.032	0.017
F8	4110	4258 – 4275	0.016	0.032	0.017
F9	3783	3884 – 3904	0.016	0.033	0.017

EOS modifications based on the abovementioned changes resulted in the decrease of the liquid drop out of the gas condensate mixtures. However, there are no acceptable experimental evidence that confirms any decrease in the richness of gas condensate fluids due to pore confinement effects, if anything liquid drop-out would be expected to increase, at least initially, due to increased heavy molecules-pore wall interactions. Therefore, the modified EOS obtained based on matching confined Pdew were further modified to reach the same MLDO for bulk and confined fluids. Based on the above modifications, phase envelope for each gas condensate mixture was plotted with the aid of PVTi module of Schlumberger Eclipse software package. Figure 5.3 compares the phase envelopes of confined and bulk state of the F7 gas condensate mixture.

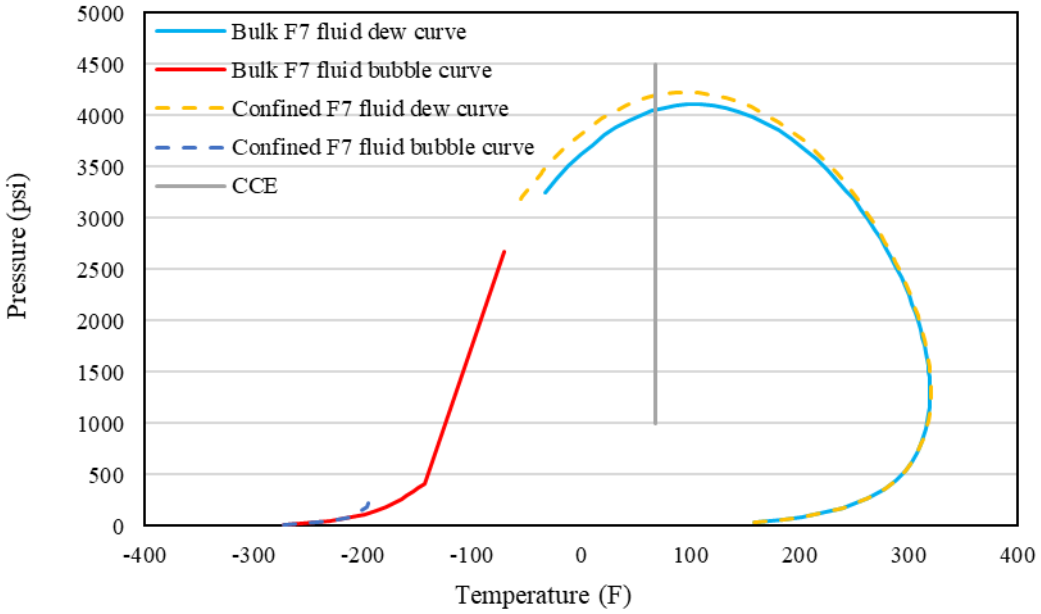

Figure 5.3: Comparison of bulk and confined F7 fluid phase envelopes.

As it can be observed, unlike the case of single component fluid, the phase envelope of F7 fluid has shifted upward due to the effects of pore confinement. As a result, the Pdew of the gas condensate mixture is higher in confined space compared to the bulk state.

Vapour and liquid viscosities for the confined and bulk fluids are compared in Figure 5.4.

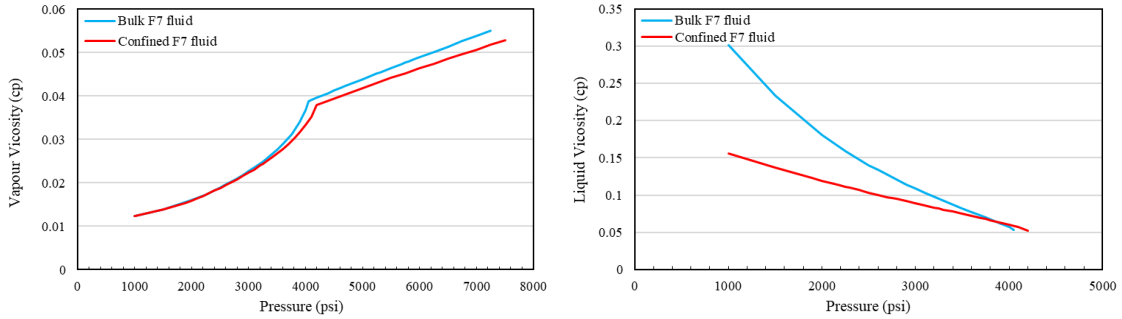

(a) (b)

Figure 5.4: Comparison of bulk (blue) and confined (red) F7 fluid (a) vapour viscosity, and (b) liquid viscosity

As it can be observed, up to the pressures of around 3000 psi, confined and bulk fluid vapour viscosities are similar. However, when pressure increases to values higher than 3000 psi, bulk and confined vapour viscosities tend to deviate from each other. When bulk and confined fluids are in the single phase state, i.e. for pressures higher than 4000 psi, confined fluid vapour viscosity is lower than bulk fluid vapour viscosity. This could be attributed to the higher interactions of pore walls and heavier molecules of confined fluid which results in the higher density of the gas condensate mixtures in the vicinity of the pore walls. However, since the heavier molecules are more attracted to the pore walls, the remainder of the gas condensate mixture, which would be more of gas like behaviour, within the pore would have lower density and lower content of heavier molecules results in lower viscosity of the gas. It can also be observed that due to the confinement effects, liquid viscosity of confined fluid is lower than the liquid viscosity of the bulk fluid. Table 5.4 compares the simulated liquid density of the bulk and confined fluid obtained from PVTi at 4 different pressures below Pdew. As it can be observed, apart from the pressure point of 4000 psi which is very close to the Pdew of the gas condensate mixture, the liquid density of the bulk fluid is higher than the liquid density of the confined fluid. Liquid viscosity of the confined fluid is predicted to be lower mainly due to using lower Tc and Pc for confined fluids compared to bulk fluids. However, a rigorous experimental or theoretical method is needed to confirm the change in the viscosity of the confined fluid.

Table 5.4: Simulated liquid density of bulk and confined F7 fluid at different pressures.

Pressure (psi)	Liquid density (cp)	
	bulk	confined
4000	25.5	26.6
3500	30.1	29.5
3000	33.0	31.7
2500	35.6	33.6

As discussed earlier, the simulated LDO were fitted in a manner that the MLDO of both confined and bulk fluid be the same. Since, there was no evidence for decrease in liquid dropout, the confined fluid EOS model was tuned based on the results of experimental bulk LDO measurements performed. The comparison between bulk and confined F7 fluid LDO is shown in Figure 5.5.

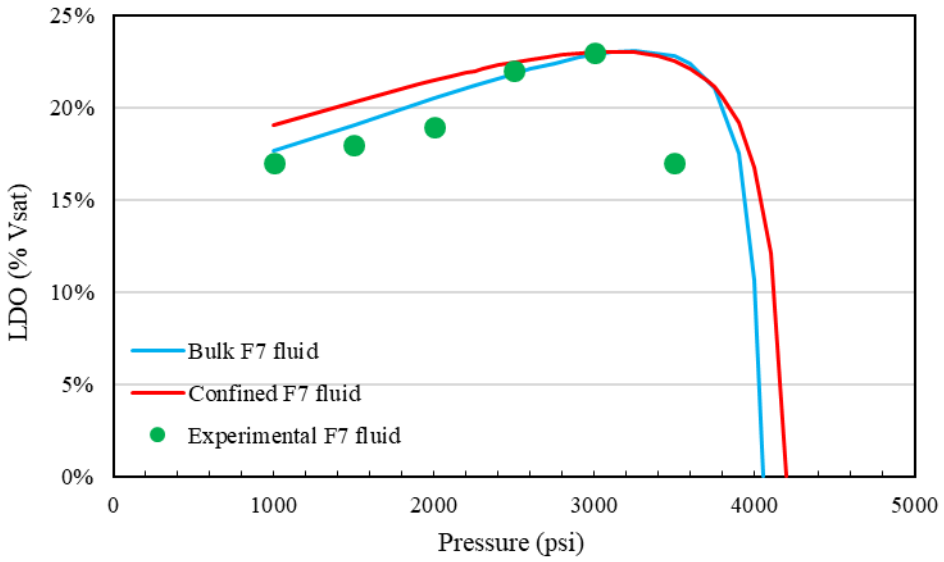

Figure 5.5: Experimental bulk and simulated bulk and confined liquid dropout of the F7 fluid sample

Similar trends were observed for other gas condensate fluid mixtures. The results of the comparison between confined and bulk state of other fluid mixtures are presented in Appendix 1.

5.5 Empirical Correlations for BIP_{total}

In this section, based on the experimentally determined values for $BIP_{confined}$, the A_{fw} values would be determined. After that, the impacts of temperature on the $BIP_{confined}$ would be examined and the dependency of A_{fw} on temperature would be formulated. The

capability of the proposed correlation for the prediction of confined Pdew based on fluid composition will be examined at the end.

5.5.1 Estimation of the Effects of Fluid Type on A_{fw}

As mentioned earlier, A_{fw} is the affinity of the fluid towards the wall surface. Hence, A_{fw} is dependent on both fluid component types and rock type. The results of the experiments for F1 to F4 fluid samples which comprise of C1 and C5 are summarized in table 5.5.

Table 5.5: A summary of the properties, bulk and confined BIP values for F2 to F4 fluid samples and EF2 core sample used in this study.

Fluid	Composition (mole %)		Bulk Pdew (psi)	Range of measured confined Pdew (psi)	BIP_{bulk}	$BIP_{confined}$	α
	C1	nC5					
F2	86	14	2493	2562 – 2581	0.001	0.020	20.0
F3	92.2	7.8	2213	2264 – 2281	0.001	0.027	20.6
F4	94.6	5.4	1891	1915 – 1935	0.002	0.033	21.7

With the experimentally determined values for α, considering that all experiments have been conducted on the same rock sample, the experimental values for the term A_{fw} for each fluid can be determined using the rearranged form of equation 5.19. Table 5.6 shows the values for A_{fw} corresponding for F1 to F4 fluid samples and EF2 core sample. As it can be observed, the difference between A_{fw} values is very marginal, which suggests that the proposed method can be used with an acceptable accuracy for a specific system of gas condensate mixture and rock type.

Table 5.6: A_{fw} Values corresponding to F1 to F4 fluid samples and EF2 core sample.

Fluid	A_{fw}
F2	19.63
F3	20.36
F4	21.54

Table 5.7 shows the BIP values as well as α, and A_{fw} for other fluid types used in this study. As it can be observed, for other fluid samples comprising of similar components,

the values of the term A_{fw} are almost the same too. These results suggest that a single value of A_{fw} can be used for these fluids with different compositions.

Table 5.7: Values for BIP_{bulk}, BIP_{total}, $BIP_{confined}$, α, and A_{fw} corresponding to F5 to F9 fluid samples and EF2 core sample.

Fluid	Composition (mole%)			BIP_{bulk}	BIP_{total}	$BIP_{confined}$	α	A_{fw}
	C1	nC8	nC10					
F5	92	-	8	0.039	0.078	0.039	1.0	0.86
F6	95.9	-	4.1	0.041	0.081	0.040	1.0	0.91
F7	92.3	7.7	-	0.016	0.032	0.017	1.1	0.95
F8	90	10	-	0.016	0.032	0.017	1.1	0.94
F9	95.1	4.9	-	0.016	0.033	0.017	1.1	1.04

5.5.2 Estimation of the Effects of Temperature on A_{fw}

In order to estimate the dependency of A_{fw} on temperature, the results of experiments conducted to at different temperatures were used following the same procedure as that described above. In other words, first, bulk fluid EOS was tuned based on the obtained experimental data. Then, critical properties of the components were modified based on equation 5.14 and 5.15. Finally, by only changing the BIP, Pdew of the confined fluid was matched with the measured experimental range. Table 5.8 shows the values for BIP_{bulk}, BIP_{total} and $BIP_{confined}$ as well as the parameters α and A_{fw} of the F7 fluid sample at different temperatures.

Table 5.8: Values for BIP_{bulk}, BIP_{total}, $BIP_{confined}$, α, and A_{fw} corresponding to F7 fluid sample and EF2 core sample at different temperatures.

Temperature (°C)	BIP_{bulk}	BIP_{total}	$BIP_{confined}$	α	A_{fw}
20	0.016	0.032	0.017	1.1	0.95
40	0.010	0.024	0.014	1.4	1.26
60	0.017	0.029	0.012	0.7	0.61

In order to obtain the relation between temperature and A_{fw}, a trend line for a plot of A_{fw} versus temperature was fitted as depicted in Figure 5.6. As it can be observed, the dependency of A_{fw} on the temperature was found to be non-monotonic that can be expressed by a second order polynomial.

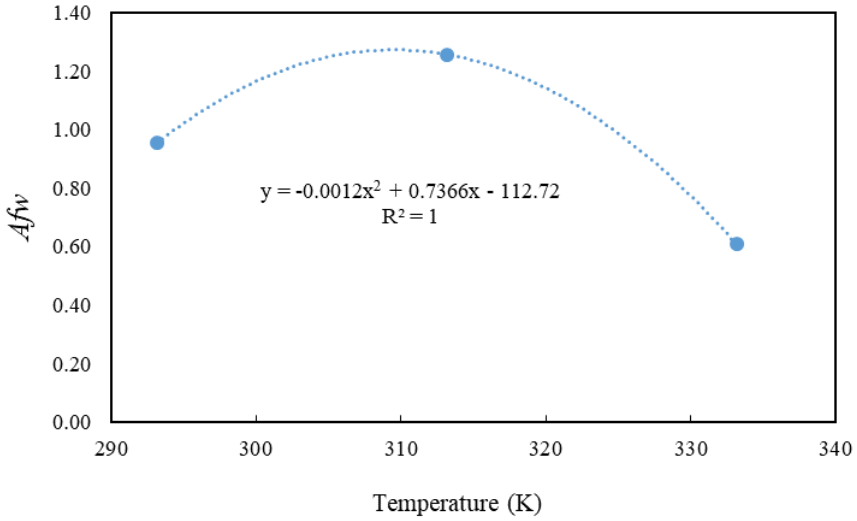

Figure 5.6: Plot of A_{fw} versus temperature for F7 fluid sample and EF2 core sample

It should be mentioned that the equation presented in Figure 5.6 is only specific to the fluid type and the core sample used in this study.

5.5.3 Estimation of the Effects of Net Stress on A_{fw}

In chapter 4, it was found that net stress could be effective on the extent of confinement effects, especially for fluid samples containing heavier molecules like nC8 and nC10. In this section the effects of net stress on the proposed correlation for EOS modification are discussed.

Nazari Moghaddam and Jamiolahmady (2016) observed that increasing net stress could reduce the average pore radius of the porous medium. They estimated pore size distribution of an Eagle Ford core sample under different net stress values. In their study, it was assumed that pore size distribution would be affected uniformly by geo-mechanical stress. Hence, they obtained the pore size distribution of the Eagle Ford core sample as depicted in Figure 5.7. Based on this Figure, average pore radius of the Eagle Ford core sample reduces from 54nm to 45nm and 38nm, when the net stress increases from 500 psi to 1000 psi and 2000 psi, respectively. Similar average pore radius values have been used in this study. The modified critical properties of C1, nC5, nC8 and nC10 components, which are obtained for different net stress values based on equations 5.14 and 5.15 are presented in table 5.9. It should be noted that for each net stress value, the corresponding average pore radius is used.

Table 5.9: Confined critical properties of C1, nC5, nC8 and nC10 for different net stress values.

Component / Net stress (psi)	Tcp (°F)			Pcp (psi)		
	500	1000	2000	500	1000	2000
C1	-120.33	-121.07	-121.90	655.50	653.31	650.90
C5	375.40	373.36	371.11	479.87	478.09	476.13
C8	548.91	545.86	542.50	352.45	350.84	349.05
C10	642.26	638.70	634.77	298.67	297.20	295.58

As expected, reducing the average pore size resulted in the further reduction of confined critical properties. These properties were used in the equations of state modified for confined fluid Pdew estimations. In order to evaluate the impacts of net stress on the EOS of confined fluids, F4, F5 and F7 fluid samples were considered. Based on the results of the experiments, and applying modified critical properties and also fitting the BIP values for confined fluid samples, the estimated values of BIP_{bulk}, BIP_{total}, $BIP_{confined}$, α, and A_{fw} for F4 fluid sample and different net stress values are presented in table 5.10.

Table 5.10: Values for BIP_{bulk}, BIP_{total}, $BIP_{confined}$, α, and A_{fw} corresponding to F4 fluid sample and EF2 core sample at different net stress values.

Net stress (psi)	BIP_{bulk}	BIP_{total}	$BIP_{confined}$	α	A_{fw}
500	0.002	0.034	0.033	21.7	21.54
1000	0.002	0.036	0.035	23.3	23.10
2000	0.002	0.040	0.039	25.8	25.62

The estimated values of BIP_{bulk}, BIP_{total}, $BIP_{confined}$, α, and A_{fw} for F5 and F7 fluid samples are presented in table 5.11 and 5.12, respectively.

Table 5.11: Values for BIP_{bulk}, BIP_{total}, $BIP_{confined}$, α, and A_{fw} corresponding to F5 fluid sample and EF2 core sample at different net stress values.

Net stress (psi)	BIP_{bulk}	BIP_{total}	$BIP_{confined}$	α	A_{fw}
500	0.039	0.078	0.039	1.0	0.86
1000	0.039	0.082	0.042	1.1	0.94
2000	0.039	0.087	0.048	1.2	1.06

Table 5.12: Values for BIP_{bulk}, BIP_{total}, $BIP_{confined}$, α, and A_{fw} corresponding to F7 fluid sample and EF2 core sample at different net stress values.

Net stress (psi)	BIP_{bulk}	BIP_{total}	$BIP_{confined}$	α	A_{fw}
500	0.016	0.032	0.017	1.1	0.95
1000	0.016	0.038	0.022	1.4	1.26
2000	0.016	0.047	0.032	2.0	1.81

The relationship between A_{fw} and net stress can be better evaluated if the corresponding average pore radius of the core for each net stress is to be considered versus A_{fw} values. Accordingly, Figure 5.7 shows the corresponding graphs of A_{fw} versus $\left(\frac{\sigma}{r_p}\right)$ for F4, F5 and F7 fluid samples. Based on the data of these plots, A_{fw} was found to be a second order polynomial function of $\left(\frac{\sigma}{r_p}\right)$, which is quite similar to the tendency of the critical properties shift to $\left(\frac{\sigma}{r_p}\right)$.

(a)

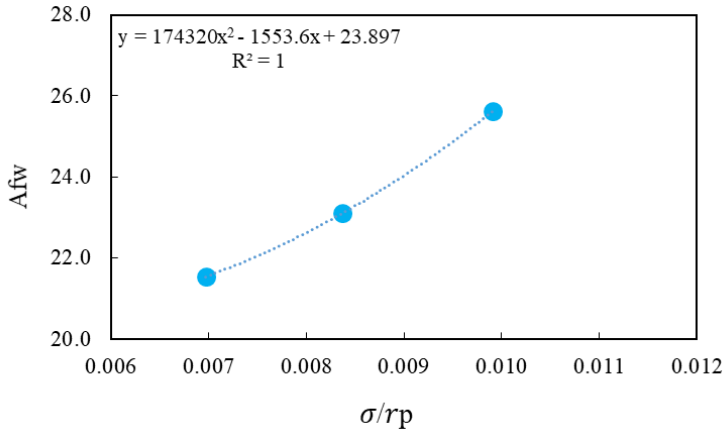

(b)

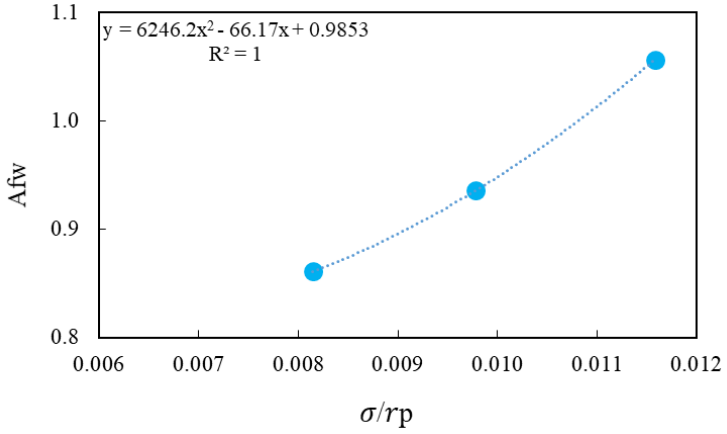

(c)

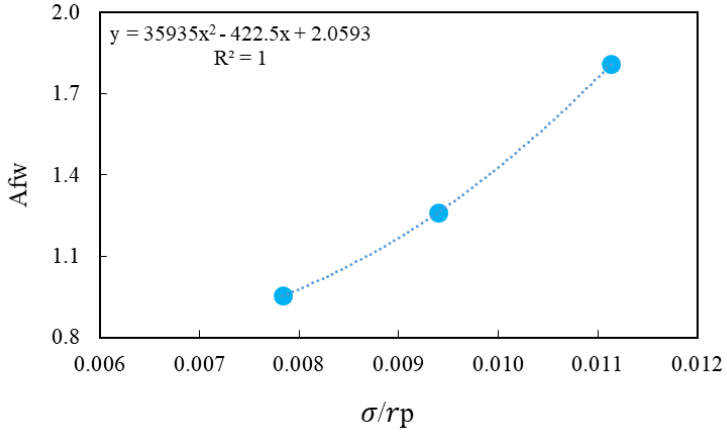

Figure 5.7: Plot of A_{fw} versus $\left(\frac{\sigma}{r_p}\right)$ obtained at different net stress for (a) F4, (b) F5, and (c) F7 fluid samples.

5.6 Predictability of the Proposed Empirical Correlation for Confined Pdew

In order to examine the accuracy of the proposed correlation, the obtained A_{fw} values for each fluid comprising of definite components would be examined. In other words, using

the experimentally determined A_{fw} for a specific fluid sample, confined Pdew of other fluid samples which comprise of similar components but not used for the development of A_{fw} expression are predicted using the same A_{fw}.

In this section, only the predictability of A_{fw} for the fluid F2 sample comprising C1+nC5, F5 fluid sample comprising of C1+nC10, and F7 fluid sample comprising of C1+nC8 are discussed. The accuracy of using other A_{fw} values for other fluids is demonstrated in Appendix 1.

A summary of the data to examine the predictability of the proposed correlation is shown in table 5.13 to table 5.15 for F2, F4 and F7 samples, respectively. For F2 sample, A_{fw} was calculated to be 19.63, for F5 fluid sample, A_{fw}, was calculated to be 0.86 and for F7 sample it was calculated to be 0.95. These values were used for the calculation of corresponding α for other fluids with similar components.

Table 5.13: Predicted Pdew for F3 and F4 fluid samples using measured and calculated data of F2 fluid sample

Fluid	BIP_{bulk} from experiments	A_{fw}	α	BIP_{total}	Confined Pdew (psi)
F2	0.001	19.63	20.0	0.021	2572
F3	0.001	19.63	19.8	0.021	2262
F4	0.002	19.63	19.8	0.031	1909

Table 5.14: Predicted Pdew for F6 fluid sample using measured and calculated data of F5 fluid sample.

Fluid	BIP_{bulk} from experiments	A_{fw}	α	BIP_{total}	Confined Pdew (psi)
F5	0.039	0.86	1.0	0.078	6052
F6	0.041	0.86	0.9	0.079	5477

Table 5.15: Predicted Pdew for F8 and F9 fluid samples using measured and calculated data of F7 fluid sample.

Fluid	BIP_{bulk} from experiments	A_{fw}	α	BIP_{total}	Confined Pdew (psi)
F7	0.016	0.95	1.1	0.032	4193
F8	0.016	0.95	1.1	0.032	4273
F9	0.016	0.95	1.0	0.032	3866

In order to calculate the error of the proposed correlation for the prediction of the confined Pdew, the difference between measured bulk and confined Pdew was calculated for

different fluid samples and it was compared with the corresponding predicted value as expressed by the below expressions.

$$Error(\%) = \frac{(measured\ confined\ Pdew - measured\ bulk\ Pdew) - (predicted\ confined\ Pdew - measured\ bulk\ Pdew)}{(measured\ confined\ Pdew - measured\ bulk\ Pdew)} \times 100$$

Since, the experimental results of the confined Pdew include a range and has an upper and a lower band, two error values for each prediction were calculated. Table 5.16 shows the results of the error estimations for different fluid samples.

Table 5.16: Error values for predicted confined Pdew based on the proposed correlation

Fluid	Bulk Pdew (psi)	Range of measured confined Pdew (psi)	Predicted confined Pdew (psi)	Error (%) compared to	
				Lower Pdew	Upper Pdew
F2*	***2493***	***2562 – 2581***	***2572***	***-14.5***	***+10.2***
F3	2213	2264 – 2281	2262	+3.9	+27.9
F4	1891	1915 – 1935	1909	+25.0	+59.1
F5*	***5784***	***6041 – 6063***	***6052***	***-4.3***	***+3.9***
F6	5264	5498 – 5519	5477	+9.0	+16.5
F7*	***4052***	***4181 – 4205***	***4193***	***-9.3***	***7.8***
F8	4110	4258 – 4275	4273	-10.1	+1.2
F9	3783	3884 – 3904	3866	+17.8	+31.4

*Used as the source data for Pdew predictions

It can be observed that the accuracy of the proposed correlation is reasonably acceptable. For most cases, the correlation slightly under predicts the confined Pdew of the gas condensate mixtures, except for the case of the F8 sample, where it slightly over-predicted. The error range for the predicted confined Pdew of F3 sample is within 3.9 and 27.9%, while the corresponding value for F4 sample are between 25.0 and 59.1%. This higher error for F4 sample is mainly due to the very small difference between measured bulk and confined Pdew. The error range for the predicted confined Pdew of F6 fluid is between 9.0 and 16.5%. The correlation performs better for F8 fluid sample where the error range is between -10.1 and 1.2% as compared to corresponding value of 17.8 and 31.4% for the F9 fluid sample.

As mentioned before, other correlations available in the literature, are based on single component fluids and predicted an incorrect trends of lower confined Pdew for gas condensate mixtures. Therefore, it can be stated that the correlation proposed here is a

reasonably good approach for predicting confined Pdew of gas condensate phase behaviour studies in unconventional reservoirs.

5.6 Concluding Remarks on Pore Confinement Induced EOS Modifications

- Proposed approaches available in the literature can properly predict the phase behaviour of the confined single component fluids. However, for any type of porous medium, specific tuning coefficients need to be used. In this study the proposed equations were used and modified based on the experimental results for a real unconventional core sample and C2 as the single component fluid. Average pore radius obtained from MICP analysis was used to be considered as the representative pore radius for the porous medium.
- For gas condensate mixtures, there was significant disagreement between the trends obtained from the proposed theoretical approaches in the literature and experimental results. That is, all proposed approaches, which have been reported previously to modify the EOS for confined fluids, suggested that confined Pdew of fluid samples reduces since they only considered the effects of pore confinement on the shift of critical properties for single component fluids. However, Pdew of gas condensate mixtures increase due to pore confinement effects. Therefore, in this study, another additional modification was suggested to properly match the Pdew of the confined gas condensate mixtures. This method was based on the addition of the fluid-wall molecular interactions in the binary interaction parameters used for gas condensate mixtures.
- For binary gas condensate mixtures, total binary interaction parameter (BIP_{total}), i.e. the interaction parameter which takes into account the effects of the fluid-fluid interactions (BIP_{bulk}) as well as fluid-wall interaction ($BIP_{confined}$), was suggested to be calculated according to the expression $BIP_{total}=BIP_{bulk}+BIP_{confiend}$. BIP_{bulk} can be obtained by bulk Pdew measurements. $BIP_{confined}$ was suggested to be based on the LJ interaction potential between fluid and pore walls. A new term, α, was defined as the ratio of the $BIP_{confined}/BIP_{bulk}$ which was considered to be dependent on A_{fw}, fluid-wall and fluid-fluid LJ interaction potential. In the proposed correlation, the term A_{fw} was defined as the fluid-wall affinity coefficient. This term can be obtained experimentally and is specific for any rock-fluid system. In this study, the dependency of this term to different parameters including fluid

type, temperature and net stress was examined. It was observed that the values A_{fw} for gas condensate fluids comprising of similar components are within the same range, while when components in different fluids are different from each other, A_{fw} might significantly vary. Moreover, it was observed that A_{fw} does not show any monotonic behaviour with temperature. For instance, for the fluid used in this study, A_{fw} was found to first increase and then decrease with increasing temperature expressed by a quadratic function. The dependency of A_{fw} on net stress was well correlated with considering the change in the size of the pores due to geo-mechanical forces. It was observed that A_{fw} is a second order polynomial function of $\left(\frac{\sigma}{r_p}\right)$. This relation was very similar to that proposed for the shifts in critical properties.

- For any set of fluid samples with similar components, one set of experiments were used to fix the A_{fw} coefficients of this correlation and then it was used to predict the Pdew of other gas condensate fluids which had not be used for tuning the coefficients of the correlation. The proposed method showed very good predictability for binary gas condensate mixtures whose data had not been used for its development. The range of the error was satisfactory for all fluid types. However, the coefficients of the correlation depends on the rock under study and hence for other rocks they might need to be adjusted with limited number of experimentally measured data points.

Chapter 6: Numerical Simulations of Unconventional Gas Condensate Reservoirs

In this chapter, results of a series of CMG-GEM-based single-well compositional simulations performed to investigate the impact of confinement on gas and condensate recovery are discussed. Sensitivity of different parameters including hydraulic fracturing, confinement effects, adsorption-desorption, and diffusion for the considered unconventional gas condensate reservoir model, is studied. The impacts of pore confinement effects on the extent of the production are evaluated using one of the fluid sample prepared for the experiments described in previous chapters. The EOS model presented in chapter 5 is implemented in the simulation model. In unconventional gas reservoirs, it is believed that adsorption and desorption can influence the storage and fluid flow calculations. Furthermore, the transport in unconventional reservoirs within matrix is influenced by the diffusion as well. Therefore, the impacts of considering adsorption-desorption phenomena and diffusion on the production data in the considered gas condensate reservoir model are also investigated. It should be mentioned that the numerical simulations performed in this study can only be considered as a starting point for the analysis of the effects of pore confinement on the performance of gas condensate flow at reservoir scale. Hence, a wider range of parameters with more in depth analysis will be required for a better evaluation of the pore confinement effects in gas condensate unconventional reservoirs.

6.1 Reservoir Model Description

Compositional simulations of a Cartesian reservoir model were performed using CMG-GEM to investigate the impacts of pore confinement. Series of sensitivity on different parameters influencing production from unconventional reservoirs were carried out. The base model used in this study, was a reservoir model with a single horizontal well penetrating in the middle of the reservoir. The basic properties of the model are presented in table 6.1.

Table 6.1: Basic properties of the base Cartesian reservoir model.

Properties	Values
Reservoir Dimensions (ft)	(30*15)*(30*15)*(10*15)
Porosity (%)	15
Horizontal matrix permeability (mD)	0.0044
Vertical matrix permeability (mD)	0.00044
Fluid	Fluid 7 (0.923C1+0.077C8)
Kr	HW measured kr
Diffusion	No
Adsorption	No

Reservoir rock properties, i.e. porosity and permeability, were selected to be similar to those of the EF2 core sample. The F7 fluid sample was used. The confined properties of the fluid sample were estimated by the modified EOS based on the approach presented in chapter 5. The initial water saturation was set to be zero. In the base model, diffusion and adsorption were ignored, however, the impacts of these parameters on the production of the reservoir model were investigated later. Figure 6.1, shows the geometry of the reservoir model, which consisted of 15, 15 and 10 grid blocks in x, y and z directions, respectively. The horizontal well was penetrated into the 5th grid block in the y-direction. It was perforated through 11 grid blocks from 10th to 20th grid in the x direction.

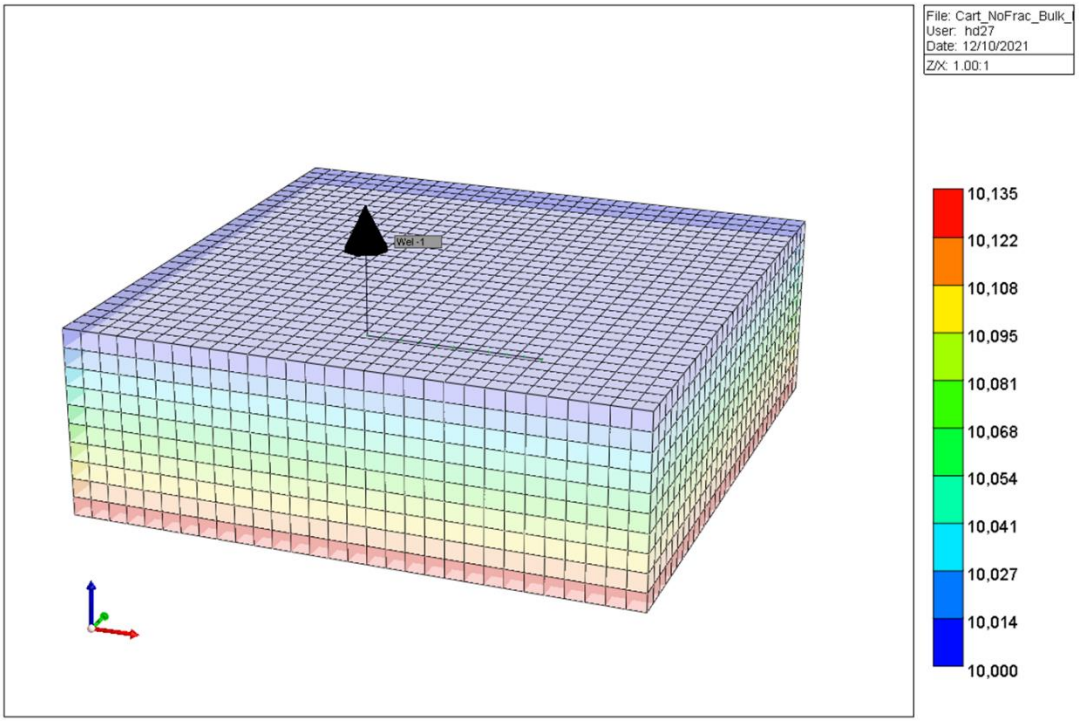

Figure 6.1: Geometry of the Cartesian reservoir model.

It should be mentioned that in the simulations, a gas-condensate kr data set, which has been measured on an Eagle Ford core sample and corrected for the effects of capillary

end effects was used. These kr data are the measured steady state relative permeabilities of gas and condensate. This kr-set are shown in Figure 6.2.

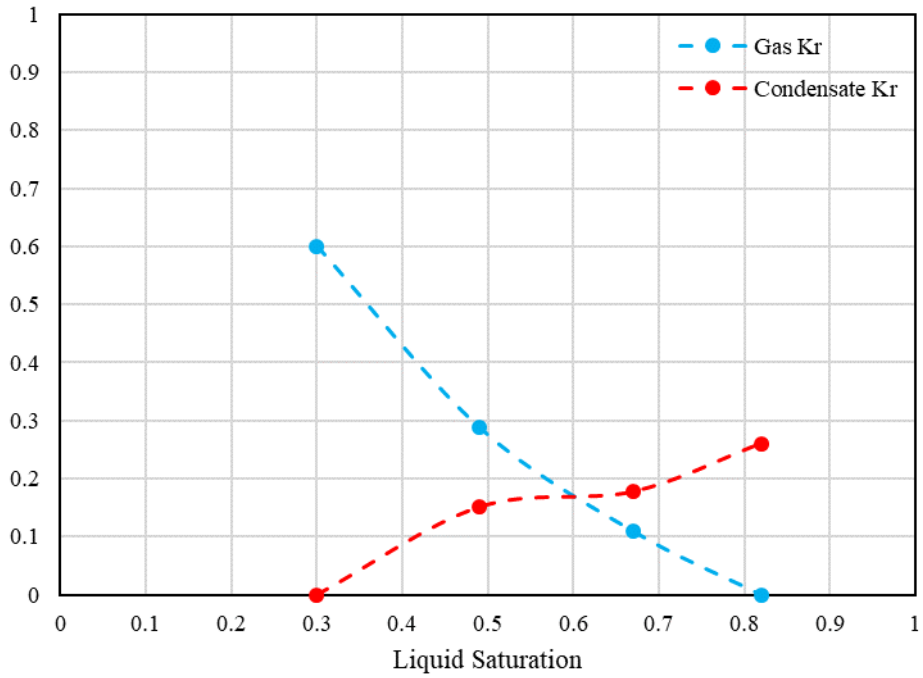

Figure 6.2: Experimentally measured relative permeability data set for an Eagle Ford core sample used in the reservoir simulations.

The simulations were performed with constant bottom hole pressure (BHP) control mode. There were two different schemes of production, i.e. single phase production and two phase production. In single phase production scheme, both external pressure (initial reservoir pressure) and BHP were above the Pdew of the gas condensate fluid. On the other hand, in two phase production scheme, the external pressure was slightly above the Pdew of gas condensate fluid while BHP was below the Pdew of the gas condensate fluid.

6.2 Simulation Results and Sensitivity Analysis

After initializing the reservoir model, impacts of different parameters were investigated. First, using the base model, the impacts of confinement effects on the production of gas and condensate under single and two phase flow conditions were studied. Then a hydraulic fracturing scheme was implemented in the model, and based on the presence of hydraulic fractures within the model the impacts of different parameters including, fluid

type, adsorption, and diffusion were investigated with bulk and confined fluid properties. It should be mentioned that since different fluid models were used for the effects of pore confinement, the production values reported in this study are in reservoir condition to eliminate the impacts of formation volume factors on the analysis of the results.

6.2.1 Impacts of Pore Confinement Effects on the Production Data using Base Reservoir Model

The performance of the single-well reservoir model producing under either single or two phase flow conditions, with bulk and confined fluid models is presented in this section. Figure 6.3 shows the comparison between gas production rates for the reservoir producing under single phase flow conditions. The external reservoir pressure was set to be 5500 psi. Two simulations at two pressure drop (DP) values of 500 and 1000 psi with respective BHP of 5000 psi and 4500 psi were performed.

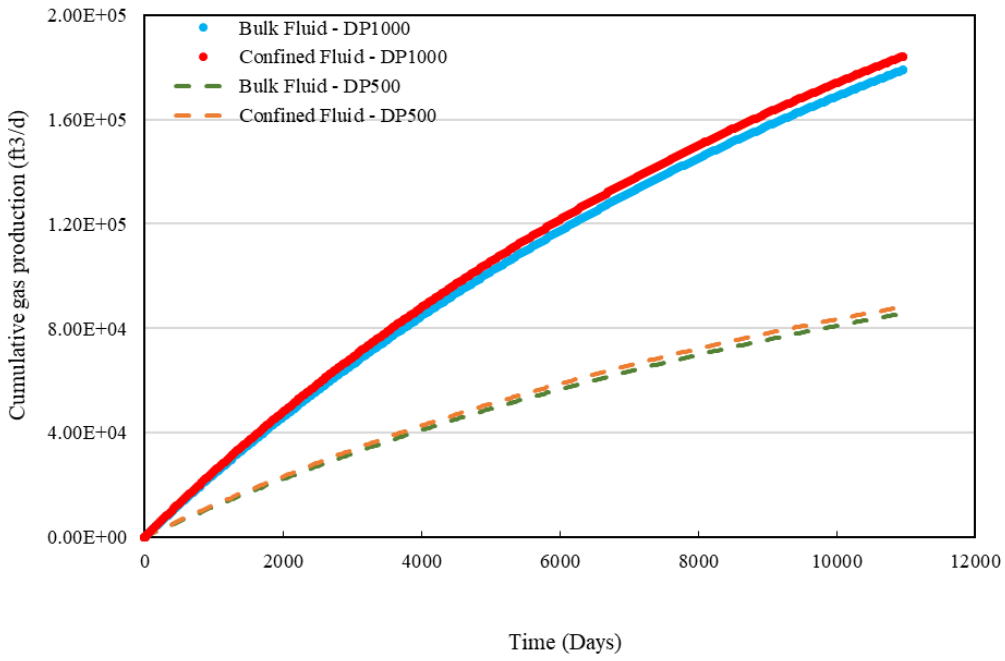

Figure 6.3: Cumulative gas production of the horizontal well base model flowing under single phase conditions with F7 bulk and confined fluid models at 2 different DP values of 500 and 1000 psi.

Table 6.2 summarizes the tabulated total production of the cases shown in Figure 6.3. As it can be observed in Figure 6.3, the cumulative production with confined fluid is slightly higher than the production with bulk fluid model (cumulative production is 3% higher for the confined fluid case). This is mainly attributed to viscosity of the confined fluid model

being slightly lower than that of bulk fluid model. As expected reducing the DP from 1000 to 500 psi resulted in lower production.

Table 6.2: A summary of the cumulative gas production data for the base case flowing under single phase flow conditions using bulk and confined fluid models at two DP values of 500 and 1000 psi

Fluid model	Cumulative gas production (ft^3*10^3)	Pressure drop (psi)	Difference between bulk and confined production (%)
Bulk	178.9	1000	2.9
Confined	184.2		
Bulk	85.7	500	2.9
Confined	88.2		

Figure 6.4 compares the gas viscosity of the bulk and confined fluid models in the pressure range of the simulations performed for the single phase gas flow case whose results are presented in Figure 6.3. It has already been demonstrated in literature that pore confinement would result in the reduction of the viscosity of the confined fluids (Wang *et al.*, 2013).

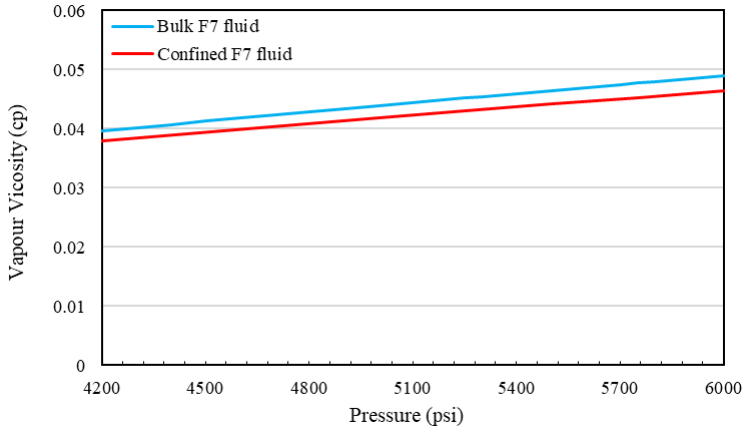

Figure 6.4: Vapour viscosity of the single phase F7 fluid model.

Two phase simulations were conducted at three different DP values of 500, 750 and 1000 psi. The results of these simulations are presented in Figures 6.5 and 6.6. In these simulations the external pressure was set to be 4300 psi, which is almost 250 psi higher than the bulk F7 fluid Pdew and almost 100 psi higher than the confined F7 fluid Pdew. As expected and noted higher DP results in higher gas and condensate production rates.

From data of Figure 6.5, it can be observed that at all DP values, using confined fluid model results in higher gas production.

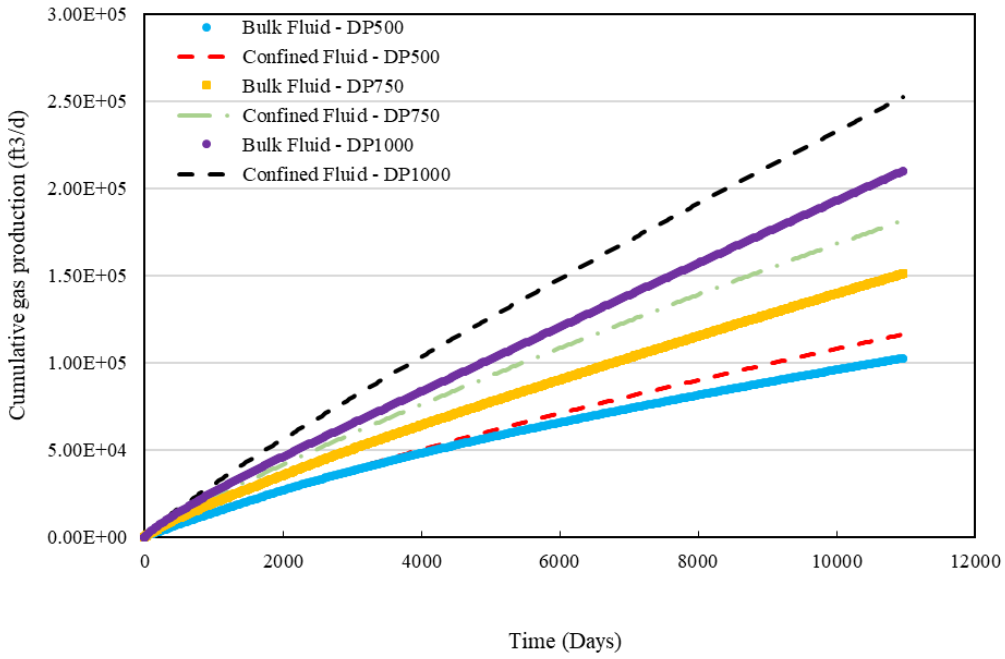

Figure 6.5: Cumulative gas production for the horizontal well base model flowing under two phase flow conditions using bulk and confined F7 fluid models at 3 different DP values of 500, 750, and 1000 psi.

Table 6.3 shows the tabulated summary of the cumulative gas production for two phase flow simulations presented in Figure 6.3.

Table 6.3: Summary of the cumulative gas production for the base case flowing under two phase conditions using bulk and confined fluid models at three DP values of 500, 750 and 1000 psi.

Fluid model	**Cumulative gas production (ft^3*10^3)**	**Pressure drop (psi)**	**Difference between bulk and confined production (%)**
Bulk Confined	210.2 252.3	1000	20.1
Bulk Confined	151.1 181.7	750	20.2
Bulk Confined	102.7 116.3	500	13.3

The comparison of two phase flow results with bulk and confined fluids can be better made considering the condensate production data as shown in Figure 6.6.

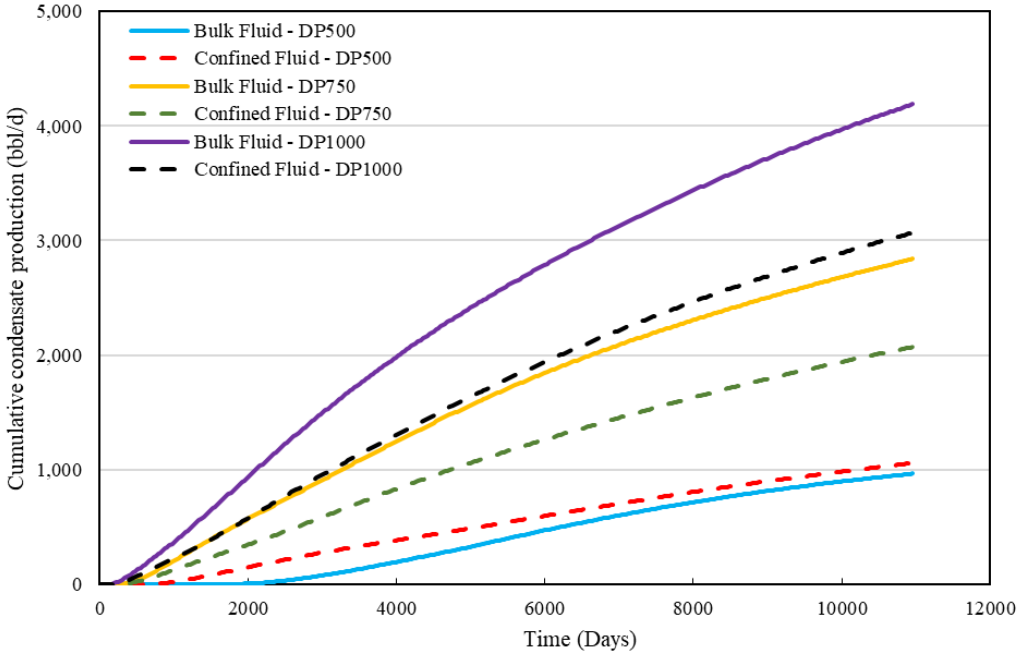

Figure 6.6: Cumulative condensate production for the horizontal well base model flowing under two phase conditions using bulk and confined F7 fluid models at three different DP values of 500, 750, and 1000 psi.

From Table 6.3, it is observed that the difference between the gas production with bulk and confined fluid for two phase flow is much higher than single phase flow. However, as illustrated in Figure 6.6, the condensate production is higher for the bulk fluid model at DP values of 750 and 1000 psi. This is mainly due to the fact that more of the heavier components of gas condensate mixture, drops out of the gas due to increased interactions of confined liquid with the pore walls. As a result, the gas phase in the confined state has lower content of heavy components which makes the flow of gas easier due to lower viscosity and hence more production as shown in Figure 6.5. For the liquid phase, on the other hand, the mobility of heavier liquid phase reduces because of increased fluid-wall interactions.

For the case with DP of 500 psi, since BHP of the model is very close to the Pdew of the bulk fluid, it takes longer for the pressure disturbance to reach to a point that makes the condensate mobility to be high enough to exceed the critical condensation saturation and have considerable condensate production. This is why the condensate production in the reservoir model with bulk fluid is negligible until 2000 days of production. While, the condensate production for the confined fluid is negligible till 500 days of production. As it can be observed, towards the end of the simulation, the difference between condensate production with bulk and confined fluid reduces at DP of 500 psi.

6.2.2 Impacts of Pore Confinement Effects on the Production Data using Hydraulically Fractured Reservoir Model

Economical production from unconventional reservoirs is feasible with the combination of drilling horizontal wells as well as hydraulic fracturing operations. Therefore, in the study of any unconventional reservoir, it is very important to take into account the impacts of fractured wells. Hence, in this section, the effects of pore confinement on the performance of a reservoir model with hydraulic fractures are discussed.

It should be mentioned that the selected reservoir model was bigger than the base reservoir model. The basic properties of the reservoir model are summarized in Table 6.4. Any modifications made on this model would be mentioned in the respective section. In this study, the horizontal well is stimulated by a single stage fracturing scheme comprising of 4 fractures with similar half-length of 150 ft. Fractures were evenly spaced and propagated. Fracture permeability and relative permeability were obtained from experimental data measured in the HW-GC laboratory. Figure 6.7 shows the relative permeability data used for the fractures.

It should be noted due to very low flow velocities in the matrix of low permeability rock, the impact of velocity on kr was ignored. Coupling refers to an increase in kr when either velocity increases or IFT decreases (Jamiolahmady *et al.*, 2009). Also, the HW-GC team have demonstrated that the negative of impact of inertia within fracture could affect flow performance of a fractured well (Mahdiyar *et al.* 2011). To take into account the impacts of non-Darcy inertial flow in the hydraulic fractures, single phase inertia factor of 351000 1/m which is the measured value corresponding to the fracture properties used in this study was employed.

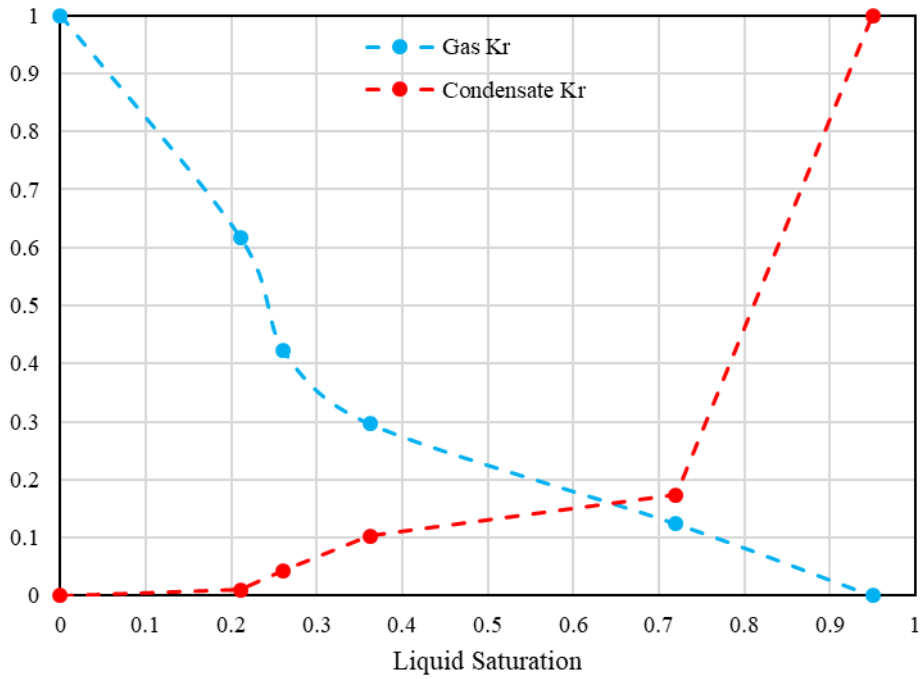

Figure 6.2: Experimentally measured relative permeability data set hydraulic fractures used in the reservoir simulations

Table 6.4: Basic properties of the Cartesian reservoir model with hydraulic fractures.

Properties	**Values**
Reservoir Dimensions (ft)	(60*15)*(60*15)*(10*15)
Porosity (%)	15
Horizontal matrix permeability (mD)	0.0044
Vertical matrix permeability (mD)	0.00044
Fluid	Fluid 7 (0.923C1+0.077C8)
Kr	HW measured kr

Figure 6.7 shows a schematic diagram of the hydraulic fractures used in the model simulated here. It should be mentioned that the reservoir model used in this section did not have any natural fractures. Hence, a single porosity reservoir model was considered. The impacts of the presence of natural fractures will be discussed in the next section of this chapter.

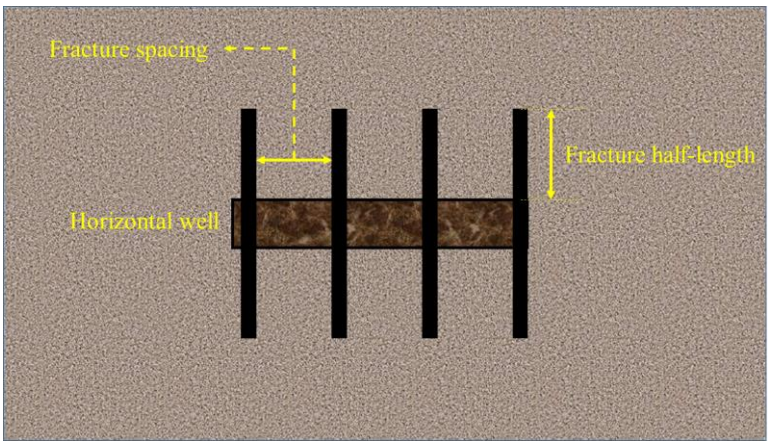

Figure 6.7: A schamtic representation of hydraulic fracture configurations.

It should be mentioned that, as depicted in Figure 6.8, local grid refinement (LGR) was performed for near fracture grid blocks. The number of refinement in I- and J-directions was set to be 7 where the refined grids were logarithmically spaced.

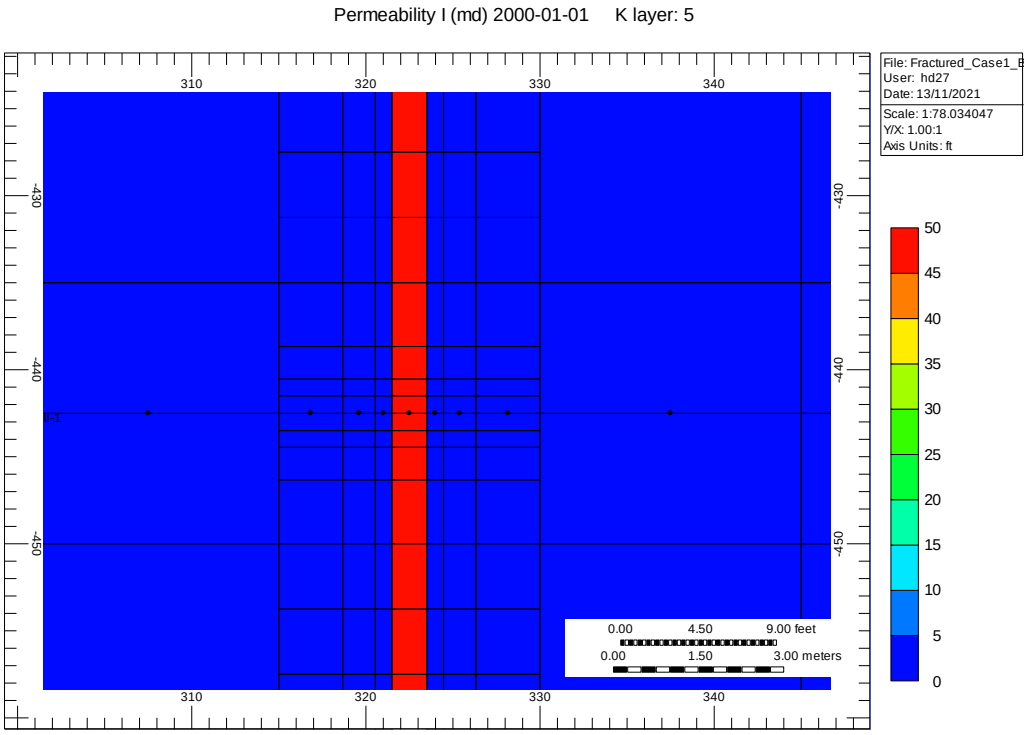

Figure 6.8: Local grid refinement for near fracture grid blocks.

Apart from fracture half-length values, other properties of the fractures for different cases were similar and are presented in Table 6.5.

Table 6.5: Parameters of hydraulic fractures used in this study.

Parameter	Values
Fracture width	0.01 ft
Fracture intrinsic permeability	146000 mD
I-direction LGR	7
J-direction LGR	7
Fracture height	75 ft
Fracture spacing	85 ft

Figure 6.9, shows the results of single phase simulations with reservoir external pressure of 6500 psi and at two different DP values of 1000 and 2000 psi for the horizontal fractured well. The performance of the reservoir model with bulk and confined fluid models are compared in this figure. As it can be observed, similar to the results of the base case simulations, gas production for the model with confined fluid is slightly higher compared to the gas production with bulk fluid.

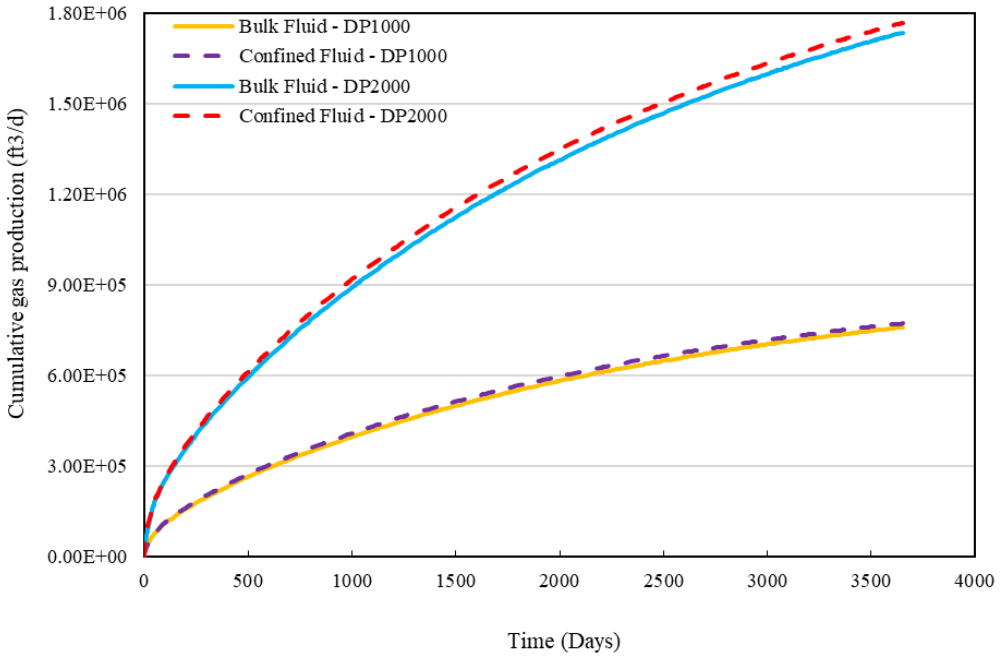

Figure 6.9: Cumulative gas production for the fractured horizontal well model flowing under single phase flow conditions using bulk and confined F7 fluid models at two different DP values of 1000 and 2000 psi.

Table 6.6 shows the tabulated cumulative gas production data for the cases shown in Figure 6.9.

Table 6.6: A summary of the cumulative gas production for the fractured well model flowing under single phase conditions using bulk and confined F7 fluid model at 2 DP values of 1000 and 2000 psi.

Fluid model	Cumulative gas production (ft^3*10^3)	Pressure drop (psi)	Difference between bulk and confined production (%)
Bulk Confined	1736.2 1768.5	2000	+1.9
Bulk Confined	760.2 773.4	1000	+1.7

The results of cumulative gas production for two phase flow simulations are presented in Figure 6.10. In these two phase flow simulations, similar to the base case two phase flow simulations, the external pressure was 4300 psi and three different DP values of 500 psi, 1000 psi and 2000 psi were considered. The effects of confinement are compared in this figure.

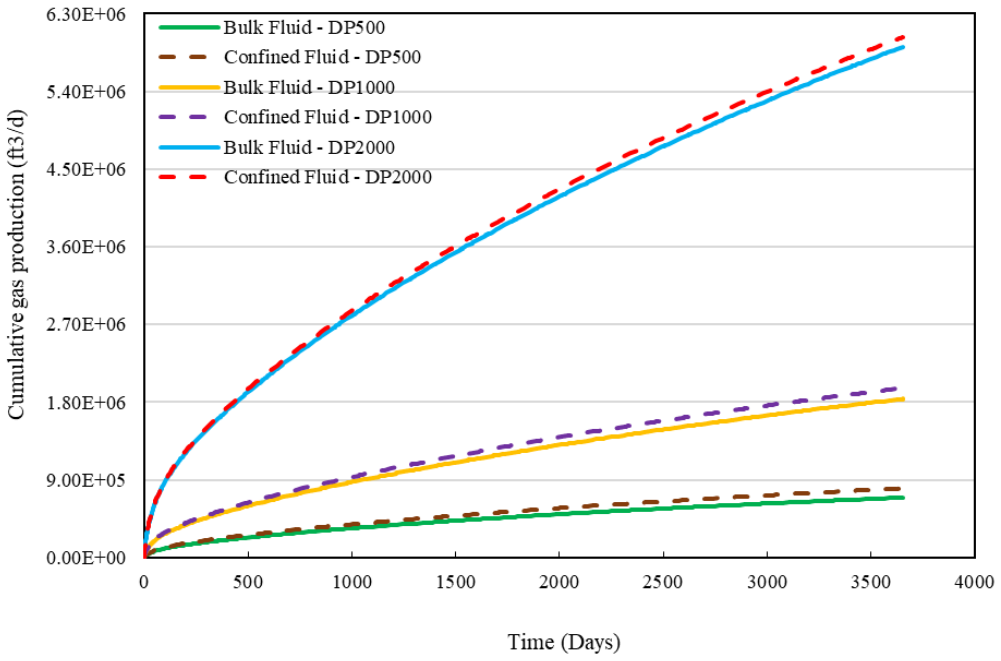

Figure 6.10: Cumulative gas production for the fractured horizontal well model flowing under two phase flow conditions using bulk and confined F7 fluid models at 3 different DP values of 500, 1000, and 2000 psi.

Table 6.7 shows the tabulated cumulative gas production data for the cases shown in Figure 6.10.

Table 6.7: A summary of the cumulative gas production for the fractured well model flowing in two phase with bulk and confined F7 fluid model with 3 DP values of 500, 1000 and 2000 psi.

Fluid model	Cumulative gas production (ft^3*10^3)	Pressure drop (psi)	Difference between bulk and confined production (%)
Bulk Confined	5918.1 6028.0	2000	+1.9
Bulk Confined	1836.8 1963.6	1000	+6.9
Bulk Confined	694.3 801.4	500	+15.4

As it can be observed, for all cases, the performance of the reservoir model with confined fluid model in terms of gas production is slightly better.

To better evaluate the performance of the reservoir models under the effects of pore confinement, reservoir condensate production for two phase flow simulations at different DP values with confined and bulk fluid models are compared in Figure 6.14.

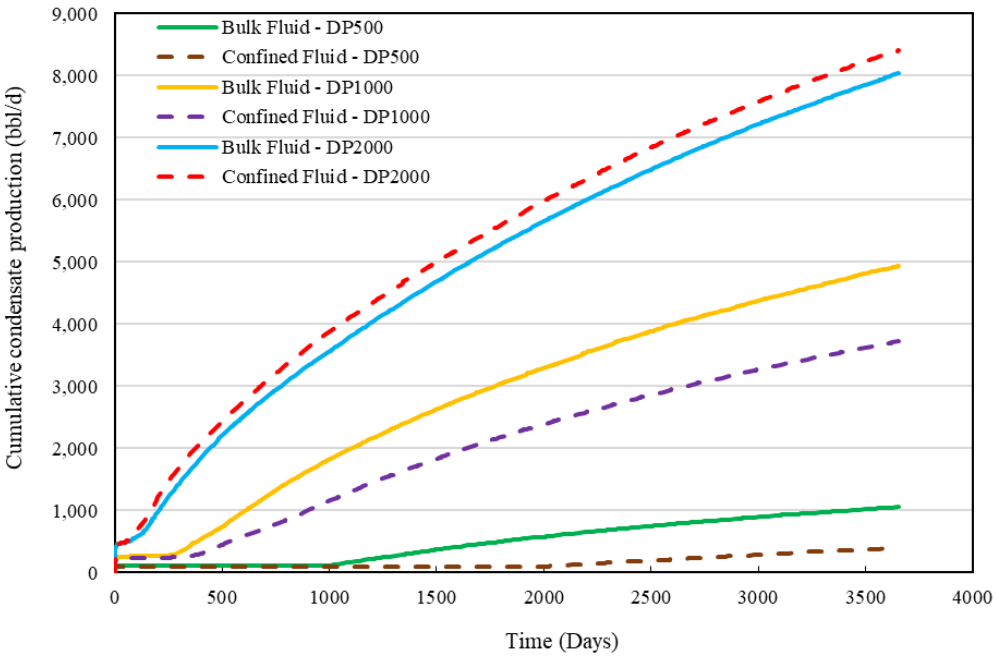

Figure 6.11: Cumulative condensate production for the fractured horizontal well model flowing under two phase flow conditions using bulk and confined F7 fluid models at 3 different DP values of 500, 1000, and 2000 psi.

As it can be observed, for the two cases with DP values of 500 psi and 1000 psi, the cumulative condensate production with bulk fluid model is higher. However, for the case

with DP of 2000 psi, condensate cumulative production with confined fluid model is higher. This could be mainly due to the variations in liquid drop out. It can be observed in Figure 6.12 that the LDO of the confined fluid model is slightly higher than the bulk fluid model at 2300 psi which is the well bottom hole flowing pressure. As a result, condensate production at the reservoir is higher for the confined fluid model compared to the bulk fluid model due to higher saturation of condensate in the near wellbore region. As it is noted in this figure, the bulk and confined fluid LDO values are almost the same for 3800 and 3300 psi. As described in Chapter 5, there were no experimental evidence that the richness of the fluid would change due to confinement effects. As a result, the MLDO of the fluids were tuned to be the same, however, LDO of the fluids could vary due to interactions between rock and fluids. It should be noted that lower condensate production from unconventional gas condensate reservoirs is in line with actual production data (Luo *et al.*, 2021).

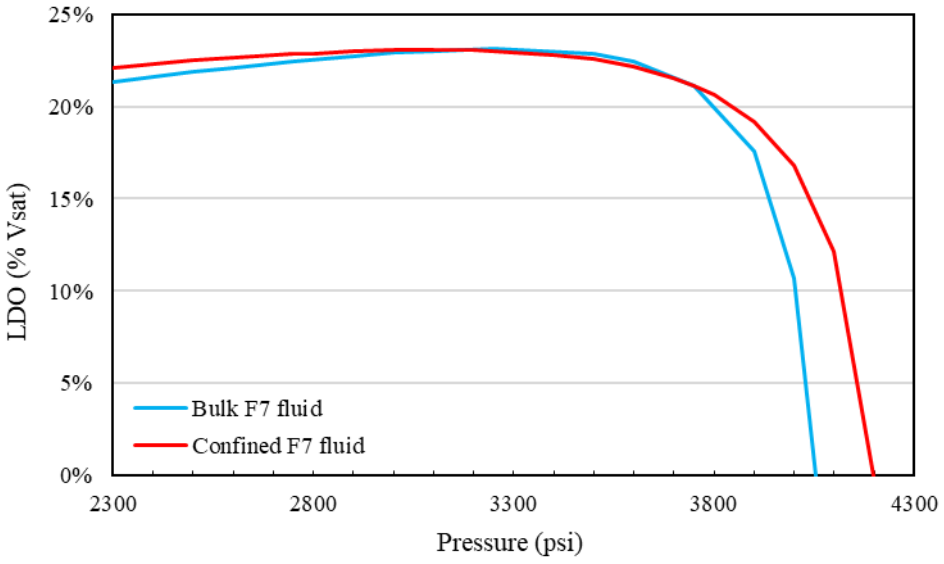

Figure 6.12: Liquid drop out of the bulk and confined F7 fluid model.

6.2.3 Dual Porosity and Dual Permeability Hydraulically and Naturally Fractured Reservoir Models

Another important aspect of unconventional reservoirs is the natural fractures which exist in these reservoirs. There are four different types of widely used models, namely dual porosity, dual permeability, subdomain and MINC (Multiple INteracting Continua) for simulating naturally fractured reservoirs. It has been suggested that for the simulation of

unconventional reservoirs, Logarithmically Spaced, locally Refined, Dual Permeability (LS-LR-DK) fractured reservoir models would be the best approach which gives satisfactory results (Rubin, 2010). In dual permeability models (also known as Dual Poro – Dual Perm models), unlike, standard dual porosity models, fluid flow within matrices is not ignored. As a result, additional fluid flow equations are solved for dual permeability models, which take into account the matrix-to-matrix fluid flow. The CPU usage and run time for dual permeability models are higher than dual porosity models, however, it would result in more realistic simulation results. Hence, here, dual permeability (Dualperm-Dualporo), as well as dual porosity, models were considered for the cases with confined and bulk fluid models.

Figure 6.13 shows an illustration of dual porosity and dual permeability models. In summary, dual porosity model is a reservoir model in which both matrices and fractures contribute to the storage of the fluid within the reservoir but there is no flow from matrix to matrix and only fractures play a part for flow of fluid to the wellbore. However, in dual permeability-dual porosity reservoir model (which for simplicity will be referred to as dual permeability model from now on in this text) matrices and fractures contribute not only to the fluid storage, but also to the fluid flow within the reservoirs.

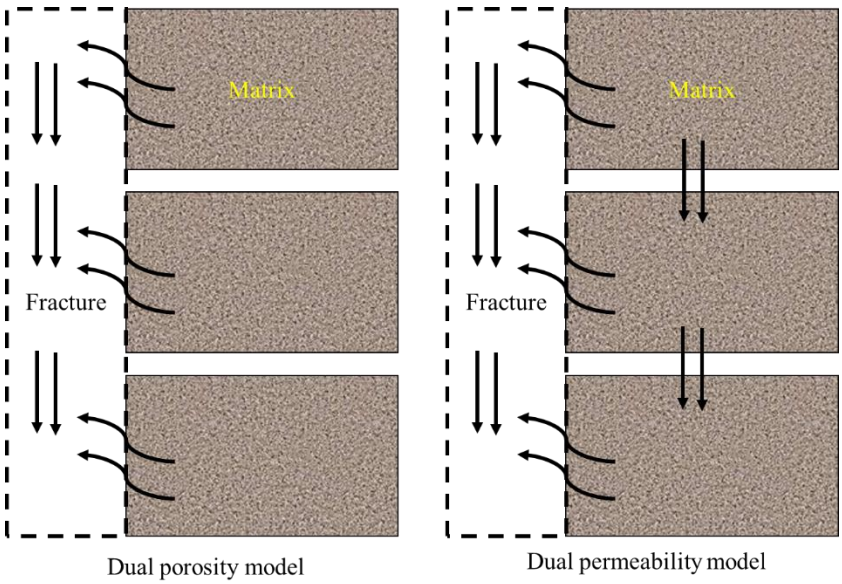

Figure 6.13: A schematic illustration of dual porosity and dual permeability models for the simulation of naturally fractured reservoirs

In this section the results of the simulations with dual porosity model and dual permeability model are compared.

Figure 6.14 shows the comparison between the performance of the dual porosity model for single phase flow simulations using bulk and confined fluids at the DP value of 1000 psi.

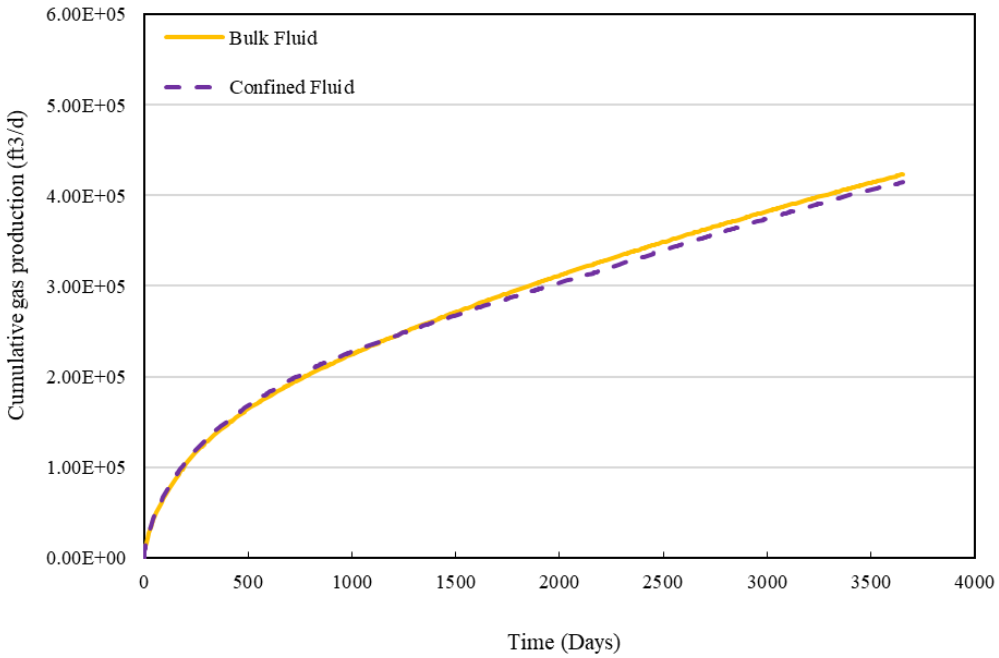

Figure 6.14: Cumulative gas production for the fractured horizontal well and dual porosity model flowing under single phase flow conditions using bulk and confined F7 fluid models at DP value of 1000 psi.

As it can be observed, unlike the single-porosity case, the performance of the dual porosity model with the bulk fluid is slightly better than that with the confined fluid.

The results of the dual permeability models for the single-phase flow simulations using bulk and confined fluids at DP of 500 psi are presented in Figure 6.15. As opposed to dual porosity model, these data demonstrate that the well performance is better when using the confined fluid EOS model.

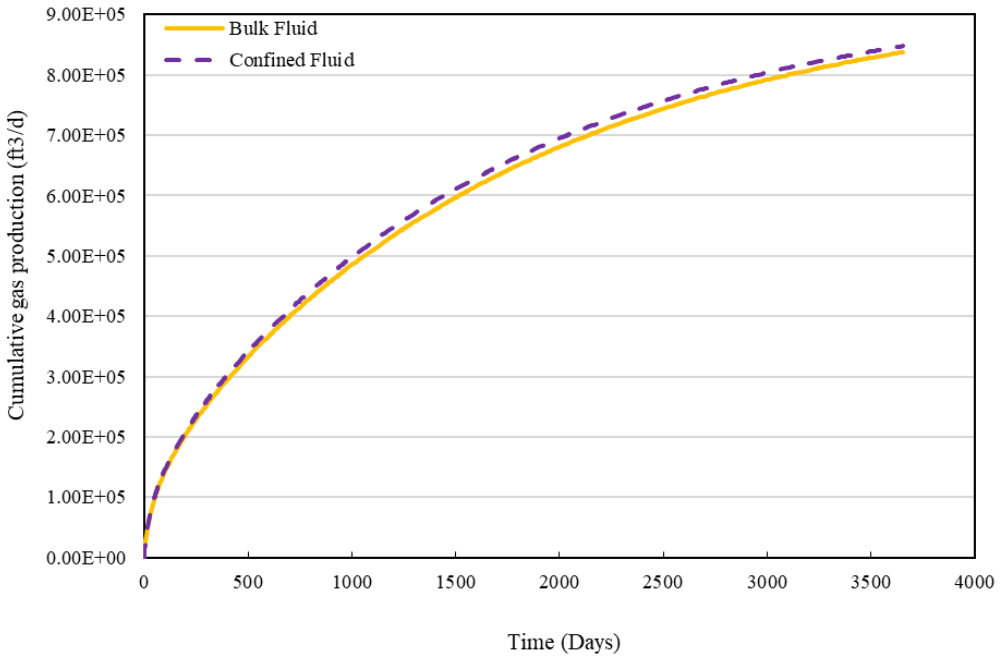

Figure 6.15: Cumulative gas production for the fractured horizontal well and dual permeability model flowing under single phase flow conditions using bulk and confined F7 fluid models at DP value of 1000 psi.

A summary of the results of the dual porosity model and dual permeability model demonstrated in Figures 6.14 and 6.15 are compared in Table 6.8.

Table 6.8: A summary of the cumulative gas production for the dual porosity and dual permeability models with the fractured well model flowing in single phase with bulk and confined F7 fluid model with DP value of 1000 psi.

Fluid model	**Cumulative gas production (ft^3*10^3)**	**Simulation Model**	**Difference between bulk and confined production (%)**
Bulk	423.5	Dual Poro	-2.1
Confined	414.5		
Bulk	837.8	Dual Perm	+1.2
Confined	847.6		

The impacts of confinement on the performance of the dual porosity model was also investigated in two phase flow simulations. Figure 6.16 shows the results of two phase flow simulations for dual porosity and dual permeability models at DP of 500 psi using both bulk and confined F7 fluid models. As it can be observed for both dual porosity and dual permeability models, the well performance is better when using confined fluid. Moreover, the difference between the performance of the dual porosity and dual permeability is significant. As mentioned, a dual permeability reservoir model is considered to be more representative of fluid flow in real unconventional reservoirs as

the physics of fluid flow considered in this approach resembles more to what actually takes place in these reservoirs.

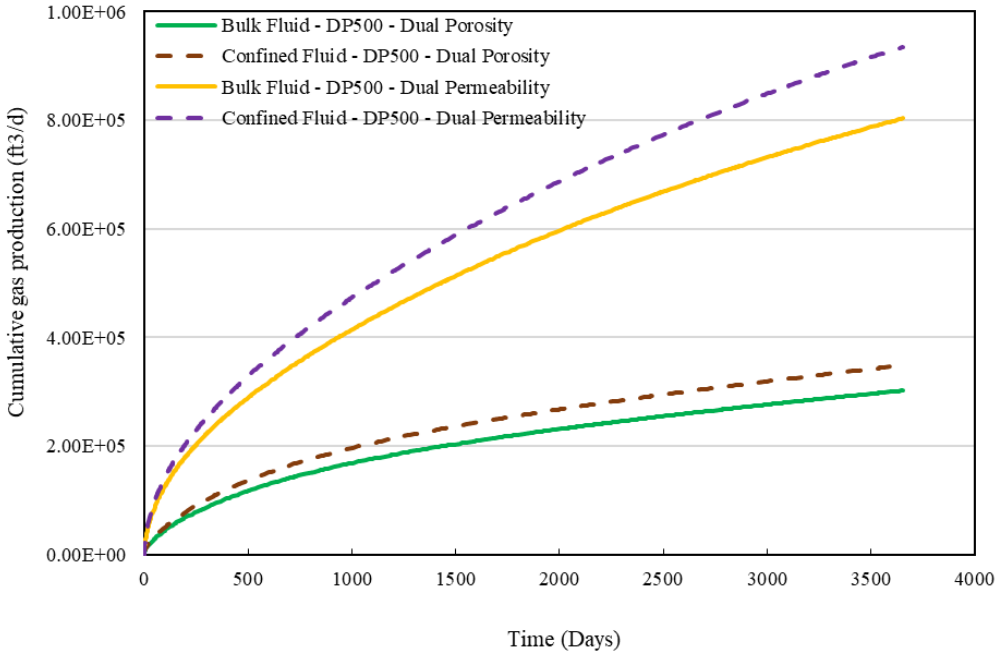

Figure 6.16: Cumulative gas production for the dual porosity and dual permeability models with fractured horizontal well model flowing under two phase flow conditions using bulk and confined F7 fluid models at DP value of 500 psi.

The tabulated cumulative gas production data of Figure 6.16 are presented in Table 6.9.

Table 6.9: A summary of the cumulative gas production for the dual porosity and dual permeability models with the fractured well model flowing in two phase with bulk and confined F7 fluid model with DP value of 500 psi.

Fluid model	**Cumulative gas production (ft^3*10^3)**	**Simulation Model**	**Difference between bulk and confined production (%)**
Bulk Confined	302.1 348.7	Dual Poro	+15.4
Bulk Confined	803.4 934.8	Dual Perm	+16.4

Figure 6.17 shows the condensate production of the models demonstrated in Figure 6.16. Similar to the base case model, condensate production for the models with the bulk fluid model is higher than that with the confined fluid model. Also, condensate production in the dual porosity model is better compared to that in the dual permeability model.

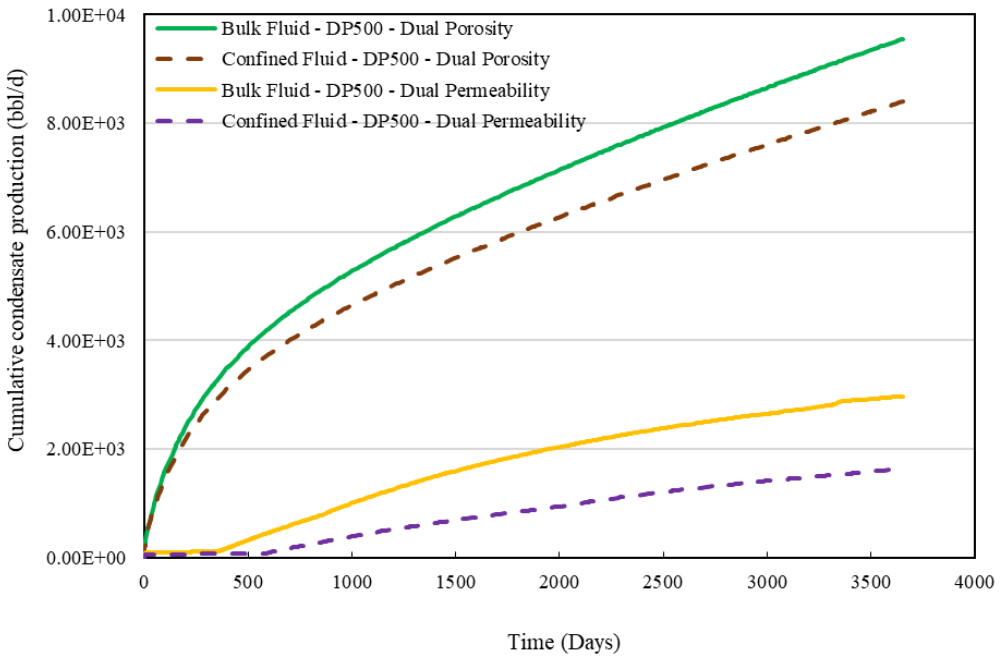

Figure 6.17: Cumulative condensate production for the dual porosity and dual permeability models with fractured horizontal well model flowing under two phase flow conditions using bulk and confined F7 fluid models at DP value of 500 psi.

Another important aspect of dual permeability fractured reservoir modelling is the impacts of near fracture zone (NFZ) grid properties. Hence, different reservoir models with different permeability values, which were assigned to near fracture zone grid blocks, were considered. The impacts of confined and bulk fluid properties were then investigated with these modifications. NFZ grid blocks permeability values for the two different cases are summarized in Table 6.9. Figure 6.18 compares the permeability distribution of the two sets of modified NFZ grid blocks and the non-modified NFZ grid blocks.

Table 6.9: Case 1 and Case 2 NFZ grid blocks permeability modified values

Parameter	Value for Case 1 NFZ modifications	Value for Case 1 NFZ modifications
K_x	1 mD	10 mD
K_y	1 mD	10 mD
K_z	0.1 mD	1 mD

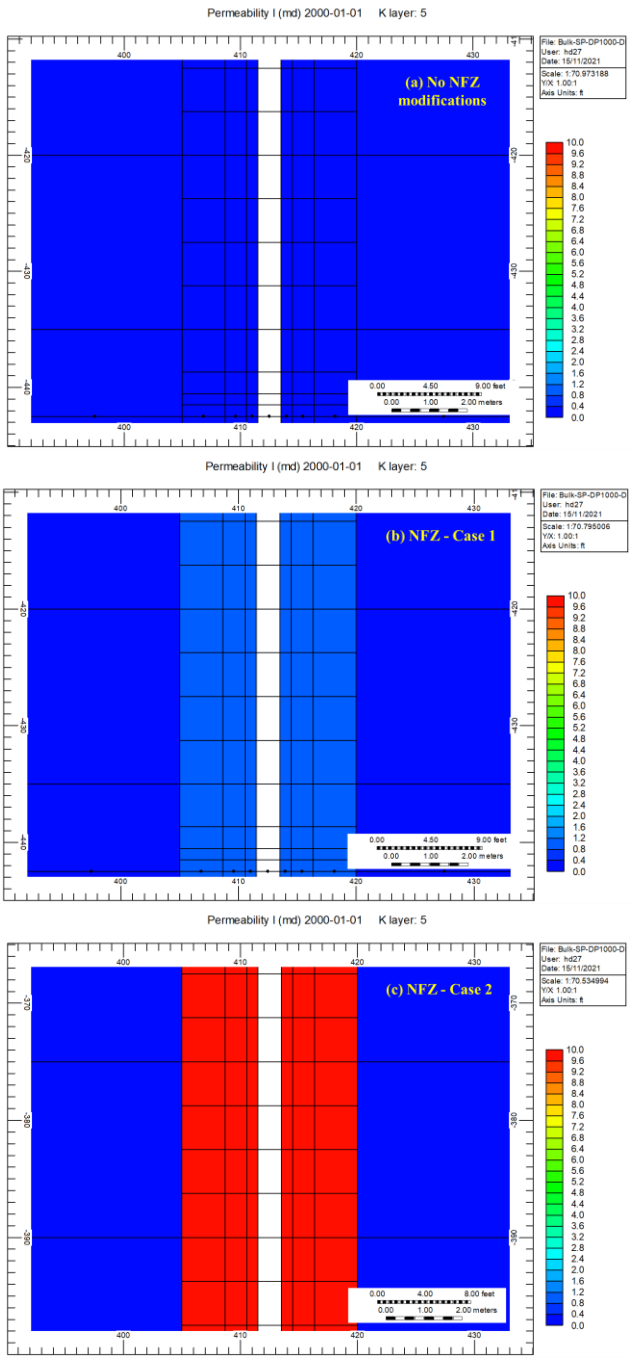

Figure 6.18: Comparison of the permeability variations in the NFZ grid blocks for (a) no NFZ modifications, (b) Case 1 NFZ modifications, and (c) Case 2 NFZ modifications

Figure 6.19 compares the simulations results of the models with original NFZ grid blocks permeability and, Case 1 and Case 2 NFZ modifications, all using the bulk fluid and producing under the single phase flow conditions at DP of 1000 psi.

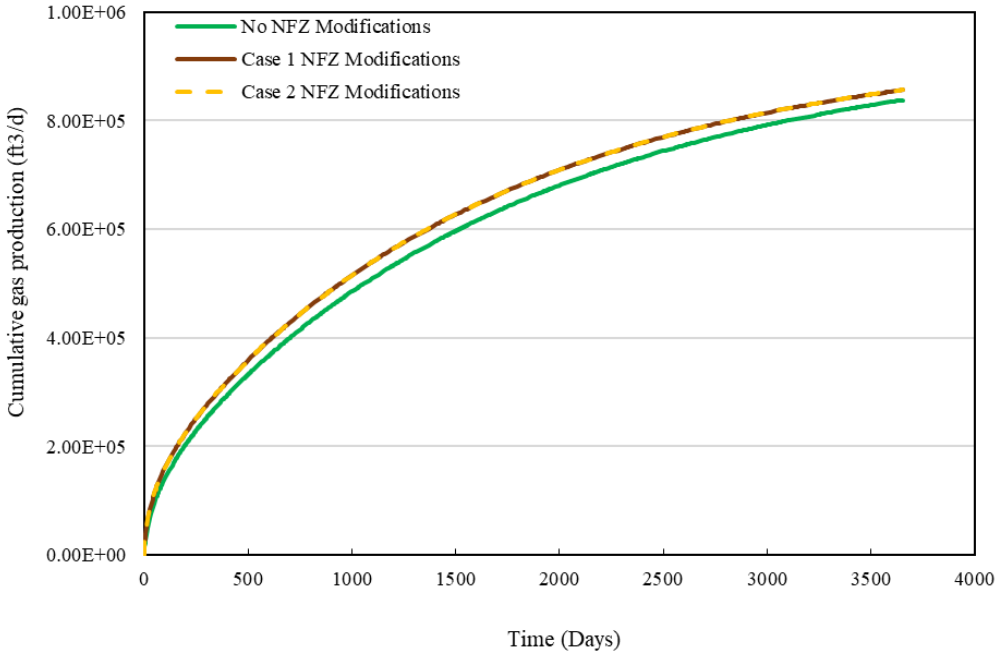

Figure 6.19: Cumulative gas production for the fractured well and dual permeability model flowing in single phase with bulk fluid model with DP value of 1000 psi for no NFZ, Case 1 and Case 2 NFZ modifications.

It is noted that the difference between cases of NFZ modifications is found to be marginal. Additionally, the presence of matrix grid blocks adjacent to hydraulic fractures with higher permeability, slightly increases the production.

In the next step, the difference between using confined and bulk fluid models was investigated. For this purpose, the performance of the reservoir models with confined and bulk fluid models under two phase flow conditions at DP of 1000 psi was studied for different cases of NFZ modifications. Figure 6.20 shows the results of this comparison.

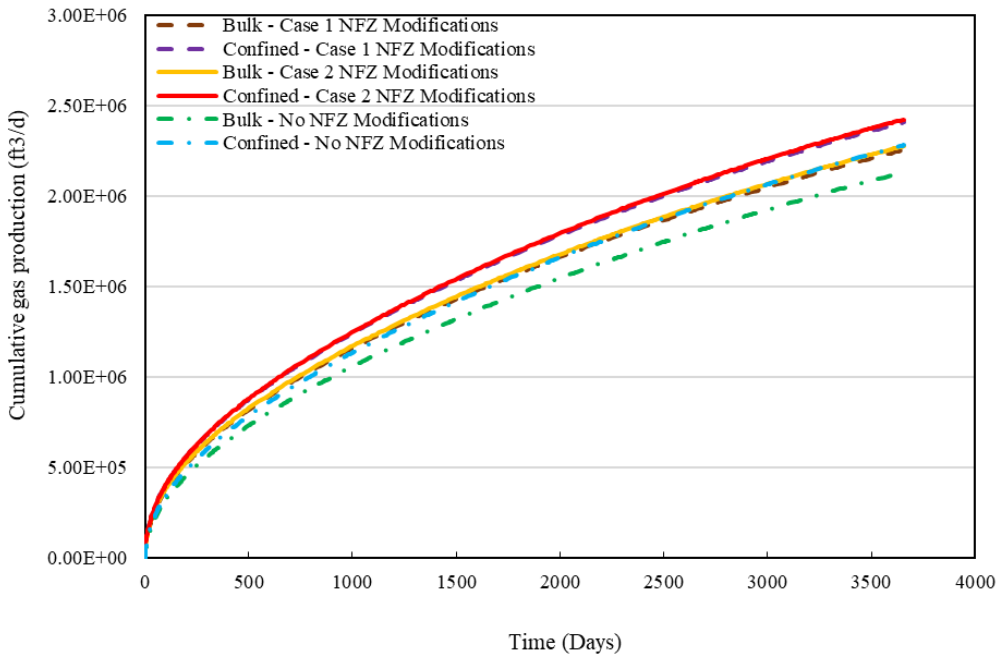

Figure 6.20: Cumulative gas production for the fracture well and dual permeability model flowing in two phase with bulk and confined F7 fluid models with DP value of 1000 psi for no NFZ, Case 1 and Case 2 NFZ modifications.

The results show that, NFZ grid block modifications, as expected, improve the performance of the reservoir model. It is noted that similar to the model flowing under single phase conditions, the difference between the two cases of NFZ is marginal when under two phase flow conditions as well. Additionally, the gas production with the confined fluid model is higher than that with the bulk fluid model almost to the same extent for cases with and without NFZ grid blocks.

Figure 6.21, shows the spatial pressure variations for the NFZ grid blocks after 1 month of production for the 3 cases with different NFZ modifications.

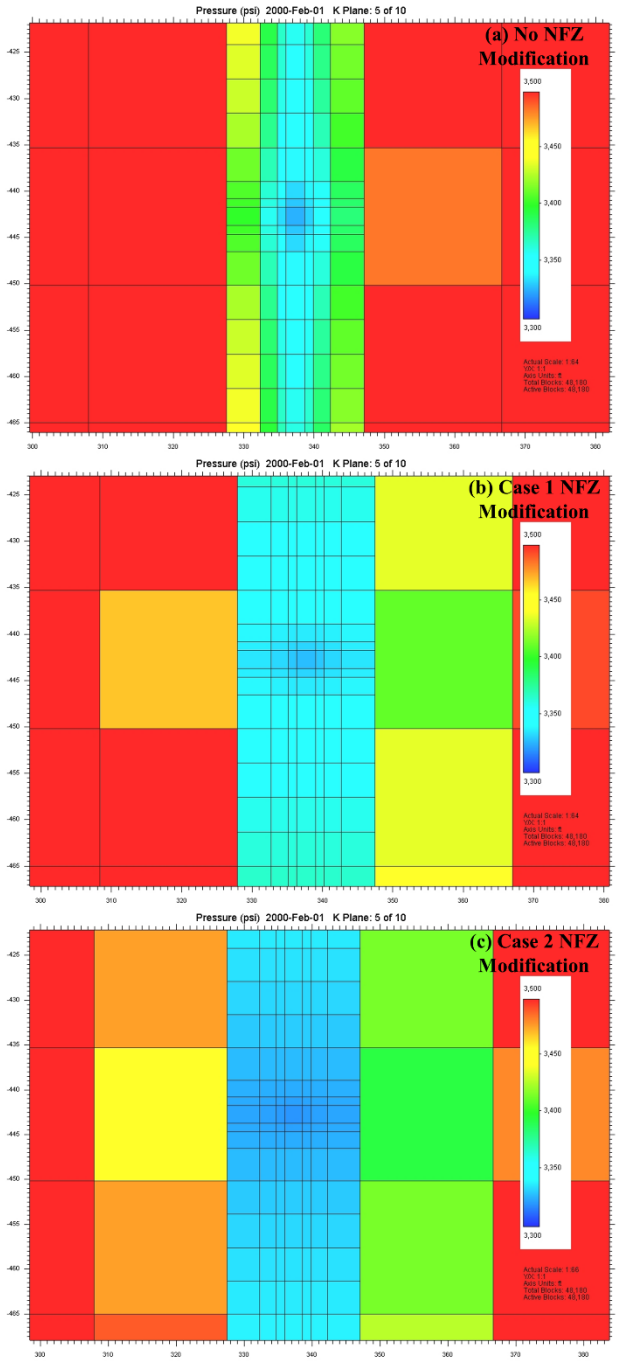

Figure 6.21: Comparison of the pressure variations in the NFZ grid blocks for (a) no NFZ modifications, (b) Case 1 NFZ modifications, and (c) Case 2 NFZ modifications

As mentioned before, the importance of NFZ modifications is in history matching of the production data from such reservoirs. However here it is shown that their presence do not change the overall trend of results of confined versus bulk fluid cases.

6.2.4 Impacts of Adsorption on the Performance of Models with Bulk and Confined Fluid

In conventional reservoirs, fluid is stored in the reservoir via two main ways of free fluid and soluble fluid. For instance, initial gas in place (IGIP) of a conventional saturated reservoir is the combination of the free gas which exist in the pores and the gas which is dissolved in liquids existing in the reservoir. However, for unconventional reservoirs, apart from the two abovementioned ways of fluid storage, fluids can be contained in the reservoir by adsorption. Adsorption depends on the pressure and temperature. Higher temperature and lower pressure would result in a process called desorption which is the opposite of adsorption. Desorption is one of the main mechanisms of production in unconventional reservoirs.

In this section, the impacts of adsorption on the performance of the fractured dual permeability reservoir model are investigated. It should be mentioned that for all of the remaining simulations in this study, dual permeability reservoir model without any NFZ modifications has been used. Generally, in unconventional reservoirs, the adsorption of lighter components, e.g. C1, C2, N2 or CO2, is of interest. Accordingly, in this study, the sensitivity analysis was performed based on the adsorption of the C1 as the light component and the impacts of adsorption of C8 on the production is ignored. In commercial reservoir simulation packages, including CMG-GEM (2017), there are two formats to input adsorption isotherms. The first format is to input a table of adsorption isotherm, which include the data of the amount of adsorbed fluid versus pressure. The second format, deals with Langmuir adsorption isotherm. Langmuir adsorption isotherm was briefly introduced in chapter 2. Figure 6.25 shows a typical Langmuir adsorption isotherm.

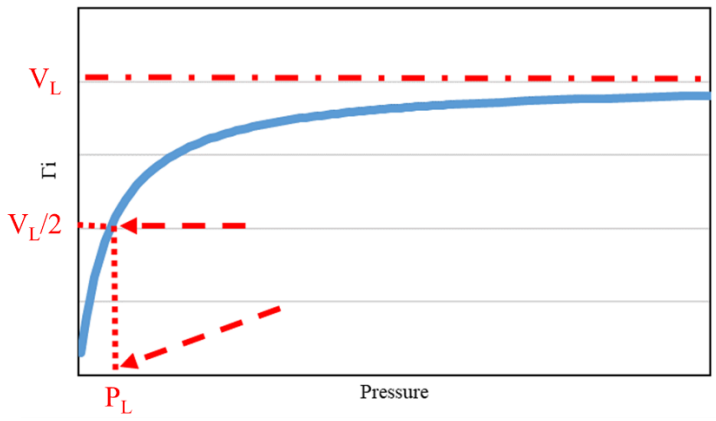

Figure 6.22: Typical representation of Langmuir isotherm

As depicted in Figure 6.22, any Langmuir isotherm can be expressed by two parameters. V_L is the maximum adsorbed amount of the adsorbate, and P_L corresponds to the pressure at which the adsorption is half of its maximal value, i.e. it is equal to $V_L/2$. In this study, different values of Langmuir adsorption parameters were considered for C1 to investigate the effects of adsorption on the performance of the dual permeability reservoir model. Table 6.10 shows different adsorption constant values used for this study.

Table 6.10: Langmuir adsorption parameters for different cases used in this study

Case	$1/P_L$ (1/psi)	V_L (gmol/lb)
Case 1	0.002	0.1
Case 2	0.004	0.2
Case 3	0.008	0.4

Corresponding adsorption isotherms for these three different cases as defined by the parameters presented in Table 6.5, are shown in Figure 6.23.

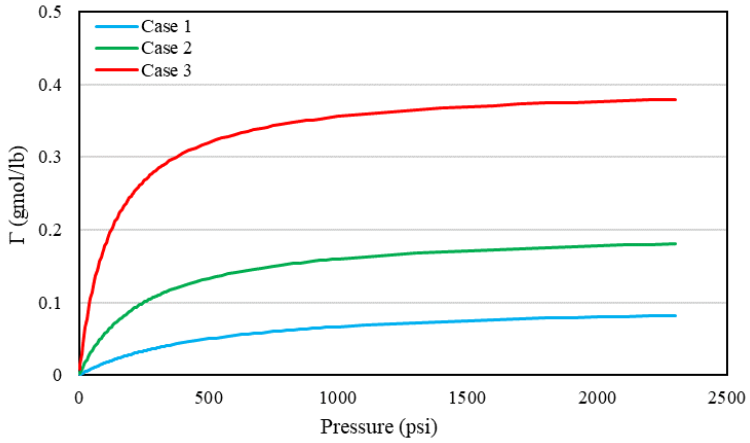

Figure 6.23: Different cases of Langmuir adsorption isotherms for C1 used in this study

The performance of the reservoir with bulk fluid for 3 different cases of adsorption isotherms and the performance of the reservoir without considering adsorption are compared in Figure 6.24. It should be mentioned that the two phase flow simulations results are considered for this section. The range of DP imposed is different from those used in the previous sections. The main reason for the selection of the new DP values, is the fact that to investigate the impacts of adsorption on the production, reservoir pressure should decrease considerably as the desorption process becomes noticeable when the producing pressure is in the range of P_L or lower pressures. Accordingly, the simulations were set to produce at BHP of 300 psi with the external pressure of 4300 psi. The gas

production is slightly higher for the cases with adsorption, however, despite significant changes in the adsorption level, the impact on the gas production is minimal.

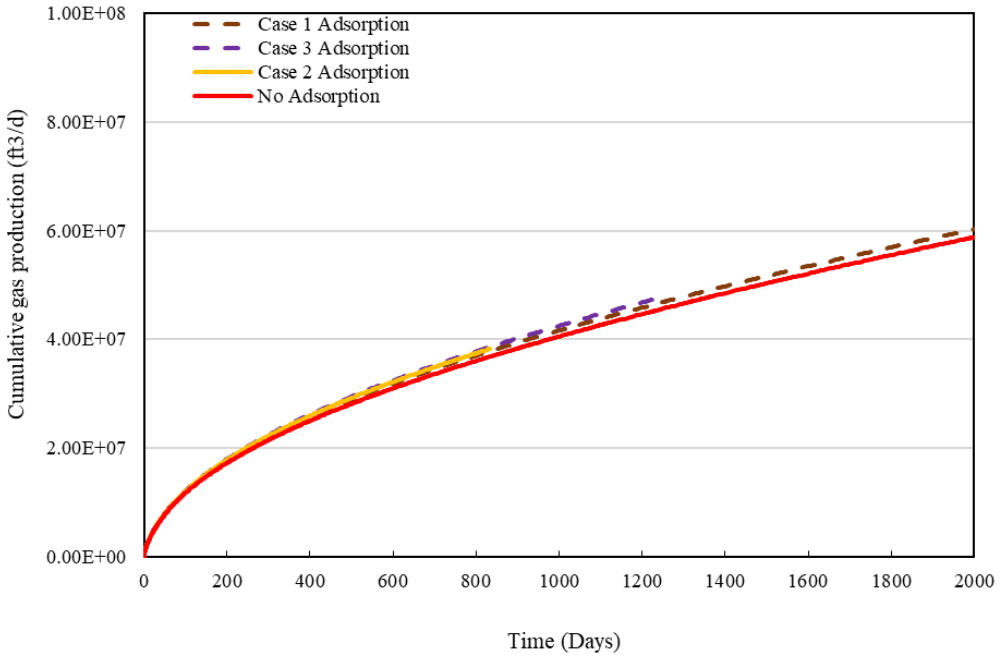

Figure 6.24: Cumulative gas production for the fractured well for dual permeability models flowing in two phase with bulk fluid model with DP value of 2000 psi for different cases of adsorption isotherms.

The impacts of pore confinement effects on production in the presence of adsorbed gas was also investigated. The results of the comparison of the performance of the reservoir with confined and bulk fluid models with and without considering Case 1 gas adsorption isotherm with the highest desorption level are presented in Figure 6.28. Again the trend is similar to the previously presented simulations results, i.e., slightly higher production using the confined fluid.

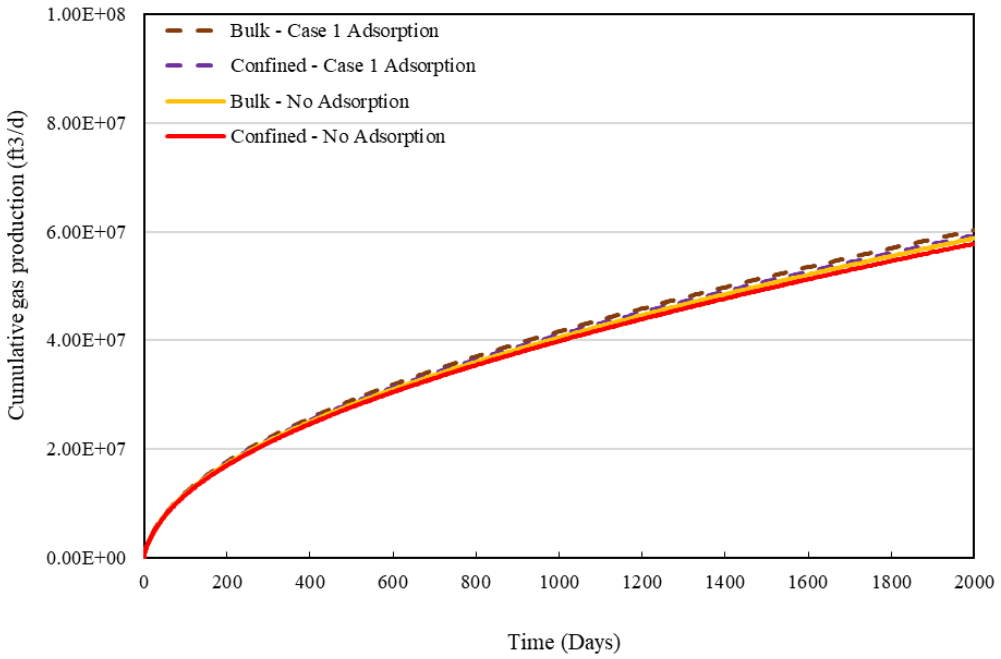

Figure 6.25: Cumulative gas production for the fractured well for dual permeability models flowing in two phase with bulk and confined fluid models with DP value of 2000 psi for cases without adsorption and Case 1 adsorption isotherms.

The results of the simulation for condensate production of the cases presented in Figure 6.25 are displayed in Figure 6.26. As it can be observed, adsorption does not contribute to any significant difference in condensate production because desorption of C1 is primarily in the gas phase.

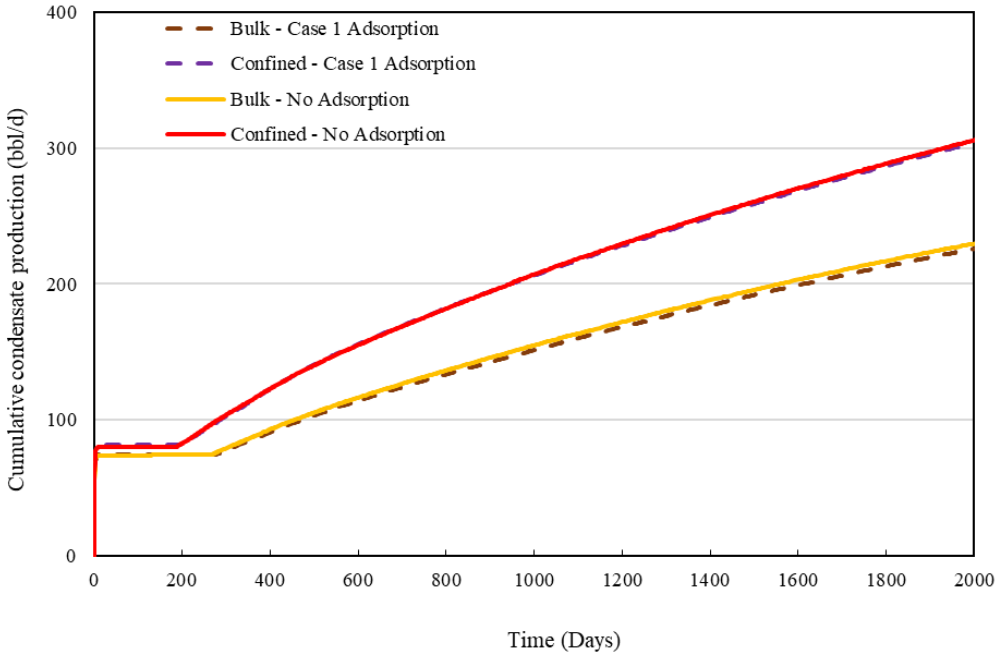

Figure 6.26: Cumulative condensate production for the fractured well for dual permeability models flowing in two phase with bulk and confined fluid models with DP value of 2000 psi for cases without adsorption and Case 1 adsorption isotherms.

6.2.5 Impacts of Matrix to Fracture Gas Diffusion on the Performance of Models with Bulk and Confined Fluid

Production from fractured unconventional reservoirs takes place by three different flow regimes. Darcy flow, non-Darcy flow and diffusion flow regimes control the production and fluid flow. Within the fractures, depending on its conductivity, both Darcy and non-Darcy flow can exist. However, due to high conductivity of the fractures, the production from fractures is usually associated with non-Darcy flow. In matrices, on the other hand, it is not very common to have non-Darcy inertial flow apart from near wellbore regions in high permeable reservoirs. The impact of coupling in the considered unconventional gas-condensate reservoirs were also ignored here. Therefore, it can be stated that, Darcy flow is one of the main flow regimes in matrices of unconventional reservoirs. However, diffusion flow can also exist in matrices of unconventional reservoirs. The driving force for Darcy flow is DP. Matrix to fracture diffusion flow, on the other hand, is as a result of the difference between the concentrations of the components in the matrix and fracture, and that is the reason why higher diffusion occurs at fracture and matrix interface, where the concentration difference is the highest, rather than in the matrix itself.. In commercial simulation packages like CMG-GEM, the following equation is used for the calculation of the rate of diffusion in fractured reservoirs.

$$Rate = \frac{Area}{Separation} \times \frac{D}{\tau} \times \varphi \times S_g \times \{C(k, gas, i) - C(k, gas, j)\} \qquad \text{Eq. 6.1}$$

where D is the diffusion coefficient and τ is the tortuosity.

It is to note that diffusion is an essential element in modelling any process which involves the injection of the gas. For instance, during CO_2 injection into gas condensate reservoirs, one of the main mechanisms contributing to the production is the vaporization of the condensate. In this study, however, our interest is to explore the impacts of diffusion on the extent of confinement. For the purpose of investigating the impacts of diffusion on the performance of the considered fractured reservoir model, new models were set-up. The tortuosity of these models was set to 1.5 which is within the lower band of typical range of tortuosity values for unconventional reservoirs. Based on the sensitivity on the diffusion coefficient and tortuosity, it was observed that changing the tortuosity and diffusion coefficient within the two orders of magnitude did not show any significant difference on the results. Different cases with various diffusion coefficients for C1 and nC8 components were considered. The impacts of having simultaneous effects of adsorption and diffusion were also investigated.

Table 6.11 shows the parameters used for different cases with various coefficient values used for gas phase matrix to fracture diffusion in two phase fluid flow simulations. It should be mentioned that Case 3 was also considered to explore the simultaneous impacts of adsorption and diffusion using the Case 1 adsorption isotherm as the case with the highest desorption.

Table 6.11: Diffusion parameters for different cases of simulations

Case	Diffusion coefficient (cm^2/s)		Tortuosity	Adsorption isotherm case
	C1	nC8		
Case 1	0.048	-	1.5	-
Case 2	0.048	0.006	1.5	-
Case 3	0.048	0.006	1.5	Case 1 adsorption isotherm

First the results of the simulations with bulk and confined fluid for the Case 1 diffusion coefficient versus the case where diffusion is not considered were compared as shown in Figure 6.29. Again the trend is similar to the previously presented simulations results, i.e., slightly higher gas production using the confined fluid model. Also it was observed that the Case 1 diffusion does not contribute to any significant change in the gas production. As will be shown later the difference between cases with different diffusion coefficients is minimal, i.e. similar observations are expected for diffusion Cases 2 and 3.

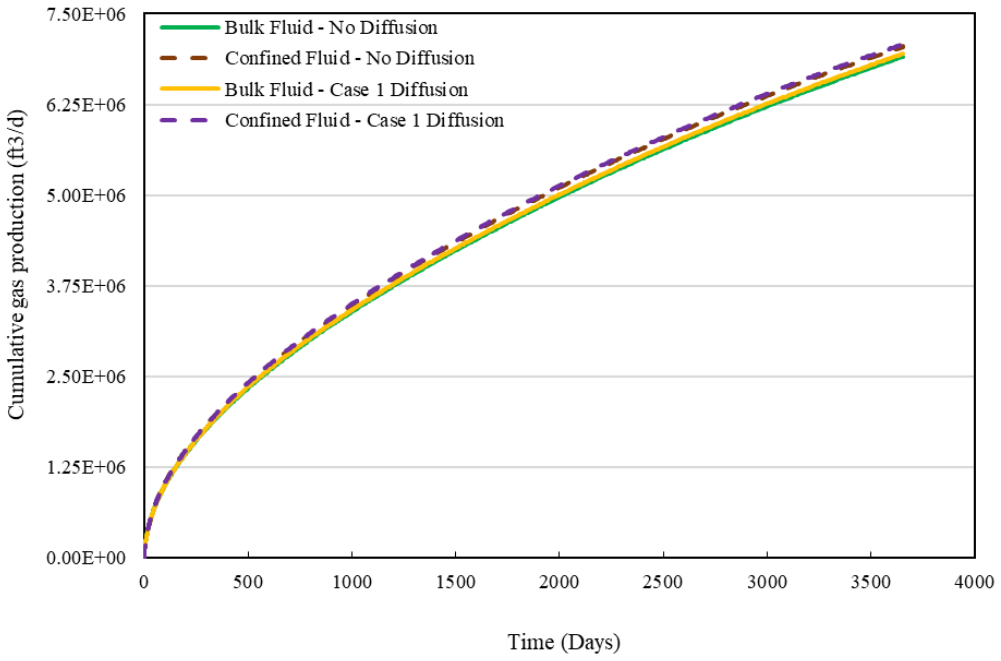

Figure 6.27: Cumulative gas production for the fractured well for dual permeability reservoir type flowing in two phase with bulk and confined fluid models with DP value of 2000 psi for cases with Case 1 diffusion coefficients and without diffusion.

Figure 6.28 shows the condensate production for cases demonstrated in Figure 6.27. As it can be observed, for the Case 1 diffusion, condensate production is lower for both bulk and confined fluid compared to the case without diffusion.

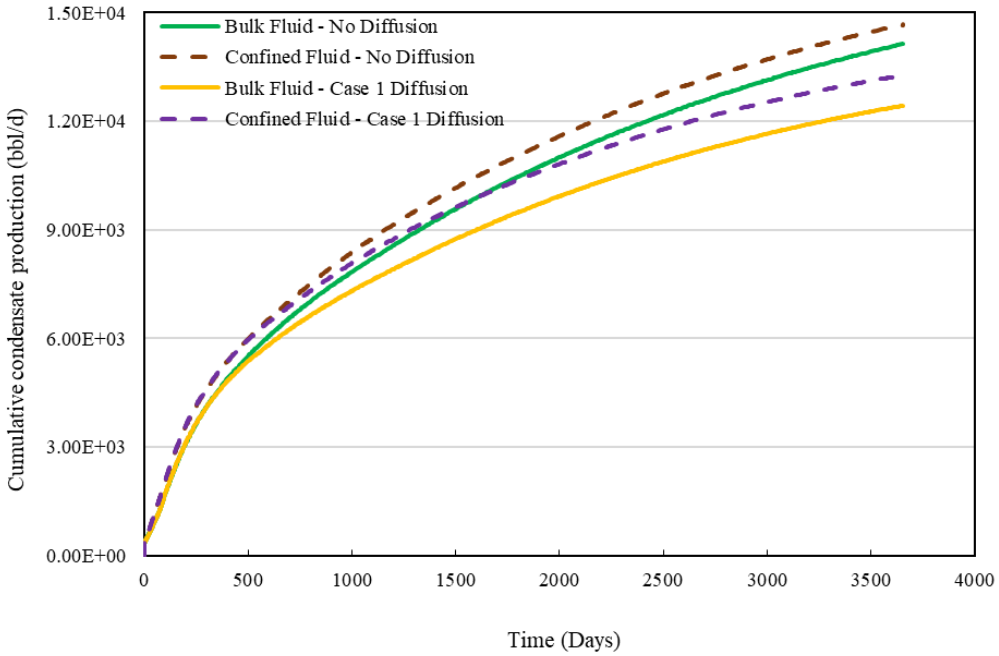

Figure 6.28: Cumulative condensate production for the fractured well for dual permeability reservoir type flowing in two phase with bulk and confined fluid models with DP value of 2000 psi for cases with Case 1 diffusion coefficients and without diffusion.

In order to better demonstrate the impacts of diffusion on condensate production, Figure 6.28 shows oil saturation variations in the fractures for cases without diffusion and Case 1 diffusion.

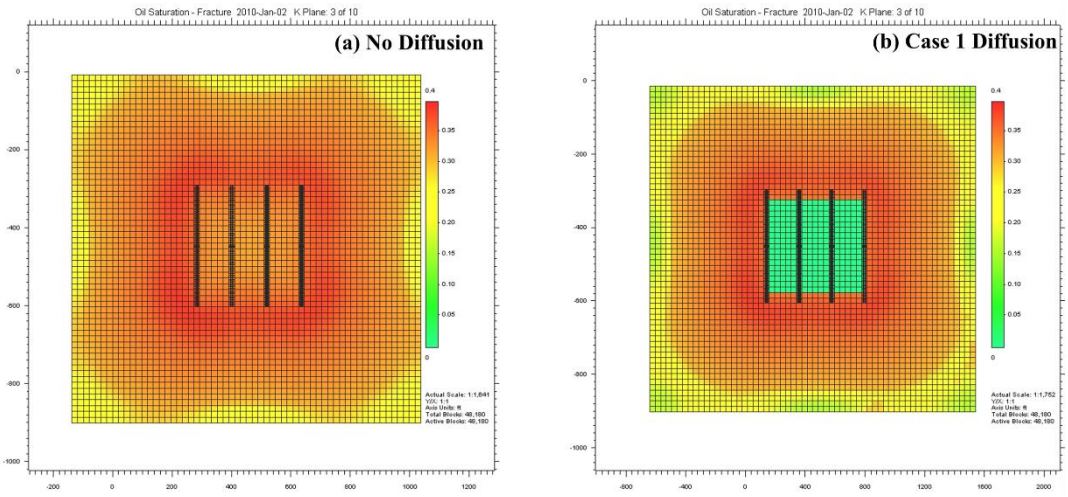

Figure 6.29: Fracture oil saturation after 10 years of production for the fractured well for dual permeability reservoir type flowing in two phase with bulk fluid models with producing DP value of 2000 psi for (a) no diffusion case and (b) Case 1 diffusion coefficients.

This figure shows oil saturation variations in fractures for the simulation with no diffusion and Case 1 diffusion coefficients. As it can be observed in this figure, for the Case 1 diffusion, the oil saturation in fractures in the regions of hydraulic fractures are close to zero. Also, natural fracture oil saturation towards the outer boundary of the reservoir is clearly lower for the case with diffusion. This implies that gas diffusion from matrix to fracture has resulted in the vaporization of condensate within fractures and consequently the reduction of oil saturation in fractures.

The results of the gas production data for the cases with different diffusion coefficients are presented in Figure 6.30. All the simulations have been performed at DP of 2000 psi and under two phase flow conditions.

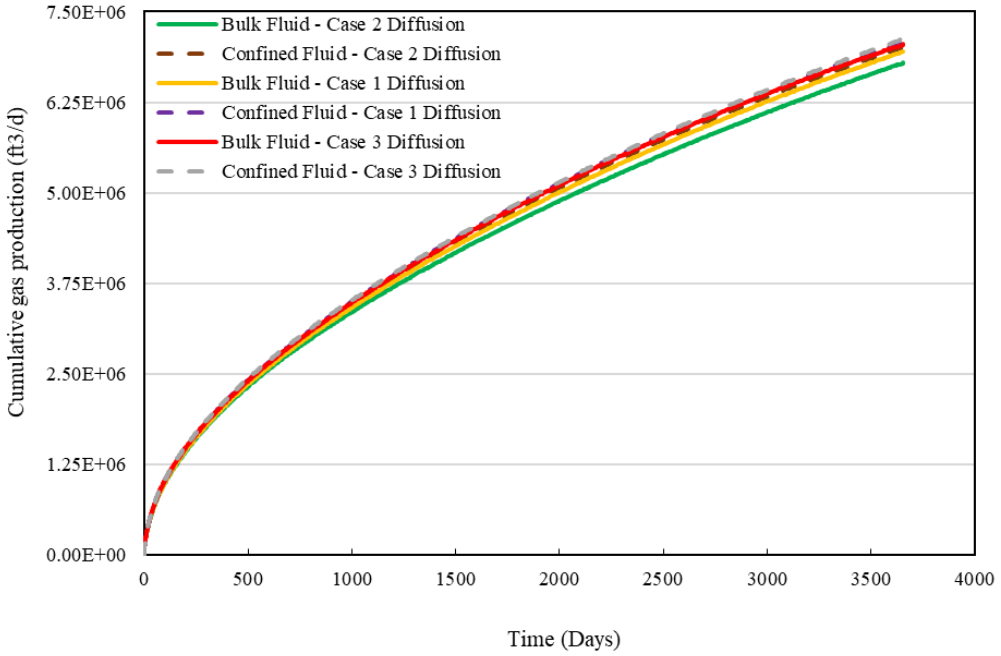

Figure 6.30: Cumulative gas production for the fractured well for dual permeability reservoir type flowing in two phase with bulk and confined fluid models with DP value of 2000 psi for different cases of diffusion coefficient.

Table 6.10 summarizes the cumulative gas production data of Figure 6.29.

Table 6.10: A summary of the cumulative gas production for the dual permeability model with the well and Case 2 hydraulic fracture model flowing in two phase with bulk and confined F7 fluid model with DP value of 2000 psi for different cases of diffusion coefficient.

Case	**Cumulative gas production (ft^3*10^3)**	**Fluid model**	**Difference between bulk and confined production (%)**
Case 1	6946.9 7079.1	Bulk Confined	+1.9
Case 2	6792.4 7009.1	Bulk Confined	+3.2
Case 3	7048.1 7121.8	Bulk Confined	+1.0

Figure 6.30 shows the results of the similar simulations as per Figure 6.29 for condensate production. Again, it can be observed that the condensate production is generally higher for the cases with diffusion. The trend for the effects of confinement on condensate production is also similar to that observed in previous sections for DP value of 2000 psi, i.e. condensate production is higher with the confined fluid model compared to that with the bulk fluid model.

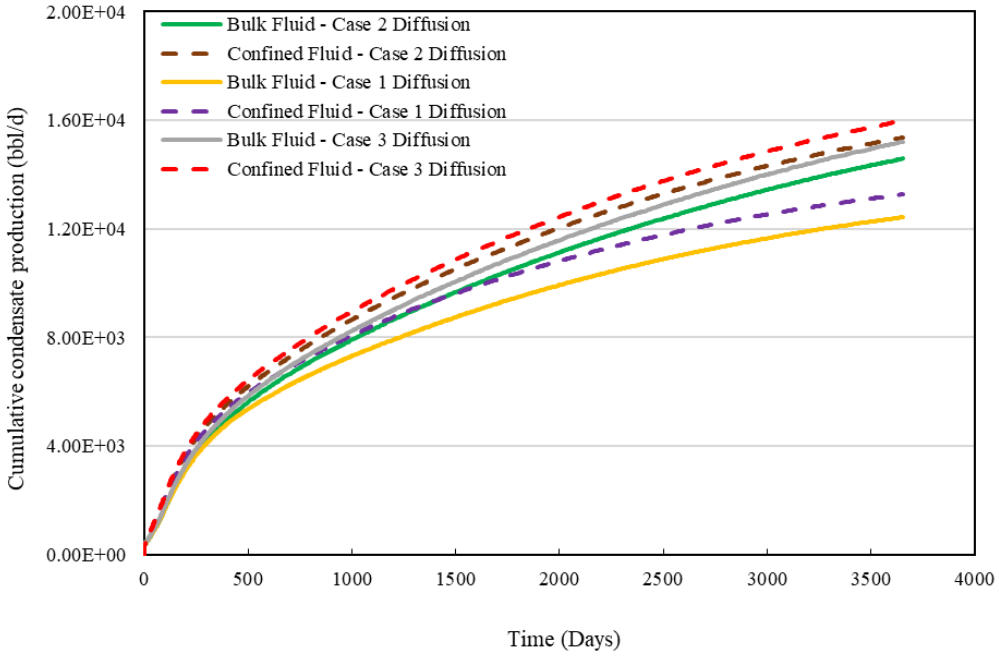

Figure 6.30: Cumulative condensate production for the well with Case 2 hydraulic fracture for dual permeability reservoir type flowing in two phase with bulk and confined fluid models with DP value of 2000 psi for cases with Case 1 diffusion coefficients and without diffusion.

As it can be observed, for all cases of diffusion coefficients, the difference between the productions of the cases with different diffusion coefficients is marginal. The impact of pore confinement effects on the gas production, with using different fluid sample models seems to be more important than diffusion taking place between matrix and fracture. However, it should be noted that matrix to fracture gas phase diffusion mainly contribute to the interaction between the regions with high and low condensate values. Hence in a fractured reservoir, where the pressure drop across the fracture-matrix interface is significant, in case of having diffusion, it is likely that the condensate in fractures is vaporized due to diffusion of gas from matrix to fractures.

6.3 Conclusions

In this chapter, confined and bulk fluid models were employed to compare the performance of series of single well unconventional gas-condensate reservoir models to evaluate the pore confinement effects. Several sensitivities were run to investigate the impacts of different parameters including hydraulic fracturing, NFZ modifications, adsorption, and matrix-fracture gas diffusion. It should be mentioned that the numerical simulations performed in this study can only be considered as a starting point for the

analysis of the effects of pore confinement on the performance of gas condensate flow at reservoir scale and a wider range of parameters should be considered for a more in depth investigations. Following findings can be summarised from the results of the numerical simulations performed in this chapter.

- For single phase flow simulations, it was observed that employing the confined fluid model resulted in higher gas production. Single phase flow is mainly governed by the viscosity of the flowing fluid and also the pressure drop. Hence, the main reason for the slightly higher cumulative gas production when using the confined compared to bulk fluid model was attributed to the lower gas viscosity for the confined fluid.
- Similarly, for two phase flow simulations, since confined gas viscosity was lower, gas production using the confined fluid model was also higher than the case using the bulk fluid model. The flowing gas components of the confined fluid has lower density and hence lower viscosity, due to higher interactions taking place between heavier fluid molecules and pore walls which attracts the heavier molecules towards the pore walls. Hence, confined gas viscosity becomes lower and would have lower resistance for the flow towards well.
- It was observed that the dual permeability reservoir model resulted in much higher production compared to the corresponding dual porosity model. This highlights the importance of the flow within matrices. That is, although fractures can be considered as the main flow path for the fluids, matrices are the main contributor for the overall production of unconventional reservoirs. Using the confined fluid model did not change this trend. The trends mentioned above for the effect of confinement for single-porosity model was also observed for the dual porosity and dual permeability models with natural fractures.
- NFZ grid block modifications slightly improved gas production for both confined and bulk fluid models but did not alter the trends mentioned above for the effect of confinement. It is suggested that, although NFZ modifications may not significantly increase the production from the reservoirs, it can be considered as a suitable option for tuning during history matching from unconventional reservoirs.
- The impacts of adsorption on the production was not very significant, and hence the above mentioned trends for the effect of confinement was unchanged. The effect adsorption is expected to be more important if the reservoir pressure reduces

to the range at which the slope in the adsorption isotherm is very high. It should also be noted that adsorption plays an important role on the storage capacity of unconventional reservoirs.

- Matrix to fracture gas phase diffusion did not significantly change gas production and hence the confinement effects trends were preserved. The main contribution of the diffusion in unconventional reservoirs, is its impacts on the vaporization of the condensate which usually exist in natural fractures within porous medium.

Chapter 7: Summary, Conclusions and Recommendations for Future Studies

7.1 Summary

Unconventional reservoirs have gained a lot of attention in recent years due to globally increasing energy demands. However, understanding the mechanisms, which affect their fluid flow and phase behaviour is still a challenge due to the complexity of these reservoirs and little experimental data to verify the proposed theoretical methods.

Increased fluid-wall interactions in nanopores of unconventional rocks could alter the phase behaviour of residing fluids. This is known as the pore confinement effect. The main objective of this research was to study the impacts of confinement effects on the phase behaviour of gas condensate fluids. In this research, several experiments were performed following a newly proposed experimental method, which is suitable for real unconventional rocks and multi-component gas condensate fluids, to investigate the impacts of different parameters including fluid composition, net stress and temperature on the extent of pore confinement effects in real shale core samples. The results of these Pdew measurements were then used to propose a formulation which was in turn applied to modify an Equation of State (EOS) that expresses the confinement effect. Series of single-well numerical simulations were carried out that used this modified EOS. In the following section, a summary of the conducted experiments, EOS modelling and simulations performed are described.

After performing bulk Pdew for a binary gas condensate mixture, three different core samples including a shale core sample, and two tight cores, with different ranges of permeability were selected to perform the porous medium Pdew measurements. These experiments performed on tight cores served as the validation step of the method proposed to measure the Pdew of the gas condensate mixture within real porous media. That is, measurements conducted within these tight cores correctly did not show any significant difference between bulk and porous medium but those within real shale cores demonstrated an increase in confined Pdew compared to the bulk Pdew, . The experimental steps followed in this study are presented in chapter 3 of this research.

After validation of the experimental method, in chapter 4, first by using C2 as the single component fluid, its confined Pdew within a porous medium was measured. Then, Pdew of various gas condensate mixtures in two shale core samples at different conditions were measured. The impact of fluid composition, temperature, net stress and rock type were studied using 9 different gas condensate fluids at three different temperatures and three different net stress values. In total, 23 different sets of experiments were performed in this study.

Based on the experimental results presented in chapter 4, a new approach for modification of the EOS for confined fluids was discussed in chapter 5. For this purpose, a new term was added to the binary interaction parameter (BIP) of the confined fluid. A formulation specific to the rock type, which was based on Lennard Jones (LJ) potential, was proposed to calculate the change in BIP due to confinement. The predictability of the proposed method was found to be satisfactory.

In chapter 6, the results of series of single-well numerical reservoir simulations that were performed using the GEM (CMG) software to evaluate the impact of confinement on the considered reservoir performance, were discussed. CMG is a compositional simulator, which is widely used for the simulation of unconventional reservoirs. Using a Cartesian reservoir model with a horizontal well, several sensitivity analysis were performed on the impacts of confinement varying different parameters including near fracture zone grid blocks permeability, adsorption, diffusion, and dual porosity versus dual permeability models.

7.2 Conclusions

In this section, the main conclusions obtained based on experimental and theoretical investigations performed in this study are presented.

Impacts of pore confinement effects on the Pdew of single component fluid and gas condensate mixtures: It was observed that pore confinement effects have two different impacts on single component fluid and gas condensate mixtures. For single component fluid, Pdew decreased as a result of pore confinement effects. However, for gas condensate mixtures, Pdew increased due to pore confinement effects.

Impacts of gas condensate composition on pore confinement effects: In gas condensate mixtures with similar components, as the concentration of the heavier component

increased, the confined Pdew was higher. The richness of the gas condensate mixture which is represented by its MLDO, was not as an important factor as the presence of heavier components in the mixture. In other words, it is possible that the pore confinement effects would be higher for a gas condensate mixture with similar MLDO compared to another gas condensate, mainly due to the presence of heavier molecules.

Impacts of temperature on pore confinement effects: Initially, by an increase in temperature, the difference between confined Pdew and bulk Pdew increased. However, further increase in the temperature resulted in a considerable decrease in the difference between bulk and confined Pdew.

Impacts of net stress on pore confinement effects: The impacts of net stress was shown to be highly dependent on the fluid type. For lean fluids, or fluids with very low content of heavier components, the net stress had negligible impacts on the extent of the confinement effects. However, when gas condensate mixture contained heavier molecules, the impacts of net stress was not negligible anymore.

Proposed correlations in literature: Proposed approaches available in the literature can properly predict the phase behaviour of the confined single component fluids. However, for any type of porous medium, specific tuning coefficients need to be used. For gas condensate mixtures, there is a significant disagreement between the trends obtained from the proposed theoretical approaches in the literature and the experimental results presented here. That is, all proposed approaches, which have been reported previously to modify the EOS for confined fluids, suggested that confined Pdew of fluid samples would reduce since they only considered the effects of pore confinement on the shift of critical properties for single component fluids. However, it is shown here that Pdew of gas condensate mixtures increase due to pore confinement effects.

Proposed formulation for BIP calculations: In this study, a new modification to BIP was suggested using LJ potentials concept to allow an EOS to properly match the Pdew of the confined gas condensate mixtures. The range of errors for the proposed equation was satisfactory. The coefficients of the proposed formulation depend on the rock under study and hence for other rocks they might need to be adjusted albeit with limited requiring number of measured data points.

Unconventional reservoir performance using numerical simulations: Impacts of different parameters and mechanisms on the performance of a single-well model was investigated in series of numerical simulations. It was observed that for almost all cases the simulated

gas production data from the unconventional reservoir models with confined fluid were slightly higher compared to those from the models with bulk fluid. For the case of condensate production, it was observed that when pressure drawdown (DP) was low, models with bulk fluid produced more condensate. However, when DP increased, models with confined fluid produced more mainly due to higher liquid drop out. It was also observed that implementing dual permeability model, resulted in significantly higher gas production compared to dual porosity model. The impacts of adsorption and matrix to fracture gas diffusion on the production were also investigated. It was observed that changing these two parameters over a wide range do not contribute to a significant change in gas production. However, considering matrix to fracture gas diffusion resulted in higher condensate production as the gas phase can evaporate the condensate which drops out within the fractures with a lower pressure compared to the matrix. Including dual porosity, dual permeability, adsorption or diffusion did not alter the overall trend observed when a confined fluid model rather than a bulk fluid model was used in these models.

7.3 Recommendations for Future Studies

The current study only serves a starting point for a newly developed experimental method and corresponding modelling approach for gas condensate fluid phase behaviour in unconventional reservoirs. Undoubtedly, apart from performing more experiments to consolidate the findings of this study, there are several other questions which need to be answered to get a better understanding of the observed findings. In this section, some recommendations for future studies are presented which can be followed to answer some of the unanswered questions on the effect of confinement in unconventional reservoirs.

Impacts of fluid composition and temperature on pore confinement effects: In this study it was observed that fluid composition and the presence of heavier components influence the extent of the effects of pore confinement. It is suggested that more experiments to be conducted on different binary and ternary gas condensate mixtures to consolidate these findings. Using multi-component real gas condensate mixtures at a later stage can also be extremely helpful to verify the reliability of the proposed experimental and theoretical methods. Three different experiments were performed in this study to investigate the effects of temperature. Only one fluid was used for these experiments. More experiments are required to study the effects of temperature. Especially, since the range of the reservoir

temperature for unconventional is generally higher than those considered in this study, further knowledge can be acquired. Also, different types of fluids with different components can be used. The modified phase behaviour modelling approach and proposed formulation in this study can then be further improved with additional experimental data.

Experimental and theoretical determination of uncertain parameters: In this study, it was assumed that pore confinement does not change the MLDO of the fluids because there is no experimental evidence for having different MLDO for confined fluids. Moreover, the viscosity of the confined fluid was estimated based on the proposed modified EOS. There is no experimental evidence or a proper theoretical study conducted to investigate the change in the LDO or viscosity of gas condensate mixtures due to the effects of pore confinement. Hence, it is suggested that further theoretical investigations and novel experiments to be performed in order to determine other properties of the fluids under confinement in unconventional rocks. These parameters can then be implemented in the Eos modifications applied for unconventional reservoirs. Performing experiments on synthetic porous medium using the proposed method in this study would bring some benefits to the current state of the knowledge about unconventional reservoirs. Firstly, the integrity of the proposed method would further be evaluated. Second, using synthetic porous medium, some of the parameters including the mineralogy and pore size distribution can be controlled. Hence, comparing the results of the experiments conducted on synthetic and real porous media would give more insightful knowledge about the pertinent parameters regarding the pore confinement effects.

Applications of the proposed correlation for EOS modifications: In this study, the proposed correlation has been developed based on binary mixtures, which can be extended to multi-components mixtures. It should be mentioned that, in order to find an acceptable correlation for multicomponent mixtures, further experiments using various components are required. To modify the equation proposed here to multi-components gas condensate mixtures, one approach could be to obtain the net interaction potential between different pair of components of a multicomponent gas condensate mixture by applying a suitable mixing rules. Then, terms α, which is the ratio of the confined BIP to the bulk BIP and A_{fw}, which is the fluid-wall affinity coefficient, can be estimated.

Adsorption and desorption: The sorption-desorption mechanism taking place in unconventional reservoirs is of great importance and should carefully be taken into account in any study for unconventional reservoirs performance. The sorption-desorption

mechanism is particularly important for dry gas or lean gas condensate reservoirs production estimations. Experimentally determined adsorption and desorption isotherms are very important in the study of fluid flow and phase behaviour in unconventional reservoirs. The results of the experiments performed on the phase behaviour of confined fluid along with the adsorption isotherms can provide more accurate information about the physics of fluid flow in unconventional reservoirs which would result in a more representative modelling of these reservoirs. The results of adsorption isotherms would give valuable information regarding the extent of the impacts of adsorption on permeability change within unconventional reservoirs.

At a higher level and for other applications of the study of the phase behaviour of fluids within unconventional reservoirs, following aspects could also be implemented using novel experimental and theoretical approaches.

CO2 EOR in unconventional gas condensate reservoirs: CO2 EOR processes are considered to be one of the most prosperous approaches for enhancing the production from hydrocarbon reservoirs. The impact of CO2 on the production from unconventional reservoirs has recently been the subject of many studies. However, still there are a lot of questions, which need to be answered regarding the application of CO2 EOR, especially for gas condensate reservoirs. The phase behaviour and properties of CO2 and resident fluids are also expected to be affected by the confinement effect. Hence, experimental data on the enhanced condensate recovery from unconventional reservoirs, can provide new insights for CO2 EOR in unconventional reservoirs. Also, experimental studies can be performed to investigate the potential of unconventional reservoirs for CO2 storage as absorbed or free gas. Modelling of these processes can provide better knowledge on the benefits of using CO2 for EOR and storage purposes.

Multi-scale unconventional rock modelling: The mechanisms taking place in unconventional porous media involves the interactions at molecular levels. However the resultant impact can affect the reservoir at much larger scales. Hence, a more in-depth approach for linking experimental and theoretical studies in such a way to properly takes into account multi-scale phenomena in unconventional reservoirs is desired. Moreover, the impacts of different pertinent parameters on the performance of the unconventional reservoir models should be investigated more deeply by such numerical simulations.

Diffusion in unconventional reservoirs: In any study of unconventional reservoirs, diffusion coefficients and how the diffusive flow is considered is very important.

Different models for estimating diffusion exist in the literature. However, a combined experimental and theoretical approach to estimate the diffusion coefficient with the main focus on unconventional reservoirs is lacking, which can be a subject of a future study especially when it is linked to confinement effects.

Fluid flow and geomechanical effects in unconventional reservoirs: There are very limited data available on gas-condensate flow in unconventional rocks. In the numerical simulations performed in this study, the stress dependency of porosity and permeability of unconventional rocks was ignored. Also, the impacts of gas slippage effects on fluid flow in the presence of liquid film is not very well documented. There are no experimentally measured data on gas-condensate relative permeability (except the limited data measured in by HW-GC team). Once the impacts of the above mentioned parameters have been verified experimentally, appropriate theoretical models can be developed to consider simultaneous effects of geomechanical and gas slippage effects in unconventional reservoirs fluid flow.

Flexible source codes for unconventional reservoir simulations: Commercial softwares and simulation packages do not have sufficient flexibility to study unconventional reservoirs including the details of all mechanisms influencing the performance of unconventional reservoirs. The development of a new set of numerical codes for unconventional reservoirs with the possibility to explicitly modify the properties according to the experimentally obtained data and newly proposed models for different mechanisms including geomechanical effects, pore confinement effects, adsorption-desorption effects, gas slippage and Knudsen diffusion effects, and capillary pressure effects will be beneficial.

Application of data science in unconventional reservoirs: Considering the current tendency in the applications of data science in engineering fields, very little is known about artificial intelligence and data science approaches in unconventional reservoir engineering. Hence, employing data science techniques can shed light onto some of the main features of unconventional reservoirs.

Appendix 1: Comparison of Bulk and Confined Phase Behaviour of Different Fluids based on the Proposed EOS Modification.

In chapter 5, the main focus was based on F7 fluid sample results. In this section the bulk and confined dew curve, vapour and liquid viscosity of other fluid samples used in this study are compared. Figure A.2 to A.8 show the graphs. As it can be observed, the trends are very similar to that of F7 fluid sample. Predicted vapour viscosity for bulk fluid is higher than confined fluid vapour viscosity. Similarly, the predicted liquid viscosity for bulk fluid is higher than the liquid viscosity of confined fluids. Regarding the dew curve, for most components and over a wide range of temperature, the Pdew of bulk fluid is predicted to be lower than that of confined fluid.

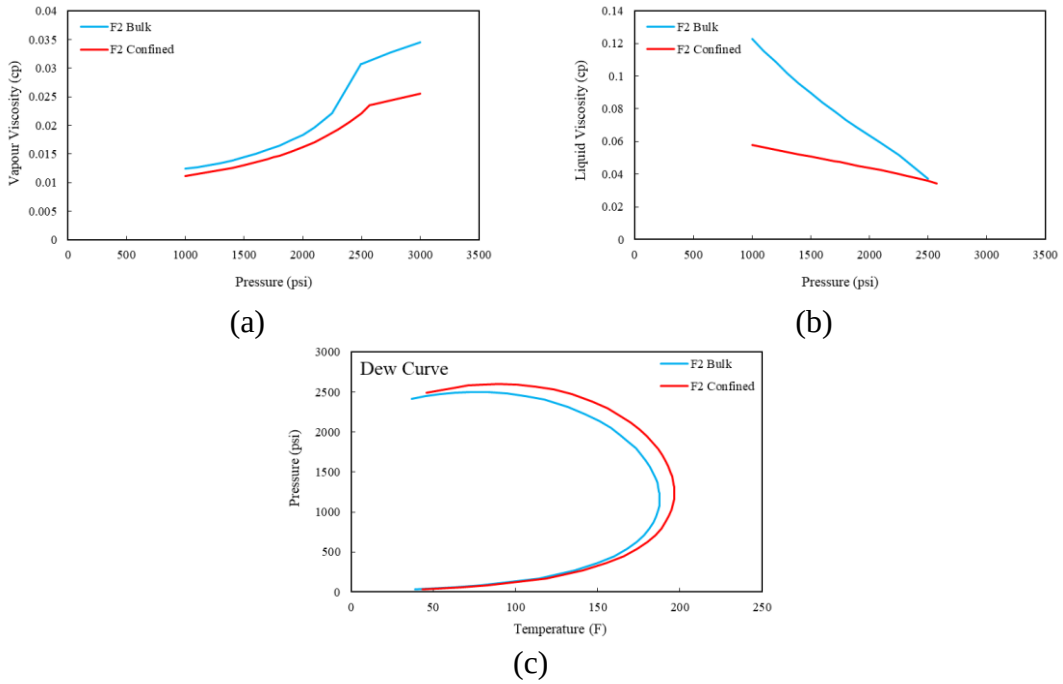

Figure A.2: Comparison of F2 sample bulk and confined (a) vapour viscosity, (b) liquid viscosity, and (c) dew curves.

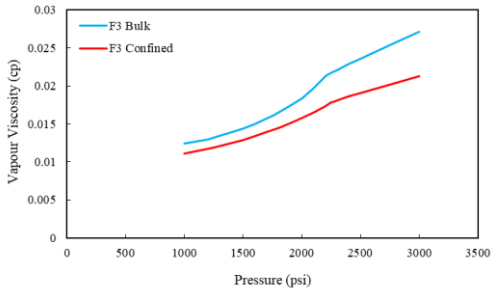

(a)

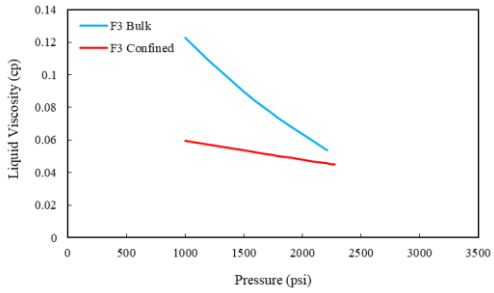

(b)

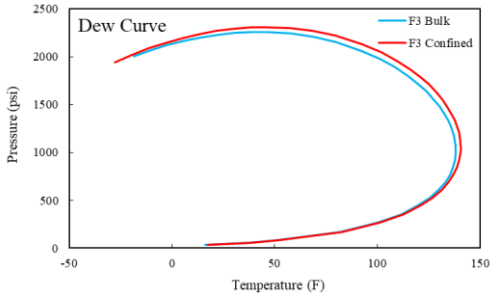

(c)

Figure A.3: Comparison of F3 sample bulk and confined (a) vapour viscosity, (b) liquid viscosity, and (c) dew curves.

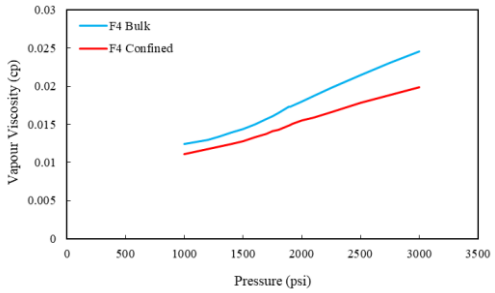

(a)

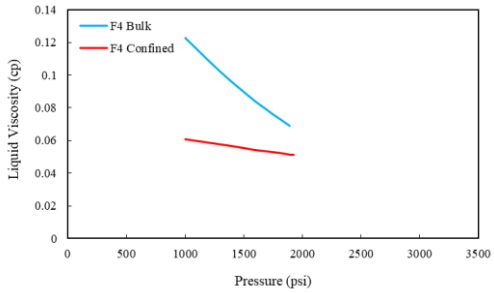

(b)

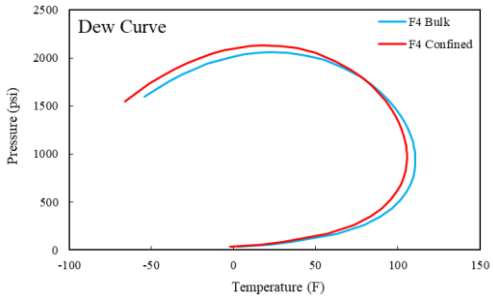

(c)

Figure A.4: Comparison of F4 sample bulk and confined (a) vapour viscosity, (b) liquid viscosity, and (c) dew curves.

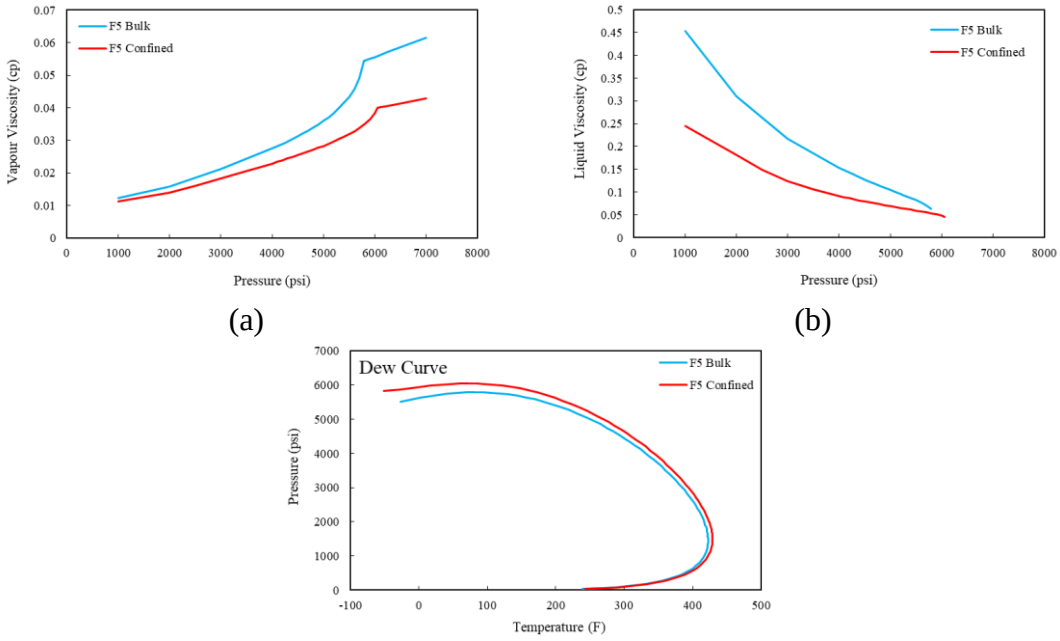

Figure A.5: Comparison of F5 sample bulk and confined (a) vapour viscosity, (b) liquid viscosity, and (c) dew curves.

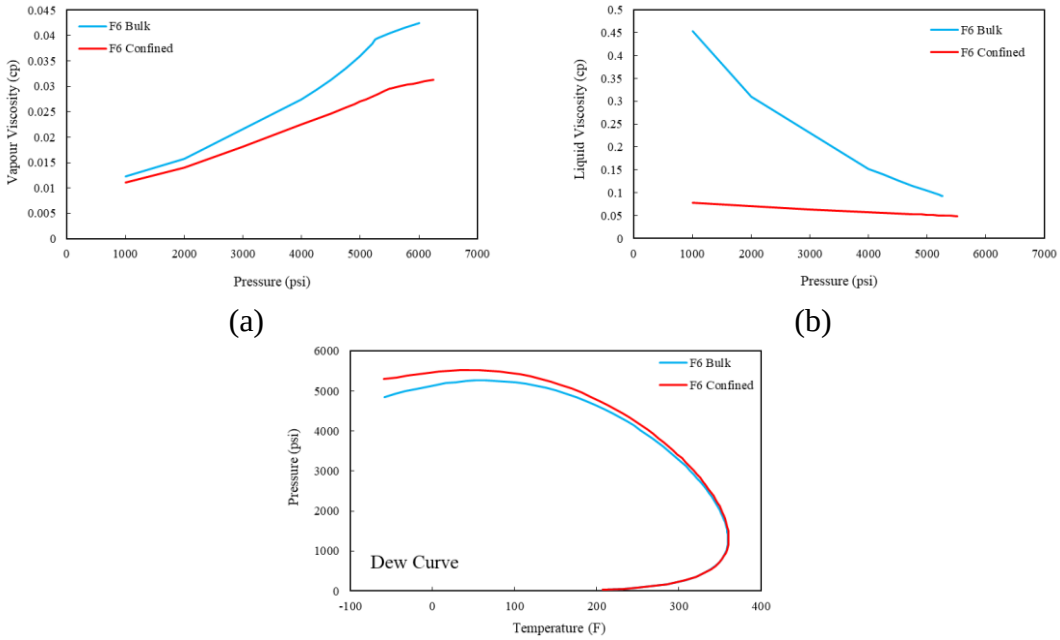

Figure A.6: Comparison of F6 sample bulk and confined (a) vapour viscosity, (b) liquid viscosity, and (c) dew curves.

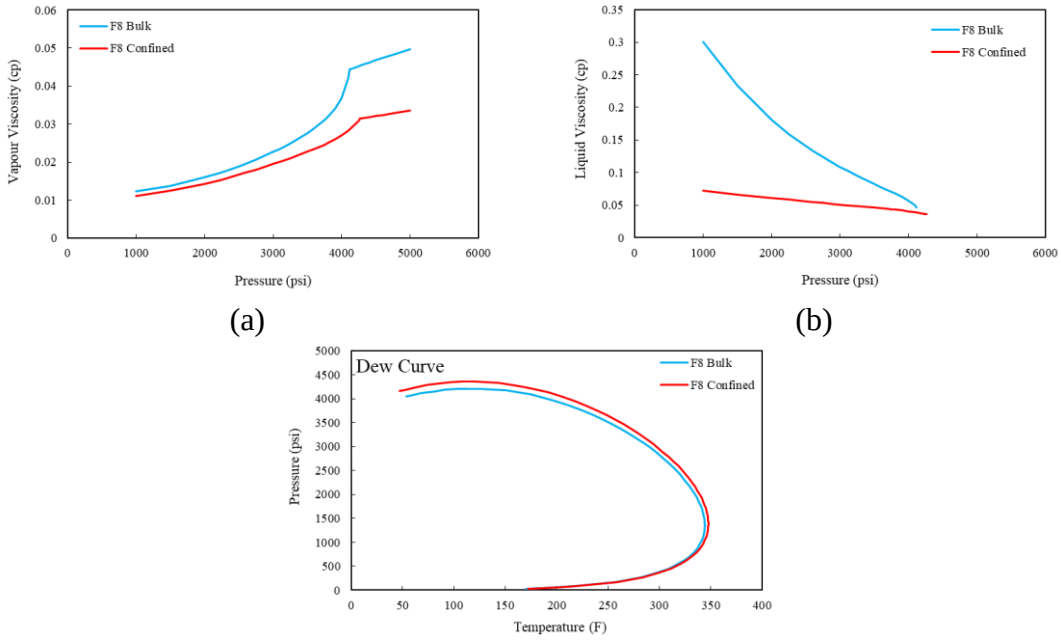

Figure A.7: Comparison of F8 sample bulk and confined (a) vapour viscosity, (b) liquid viscosity, and (c) dew curves.

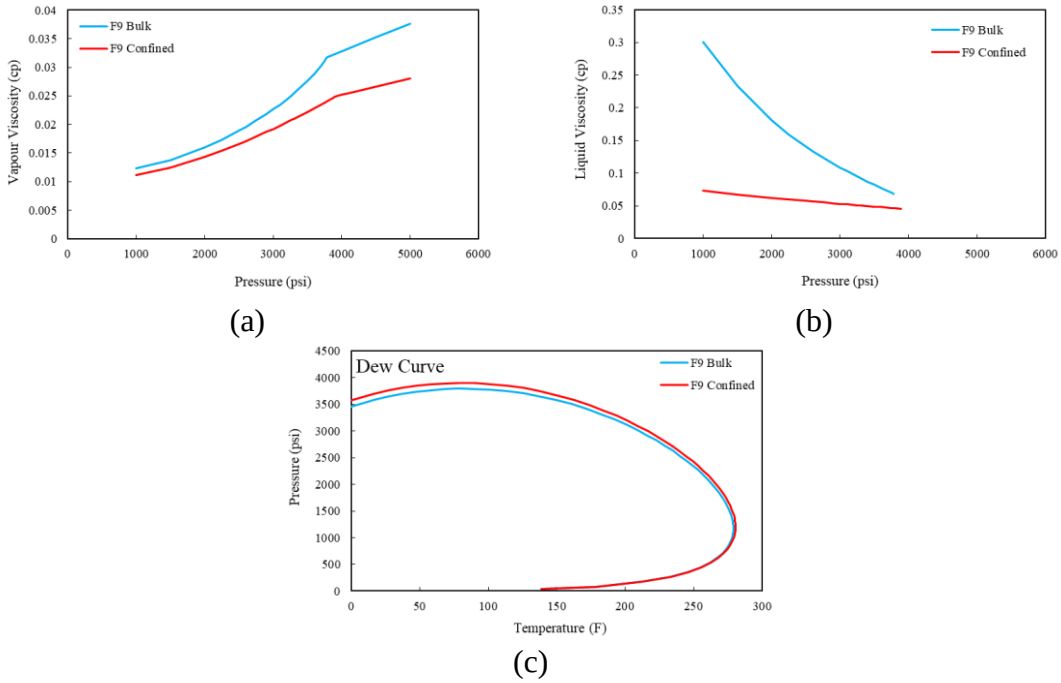

Figure A.8: Comparison of F9 sample bulk and confined (a) vapour viscosity, (b) liquid viscosity, and (c) dew curves.

In chapter 5 the predictability of the proposed correlation for different types of fluids were presented. In this section, the results of the error analysis with considering the experimental data of other fluids as the source data for the analysis are presented.

- Error Analysis for C1+nC5 Mixtures

Fluid	Bulk Pdew (psi)	Range of measured confined Pdew (psi)	Predicted confined Pdew (psi)	Error (%) compared to	
				Lower Pdew	Upper Pdew
F2	2493	2562 – 2581	2587	-36.2	-6.8
F3*	***2213***	***2264 – 2281***	***2273***	***-17.6***	***+11.8***
F4	1891	1915 – 1935	1918	-12.5	+38.6

*Used as the source data for Pdew predictions

Fluid	Bulk Pdew (psi)	Range of measured confined Pdew (psi)	Predicted confined Pdew (psi)	Error (%) compared to	
				Lower Pdew	Upper Pdew
F2	2493	2562 – 2581	2599	-53.6	-20.5
F3	2213	2264 – 2281	2288	-47.1	-10.3
F4*	***1891***	***1915 – 1935***	***1925***	***-41.7***	***+22.7***

- Error Analysis for C1+nC10 Mixtures

Fluid	Bulk Pdew (psi)	Range of measured confined Pdew (psi)	Predicted confined Pdew (psi)	Error (%) compared to	
				Lower Pdew	Upper Pdew
F5	5784	6041 – 6063	6084	-16.7	-7.5
F6*	***5264***	***5498 – 5519***	***5509***	***-4.7***	***+3.9***

- Error Analysis for C1+nC8 Mixtures

Fluid	Bulk Pdew (psi)	Range of measured confined Pdew (psi)	Predicted confined Pdew (psi)	Error (%) compared to	
				Lower Pdew	Upper Pdew
F7	4052	4181 – 4205	4185	-9.3	7.8
F8*	***4110***	***4258 – 4275***	***4267***	***-6.1***	***+4.8***
F9	3783	3884 – 3904	3859	+24.8	+37.2

Fluid	Bulk Pdew (psi)	Range of measured confined Pdew (psi)	Predicted confined Pdew (psi)	Error (%) compared to	
				Lower Pdew	Upper Pdew
F7	4052	4181 – 4205	4219	-29.5	-9.2
F8	4110	4258 – 4275	4291	-22.3	-9.7
F9*	***3783***	***3884 – 3904***	***3894***	***-9.9***	***+8.3***

References

A. Russo, P., Ribeiro Carrott, M. M. L. and M. Carrott, P. J. (2011) 'Hydrocarbons adsorption on templated mesoporous materials: effect of the pore size, geometry and surface chemistry', *New Journal of Chemistry*, 35(2), pp. 407–416. doi: 10.1039/C0NJ00614A.

Afidick, D., Kaczorowski, N. J. and Bette, S. (1994) 'Production performance of a retrograde gas reservoir: a case study of the arun field', *SPE - Asia Pacific Oil & Gas Conference*, pp. 73–80. doi: 10.2118/28749-MS.

Al-Kindi, I. and Babadagli, T. (2021) 'Revisiting Kelvin equation and Peng–Robinson equation of state for accurate modeling of hydrocarbon phase behavior in nano capillaries', *Scientific Reports 2021 11:1*, 11(1), pp. 1–14. doi: 10.1038/s41598-021-86075-8.

Alafnan, S. *et al.* (2021) 'Langmuir adsorption isotherm in unconventional resources: Applicability and limitations', *Journal of Petroleum Science and Engineering*. Elsevier B.V. doi: 10.1016/j.petrol.2021.109172.

Alfi, M., Nasrabadi, H. and Banerjee, D. (2016) 'Experimental investigation of confinement effect on phase behavior of hexane, heptane and octane using lab-on-a-chip technology', *Fluid Phase Equilibria*, 423, pp. 25–33. doi: 10.1016/j.fluid.2016.04.017.

Andrade, D. de C. J. de and Nojabaei, B. (2021) 'Phase behavior and composition distribution of multiphase hydrocarbon binary mixtures in heterogeneous nanopores: a molecular dynamics simulation study', *Nanomaterials 2021, Vol. 11, Page 2431*, 11(9), p. 2431. doi: 10.3390/NANO11092431.

Annual Energy Outlook 2021 (no date). Available at: https://www.eia.gov/outlooks/aeo/ (Accessed: 30 October 2021).

Barsotti, E. *et al.* (2016) 'A review on capillary condensation in nanoporous media: Implications for hydrocarbon recovery from tight reservoirs', *Fuel*. Elsevier Ltd, pp. 344–361. doi: 10.1016/j.fuel.2016.06.123.

Barsotti, E. *et al.* (2018) 'Capillary condensation of binary and ternary mixtures of n-pentane–isopentane–co2 in nanopores: an experimental study on the effects of composition and equilibrium', *Langmuir*, 34(5), pp. 1967–1980. doi: 10.1021/ACS.LANGMUIR.7B04134.

Barsotti, E. and Piri, M. (2021) 'Effect of pore size distribution on capillary condensation in nanoporous media', *Langmuir*, 37(7), pp. 2276–2288. doi: 10.1021/ACS.LANGMUIR.0C02775.

Belmabkhout, Y., Frère, M. and Weireld, G. De (2004) 'High-pressure adsorption measurements. A comparative study of the volumetric and gravimetric methods', *Measurement Science and Technology*, 15(5), p. 848. doi: 10.1088/0957-0233/15/5/010.

Beskok, A. and Karniadakis, G. E. (1999) 'Report: A model for flows in channels, pipes, and ducts at micro and nano scales', *Microscale Thermophysical Engineering*, 3(1), pp. 43–77. doi: 10.1080/108939599199864.

Brusilovsky, A. I. (1992) 'Mathematical simulation of phase behavior of natural multicomponent systems at high pressures with an equation of state', *SPE Reservoir Engineering*, 7(01), pp. 117–122. doi: 10.2118/20180-PA.

Cipolla, C. L. *et al.* (2009) 'Fracture design considerations in horizontal wells drilled in unconventional gas reservoirs', *Society of Petroleum Engineers - SPE Hydraulic Fracturing Technology Conference 2009*, pp. 366–375. doi: 10.2118/119366-MS.

Coutinho, J. A. P., Kontogeorgis, G. M. and Stenby, E. H. (1994) 'Binary interaction parameters for nonpolar systems with cubic equations of state: a theoretical approach 1. CO2/hydrocarbons using SRK equation of state', *Fluid Phase Equilibria*, 102(1), pp. 31–60. doi: 10.1016/0378-3812(94)87090-X.

Cui, G. *et al.* (2018) 'Why shale permeability changes under variable effective stresses: New insights', *Fuel*, 213, pp. 55–71. doi: 10.1016/J.FUEL.2017.10.068.

Darabi, H. *et al.* (2012) 'Gas flow in ultra-tight shale strata', *Journal of Fluid Mechanics*, 710, pp. 641–658. doi: 10.1017/JFM.2012.424.

Devegowda, D. *et al.* (2012) 'Phase behavior of gas condensates in shales due to pore proximity effects: Implications for transport, reserves and well productivity', in *Proceedings - SPE Annual Technical Conference and Exhibition*. Society of Petroleum Engineers (SPE), pp. 4197–4218. doi: 10.2118/160099-ms.

Diestler, D. J. *et al.* (1998) 'Thermodynamics of a fluid confined to a slit pore with structured walls', *The Journal of Chemical Physics*, 100(12), p. 9140. doi: 10.1063/1.466668.

Dong, T. *et al.* (2018) 'The effect of thermal maturity on geomechanical properties in shale reservoirs: An example from the Upper Devonian Duvernay Formation, Western Canada Sedimentary Basin', *Marine and Petroleum Geology*, 97, pp. 137–153. doi: 10.1016/J.MARPETGEO.2018.07.007.

Dong, X. *et al.* (2016) 'Phase equilibria of confined fluids in nanopores of tight and shale rocks considering the effect of capillary pressure and adsorption film', *Industrial and Engineering Chemistry Research*, 55(3), pp. 798–811. doi: 10.1021/ACS.IECR.5B04276.

Donnelly, B. *et al.* (2016) 'Capillary pressure – saturation relationships for gas shales measured using a water activity meter', *Journal of Natural Gas Science and Engineering*, 33, pp. 1342–1352. doi: 10.1016/J.JNGSE.2016.05.014.

Gensterblum, Y. *et al.* (2015) 'Gas transport and storage capacity in shale gas reservoirs – A review. Part A: Transport processes', *Journal of Unconventional Oil and Gas Resources*, 12, pp. 87–122. doi: 10.1016/J.JUOGR.2015.08.001.

Zarragoicoechea, G. J. and Kuz, V. A. (2002) 'van der Waals equation of state for a fluid in a nanopore', *Physical review. E, Statistical, nonlinear, and soft matter physics*, 65(2 Pt 1). doi: 10.1103/PHYSREVE.65.021110.

Haider, B. A. (2015) 'Impact of capillary pressure and critical properties shift due to confinement on hydrocarbon production from shale reservoirs'.

Hamada, Y., Koga, K. and Tanaka, H. (2007) 'Phase equilibria and interfacial tension of fluids confined in narrow pores', *The Journal of Chemical Physics*, 127(8), p. 084908. doi: 10.1063/1.2759926.

Hanarpour, M. and Mahmood, S. M. (1988) 'Relative-permeability measurements: an overview', *Journal of Petroleum Technology*, 40(08), pp. 963–966. doi: 10.2118/18565-PA.

Herdes, C. *et al.* (2018) 'Combined experimental, theoretical, and molecular simulation

approach for the description of the fluid-phase behavior of hydrocarbon mixtures within shale rocks', *Energy & Fuels*, 32(5), pp. 5750–5762. doi: 10.1021/ACS.ENERGYFUELS.8B00200.

Hill, T. L. (1962) 'Thermodynamics of small systems', *The Journal of Chemical Physics*, 36(12), p. 3182. doi: 10.1063/1.1732447.

Hui, W. *et al.* (2019) 'Review of molecular simulation method for gas adsorption/desorption and diffusion in shale matrix', *Journal of Thermal Science*, 28(1), pp. 1–16. doi: 10.1007/s11630-018-1053-9.

Fahimpour, J. (2015) 'Wettability alteration of carbonate rocks to alleviate condensate blockage around gas-condensate wells'.

Jamiolahmady, M. *et al.* (2009) 'A generalized correlation for predicting gas–condensate relative permeability at near wellbore conditions', *Journal of Petroleum Science and Engineering*, 66(3–4), pp. 98–110. doi: 10.1016/J.PETROL.2009.02.001.

Jarvie, D. M. (2012) 'Shale resource systems for oil and gas: part 1—shale-gas resource systems', *AAPG Memoir*, 97, pp. 69–87. doi: 10.1306/13321446M973489.

Jiang, J. *et al.* (2005) 'Adsorption and separation of linear and branched alkanes on carbon nanotube bundles from configurational-bias Monte Carlo simulation', *Physical Review B*, 72(4), p. 045447. doi: 10.1103/PhysRevB.72.045447.

Jin, Z. and Firoozabadi, A. (2016) 'Thermodynamic modeling of phase behavior in shale media', *SPE Journal*, 21(01), pp. 190–207. doi: 10.2118/176015-PA.

Li, L. and Sheng, J. J. (2017) 'Nanopore confinement effects on phase behavior and capillary pressure in a Wolfcamp shale reservoir', *Journal of the Taiwan Institute of Chemical Engineers*, 78, pp. 317–328. doi: 10.1016/J.JTICE.2017.06.024.

Liu, X. and Zhang, D. (2019) 'A review of phase behavior simulation of hydrocarbons in confined space: Implications for shale oil and shale gas', *Journal of Natural Gas Science and Engineering*, 68, p. 102901. doi: 10.1016/J.JNGSE.2019.102901.

Luo, S. *et al.* (2021) 'Multiscale pressure/volume/temperature simulation of decreasing condensate/gas ratio at greater than dewpoint pressure in shale gas-condensate reservoirs', *SPE Journal*, 26(06), pp. 4174–4186. doi: 10.2118/203905-PA.

Luo, S., Lutkenhaus, J. L. and Nasrabadi, H. (2018a) 'Multiscale fluid-phase-behavior simulation in shale reservoirs using a pore-size-dependent equation of state', *SPE Reservoir Evaluation & Engineering*, 21(04), pp. 806–820. doi: 10.2118/187422-PA.

Luo, S., Lutkenhaus, J. L. and Nasrabadi, H. (2018b) 'Use of differential scanning calorimetry to study phase behavior of hydrocarbon mixtures in nano-scale porous media', *Journal of Petroleum Science and Engineering*, 163, pp. 731–738. doi: 10.1016/J.PETROL.2016.12.019.

Luo, S., Nasrabadi, H. and Lutkenhaus, J. L. (2016) 'Effect of confinement on the bubble points of hydrocarbons in nanoporous media', *AIChE Journal*, 62(5), pp. 1772–1780. doi: 10.1002/AIC.15154.

Ma, Y., Jin, L. and Jamili, A. (2013) 'Modifying van der waals equation of state to consider influence of confinement on phase behavior', *Proceedings - SPE Annual Technical Conference and Exhibition*, 6, pp. 4643–4654. doi: 10.2118/166476-MS.

Mahdiyar, H., Jamiolahmady, M. and Sohrabi, M. (2011) 'Improved Darcy and non-

Darcy flow formulations around hydraulically fractured wells', *Journal of Petroleum Science and Engineering*, 78(1), pp. 149–159. doi: 10.1016/J.PETROL.2011.05.013.

Morishige, K. and Shikimi, M. (1998) 'Adsorption hysteresis and pore critical temperature in a single cylindrical pore', *The Journal of Chemical Physics*, 108(18), p. 7821. doi: 10.1063/1.476218.

Mulliken, C. A. and Sandler, S. I. (2002) 'The prediction of co2 solubility and swelling factors for enhanced oil recovery', *Industrial and Engineering Chemistry Process Design and Development*, 19(4), pp. 709–711. doi: 10.1021/I260076A033.

Nazari Moghaddam, R. (2016) 'Study of fluid flow in unconventional reservoir rocks : assessing flow regimes, geomechanics and capillary end effects'. Available at: https://www.ros.hw.ac.uk/handle/10399/3431 (Accessed: 29 November 2021).

Nazari Moghaddam, R. and Jamiolahmady, M. (2016a) 'Fluid transport in shale gas reservoirs: Simultaneous effects of stress and slippage on matrix permeability', *International Journal of Coal Geology*, 163, pp. 87–99. doi: 10.1016/J.COAL.2016.06.018.

Nazari Moghaddam, R. and Jamiolahmady, M. (2016b) 'Slip flow in porous media', *Fuel*, 173, pp. 298–310. doi: 10.1016/J.FUEL.2016.01.057.

Nazari Moghaddam, R. and Jamiolahmady, M. (2019) 'Steady-state relative permeability measurements of tight and shale rocks considering capillary end effect', *Transport in Porous Media 2019 128:1*, 128(1), pp. 75–96. doi: 10.1007/S11242-019-01236-8.

Nelson, P. H. (2009) 'Pore-throat sizes in sandstones, tight sandstones, and shales', *AAPG Bulletin*, 93(3), pp. 329–340. doi: 10.1306/10240808059.

Péneloux, A., Rauzy, E. and Fréze, R. (1982) 'A consistent correction for Redlich-Kwong-Soave volumes', *Fluid Phase Equilibria*, 8(1), pp. 7–23. doi: 10.1016/0378-3812(82)80002-2.

Peng, D.-Y. and Robinson, D. B. (1976) 'A new two-constant equation of state', *Industrial and Engineering Chemistry Fundamentals*, 15(1), pp. 59–64. doi: 10.1021/I160057A011.

Rubin, B. (2010) 'Accurate simulation of non-darcy flow in stimulated fractured shale reservoirs.' Available at: http://onepetro.org/SPEWRM/proceedings-pdf/10WRM/All-10WRM/SPE-132093-MS/1744307/spe-132093-ms.pdf/1. SPE 132093.

Salahshoor, S. and Fahes, M. (2020) 'Experimental determination of the dew point pressure for bulk and confined gas mixtures using an isochoric apparatus', *Fluid Phase Equilibria*, 508, p. 112439. doi: 10.1016/j.fluid.2019.112439.

Salahshoor, S., Fahes, M. and Teodoriu, C. (2018) 'A review on the effect of confinement on phase behavior in tight formations', *Journal of Natural Gas Science and Engineering*. Elsevier B.V., pp. 89–103. doi: 10.1016/j.jngse.2017.12.011.

Sanaei, A., Jamili, A. and Callard, J. (2014) 'Effect of pore size distribution and connectivity on phase behavior and gas condensate production from unconventional resources', in *Society of Petroleum Engineers - SPE USA Unconventional Resources Conference 2014*. Society of Petroleum Engineers, pp. 85–97. doi: 10.2118/168970-ms.

Shapiro, A. A. and Stenby, E. H. (1997) 'Kelvin equation for a non-ideal multicomponent mixture', *Fluid Phase Equilibria*, 134(1–2), pp. 87–101. doi: 10.1016/S0378-3812(97)00045-9.

Shinta, A. A. and Firoozabadi, A. (1997) 'Predicting phase behavior of water/reservoir-crude systems with the association concept', *SPE Reservoir Engineering*, 12(02), pp. 131–137. doi: 10.2118/27872-PA.

Sigmund, P. M. *et al.* (1973) 'Retrograde condensation in porous media', *Society of Petroleum Engineers Journal*, 13(02), pp. 93–104. doi: 10.2118/3476-PA.

Singh, S. K. *et al.* (2009) 'Vapor-liquid phase coexistence, critical properties, and surface tension of confined alkanes', *Journal of Physical Chemistry C*, 113(17), pp. 7170–7180. doi: 10.1021/jp8073915.

Slot-Petersen, C. (1989) 'A systematic and consistent approach to determine binary interaction coefficients for the Peng-Robinson equation of state (includes associated papers 20308 and 20393)', *SPE Reservoir Engineering*, 4(04), pp. 488–494. doi: 10.2118/16941-PA.

Tan, S. P., Barsotti, E. and Piri, M. (2020) 'Criticality of confined fluids based on the tensile strength of liquids'. doi: 10.1021/acs.iecr.0c01848.

Tan, S. P. and Piri, M. (2015) 'Equation-of-state modeling of confined-fluid phase equilibria in nanopores', *Fluid Phase Equilibria*, 393, pp. 48–63. doi: 10.1016/j.fluid.2015.02.028.

Technical Writing, M. (2017) 'Autopore ® v series mercury intrusion porosimeter'.

Teklu, T. W. *et al.* (2014) 'Phase behavior and minimum miscibility pressure in nanopores', *SPE Reservoir Evaluation & Engineering*, 17(03), pp. 396–403. doi: 10.2118/168865-PA.

Travalloni, L. *et al.* (2010) 'Thermodynamic modeling of confined fluids using an extension of the generalized van der Waals theory', *Chemical Engineering Science*, 65(10), pp. 3088–3099. doi: 10.1016/J.CES.2010.01.032.

Venkatramani, A. V. and Okuno, R. (2015) 'Characterization of water-containing reservoir oil using an EOS for steam injection processes', *Journal of Natural Gas Science and Engineering*, 26, pp. 1091–1106. doi: 10.1016/J.JNGSE.2015.07.036.

Wang, L. *et al.* (2014) 'Experimental study and modeling of the effect of nanoconfinement on hydrocarbon phase behavior in unconventional reservoirs' SPE-169581-MS. doi: 10.2118/169581-MS.

Wang, L. *et al.* (2016) 'Effect of pore-size distribution on phase transition of hydrocarbon mixtures in nanoporous media', *SPE Journal*, 21(06), pp. 1981–1995. doi: 10.2118/170894-PA.

Wang, Y., Yan, B. and Killough, J. (2013) 'Compositional modeling of tight oil using dynamic nanopore properties', *Proceedings - SPE Annual Technical Conference and Exhibition*, 3, pp. 2287–2299. doi: 10.2118/166267-MS.

Washburn, E W and Washburn, Edward W (1921) 'Note on a method of determining the distribution of pore sizes in a porous material', *Proceedings of the National Academy of Sciences of the United States of America*, 7(4), p. 115. doi: 10.1073/PNAS.7.4.115.

Zarragoicoechea, G. J. and Kuz, V. A. (2004) 'Critical shift of a confined fluid in a nanopore', *Fluid Phase Equilibria*, 220(1), pp. 7–9. doi: 10.1016/j.fluid.2004.02.014.

Zhang, K. *et al.* (2018) 'Thermodynamic phase behaviour and miscibility of confined fluids in nanopores', *Chemical Engineering Journal*, 351, pp. 1115–1128. doi:

10.1016/J.CEJ.2018.06.088.

Zhang, K., Jia, N. and Liu, L. (2019) ‘Generalized critical shifts of confined fluids in nanopores with adsorptions’, *Chemical Engineering Journal*, 372, pp. 809–814. doi: 10.1016/j.cej.2019.04.198.

Zhang, S. *et al.* (2018) ‘Paleoenvironmental conditions, organic matter accumulation, and unconventional hydrocarbon potential for the Permian Lucaogou Formation organic-rich rocks in Santanghu Basin, NW China’, *International Journal of Coal Geology*, 185, pp. 44–60. doi: 10.1016/J.COAL.2017.11.012.

Zhang, W.-M., Meng, G. and Wei, X. (2012) ‘A review on slip models for gas microflows’, *Microfluidics and Nanofluidics 2012 13:6*, 13(6), pp. 845–882. doi: 10.1007/S10404-012-1012-9.

Zudkevitch, D. and Joffe, J. (1970) ‘Correlation and prediction of vapor-liquid equilibria with the redlich-kwong equation of state’, *AIChE Journal*, 16(1), pp. 112–119. doi: 10.1002/AIC.690160122.